The role of Signal Transducer and Activator of Transcription 3 (STAT3) in neuronal pathways of Neonatal Hypoxic Ischaemic Encephalopathy

Konstantina Tetorou

University College London (UCL)

A thesis submitted for the degree of Doctor of Philosophy in Neuroscience to University College London 2023

Declaration

I, Konstantina Tetorou confirm that the work presented in this thesis is my own. Where information has been derived from other sources, I confirm that this has been indicated in the thesis.

Abstract

Hypoxic-ischaemic encephalopathy is a leading cause of child mortality and morbidity. Hypoxia-ischaemia (HI) strongly up-regulates Signal Transducer and Activator of Transcription 3 (STAT3) in the immature brain. There is need for development of alternative therapies for neonatal HI brain damage since the only available treatment therapeutic hypothermia (TH) has rather limited effectiveness and application, especially for infection-sensitised HI cases. We, as well as others, have shown that HI strongly upregulates STAT3 transcription factor in the immature brain and that systemic pharmacological STAT3 inhibition with WP1066 provides short-term neuroprotection. We hypothesised that STAT3 is involved in HI and that two compounds would have therapeutic activity in HI injury: WP1066: a pharmacological Janus Kinase 2 (JAK2) inhibitor of STAT3 and curcumin, a plant-derived compound with anti-inflammatory, antioxidative properties. Furthermore, we hypothesised that microglia-specific TGβR1 deletion, would provide neuroprotection, as it has been described that TGFβ, a pleiotropic cytokine, increases STAT3 phosphorylation.

WP1066 potential neuroprotective role was evaluated through intraperitoneal application on a postnatal day 9 neonatal C57Bl/6 HI mouse model, in different doses and time points and demonstrated short- and long-term neuroprotective effects at an optimal dose of 80μg/g body weight.

The intraperitoneal administration of curcumin in DMSO solution to postnatal day 9 HI animals showed clear neuroprotection. However, curcumin's poor bioavailability necessitated further optimisation to make the product suitable for clinical use. Thus, we synthesised curcumin-loaded microspheres P(3HB) and the results showed that intranasal administration after HI is neuroprotective.

Additionally, microglial-specific TGFβR-1 deletion provides neuroprotective effect, by increasing the anti-inflammatory microglial levels as assessed with immunofluorescence analysis, thus inducing repair after HI insult. Finally, we established a new infection-sensitised HI model, based on *E.coli* intravaginal maternal injection.

We conclude that both WP1066 and curcumin treatments reduce brain damage after HI insult and could be considered as potential treatment for the condition. Overall, all treatments have an effect on STAT3 phosphorylation, which points towards a detrimental role of STAT3 in HI.

Impact Statement

This study is based on a well-established mouse model of neonatal hypoxic-ischaemic (HI) brain damage, and specifically focuses on exploring the neuropathological role of STAT3 in this condition and the development of new treatments for neonatal HI. Neonatal HI brain injury evolves following deprivation of blood and oxygen flow to the brain of the infant, either around, at the time of birth affecting 1 to 3 per 1000 live births yearly[1]. It is the cause of about 1 million neonatal deaths per annum and 40% of the surviving affected children are likely to develop severe disabilities, such as epilepsy, cerebral palsy, and mental retardation. The only available treatment for HI is therapeutic hypothermia, but its efficacy is rather limited, with beneficial effects in only 1 per 7-8 treated children. Moreover, in cases of pre-exposure to bacterial infection, TH is not applicable[2–4], as suggested by an *in vivo* study[5], due to the inter-individual variability. This makes neonatal HI one of the top 20 leading causes of burden of disease, especially in terms of disability-adjusted life years. Therefore, further research into drug development for HI is vital for improvement of public health care.

The successful outcome of our research will elucidate new evidence for the pathological mechanism of HI brain damage. Additionally, novel drug-directed strategies in neonatal HIE will be developed as an alternative to therapeutic hypothermia. We focused on two widely available and well-studied compounds: WP1066, an inhibitor of STAT3, a transcription factor strongly upregulated after neonatal HI, and curcumin, a dietary molecule, anti-inflammatory, anti-oxidant known for its remarkable health advantages. At the same time, we assessed the role of microglia-specific TGFβR-1 deletion on HI damage as TGFβ1 cytokine increased

STAT3 phosphorylation on an HI rodent model, and established a new infection-sensitised HI model based on intravaginal maternal infection with *E.coli* K12 strain.

The two molecules were tested in a mouse model of neonatal HI and each demonstrated a satisfactory level of neuroprotection. Specifically, this research demonstrates the beneficial effects of WP1066 in an optimal dose of 80μg/g body weight, applied immediately, 1 or 2h post-HI in a postnatal day 9 mouse model. Additionally, this current study showed the neuroprotective effect of curcumin treatment dissolved in DMSO, but due to its toxic effects in humans we tested the application of curcumin encapsulated in P(3HB) microspheres, resulting in neuroprotective effects in different formulations.

Our results open the door to future research that should focus on establishing a new translational formulation for WP1066 application and combining it with therapeutic hypothermia, which will allow us to investigate the effect of combined treatments after HI brain damage in term infants.

The neuroprotective effect of curcumin and drug development is challenging due to its unknown target molecule. This current study aimed to overcome this challenge by assessing whether WP1066 and curcumin provide neuroprotective effect via the STAT3 pathway. Therefore, we can assume that one of curcumin's targets is possibly STAT3. The possibility to have, in the future, two potential new pharmacological compounds available for the treatment of neonatal normal and infection-sensitised HI could reduce the suffering of millions of children and their families and will reduce costs on the healthcare system making this research of great value to the society worldwide.

Acknowledgments

First of all, I owe my deep gratitude to my primary supervisor, Doctor Mariya Hristova, for her constant support, guidance, patience and encouragement. Thank you for accepting me into the lab for my Master's project and then for my PhD, for teaching me, inspiring me, being a friend, mentor other than an excellent supervisor. It is my honour to be part of this team.

I would like to thank my secondary supervisor, Prof Sigrun Lange, for her valuable support during this PhD, for her wise suggestions and input. I want to particularly thank her for helping me and guiding me, allowing me to learn all about western blots, and recommendations on my project.

I wholeheartedly thank Doctor Claudia Sisa, my fellow PhD student on the first year of my PhD, for her unstoppable support and guidance. Thank you for teaching me animal techniques, guiding me every day, and sharing with me all your experience. Claudia, you've been and are an amazing friend and listener, always keeping your positivity and calmness, you are a real inspiration.

I am thankful to UCL Cruciform BSU team. Thank you, Jayne Holby, Gabi Sturgis, Matthew Lawson, Irene Lopez, George Martin, Jamie Delicata, Patience Madzivanyika, for all your technical and veterinary support and for bearing with all my requests and questions. All the animal work in this PhD wouldn't have been possible without you.

I would also like to thank all the Master and BSc students who have assisted and contributed to this project: Miruna Nitu, Ishrat Hussain, Lubnaa Ghoora, Dayana Paulose, Christina Kostakou, Marwa Galaleldin, Amy Coombes, Elentina Gjonti, Jude

Alwan, Naomi Wawa, Elisa Mohd Faizal. I am thankful to my fellow PhD students, Dipa Begum, Runci Li for helping me during the last year of my PhD. Special thanks to Mr Daniel Hill, fellow PhD student from Cordeiro's lab, for his help with planning and conducting the toxicity assays.

I am grateful to A.G. Leventis Foundation for funding partially this project.

I am thankful to Prof Ipsita Roy for providing help with encapsulation of curcumin, and Dr Somavarapu Satyanarayana for his advice on the toxicity assays. A deep thank you to my graduate tutor Dr Sioban Sengupta, for her advice and academic support during this PhD and to all the administrative, finance team at Institute for Women's health, UCL for helping me with the bureaucracy related to this PhD.

A huge thank you to all my colleagues at Institute for Women's Health, who became good friends over the past 4 years. I wholeheartedly thank Dr Riccardo Privolizzi, for the continuous support and advice during my PhD, you've been and are a wonderful friend, Dr Juan Antinao for helping me with all the qPCRs for this PhD and bearing all my questions, Dr Nandaki Keshavan, for supporting me throughout this PhD, Dr Tania Castillo-Fernandez you've been a great friend and mentor for me, thank you, Dr Ashley Boyle, for your support on the infection-sensitised HI experiments, Dr Ellie Chilcott, Hester Chu and Anna Keegan, my office friends for always listening me and advising me. I am going to miss you all!

A deep thank you to my friends in London and Greece who supported me throughout this PhD, listening to me and always believed in me. Finally, I am grateful to my family, my mum, my dad and my sister, for the endless support. The deepest thank you goes to them, who believed in me, taught me to smile in any situation, experienced this

journey with me and made my life easier many times when needed! Thank you for always being by my side and I hope I made you proud!

Table of Contents

Index of tables

Index of figures

List of Abbreviations

ABC	Avidin-biotin conjugates
AIF	Apoptosis-Inducing Factor
ATP	Adenosine Triphosphate
BAK	Bcl-2-antagonist killer
BAX	Bcl-2-associated X protein
BBB	Blood Brain Barrier
BCA	Bicinchoninic Acid
BCL2	B-cell lymphoma 2
BMP	Bone Morphogenetic Protein
BRG1	Brahma-Related Gene 1
BSA	Bovine Serum Albumin
BW	Body Weight
CAT	Catalase
CC3	Cleaved Caspase-3 Enzyme
CHCl3	Chloroform
CHD7	Chromodomain Helicase DNA Binding Protein 7
CNP	Cyclic Nucleotide 3'-Phosphohydrolase
CNS	Central Nervous System
CPAI	plasminogen activator inhibitor
CSF	Cerebrospinal Fluid
CXC	Chemokine (C-X-C motif) ligand 1
DAB	Diaminobenzidine
DMSO	Dimethyl Sulfoxide

DNA	Deoxyribonucleic Acid
E.coli	Escherichia coli
EEG	Electroencephalography
EGF	Epidermal Growth Factor
ERK	Extracellular Signal-regulated Kinase
e-NOS	Endothelial NOS
Fe	Iron
FGF2	Fibroblast Growth Factor 2
FTIR	Fourier-Transform Infrared Spectroscopy
GalC	Galactosylceramidase
GAS	Gamma-activated Sites
GFAP	Glial Fibrillary Acidic Protein
GPx	Glutathione Peroxidase
GPx/cr	Glutathione Peroxidase/ creatinine
GSK3β	Glycogen synthase kinase 3
H2O2	Hydrogen Peroxide
HDAC	Histone Deacetylase
HI	Hypoxia-ischaemia
HIE	Hypoxic-ischaemic encephalopathy
HIF-1α	Hypoxia-Inducible Factor 1-alpha
HRP	Horseradish Peroxidase
ICAM1	Intercellular Adhesion Molecule 1
IHC	Immunohistochemistry
IL	Interleukin
INFχ	Interferonχ

Intraperitoneal	i.p.
iNOS	Inducible Nitric Oxide Synthetase
JAK 2	Janus Kinase 2
Jnk	Jun N-terminal kinase
LAMP1	Lysosomal Associated Membrane Protein 1
LIF	Leukemia Inhibitory Factor
LPS	Lipopolysaccharide
MAG	Myelin-associated Glycoprotein
MAPK	Mitogen-activated Protein Kinase
MBP	Myelin Basic Protein
MCP	Monocyte Chemoattractant Protein-1
MIP	Macrophage Inflammatory Protein
MMPs	Metalloproteins
MOG	Myelin Oligodendrocyte Protein
MRI	Magnetic Resonance Imaging
NE	Neonatal Encephalopathy
NF-kB	Nuclear Factor kappa B
NG2	Neuron-Glial Antigen 2
NICE	National Institute for Health and Care Excellence
NK	Natural Killer
NLRP3	NOD-like receptor family pyrin domain containing 3
NMDA	N-methyl-D-asparate
NO	Nitric Oxide
NOR	Novel Object Recognition
NOS	Nitric oxide synthase

Nrf2	Nuclear Factor Erythroid-2-Related Factor 2
n-NOS	Neuronal NOS
OD	Optical Density
Olig 1	Oligodendrocyte transcription factor 1
OLV	Optical Luminosity Value
OPCs	Oligodendrocyte Progenitor cells
O_4	Tetraoxygen
Pax	Paired Box genes
PB	Phosphate Buffer
PBS	Phosphate Buffer Saline
PC	Phosphatidylcholine
PDGFRα	Platelet-Derived Growth Factor Receptor α
PFA	Paraformaldehyde
PHB	Prohibitin
PKC	Protein Kinase C
PLGA-PEG	Poly (lactic-co-glycolic acid)-poly (ethylene glycol)
PLP	Proteolipid Protein
P	Postnatal day
PS	Phosphatidylserine
PUFA’s	Polyunsaturated Fatty Acids
PVA	Polyvinyl Alcohol
PVL	Periventricular Leukomalacia
PHA	Polyhydroxyaklanoates
ROS	Reactive Oxygen Species
RT	Room Temperature

SD	Standard Deviation
SEM	Standard Error of the Mean
SMAD	Suppressor of Mothers against Decapentaplegic
SOD	Superoxide Dismutase
STAT3	Signal transducer and activator of transcription 3
SVZ	Subventricular Zone
TGFβR1	Transforming Growth Factor Beta Receptor 1
TH	Therapeutic hypothermia
TLR	Toll-Like Receptor
TNFα	Tumour Necrosis Factorα
tPA	Tissue Plasminogen Activator
TUNEL	Terminal deoxynucleotidyl transferase d-UTP nick-end labelling
VEGF	Vascular Endothelial Growth Factor
Wnt	Wingless-Related Integration Site

Chapter 1: Introduction

1.1 Neonatal Encephalopathy and Hypoxia Ischaemia

Neonatal encephalopathy (NE) is a clinical constellation of abnormal neurological function that has multifactorial aetiology, including hypoxia-ischaemia (HI). This condition affects 1 to 3 per 1000 live births in developed countries, increasing to 26 per 1000 in the developing world[6], and is a major cause of brain damage and neurologic deficits in term and preterm infants. HI is a consequence of interrupted blood and oxygen supply to the fetal brain around and/or at the time of birth due to severe asphyxia. Despite the advantages in neonatal health care, a quarter of all neonatal deaths is a consequence of severe birth asphyxia[6]. About 40% of the affected infants die in the neonatal period and 30% of the surviving children develop long term neurological deficits[7] including cerebral palsy, seizures, and cognitive and memory impairment[6,8].

A number of risk factors for neonatal HI have been suggested, including antepartum conditions, such as maternal diabetes, pre-eclampsia and cardiac disease, and the less common intrapartum events of breech presentation, viral and bacterial infections, maternal fever in labour[8], instrumental delivery and cord prolapse[9]. Furthermore, socio-economic conditions, age and maternal BMI are studied risk factors for the disease[8]. Neonatal HI, causes brain damage with respective subregional vulnerability and is an important clinical challenge due to the substantial biopsychosocial burden it places on patients, families, and global healthcare systems. Hence, treatment and molecular targets for the condition are of pivotal importance.

1.2 Regional Vulnerability

HI brain damage does not result in uniform brain injury. The mostly affected regions are cortex, pyriform cortex, external capsule, hippocampus, striatum, and thalamus due to their highest metabolic activity. Gestational age and duration of the HI event also affect the severity of the damage[10]. Specifically, at early gestational stages oxygen deprivation affects periventricular white matter, causing motor, cognitive, sensory and visual impairment[6]; whereas in term infants the most vulnerable regions appear to be the sensorimotor cortex, cerebellum, brainstem, thalamus, and basal ganglia, resulting in severe motor disabilities, including rigidity, speech difficulties and impairment of the upper limbs[6]. Additionally, longer periods of infarction and watershed are associated with increased levels of brain damage and prolonged HI[6]. It has been suggested that the highly dynamic nature of the cerebral blood vessels in the fetus, and the fluctuations of cerebral blood flow and metabolic demand that occur following HI could explain the regional vulnerability in the developing brain[11]. HI is not a single event, rather an ongoing process causing neuronal cell death over hours to days after the initial injury.

1.3 Neonatal HI pathophysiology

In more detail, the pathology of HI brain injury evolves over days via three consecutive phases (primary, secondary, and tertiary energy failure, Figure 1)[10]. Reduced fetal cardiac output and cerebral perfusion leading to lack of oxygen and glucose delivered to the brain trigger acute insult and primary energy failure[12]. Fetal brain requires a constant supply of energy in form of adenosine triphosphate (ATP) that obtains

metabolizing lactate, ketone bodies, and glucose. Comparing to adult, fetal brain has a greater ability to tolerate HI, due to its capacity to reserve energy when needed. However, in case of a critical depletion of ATP also, the fetal brain becomes susceptible to injury. Subsequently, reduced mitochondrial phosphorylation and ATP availability cause a switch from aerobic to anaerobic respiration[13,14]. This change in metabolism results in reduced production of ATP and extracellular acidosis leading to dysfunction of Na^+/K^+ pump, thus increasing the intracellular calcium influx, and reducing the membrane potential from its normal values (-70mV)[7]. The cellular swelling linked to this process is known as cytotoxic oedema and leads to necrotic cell lysis. The depolarised neuronal membrane releases high concentrations of glutamate, which would typically be cleared via the glial reuptake pumps during aerobic respiration. N-methyl-D-aspartate (NMDA) and α-Amino-3-hydroxy-5-methyl-4-isoxazolepropionic acid (AMPA) channels opening occurs also due to the high concentrations of glutamate. The presence of these 2 different receptors on distinct parts of the cell raises the possibility of a 2-stage process of excitotoxicity. NMDA receptors have a higher affinity for glutamate and flux Ca^{2+} more promptly. This could lead to loss of cell processes initially, with progression to cell death only with activation of the AMPA receptors located on the cell body[15]. The physiological activity of the NMDA receptor, a receptor of glutamate and the primary excitatory neurotransmitter in the human brain, is essential for normal neurological function, including synaptic plasticity, cognition, learning, and memory formation. However, the excessive release of glutamate under HI insult leads to the over-activation of NMDA receptors, resulting in excessive Ca^{2+} influx that activates downstream death signaling pathways and finally leads to cell necrosis or apoptosis, which is known as excitotoxicity[10,16,17]. NMDA receptors exist in neurons and glial cells of newborns[18] and are composed of

four different subunits, including the structural subunit GluN1 and the regulatory subunits GluN2 and GluN3[19]. AMPA receptors, mediate fast synaptic transmission and are tetrameric assemblies of the subunits GluR1–4 and are encoded by separate genes, which are differentially expressed throughout the central nervous system. AMPARs lacking the GluR2 subunit are permeable to Ca^{2+}, a potential mechanism of action during HI brain damage[20].

Reduced intracellular pH, due to the accumulation of protons in the extracellular environment, during primary energy failure alters the binding of Fe^{3+} causing an increase in its catalytic activity in the Harber-Weiss reaction, which generates hydroxyl radicals from hydrogen peroxide and superoxide, thus initiating lipid breakdown or peroxidation[21,22]. In areas with high levels of Fe^{3+}, such as striatum, brain lipids with increased levels of polyunsaturated fatty acids (PUFA's) are highly susceptible to this form of lipid peroxidation and Deoxyribonucleic Acid (DNA) damage. Likewise, the high level of PUFA's break down generates additional oxygen free radicals, thus further increasing oxidative stress and neuronal death[23–25].

After successful re-oxygenation, a latent-recovery phase takes place, where aerobic respiration and homeostasis are recovered[12–14,26]. Several studies highlight that during latent period no changes are observed with magnetic resonance imaging (MRI) and histological analysis[10]. Electroencephalogram (EEG) data is suppressed as well, and a delayed onset of hypoperfusion can be observed[27]. Normalised oxygen flow alongside with recovered ATP levels are also recorded on magnetic cellular spectroscopy analysis report[28]. However, as the initial insult might not be adequately compensated, the pathways involved in cell death are still active and lead to secondary energy failure within 6-12h following the primary HI event[6].

Secondary energy failure starts as early as 6 to 12h after the initial injury and involves continued excitotoxicity, mitochondrial impairment, and inflammation. In particular, there is an increased expression of pro-inflammatory cytokines, such as interleukin-1β (IL-1β), interleukin-6 (IL-6), tumour necrosis factor α (TNF-α), transforming growth factor beta (TGβ) and transcription factors, as signal transducer and activator of transcription 3 (STAT3)[29–31]. Increased pro-inflammatory cytokine expression enhances free radicals' formation, which will act as cytotoxic mediators. Because of their high metabolic demand and their energy supply to myelinated axons[32], oligodendrocyte progenitors are particularly sensitive to free radicals. Hence, in both animal models and human newborns, oligodendrocytes' degeneration is enhanced after HI damage[33], thus leading to hypomyelination[32]. Mitochondrial dysfunction causes a boost of oxidative stress by increasing catalase (CAT), superoxide dismutase (SOD), glutathione peroxidase (GPx) levels and glutathione peroxidase/creatinine ratio (GPx/cr)[17,34], which ultimately increase reactive oxygen species (ROS). At this time, the majority of cell death occurs via necrosis, apoptosis (caspase 3 dependent pathway), autophagy and apoptosis-necrosis continuum leading to cellular atrophy[35–38].

Additionally, the production of pro-inflammatory cytokines results in the recruitment of white blood cells to the brain[39]. Lymphocytes play a crucial role in the protection of the brain after HI insult. Immune cell activation is correlated to poor outcome in HI brain injury and leads to inflammatory responses[40]. In HI, glial cells release a number of cytokines and chemokines including chemokine (C-X-C motif) ligand 1 (CXC12), macrophage inflammatory protein (MIP)-1α, MIP-1β, CCL5, CCL21 and CCR6, which stimulate natural killer (NK) cells, B cells, T cells and innate T cells to migrate to site of injury[41]. The accumulation of lymphocytes is linked to the chronic response resulting

in exacerbation of the brain damage days to months after the initial HI insult through the production of pro-inflammatory cytokines[42]. However, B cells and Tregs protect the brain by producing IL-10, which is a cytokine with potent anti-inflammatory properties that plays a central role in limiting host immune response to pathogens, thus maintaining normal tissue homeostasis[43].

During the secondary energy failure, decreased mitochondrial ATP production and excessive glutamate release lead to over-activation of NMDA receptors. Subsequently, excess Ca^{2+} enters and accumulates in neuronal cells in the basal ganglia and thalamus. Thus, NO is synthesised along with ROS and free radicals' formation. Excess NO reacts with superoxide radicals and forms peroxynitrite, which is rapidly broken down to form hydroxyl radicals. The combination of excess Ca^{2+}, NO, peroxynitrite and free radicals contribute to change in mitochondrial permeabilisation and subsequent dysfunction[44,45]. Consequently, mitochondrial oxidative phosphorylation dysfunction increases the toxic levels of ROS, peroxynitrite, and superoxides, leading to upregulated trafficking of cytochrome C and apoptosis-inducing factor (AIF) into the cytoplasm. When in the cytoplasm, cytochrome C activates proteolytic enzymes caspase 3, 8 and 9, which in turn initiate apoptotic-mediated DNA fragmentation and autophagy[1]. A cascading inflammatory response also causes cell death due to the release of cytokines, and excess increased levels microglia, and astrocytes[28].

Depending on the length and the severity of the HI insult, tertiary energy failure can occur and this persists for weeks and months after the initial injury, involving remodelling and repair, astrogliosis and late cell death[6]. Additionally, it leads to long-term neurological damage and disabilities including motor and cognitive impairment[46]. Persistence of neuronal degeneration, in conjunction with synthesis of new synaptic

connections is also observed in this last tertiary phase[47]. Figure 1 summarises the pathological development of HI brain injury. The cell death mechanisms involved in the different stages of the pathophysiology can be apoptosis, necrosis and autophagy.

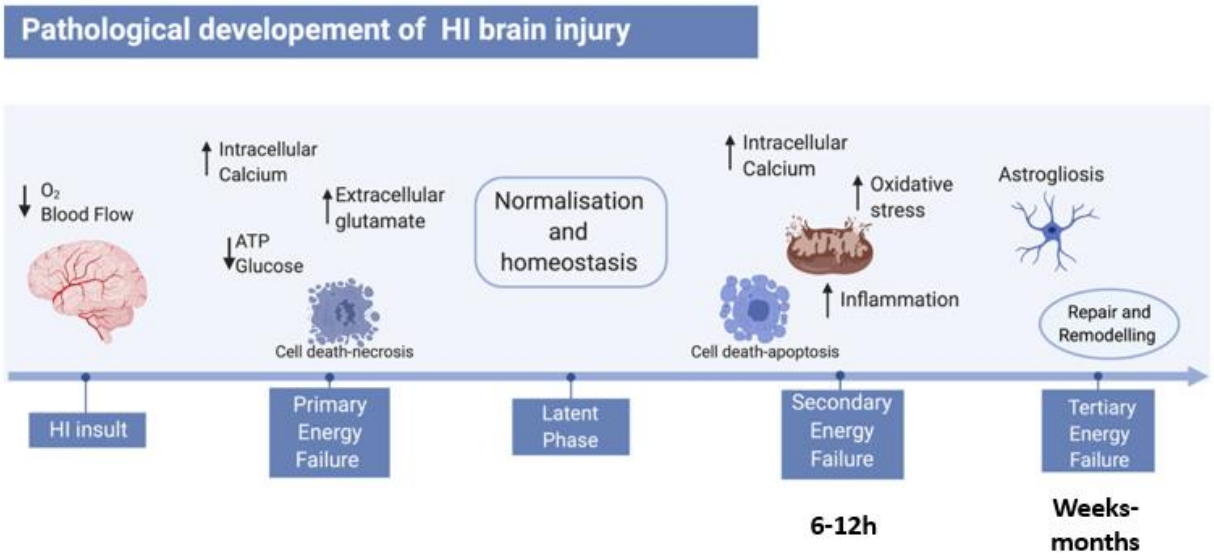

Figure 1. **Pathological development of neonatal HI brain injury.** The HI insult consists of a reduction of blood flow and oxygen to the fetal brain, leading to a primary energy failure. The main events of this phase include the reduction of ATP and glucose, the increase of intracellular calcium, therefore increase of glutamate release in the extracellular space. This scenario leads to cell death mainly via necrosis. After the primary energy failure, a latent phase begins, where the brain goes back to a “normal” state. A secondary energy failure can occur after 6 to 12h post-HI, where a second and stronger wave of cell death hits the brain, and events of inflammation, oxidative stress and mitochondrial damage occur. A tertiary energy failure can persist for months after the initial HI insult and is characterised by events such as brain remodelling and repair as well as astrogliosis (adapted from Tetorou et al., 2021)[48].

1.4 Cell death mechanisms during HI

During primary and secondary energy failure, cell death occurs as previously mentioned. Neonatal HI includes three different cell death mechanisms: apoptosis, necrosis, and autophagy[49]. Apoptosis is an active process that is crucial in normal brain development by refining cell pathways[50]. Apoptosis is the main cell death mechanism during secondary energy failure[50] and involves programmed cell death, characterised by cell shrinkage, chromatin condensation, nuclear pyknosis, plasma membrane blebbing, and DNA fragmentation[38]. The mechanisms resulting in chromatin processing during apoptosis are caspase-3 activation, and participation of AIF[51]. Both mechanisms have been recorded in animal models such as rodents, piglets, sheep and humans after HI injury causing significant damage and cell death[50]. Specifically, two main apoptotic pathways occur in the cell during HI brain damage: the extrinsic pathway mediated by death receptors and the intrinsic pathway mediated by the mitochondria[52]. The extrinsic pathway, is triggered by extracellular signals that oligomerize death receptors located on the plasma membrane[53] and the intrinsic pathway by intracellular stimuli, such as an increase of ROS, NO and Ca^{2+} caused by glutamate increase in the brain[54,55]. The extrinsic pathway activates B-cell lymphoma 2 (Bcl-2) and the Bcl-2 homologous antagonist killer (BAK1) proteins[56], followed by the release from the mitochondria to the cytosol of pro-apoptotic proteins including AIF, second mitochondria-derived activator of caspases, and endonuclease G[52], making this another way to classify apoptosis, depending on the final executor, and the involvement or not of caspases. Caspase-dependent apoptosis is initiated by cytochrome c followed by the apoptosome complex in the cytosol. This event will lead to the activation of caspase 3, resulting in DNA degradation, into pieces of about 200

to 1000 bp[57]. The caspase-independent pathway involves translocation of AIF to the nucleus mainly, leading to large-scale DNA fragmentation, into pieces of about 50,000 bp, and chromatin condensation[58,59].

Necrosis, a cell death mechanism present in secondary energy failure, is a passive cell death process, including membrane integrity loss, inflammation, cell swelling with complete organelle disruption, and cell lysis[60]. Necrosis results from Ca^{2+} entering damaged neurons and bind to mitochondrial electron transport mechanisms to disrupt metabolism and generate free radicals. Intracellular calcium activity is normally very low (~70 nM) and extracellular calcium is over 10,000 times higher (~1.2 mM). At concentrations exceeding 1 μM, Ca^{2+} activate cytosolic enzymes, including phospholipase, phosphatases, and phosphokinases that break down cell components, causing necrosis. Necrotic cells tend to be swollen and have indistinct intracellular features[61]. Additionally, a hybrid type of cell death, known as the "apoptotic-necrotic continuum", has been described after neonatal HI insult, which combines both necrotic and apoptotic characteristics[6,62].

Finally, during HI some neurons undergo autophagy[63], an adaptive process of degradation and recycling of cells' cytoplasm and organelles via a lysosomal mechanisms[44,64]. Autophagy is an essential process for the degradation and recycling of intracellular macromolecules. The most important autophagic mechanism, macroautophagy, involves the sequestration of long-lived proteins and damaged organelles in multimembrane vesicles, named autophagosomes, which then fuse with lysosomes to degrade their contents[65]. In neurons, autophagy has been demonstrated to be induced during development, starvation, neurodegeneration[66], and also after different excitotoxic stimuli[67–69]. In a Rice-Vannucci HI model has been described an increase in autophagosome formation[70,71] suggesting an enhancement of autophagy

after neonatal cerebral HI. Various animal models have investigated the cell death mechanisms described above but also the differences between preterm and term neonates affected by HI brain damage.

1.5 Preterm and term differences of HI injury

The severity of the brain damage developed after neonatal HI, is highly determined by the timing of the insult in respect to gestation as stated before. Therefore, both preterm and term animal models are used to investigate and mirror the different aspects of HI brain injury.

In preterm infants (<32 weeks of gestation) HI generally has a more complex temporal profile, with chronic nature[72,73] and is characterised by cognitive, and sensory deficits[74]. Overall, stimulation of the immature immune system may potentially result in an intense inflammatory response that is likely to be prolonged for some time[75].

At this stage, the periventricular white matter is particularly strongly hit by the insult, resulting in periventricular leukomalacia (PVL)[37,76] which sees the block in development of oligodendrocytes at the pre-oligodendrocyte stage, leading to abnormal myelination patterns typically observed in MRI scans[77,78]. Pre-oligodendrocytes susceptibility to inflammation and oxidative stress after HI results in increased cell death[33,77–80]. Preterm neurons are also vulnerable to the HI insult, as NMDA receptors are physiologically upregulated allowing Ca^{2+} to enter in higher concentrations[81], making these cells susceptible to the excitotoxicity cascade.

In term infants (>36 gestational age) HI insult causes selective damage to the sensorimotor cortex, basal ganglia, thalamus[82] and brainstem[83], resulting in severe

motor disability, including rigidity, impairment of mostly the upper limbs, and speech difficulties[83,84]. Cerebral white matter is also described as selectively sensitive to term HI injury, with abnormalities of watershed white matter and cortex present in 40–60% of patients[85].

The changes in NMDA receptor expression during neurodevelopment could explain the different patterns of injury seen in the preterm versus term infants. In a neonatal rat HI model using intracerebral injection of glutamate receptor agonist, selective white matter injury was observed at postnatal day 7(P7) (modelling preterm), while severe cortical infarction with no white matter selectivity was registered at P10 (modelling term)[86]. The same pattern was observed in a rabbit and piglet model[87]. Both preterm and term differences have been observed in HI alone and infection-sensitised HI models.

1.6 Infection-sensitised HI

Along with HI alone, infection-sensitised HI has been described. Specifically, bacterial intrauterine infection is among the factors contributing to HI brain damage. Maternal intrauterine infection during pregnancy leads to elevated fetal susceptibility to HI damage and increased risk of neonatal disability and mortality compared to HI alone[88–90]. Bacterial infection is recorded in half of all preterm births[91–93], including infections caused by chlamydia, syphilis, or gonorrhoea, and increases the risk of brain damage and intraventricular haemorrhage[94]. Preterm delivery occurs in approximately 11% of all births worldwide[92], and is mostly due to chorioamnionitis, inflammation of the extraplacental membranes or amniotic fluid, leading to fetus infection[94]. Infection-sensitised HI depends on the type of bacterial infection, differing between gram-

negative and gram-positive bacteria. Gram-negative bacteria are surrounded by a thin peptidoglycan cell wall, which itself is surrounded by an outer membrane containing lipopolysaccharide (LPS). Gram-positive bacteria lack an outer membrane but are surrounded by layers of peptidoglycan many times thicker than is found in the gram-negative.

Bacterial LPS, a main component of the outer cell membrane of most gram-negative bacteria such as *Escherichia coli (E.coli)*, sensitises the neonatal brain to HI[95] due to its strong immune-stimulatory properties[95] (Figure 2). It is therefore a commonly used agent to mimic brain infection in animal HI models. Following HI insult, LPS increases cerebral lesions and CNS damage, enhancing mortality rate due to tissue damage and exacerbated infraction volume in rodent and piglet models[5,75,95,96]. Studies suggest that the interaction between LPS and Toll-like receptors is critical for LPS-sensitised HI brain damage[97]. Specifically, a direct binding is established between LPS and myeloid differentiation primary response 88 (MyD88) adaptor protein or Toll/interleukin-1R domain-containing adaptor (TLR/IL-1R) before binding to TLR4. Following that, downstream activation of nuclear factor 'kappa-light-chain-enhancer' of activated B-cells (NF-kB) occurs by degrading IKB (enzyme complex) allowing the translocation from the cytoplasm to the nucleus[98–100]. Thus, NF-kB binds on the promoter region activating glial cells and inducing the upregulation of pro-inflammatory cytokines including TNF-α, IL-1β, IL-6, and IL-8[101], and cell adhesion molecules including P-Selectin, E-Selectin, and Intercellular Adhesion Molecule 1 (ICAM1), as show in Figure 2. A reduction in the levels of brain injury after LPS-sensitised neonatal HI has been shown in several studies using a mouse model of MyD88 deficiency[102], TNF cluster gene knock-out[103], and after pharmacological inhibition of NF-kB[98]. NF-kB translocates to the nucleus resulting in an increased pro-inflammatory response

involving activation of the inflammasome NOD-like receptor family pyrin domain containing 3 (NLRP3), caspase1, and IL-1b multi-protein complex[99,100].

Additionally, the activation of TLR4 and 3 increases glial activation, infiltration of peripheral immune cells and leads to blood brain barrier (BBB) impairments[104], while decreasing myelination[105]. This activation prior to HI insult, supresses mitochondrial respiration resulting in earlier ATP depletion during HI. *In vitro* studies have demonstrated that pro-inflammatory cytokines, including IL-1β, induce Ca^{2+} influx in the myometrial smooth muscle and could potentially influence premature maternal muscle contraction[106]. In preterm infants, pre-oligodendrocyte maturation is halted, and MRI studies have shown that this is linked to abnormal myelination, thus exacerbating HI induced damage in the preterm brain[107].

In a study from Suff and colleagues (2018), vaginal injection of *E.coli* K12 at embryonic day 16 in C57Bl/6 $Tyr^{c\text{-}2J}$ mice, resulted in bacterial ascension into the uterine cavity within 18h and caused preterm parturition and neonatal cerebral inflammation[91]. The exposure of the immature brain to an inflammatory stimulus such as bacterial infection with *E.coli* triggers an increase in the levels of pro-inflammatory cytokines and neuronal cell death, thus resulting in an abnormal development of the central nervous system (CNS)[105]. Increased levels of pro-inflammatory cytokines, including IL-6, IL-1a, IL-8 and TNF-α in the blood serum and cerebrospinal fluid (CSF) of HI affected neonates, have been positively linked to elevated pathological severity and risk of developing cerebral palsy and other motor and cognitive disabilities[96,108,109]. Thus, an antenatal pro-inflammatory stimulus makes the CNS more vulnerable to injuries, a phenomenon known as ‘’sensitisation’’[105].

Alternatively, gram-positive bacterial infection is the cause of 90% of early-onset sepsis in neonates, exacerbating HI induced damage[110]. Peptidoglycans and lipoteichoic acid present on the gram-positive cell wall were shown to sensitise the brain in a P7 Wistar rat model via interaction with TLR2, resulting in increased microglial activation and tissue loss, at a level comparable to LPS sensitisation[111]. Further studies have shown that sensitisation with an artificial TLR2 agonist, exacerbates neural loss, suppresses mitochondrial respiration and increases myelin loss following HI insult in a P8 C57Bl/6 mouse model[112]. In the same study, TLR2 knockout mice showed reduced brain damage in comparison to TLR2+/+ mice[112].

As described previously, microglial cells play an important role in the HI alone and also in LPS-sensitised HI, by displaying a pro-inflammatory microglial phenotype at 24h post-HI insult in an LPS sensitised neonatal HI rat model[100]. Simultaneously, an anti-inflammatory microglial phenotype is also recorded, highlighting the dual role of microglial cells in HI alone and LPS-sensitised HI[100]. Specifically, pro- and anti-microglia subsets accumulate at the site of damage with Interferon γ (IFNγ) leading to the production of pro-inflammatory triggered cytokines[96], while IL-4 stimulates anti-inflammatory phagocytosis of cell debris and promotes anti-inflammatory cytokines to supress neuroinflammation.

Further studies in a rodent model have shown that microglia tissue plasminogen activator (tPA) persistent stimulation during HI injury is a critical component of LPS-sensitised HI[113]. Furthermore, treatment with a mutant form of plasminogen activator inhibitor (CPAI), successfully mitigated microglial activation after insult[113], while decreasing LPS mediated NF-kB, and monocyte chemoattractant protein-1 (MCP-1) levels, and brain damage, thus highlighting the crucial role of microglia in the LPS-

sensitised HI response[113]. Along with microglia, a variety of cells are involved in HI brain damage with a number of different roles.

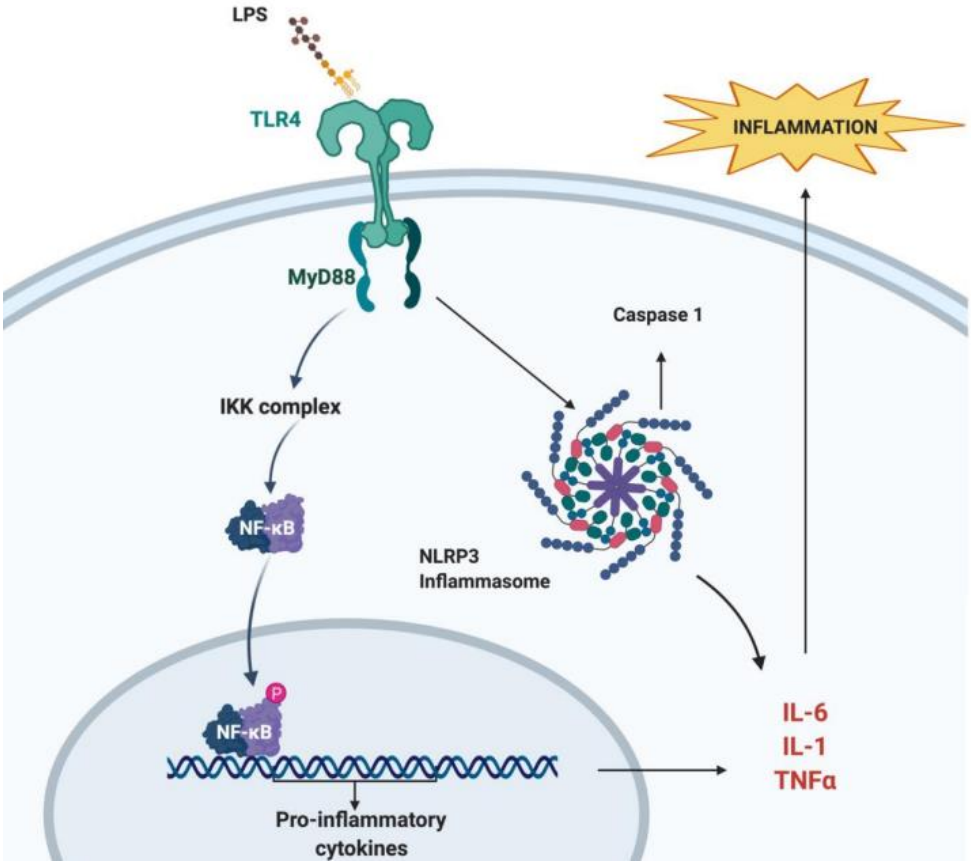

Figure 2. **Mechanisms behind LPS-sensitised neonatal HI**. A bacterial infection sensitises the brain to subsequent HI insult via the interaction of LPS with TLR4. This leads to MyD88-mediated NF-kB internalization. NF-kB activates the transcription of genes for pro-inflammatory cytokines expression. Simultaneously, the LPS interaction with TLR4 activates the NLRP3 inflammasome, which also promotes increased presence of pro-inflammatory cytokines and apoptosis. Figure created with Biorender and based on publications[48,102,114,115].

1.7 Cells of the brain affected by HI insult

HI impacts all of the brain's cells, leading to inflammatory responses and cell death. Glial cells refer to a collection of abundant cells in the CNS, including astrocytes, microglia and oligodendrocytes. Glial cells provide structural and nutritional support and protect neurons, through myelin formation, debris removal and maintenance of homeostasis[116]. They are also involved in the development of the CNS under normal physiological conditions and are critical in neuropathogenesis and in pathological conditions, as they participate in innate and adaptive immune responses.

Microglia represent 10-15% of glial cells in the brain and are the first line of immune response in the CNS[117]. More than 100 years ago, in 1913, Santiago Ramón y Cajal described microglia as the "third element" of the CNS[118]. Microglia arise from embryonic yolk sac precursors[119], maintain their CNS population by self-renewal and are not replaced by bone marrow-derived myeloid cells[118,119]. Recent studies have constructed a mouse model of microglial knockout by using transgenic methods and demonstrated that microglial replacement is combined with local microglial proliferation and infiltration of bone marrow-derived precursors to repopulate the niche[120]. Their main role is to protect the homeostasis of the neuronal cells under normal conditions[121]. Microglia eliminate microbes, dead cells, redundant synapses, protein aggregates, and other particulate and soluble antigens that may endanger the CNS. Furthermore, microglia secrete various soluble factors that contribute to different aspects of the immune response and tissue repair[122]. Microglia remain static to prevent tissue disruption but have the ability to migrate and proliferate to the place of damage during a HI insult. Microglial activation results in ROS production,

phagocytosis, release of pro- and anti-inflammatory cytokines and production of metalloproteins (MMPs), leading to breakdown of the BBB[116].

Endothelial cells, astrocytic foot processes which in normal conditions, surround brain capillaries and, during development, induce endothelial cells to form tight junctions pericytes and basement membrane of BBB limit the permeability of immune cell infiltration through tight junctions to connect adjacent cells. Within 30-60 min following HI insult, BBB leakage is present, leading to early tight junction disruption and fibre formation thus altering endothelial cell distributions[123]. Neutrophil and macrophage infiltration is promoted, releasing proteases such as MMPs, proteinase 3 and elastase, ROS, cytokines and chemokines, which subsequently deteriorate the BBB integrity[123]. Neutrophil influx blockage has been proposed as a therapeutic target with prophylactic anti-Ly6G treatment for LPS-sensitised HI brain damage in a mouse model, as the production of pro-inflammatory cytokines and MMPs is diminished[124].

Astrocytes are part of BBB, account for approximately 80% of glial cells within the CNS[125] and regulate glutamate uptake and oxidative stress levels, while maintaining homeostasis[126,127]. Astrocytes participate in synapse development, neuronal support, cerebral blood flow regulation, BBB formation and function, and control of neurotransmitters[128]. Furthermore, their morphological and functional characteristics are altered under pathological conditions, a process termed as “reactive astrogliosis,” and include their proliferation, the formation of a physical barrier to separate the injury site, the expression of intermediate filament proteins, cytokines, and chemokines, and regulation of the immune response[129]. During HI brain damage, microglial activation causes subsequent astrocyte activation, resulting in the astrocytic production of pro- and anti-inflammatory cytokines and chemokines. Therefore, hypertrophic changes are induced, characterised by glial fibrillary acidic protein (GFAP) and IL-33

upregulation[130]. On the other hand, astrocytic activation of NF-kB and hypoxia-inducible factor 1-alpha (HIF-1α) increase the expression of MMP-9 and vascular endothelial growth factor (VEGF), leading to tight junction degradation in the BBB[131].

Another category of cells involved in HI insult is oligodendrocytes, which assemble myelin in the process of myelination to permit rapid saltatory conduction along the axons in CNS[132,133]. Oligodendrocytes derive from dorsal and ventral radial glia populations in the neuroepithelial zones, which produce oligodendrocyte progenitor cells (OPCs) between 7.5 and 20 gestational weeks in human cortex and at embryonic day 16 and postnatal day 10 in the mouse cortex[132,134,135]. Neuron-glial antigen 2 (NG2) and platelet-derived growth factor receptor α (PDGFRα) are expressed from OPCs to mediate a response to PDGF and to promote OPCs proliferation prior to differentiation[136]. During differentiation (Figure 3), NG2 and PDGFRα are downregulated, and mature markers including proteolipid protein (PLP), myelin basic protein (MBP), cyclic nucleotide 3'-phosphohydrolase (CNP), and myelin oligodendrocyte protein (MOG) are expressed[137]. Oligodendrocytes continue to self-renew until the age of 50 in humans, corresponding to 2 years in mice[138]. Furthermore, OPCs express gelatinases including MMP-2 and MMP-9, facilitating cell migration and elongation of OPCs processes for myelination. During HI brain damage MMP-9 expression is decreased, as has been shown in mouse models[139].

OPCs are involved in the metabolic coupling pathway, with high metabolic demands. Due to lack of ATP during HI insult, OPCs cannot maintain the myelin and are more susceptible to the damage from ROS production and oxidative stress[140]. Olig1, an important transcription factor involved in OPC remyelination after HI brain damage, was shown to significantly decrease at 24h post-HI, whereafter it returned to normal levels between 72h and 28 days after the insult[141]. The same study showed that MBP

expression gradually diminished between 24h and 7 days, with a recovery phase between 14 and 28 days after HI insult[141]. Expressed by myelinating oligodendrocytes, MBP is the second most abundant protein in the CNS, interacting with lipids to maintain the structure of myelin and its adhesion to oligodendrocytes (Figure 3). Therefore, MBP is used as a biomarker to track the effect of HI on oligodendrocytes' repair[142–145].

Finally, OPCs amplify proliferation rates and upregulate trophic factors, which in turn increase MMP-9 expression, to induce neuroprotective effects and long-term tissue repair following HI brain damage in a rat model[146].

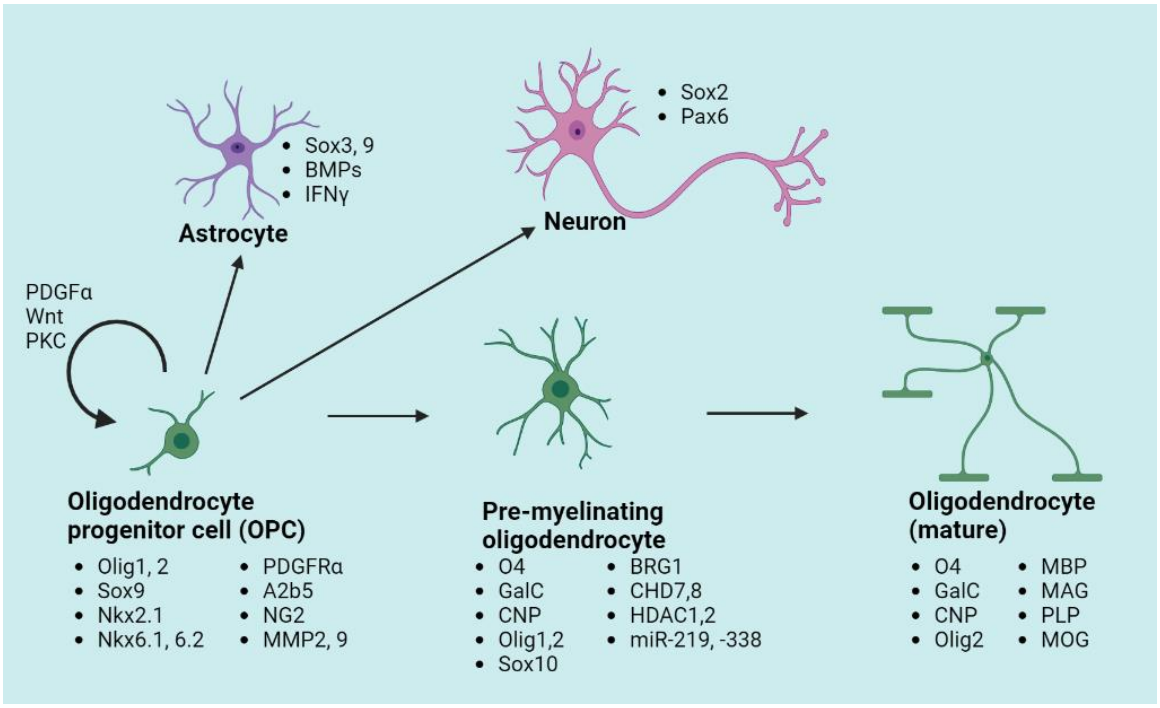

Figure 3. **The transcription factors and growth factors associated with oligodendrocyte precursor cells proliferation and differentiation into oligodendrocytes.** OPC self-renewal is dependent on PDGFα- PDGFRα, Wingless-related integration site (Wnt) signalling, and Protein kinase C (PKC) activation(Akay et al., 2021). Bone morphogenetic proteins (BMP) and IFNγ can induce OPC differentiation into astrocytes, and Sox2 and paired box genes (Pax6) can induce neuronal differentiation(Akay et al., 2021). Abbreviations: Oligodendrocyte

transcription factor (Olig 1, 2) NK2 Homebox protein 1 (Nkx2.1, Nkx6.1, 6.2), Tetraoxygen (O4), Galactosylceramidase (GalC), Brahma-related gene 1 (BRG1), chromodomain helicase DNA binding protein 7 (CHD7, 8), Histone deacetylase (HDAC1, 2), micro-RNA (miR-219, -338), Myelin-associated Glycoprotein (MAG), Wingless-related integration site (Wnt). Figure created with BioRender and based on publications[138,146,147].

1.8 Oxidative Stress

Oxidative stress involving free radicals plays a major role in HI. Molecules possessing a solitary electron in their outermost orbital shell are described as free radicals. O_2 maintains two unstable electrons, which are normally donated to nearby molecules in free radical transfers, as the mitochondrial electron transport chain, operated by eukaryotic cells for ATP production[148]. Disruption of aerobic respiration due to HI insult leads to oxidative stress, and therefore high metabolic brain regions are more susceptible to HI brain damage[149]. The neonatal cerebral tissue is especially vulnerable to the impact of oxidative stress due to elevated oxygen consumption and low antioxidant levels[150]. Primary energy failure leads to elevated Ca^{2+} and Na^{+} levels, with disruption of complex's I function, resulting in a positive feedback loop of ROS production and mitochondrial disruption[151]. Oxidative stress occurs when the equilibrium of ROS production and elimination is disrupted, allowing for ROS accumulation in the cells, although the exact mechanism of oxidative stress induced damage requires further investigation[151].

Nitric oxide synthase (NOS) is another source of ROS. NOS acts as an enzyme to synthesise the production of NO from L-arginine and oxygen. Excessive glutamate release leads to NMDA receptor coupling and Ca^{2+} influx during HI insult, which

permits NOS activation to produce NO, which subsequently reacts with superoxide free radicals to form toxic peroxynitrate followed by NO_2^+, nitrogen dioxide and hydroxyl radicals. There are three isoforms of NOS: endothelial NOS (e-NOS), neuronal NOS (n-NOS) and inducible NOS (iNOS). All three isoforms are upregulated during HI insult, with e-NOS and n-NOS upregulated immediately after reperfusion, and iNOS several hours later. e-NOS upregulation is protective, and maintains pulmonary blood flow, but n-NOS and iNOS are associated with initiation of pre-apoptotic pathways. Expressed by macrophages, dendritic cells, T-cells and microglia, the deletion of iNOS and n-NOS has been proposed as a therapeutic target, however, this is yet to be investigated in an HI infection-sensitised model[152,153]. In conclusion, oxidative stress is a main result of HI brain damage along with inflammation. It has been also reported that complement inflammatory system plays a crucial role in HI[154].

1.9 Complement System and HI

The complement system is the most potent inflammatory cascade in humans and plays a major role in innate immune defence as well as many inflammatory diseases, including HIE[155,156]. C1q is the first subcomponent of the classical complement pathway, with known functions in dendritic cell maturation, immune modulation, cell differentiation, cancer progression, which binds to antigen-antibody immune complexes on the cell surface, or to specific receptors expressed during apoptosis[157]. Then, C1q initiates the complement cascade characterised by a series of cleavages, leading to stepwise activation of a complex in the membrane activity (Figure 4). Experimental studies demonstrated that classical complement pathway activation via C1 generates pro-inflammatory mediators such as C3, C5a, which are associated with

HI brain injury[158] and that C1q is highly expressed in the brain following ischaemia[154]. Deletion of C1q reduces brain infarction and neurofunctional deficit in a mouse model of neonatal HIE[159,160], whereas failure to reduce excessive excitatory synapses during development results in epileptogenesis in C1q deficient mice[161].

C5a and C3b are intermediates in the cascade, with chemotactic and phagocytic functions, respectively[162]. C3a induces both pro- and anti-inflammatory effects that contribute to the disease phenotype. Specifically, the proinflammatory aspects of the molecule dominate the chronic phase of inflammation, whereas anti-inflammatory effects of C3a dominate the acute phase of inflammation[163]. C5aR antagonism in the acute phase improves recovery, in a mouse model of spinal cord injury. However, prolonged C5aR blockade interferes with formation of reparative scar tissue, leading to a decreased ability to confine pathology, increased spinal inflammation and reduced neurological recovery[164].

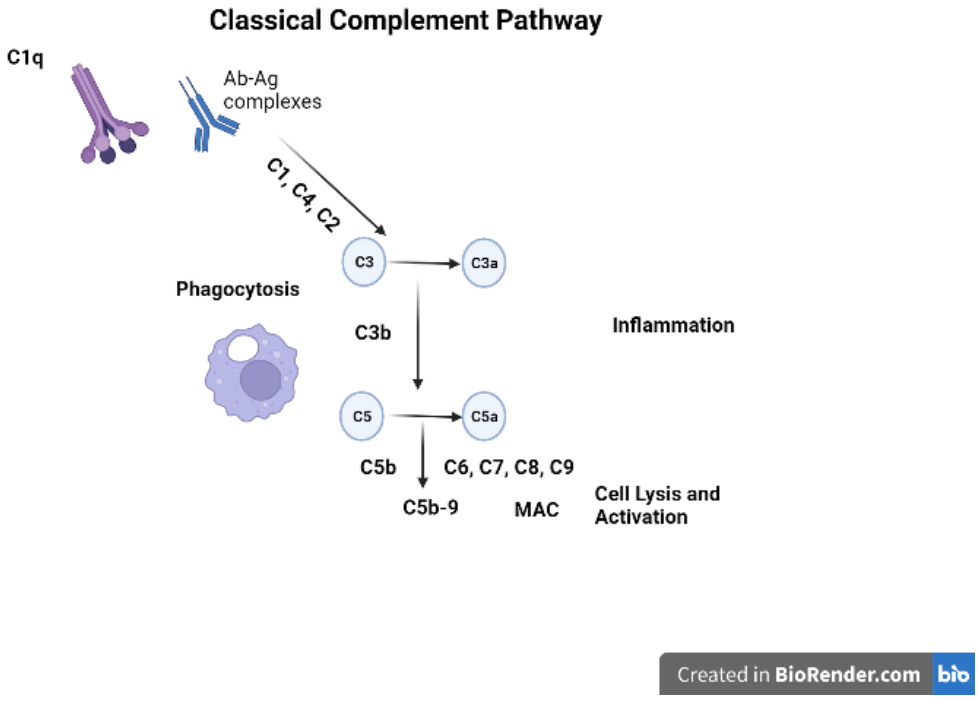

Figure 4. **The Complement Cascade in HIE**. The Classical pathway is activated by antigen/antibody complexes presented on damaged or invading cells, recognised by C1q in complex with serine proteases C1r and C1s. C1r and C1s cleave C4 and C2 to generate the classical pathway C3 convertase C4b2a. C3b protein directly binds a microbe, foreign material, or damaged tissue. C3b opsonises targets for phagocytosis and B-cell activation. Anaphylatoxins C3a, C4a, and C5a are created through enzymatic cleavage of C3, C4, and C5; while C3b, C4b, and C5b are necessary for continued propagation of the complement system towards the terminal pathway. C3a, C4a, and C5a carry out secondary cleavage actions to activate other immune systems. The terminal pathway begins with C5 cleavage by C5 convertase and cleaves C5 into C5a and C5b. C3a and C5a can attract and activate inflammatory cells. C5b binds C6, C7, C8, and multiple copies of C9 forming the membrane attack complex (MAC) complex, resulting in targeted cytolysis. Figure created with Biorender and based on publications[163].

1.10 STAT3 Pathway in HI brain damage

STAT3, is a member of the STAT family, and is a cytoplasmic transcription factor that regulates cell proliferation, differentiation, apoptosis, angiogenesis, inflammation, and immune response (Figure 5). STAT3 is strongly upregulated by HI in the immature brain[31] and in addition has important roles in acute phase response, metabolism, and is furthermore implicated in cancer progression[165].

Phosphorylation of STAT proteins, including STAT3, leads to activation followed by dimerisation and translocation to the nucleus[31]. Once in the nucleus the activated STAT dimers can bind to consensus DNA-recognition motifs, called gamma-activated sites (GAS), in the promoters of cytokine-inducible genes, resulting in transcriptional activation. This triggers the expression of pro- and anti-inflammatory molecules that

might exacerbate or reduce the damage produced in the brain[166]. STAT3 is activated by some interleukins, including IL-6, IL-11, IL-10, IL-20 and IL-22[167,168]. Furthermore, its activation is involved in more astroglial maturation and in the inflammatory response after HI brain damage[169]. An increase in phosphorylated STAT3 (activated form) has also been shown in the nucleus of glial cells following HI, accompanied by induction of mRNA of selected cytokines, including IL-6, TNF-α and IL-10. This suggests the participation of STAT3 in neonatal brain inflammation[170]. Pharmacological inhibition of glycogen synthase kinase 3β (GSK3β), a constitutive activated serine/ threonine protein kinase which controls the release of IL-6 via activation of STAT3, was shown to reduce apoptosis and inflammatory responses by down-regulating STAT3 activation, resulting in reduced brain injury after HI in a P9 mouse model[170].

Importantly, STAT3 is activated due to a Janus Kinase 2 (JAK2)-dependent phosphorylation of Tyr-705 Y705, and JAK2- independent phosphorylation of Ser-727 residues[171]. Phosphorylation of STAT3 (pSTAT3) is associated with DNA degradation[172] and post-HI events are linked with phosphorylation of both sites[173]. Tyr705 phosphorylation occurs in response to cytokine stimulation mediated by Janus kinases, specifically JAK2, leading to STAT3 homodimerization, nuclear translocation, DNA binding and transcription[174]. Tyr705 phosphorylation is followed by the phosphorylation at Ser727, which is caused by various activation signals including kinases, such as extracellular signal-regulated kinase (ERK)1/2, p38, Jun N-terminal kinase (Jnk) and mitogen-activated protein kinase (MAPK)[174]. Phosphorylation of STAT3 due to IL-6 activation results in increased levels of microglial activation and cell death[172].

Interestingly, a small pool of STAT3 has recently been discovered in mitochondria (mito-STAT3), and shown to regulate mitochondrial electron transport chain, affect

mitochondrial metabolism and cellular function[174] (Figure 5). Ser727 phosphorylation mediates mito-STAT3 activation, and it has been linked to immunological function and associated to cancer progression. Mito-Stat3 suppresses ROS formation during cancer genesis, indicating that targeting Ser727 phosphorylation and mito-STAT3 may have strong potential in treating cancer[175]. In neonatal HI brain damage an excessive formation of ROS causes cell death during the secondary energy failure as described before, so the effect of mito-STAT3 on ROS formation would potentially be critical for the progression of the condition[6].

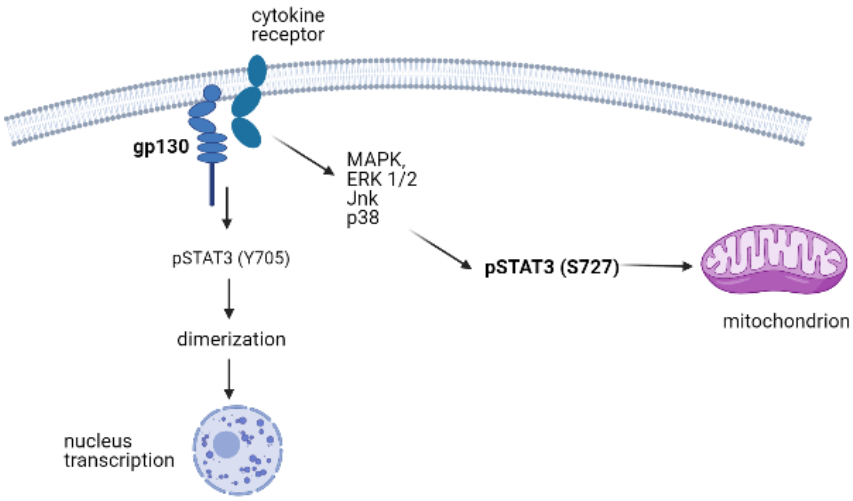

Figure 5. **STAT3 pathway after phosphorylation.** STAT3 is activated due to homodimerization of signal-transducing β-receptor (gp130), which occurs in response to cytokine stimulation mediated by JAK2. A JAK2-dependent phosphorylation of STAT3 Tyr-705 happens leading to STAT3 homodimerization, nuclear translocation[174] and a JAK2-independent phosphorylation of Ser-727 residues[171]. The phosphorylation at Ser727, which is caused by various activation signals including kinases, such as ERK1/2, p38, Jnk and MAPK[174] and mediates mito-STAT3 activation. Figure created with Biorender and based on publications[171,174,175].

In addition to being present in neurons in adult animal models of ischaemia, activated STAT3 is also present in blood vessel endothelia, astrocytes and microglia[176,177]. This potentially associates STAT3 activation with the inflammatory response within the brain, defined as neuroinflammation, and the related tissue repair[178]. STAT3 upregulation post-HI is cell and time-specific, with detrimental effect in neurons and astroglia, as its deletion in those cell types has been shown to be neuroprotective[31,179–181]. Our group recently demonstrated that global inhibition of STAT3 phosphorylation, via JAK2-blockade and brain cell type-specific deletion in neurons or astrocytes of the STAT3 gene, reduces inflammation and tissue loss in response to HI-insult[181]. This finding suggests that STAT3 is a crucial factor in neonatal HI-brain damage[181].

For the purpose of modulating STAT3 with pharmacological compounds, WP1066 is among the low-molecular-weight (368.385 g/mol) kinase inhibitors targeting JAKs. It was originally synthesised as an anti-cancer compound by modifying the structure of AG490, one of the prototypic JAK2 inhibitors[182,183]. WP1066 crosses the BBB[183] and is used for treatment of epilepsy[184] and neuropathic pain[185]. Pharmacological interference with STAT3 Tyr-705 phosphorylation through the JAK2-inhibitor WP1066 was shown to provide a protective effect similar to that seen in the neuron- and astroglia-specific STAT3 knock-out mice, but to a more moderate degree[181]. In a mouse model of HI, treatment with the inhibitor in a split dose of 80µg/g, 20 min prior and immediately after HI, significantly reduced pSTAT3 Tyr-705 phosphorylation in cortex and hippocampus at 1h post-HI, as well as astro- and microglial activation at 48h post-HI[181]. This indicates that the Jak2/STAT3 pathway affects mechanisms that can provide additive neuroprotection after HI insult.

WP1066 has low water solubility and in animal and *in vitro* studies is mostly commonly dissolved in Dimethyl Sulfoxide (DMSO) for oral or systemic administration. However,

as STAT3 is over-expressed in a number of malignancies, recent approaches have developed delivery systems where WP1066-loaded liposomes or nanoparticle formulations have been applied in clinical trials for glioblastoma[186]. WP1066-loaded liposomes or nanoparticles have also been developed to be applied orally or systemically for cancer treatment in Phase 1 Clinical trials (https://ivyfoundation.org/wp-content/uploads/2015/06/McRae-IvyFoundation-CaseStudy-STAT3-HR.pdf). Additionally, WP1066 is already in on-going cancer Clinical trials (NCT04334863, NCT01904123) and was granted Orphan Drug Status by the FDA in 2019 for glioblastoma f148 (https://news.cancerconnect.com/brain-cancer/food-drug-administration-grants-orphan-drug-status-for-wp1066-in glioblastoma) due to its ability to inhibit multiple key oncogenic transcription factors, including STAT3. The Investigational New Drug application for the study of WP1066 in the treatment of recurrent malignant glioma was recently cleared by FDA with a next step of Phase 1 open label, single arm, dose escalation study for safety, pharmacokinetics and efficacy of oral WP1066 in adult patients with recurrent malignant glioma. WP1066 has also received Rare Paediatric Disease designation for three other paediatric indications, diffuse intrinsic pontine glioma, medulloblastoma, and atypical teratoid rhabdoid tumour.

1.11 Transforming growth factor beta receptor 1 (TGFβR-1)

We further explored the correlation between STAT3 and TGFβ pathway. TGFβ is a multi-isomeric, multi-functional, pleiotropic cytokine, involved in numerous biological processes and main functions such as proliferation and differentiation[187,188]. TGFβ initiates its signal through ligand-induced heterodimerization of its two receptors

(TGFβR-1 and 2) on the cell surface. TGFβR-2 binds TGFβ and then interacts with TGFβR-1 forming complex. TGFβR-1 is phosphorylated by TGFβR-2, which leads to recruitment of signalling effectors of TGFβ, Suppressor of Mothers against Decapentaplegic (SMAD)2 or SMAD3 proteins. Then, the SMAD proteins are phosphorylated by TGFβR-1, and they form a complex with SMAD4. Subsequently, the SMAD proteins translocate to the nucleus, associating with transcription coactivators or corepressors[188]. Bain and colleagues have shown that TGFβ1-induced SMAD 2/3 phosphorylation and the combination of epidermal growth factor (EGF), a protein that stimulates cell growth and differentiation, leukemia inhibitory factor (LIF), an IL-6 class cytokine that affects cell growth by inhibiting differentiation, and TGFβ1 synergistically increased STAT3 phosphorylation over single or double cytokine combinations[179]. TGFβ and STAT3 pathways are presented in Figure 6.

TGFβ is normally present in low quantities in the brain and displays both pro- and anti-inflammatory effects. Microglia display two different activation states, as mentioned before, pro-inflammatory and anti-inflammatory, which each generate and recruit pro- and anti-inflammatory mediators respectively, following HI insult. Early pro-inflammatory microglia activation is induced following HI brain damage that triggers expression of pro-inflammatory cytokines, such as IL-1 and TNF- α, promoting inflammation and exacerbating damage. Contrary, anti-inflammatory microglia activated cells produce anti-inflammatory cytokines like IL-4 and IL-10, mediating anti-inflammatory immune response in communication with other cells and promoting healing[189].

Following HI insult TGFβ is strongly upregulated in microglia[190]. TGFβ gene deletion in an adult mouse model of HI, increased the proliferation of microglia promoted inflammation, thus highlighting the role of TGFβ as a down-regulator of microglial

activation[191]. The neuroprotective role of TGFβ is supported also by other studies where TGFβ deletion resulted in increased cell death and microgliosis in a TGF knockout mouse model[192]. Furthermore, a study on chick embryo retina demonstrated that TGFβ plays a crucial role in programmed cell death during certain periods of retinal development[193]. Altogether, these studies reveal a neuroprotective role of TGFβ, which depends on the type of injury of CNS and the developmental stage.

An altered signalling between pro- and anti-inflammatory cytokines, as a result of severe HI insult in a pre-term mouse model, causes subventricular zone (SVZ) pro-oligodendroglia precursors to differentiate into astrocytes. Therefore, astrogliogenesis is increased and affects myelination[179], since astrocytes play a stimulatory role in the survival, proliferation, maturation and function of oligodendrocytes and the migration of oligodendrocytes precursors into the lesioned areas of the CNS. Nevertheless, pharmacological inhibition of TGFβR-1 inhibits further abnormal astrogliogenesis in the post-injury recovery period, resulting in unbalanced signalling between the pro- and anti-inflammatory cytokines, following a HI insult, which influences other cellular signalling processes.

Our group recently indicated that TGFβ1 also possesses a pro-inflammatory role in the neonatal HI mouse model (unpublished data Hristova Lab). Microglia-targeted gene deletion or global pharmacological inhibition of TGFβR-1 resulted in significant decrease in microglial activation after HI. Specifically, deletion of microglia specific TGFβR-1 using a Cre-Lox-mediated knock-out (KO) in a model of severe HI brain damage, decreases microglial and astroglial activation, and tissue loss, suggesting that microglial TGFβ1 adapts a pro-inflammatory fate during and in the first 48h post-HI. In this current study, we attributed the neuroprotective mechanism of TGFβR-1 deletion to the shift of pro- to anti- inflammatory and therefore we hypothesised that

there is a shift in the ratio between the pro- and anti- inflammatory microglia in the most vulnerable brain regions after the HI insult, with more activation of the anti-inflammatory microglia to induce repair.

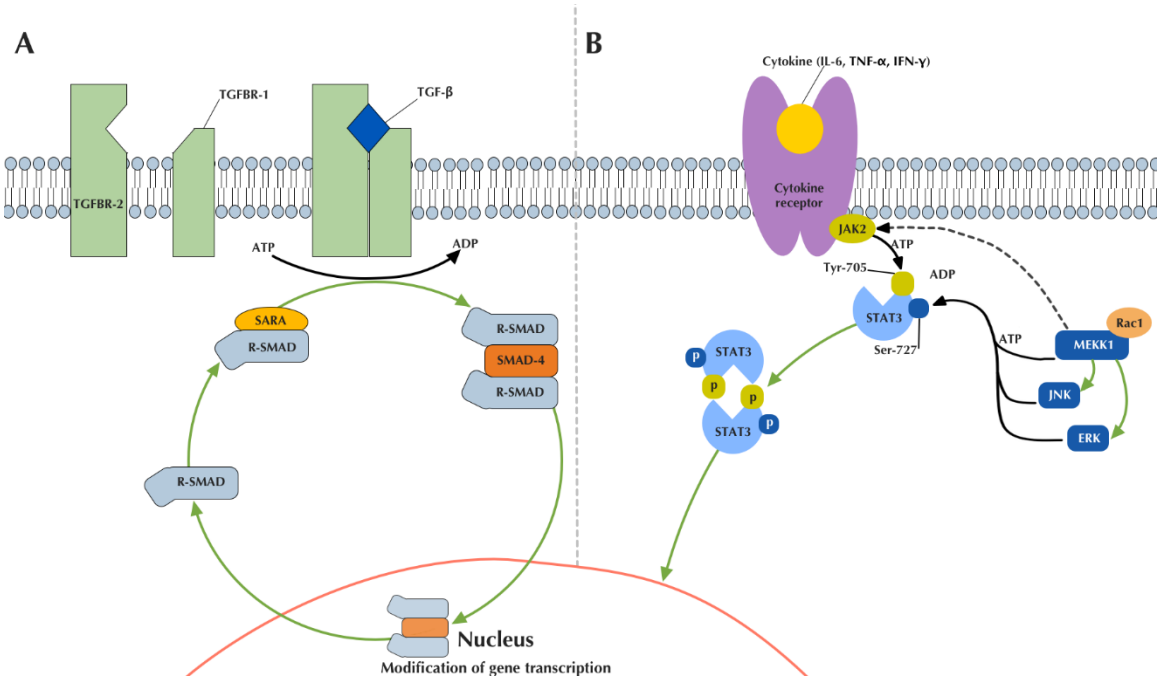

Figure 6. **TGFβ and STAT3 pathways.** (A) The receptor-regulated SMAD (R-SMAD) require TGFβ induced phosphorylation. Both receptors have a serine/threonine protein kinase in the cytoplasm. GS region of TGFβR-1 is phosphorylated by TGFβ, which then catalyses the phosphorylation of R-SMAD. R-SMADs are tethered in the cytoplasm to a SARA scaffolding (SMAD anchor for receptor activation) making them accessible to the membrane receptors. Once activated, two R-SMAD and a partner SMAD (SMAD-4) form a trimeric complex that translocate to the nucleus, where they can associate with transcription coactivators or corepressors. Although R-SMAD can return to the cytoplasm, in the nucleus they can also be subject to ubiquitylation and proteasome-dependent degradation. Modified from Massague (2000), updated from Xu and colleagues (2012) (B) STAT3 is a transcription factor, which is encoded by STAT3 gene and resides in the cytoplasm unphosporylated[194,195]. STAT3 is activated in response to numerous cytokines like IL-6, TNF-α, IFN-γ. Ligand's binding to the

receptor leads to the creation of docking sites that allow the recruitment of STAT3 through its SH2 domain. Subsequently, STAT3 is activated by the phosphorylation at Tyr-705 in the c-terminal domain by JAK2 and then undergoes dimerization via the interaction between the phospho-Tyr-705 in one monomer with the SH2 domain of the other. Growth factor receptors, such as TGFβ can activate STAT3 as well, by activating Rac1 and then MEKK1. The later can influence the phosphorylation of both sites. It acts directly over Ser-727 and also activates JNK and ERK to act on MEKK1. Additionally, MEEK1 can influence the phosphorylation of Tyr-705 by its interaction with JAK2. Ser-727 phosphorylation is not necessary to form the dimer, as the phosphorylation by JAK2 is enough to allow it, but its presence significantly enhances the process. The dimer then translocates to the nucleus and modifies the transcription of genes involved in cell proliferation, differentiation and apoptosis[196–198].

1.12 Current Treatments and Complications

Therapeutic hypothermia (TH) is the current standard treatment for neonatal HI brain damage and is recommended by the National Institute for Health and Care Excellence (NICE) guidelines. TH is a clinical procedure where the affected infants' body temperature is lowered from 36ºC to 33-35ºC for 72h[199], induced by whole-body or selective head cooling through circulation of cold fluid or air[200]. TH displayed satisfactory results in 11 clinical trials, with 40-50% effectiveness, reducing the possibility to develop cognitive impairments and disabilities[201–203].

Despite the promising results, TH also has limitations. TH has been found to only reduce the risk of infant disability and mortality by 11% and 40% of treated infants still

develop disabilities[204–206]. TH is often unavailable or ineffective in developing countries due to the use of low-technology cooling devices[207]. TH is effective if induced within a 6h time window following the HI insult, which is a problem especially in low-income locations. In these countries, the optimum therapeutic time may be missed due to delayed hospital admissions or birth complications including higher occurrence of intrauterine growth restriction and sepsis[207]. Additional limitations of TH are associated with slow drug metabolism and clearance, immunosuppression, and the increase of energy expenditure through the physiological activation of thermoregulatory mechanisms[208].

The mechanism of TH entails decrease of cerebral metabolism following brain injury, which preserves glucose levels and inhibits lactate generation. Thus, normal pH and ATP levels are preserved in the brain[209]. TH significantly inhibits superoxides and lipid peroxidation thereby decreasing the generation of ROS and correlated neuronal damage and tissue loss. Further, TH modulates and reduces pro-inflammatory cytokine production, including TNF-α, IL-1 and IL-6, which are all usually increased during HI and exacerbate neuronal injury, and increases anti-inflammatory cytokine levels, such as IL-10[210]. Neuronal cell apoptosis is also inhibited by TH, through interfering with the caspase family of proteins which play an essential role in programmed cell death. Finally, TH also increases the regulatory protein Bcl-2 reducing cytochrome c release from the mitochondria, inhibiting the expression of Bax and BAK1 affected by HI insult. Hence, TH decreases levels of caspase 3, 8 and 9[211].

In LPS-sensitised HI rat and piglet models mortality rate and brain tissue damage is upregulated even if the neonates underwent treatment with TH[212,213]. The same results have been demonstrated in clinical studies in neonates exposed to intrauterine infection, as TH does not provide neuroprotection[214]. These findings indicate that, TH

is not protective in LPS-sensitised HI cases although it is the standard current treatment for neonatal HI. Preclinical animal models of LPS-sensitisation even suggest that TH might be more damaging to the injured neonatal brain. Specifically, in a neonatal piglet model TH increased the mortality rate in LPS-sensitised HI animals compared to HI controls[215].

The mechanism by which LPS-sensitisation overcomes the neuroprotective effects of TH is still unknown. An *in vivo* murine study suggested inter-individual variability, at the damage caused by LPS-sensitised HI or HI alone in different mouse strains[5]. The results showed furthermore that genetic background might play a critical role in the individual response to both LPS-sensitised and HI injury alone[5]. Moreover, clinical results from neonates who underwent TH after HI alone in clinical studies indicated TH to be immunosuppressive[216,217], through detection of decreased numbers of leukocytes and chemokines[218]. Thus, TH might be reducing the physiological attempt of the immune system in fighting the bacterial infection, which may be detrimental for the treatment of infants affected by HI.

As gram-positive bacterial infections are shown to exacerbate HI induced damage[110,111] and to activate a different inflammatory mechanism[219], the efficacy of TH on gram-positive-sensitised HI might be different from what is described for gram-negative. Falck and colleagues showed that TH induced recovery in 80% of the P7 Wistar rats with gram-positive sensitisation[111], suggesting that the neuroprotective effects of TH might be pathogen dependent. Similarly, a retrospective clinical study demonstrated positive outcomes with TH in neonates with gram-positive sensitised HI[220]. However, TH is only partially effective in HI, but unsuccessful in gram-negative sensitised HI cases, and hence there is a need for alternative therapeutic approaches for neonatal HI. Therefore, there is a clear demand and need to develop alternative

therapies for normal and infection-sensitised HI brain damage. A variety of potential treatments have been tested in animal models and in clinical trials.

1.13 Other currently available treatments for neonatal HI

HI insult triggers an inflammatory response, oxidative stress, and cell death. An alternative approach in treating neonatal HI could be to target cell death pathways, thus modulating their downstream effectors. Several compounds have been proposed as potential neuroprotective agents in neonatal HI injury, both alone and as adjuvant therapies to TH. Combined erythropoietin, a glycoprotein hormone which increases the systemic oxygen-carrying capacity in the brain, and TH treatment was proposed to reduce brain damage and to improve motor function one year later after application in clinical trials[221]. However, in severe normal HI cases erythropoietin is not neuroprotective but actually exacerbates brain damage as shown in preclinical studies[222]. Postnatal allopurinol administration, a xanthine oxidase inhibitor which reduces the production of oxygen radicals, may provide neuroprotection to neonates with moderate HI brain damage[223,224] and antenatal administration of allopurinol to pregnant women may also attenuate HI brain damage in female neonates with therapeutic levels detected in arterial cord blood, indicating successful placental crossing whereas in males neonates no significant difference was observed[224]. In preclinical studies, allopurinol combined with TH improves neuropathological brain score, decreases levels of cleaved caspase-3, and improves functional outcome after HI[225].

Additionally, xenon, a noble, colourless, and odourless gas, causes a general reduction in excitotoxic neurotransmitter release, mainly as a potent partial NMDA

receptor antagonist, and xenon-augmented TH reduced apoptosis, and cerebral abnormalities in clinical trials[226]. Nevertheless, follow up studies suggest that xenon has no additional effects to TH in cases of moderate and severe HI[226,227]. The combination of TH and topiramate or memantine, a safe non-competitive low affinity NMDA receptor antagonist used in moderate to severe Alzheimer's disease, significantly reduced the extent of brain infarct volume in rodent and piglet models after HI insult[228–230]. Melatonin, (N-acetyl-5-methoxytryptamine), an indolamine hormone, administration combined with TH also showed neuroprotective effect in both a mouse and piglet models of neonatal HI[231–233]. Combination of deferoxamine and erythropoietin, revealed reduced neuronal damage and apoptotic markers in a rat model of neonatal HI[234]. However, further investigation of these alternative treatments and larger clinical trials for the most effective compounds tested to date are needed. There are other proposed treatments, such as curcumin, in the preclinical and clinical pipeline for neonatal HI, with many contradicting results. A common similarity between all these treatments is the targeting of similar cellular pathways involved in neonatal HI. Despite their potential, further research is required to bring the majority of these compounds into the clinic.

1.14 Curcumin

Curcumin, a natural compound also known as diferuloymethane ($C_{21}H_{20}O_6$), is the major active compound of the turmeric spice, and is isolated from the powdered dry rhizome of *Curcuma longa*. It is most frequently consumed in South Asian diets[235,236]. Except for turmeric usage as dietary pigment and its known anti-inflammatory properties from traditional medicine, modern pharmacological studies show that

curcumin provides therapeutic effects in several pathological conditions, such as cancer[237,238], inflammation[239,240], infection cardiovascular diseases[241,242], fibrosis, and neurological disorders[243]. This is partly attributed to its anti-inflammatory, anti-oxidant, anti-apoptotic, anti-microbial and ROS scavenging properties[244,245]. Curcumin is lipophilic and has the ability to cross the BBB[246] as a result of its small molecular weight (368.385 g/mol) and size, and therefore was proposed as a possible treatment in different neurodegenerative disorders, such as Alzheimer's[247] disease, Parkinson's disease and multiple sclerosis[248]. In this current study, we aimed to investigate the effects of curcumin on HI.

Curcumin acts on many important pathways involved in the pathogenesis of HI injury, making it a potential therapeutic candidate in neonatal HI brain damage[249]. Specifically, curcumin is able to increase the levels of antioxidants such as SOD, glutathione and catalases, which are all enzymes linked to neutralisation of free radicals[250]. Also, curcumin inhibits the expression of pro-inflammatory cytokines (IL-1, IL-6, TNF-α), thus mediating inflammatory pathways and was also shown to inhibit STAT3 phosphorylation[251,252].

The mechanisms of curcumin's action rely on its chemical structural properties. The o-methoxy phenolic groups[246] (Figure 6), are central for chemical reactions, allowing the transfer of electrons or donation of protons providing curcumin with ROS scavenging properties[253]. Moreover, curcumin lipophilic properties render it a particularly efficient scavenger of peroxyl radicals produced through lipid peroxidation during HI brain injury[249]. However, a limitation to the therapeutic use of curcumin is its poor bioavailability due to its low absorption, and high enzymatic degradation rate[254].

Our group recently used curcumin dissolved in DMSO as a potential treatment for hypoxic-ischaemic encephalopathy (HIE) in a P7 Rice-Vannucci murine model, and the results from that study support a dose-dependent neuroprotective effect provided by immediate and delayed intraperitoneal application following neonatal HI injury[255]. Additionally, curcumin treatment resulted in decreased pSTAT3 levels, possibly through interaction with its upstream activator IL-6[255]. The levels of mitochondrial protein prohibitin (PHB) were also increased after curcumin's treatment, a significant result as neuronal expression of PHB confers profound neuroprotection in a mouse model of focal cerebral ischemia[255,256].

Curcumin's future use and clinical application is limited as a result of its poor bioavailability and its unknown specific molecular targets. Therefore, by comparing the neuroprotective effect of WP1066 and curcumin treatment we could confirm whether STAT3 is a significant target molecule for curcumin in HI neuroprotection.

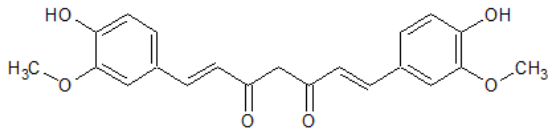

Curcumin

Figure 7. **Curcumin chemical structure**. Seven carbon structure consisting of an α, β-unsaturated β-diketone moiety, which links two aromatic rings with o-methoxy phenolic groups. Hydrophobic nature of the phenyl rings of curcumin along with hydrogen bond formation ability of the side groups are proposed to be the reasons for the aggregation in water therefore curcumin's lipophilic nature[257].

1.15 Hypothesis and Aims

We hypothesised that the involvement of STAT3 in HI is critical in inflammatory and cell death pathways, and therefore inhibition of the JAK2/STAT3 pathway with WP1066 or curcumin will reduce tissue loss, cell death, glial activation, oxidative stress and will maintain myelination, thus providing neuroprotection confirmed through improved behavioural outcomes. We further hypothesised that STAT3 and TGFβ pathways are correlated and involved in HI inflammatory pathology by reducing pro-inflammatory and increasing anti-inflammatory microglia phenotype. Finally, we hypothesised that maternal intrauterine infection with *E.coli* sensitises the neonatal brain leading to inflammatory response. Therefore, we aimed to investigate whether:

- WP1066's application provides short- and long-term neuroprotective effects after HI insult in a P9 mouse model, when administered intraperitoneally.
- Curcumin's application exhibits neuroprotective role when administered intraperitoneally dissolved in DMSO and intranasally encapsulated in P(3HB) microspheres.
- Microglial-specific TGFβR-1 deletion, reduces pro- and increases anti-inflammatory microglial activation after HI insult, therefore inducing repair as TGFβ increases STAT3 phosphorylation after HI brain damage.
- Intrauterine maternal *E.coli* K12 delivery causes sensitisation in a HI mouse model, therefore leading to inflammatory response and cell death.

The involvement of STAT3 pathway on HI brain damage has not been fully explored yet, have not yet been fully explored, which is why they were investigated in the current study. The methods used in this study include behavioural tests of cognitive, motor and memory abilities, immunohistochemical staining and confocal microscopy, cell viability assay, western blot and RT-qPCR, ELISA analysis in a HI brain damage mouse model.

The findings in this thesis contribute to a better understanding of the underlying mechanisms of HI brain damage and elucidate new evidence for potential treatments. This study will impact directly the research group, which will further explore the translational potential of WP1066's and curcumin's application in HI brain damage. Additionally, the results will contribute to the knowledge bank of the wider field of HI.

Chapter 2: Materials and Methods

All animal experiments and care protocols were approved by the Home Office and carried out according to the UK Animals (Scientific procedures) Act 1986, following the ARRIVE guidelines (PIL: I20314939, PPL: PP0028535)

2.1 Neonatal HI brain damage model

A modified version of the Rice-Vannucci model was used to induce neonatal HI brain damage in C57Bl/6 mice at P9, corresponding to term human brain maturation[70]. C57Bl/6 mice were bred in house, the holding room had a 12-12 h dark/light cycle with instant switch between light and dark with ad libitum access to food.

The animals were anaesthetised with 5% isoflurane for induction and maintained at 1.5%, while a mid-neck incision was performed. The left common carotid artery was permanently occluded with 8/0 polypropylene suture. Thus, the right hemisphere is able to act as a control to the experimental left hemisphere. Then, the animals were left to recover at 36ºC and returned to their dams for 1.5h. Subsequently, the pups were placed in a 36°C humidified hypoxic chamber and exposed to a mixture of 10% oxygen and 90% nitrogen for 60 min to induce the hypoxic insult (Figure 8). The animals were randomly assigned to different groups according to each experiment. Naïve and sham animals serve as control groups and did not undergo HI insult, although sham animals underwent anaesthesia and a mid-neck incision.

2.2 Pharmacological treatment

After the induction of HI insult, the pups were immediately treated with a single intraperitoneal injection of WP1066 (Stratech, UK, A4140) dissolved in 0.5µl 100% DMSO (Sigma-Aldrich, UK, D4540) at dosages of 40µg/g, 80µg/g, or 160µg/g body weight (BW). The concentration of 100% DMSO was chosen as both WP1066 and curcumin are insoluble in water.

2.3 Brain extraction and tissue preparation

The animals were sacrificed 48h after the HI brain insult through intraperitoneal injection of pentobarbitone and perfused with 30ml of 4% paraformaldehyde (PFA) in phosphate-buffered saline (PBS). The 48h time point was chosen as at this point inflammatory markers such as alphaM microglial activation peaks and we aimed to investigate whether WP1066's and curcumin's application can reduce the inflammatory response. At 72h after HI insult, microglia response is lower and at 98h is absent. Then, the brains were with surgical forceps after exposing the skull with surgical scissors, and post-fixed in a rotating immersion of 4% PFA in PBS at 4°C for 1h. Subsequently, the brains were cryoprotected in a solution of 30% sucrose in 0.1M phosphate buffer (PB) at 4°C on a rotator for 24h. Then, the cerebellum was removed with a scalpel blade, and the forebrains were frozen on dry ice and stored in a freezer (New Brunswick model U570) at -80°C in preparation for sectioning. Using a cryostat (LEICA CM1900), the brains were cut at -20°C and after the fusion of the corpus callosum, 50 sequential coronal sections of 40µm thickness were collected on double-gelatinised (0.5% gelatine) microscope slides, while marking the control hemisphere

with a pin puncture in the striatum. The collected slides were stored at -80°C until further use for staining[258].

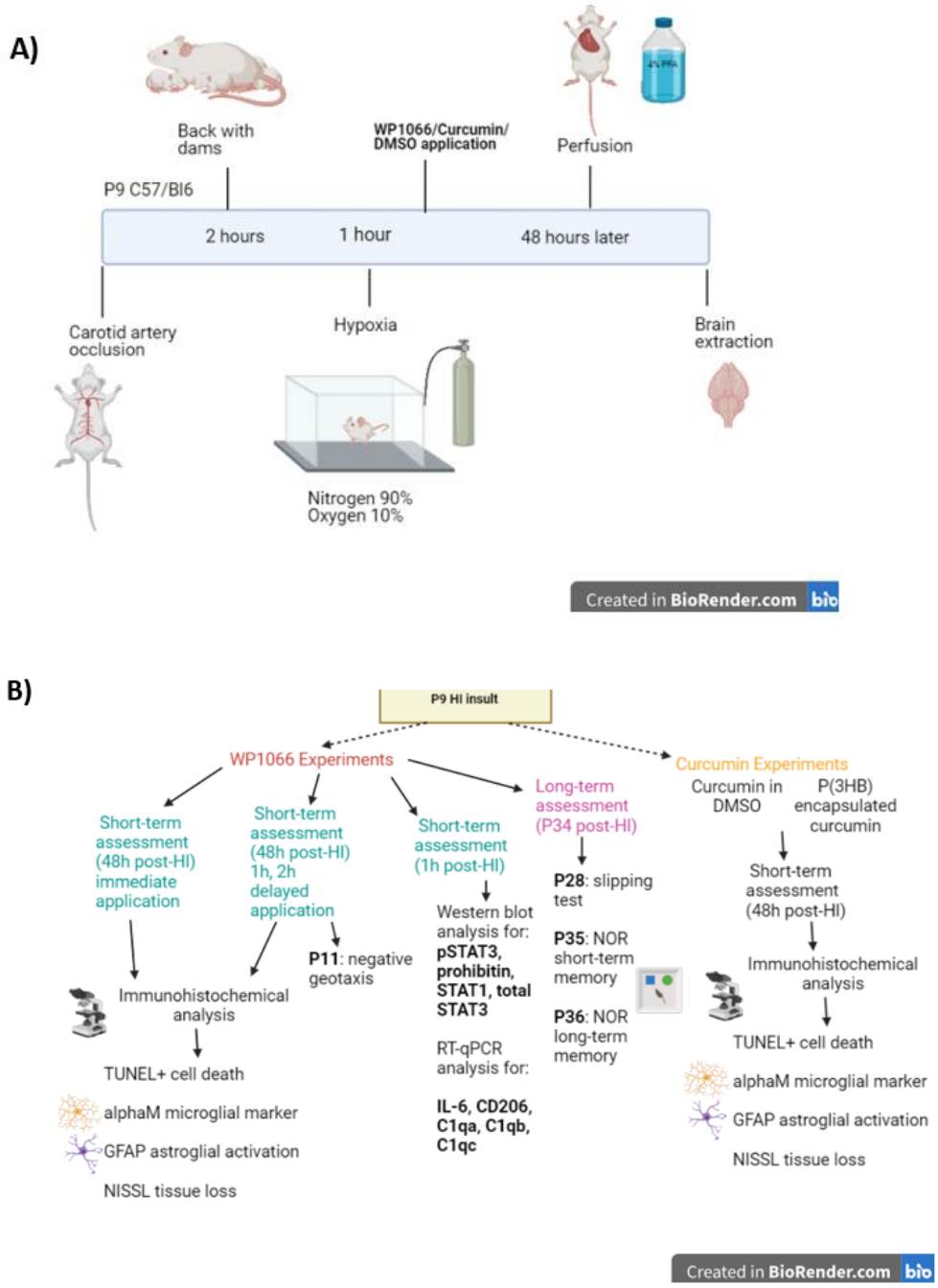

Figure 8. A) **Timeline of HI brain damage, pharmacological treatment, brain extractions. B) Experimental design for WP1066 and curcumin experiments.**

2.4 Immunohistochemistry

In preparation for each immunological staining procedure, 5 coronal sections per brain, at 400µm intervals, were retrieved from -80ºC, rehydrated with ddH_20, spread using two fine paintbrushes under a microscope and left to air dry.

2.5 Histological assessments of brain regions

The immunohistochemical and histological assessments listed below were completed in the 6 brain regions considered to be the most susceptible to the HI insult due to their high metabolic activity: cortex, pyriform cortex, external capsule, striatum, hippocampus, and thalamus (Figure 9).

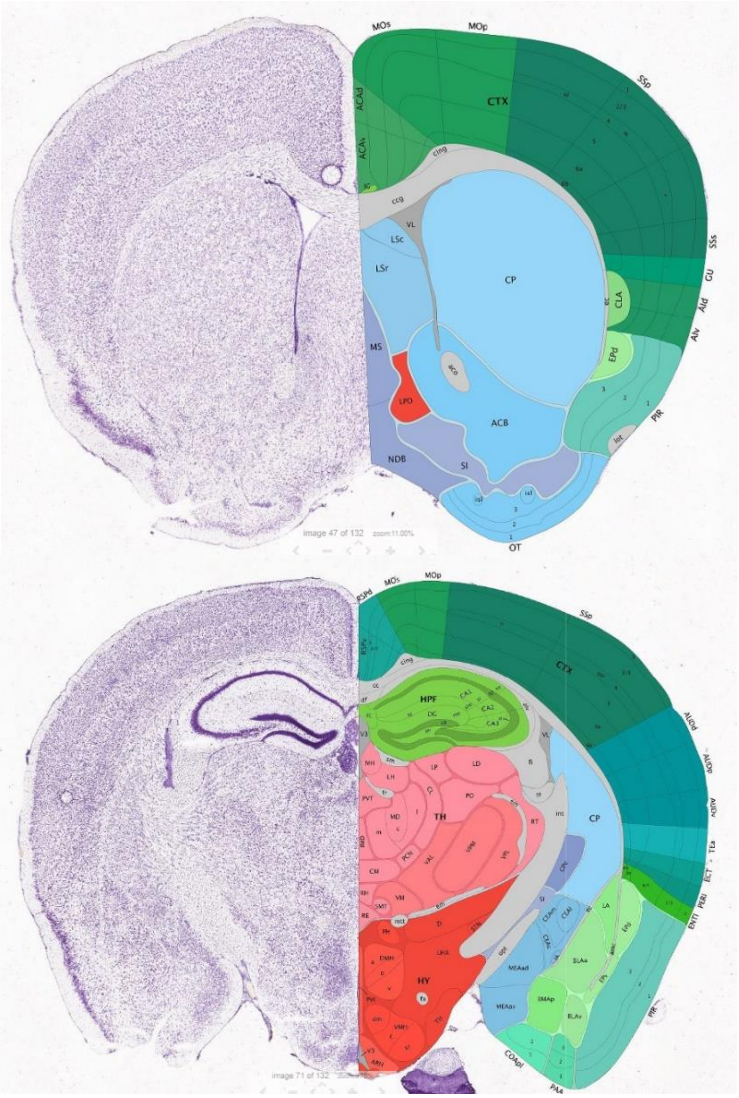

Figure 9. **Brain regions analysed, susceptible to HI damage.** Image from Interactive Atlas Viewer (P56, Coronal, Nissl Staining) (Interactive Atlas Viewer: Atlas Viewer). Panels from the Allen Reference Atlas, annotated and colour-coded using an anatomical nomenclature. CTX-cortex, PIR-pyriform cortex, CP-striatum, ec-external capsule, HIP-hippocampus, TH-thalamus.

Assessment of Microglial Activation- The selected slides for each brain were fixed in a solution of 4% formaldehyde in 0.1M PB for 5 min, followed by 2 washes in 0.1M PB. The slides were then transferred to 0.1% Bovine Serum Albumin (BSA) in 0.1M PB. Subsequently, the sections were incubated in 5% goat serum (Sigma-Aldrich, UK)

in 0.1M PB for 30 min to prevent non-specific binding of the secondary antibodies. The sections were then incubated overnight at 4^{o}C with monoclonal rat anti-alphaM (1:5000 dilution, αMβ2 integrin, Serotec, UK) primary antibody.

On the second day of staining, the slides were washed in 0.1M PB/1%BSA, 0.1MPB, and moved to 0.1M PB/1%BSA, before being incubated for 1h at room temperature (RT) with biotinylated goat anti-rat (alphaM) antibody. Exposure to the biotinylated secondary antibody was followed by washing in 2 changes of 0.1M PB/0.1%BSA, and 0.1M PB and subsequent 1h incubation with Avidin-Biotin horse radish peroxidase Complex (ABC) (1:100 dilution in 0.1M PB; Vector Laboratories, UK), according to the manufacturer's instructions for signal amplification. Following washing in 0.01M PB 3 times the slices were visualized with 3, 3' - diaminobenzidine (DAB; Fischer Scientific, UK) activated with hydrogen peroxide (H_2O_2) (Fisher Scientific, UK). The reaction mixture consisted of 0.5g/L DAB and 1:3000 dilution of H_2O_2 in 0.01M PB. The reaction was terminated through washing the sections in 0.01M PB followed by two washes in dd$H_2$0 water. The time for termination of the reaction was determined through monitoring the staining intensity under a light microscope. The slides were then left to dry, before mounting in DEPEX medium.

AlphaM score

The alphaM staining was scored semi quantitatively in each region of interest, on ipsilateral (experimental side) and contralateral hemisphere (control side), at low 10x magnification using a 0-4 scale shown in Table 1[259] and Figure 10. The score was averaged per animal then averaged per group.

*Table 1.***Scores from 0-4 given for each microglia phenotype observed.**

Score	Microglial appearance
0	No activation
1	Focal diffuse activation
2	Mild phagocytic activation affecting <50% of the region
3	Phagocytic activation affecting >50% of the region
4	Total phagocytic activation

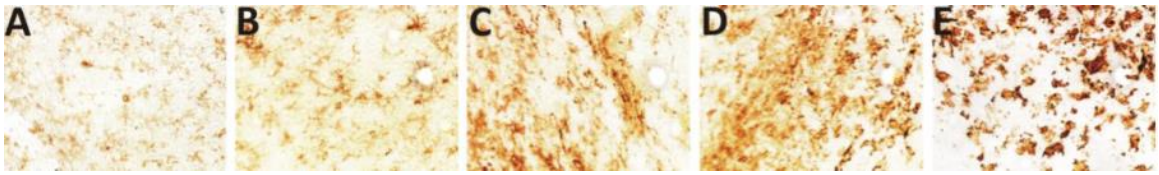

Figure 10. **alphaM immunoreactivity scores in the dorsoparietal cortex**. Brain regions were scored for alphaM immunoreactivity based on different appearance and morphology as: A. no activation (0), B. focal ramified morphology (1); C. mild diffuse predominantly ramified morphology (2); D. total widespread predominantly amoeboid, phagocytic activation (3), E. total activation, predominantly amoeboid morphology (4).

Assessment of Astroglial Activation- Activated astroglial cells were detected on brain sections using GFAP-immunoreactivity utilising the same immunohistochemical protocol described above. The primary antibody used was polyclonal rabbit anti-GFAP (1:6000 dilution, Dako, UK) and the secondary antibody was biotinylated goat anti-rabbit (1:100 dilution, Vector Laboratories, UK).

Optical Luminosity

Reactive astrogliosis was assessed through GFAP immunoreactivity measured in Optical luminosity values (OLV). Using a Sony AVT-Horn 184 3CCD (24bit RGB, 760x570 pixel resolution) colour camera, pictures of cortex, pyriform cortex, external capsule, striatum, hippocampus, and thalamus were captured, using 3 optical fields at 20x magnification for GFAP. The images of the brain sections and the surrounding glass were imported into Optimas 6.51 (Media Cybernetics), and the mean and standard deviation (SD) were obtained. The SD is subtracted from the mean for each image, and the resulting value is subtracted from the one measured from the surrounding glass to obtain the intensity of the staining[260]. Each value was averaged per region, per animal and then per experimental group.

Assessment of Myelination and Oxidative stress- Myelination and oxidative stress were detected using MBP- and iNOS- immunoreactivity on histological brain sections using the same protocol described above. The primary antibodies used were polyclonal rabbit anti-MBP (1:2000 dilution, Abcam, UK) and anti-iNOS (1:1000, Invitrogen, UK) and the secondary antibody was biotinylated goat anti-rabbit (1:100 dilution, Vector Laboratories, UK). MBP immunoreactivity was measured in external capsule, striatum with OLV as described above. iNOS+ cells were counted manually bilaterally at 20x magnification in hippocampus, on 3 optical fields and the average of the 3 counts was averaged per animal and per group. Table 2 summarises the antibodies used for immunohistochemistry.

Table 2. **List of the antibodies and their respective dilutions used to stain for activated microglial, astroglial cells, myelination and oxidative stress.**

Staining	Primary antibody	Dilution and Manufacturer	Secondary Antibody	Dilution and Manufacturer
Activated Microglia	Monoclonal Rat Anti-CD11b	1:5000 Serotec, UK	Biotinylated goat anti-rat	1:100 Vector Laboratories Inc., UK
Activated Astroglia	Polyclonal Rabbit anti-GFAP	1:6000 Dako, UK	Biotinylated goat anti-rabbit	1:100 Vector Laboratories Inc., UK
Myelination	Polyclonal Rabbit anti-MBP	1:6000, Abcam, UK	Biotinylated goat anti-rabbit	1:100 Vector Laboratories Inc., UK
Oxidative Stress	Polyclonal Rabbit anti-iNOS	1:1600, Invitrogen, UK	Biotinylated goat anti-rabbit	1:100 Vector Laboratories Inc., UK

Assessment of Cell Death- To assess the levels of cell death the Terminal transferase-mediated biotinylated d-UTP Nick-End Labelling (TUNEL) stain kit was used (Roche, West Sussex, UK). Five sections per brain were selected as before and spread as explained above. The staining was carried out according to the manufacturer's protocol, targeting fragmented DNA. DAB stage was used for visualisation and was enhanced with Cobalt/Nickel[181].

The number of TUNEL + cells, indicating cell death, was counted bilaterally at 20x magnification in all 6 regions of interest. In each brain region, 3 optical fields were assessed and the average of the 3 counts was averaged per animal and per group.

2.6 Cover Slipping

All the stained sections were air dried and then immersed 3 times for 1 min each in Xylene before being embedded in DEPEX mounting medium (Thermo Fisher, UK) and cover slipped.

2.7 NISSL staining

Tissue loss was assessed through cresyl violet staining (NISSL) on 5 sections per brain (400um apart), as described before. For the staining, the slides were fixed overnight in 4% formaldehyde in 0.1 M PB, then moved to 70% ethanol overnight. On day two the NISSL solution is made (1% cresyl violet) by mixing 2g cresyl violet powder (Acros Organics, USA) in 40 mL of 100% ethanol in a closed 50ml falcon tube, shaking and inverting for 15 minutes, adding this solution to 360mL of warm distilled water on a warming stirring plate for 20 minutes and filtering with filter paper grade 4 (GE Healthcare Life sciences Whatman, UK). On day 3 the sections were incubated stepwise as illustrated in the Table 3. Right after step 12 the slides were cover slipped as described above.

Table 3. **Reagents and time required for cresyl violet (Nissl) staining steps.**

Step	Reagents	Duration
1	Cresyl Violet	10 minutes
2	Fresh distilled water	2 minutes
3	Fresh distilled water	2 minutes
4	70%	2 minutes
5	90%	2 minutes
6	96%	2 minutes
7	96% (+ 5-7 drops of glacial acetic acid)	3-10 minutes
8	100%	2 minutes
9	Isopropanol	2 minutes
10	Xylene	2 minutes
11	Xylene	2 minutes
12	Xylene	2 minutes

Assessment of Tissue Loss

Nissl bodies located in the cytoplasm of neurons are stained with cresyl violet dye. Tissue loss was measured in cortex, pyriform cortex, hippocampus, striatum, and thalamus. Nissl-stained brain sections were scanned with Sony AVT-Horn 184 3CCD colour camera, imaged into Optimas 6.5 software and then imported in ImageJ 1.51 software for further analysis.

Intact staining of the brain regions of interest was outlined and measured bilaterally with a freehand tool. The measured value was converted into mm2 and

multiplied by 400µm to obtain the corresponding volume. The percentage of tissue loss was then calculated by comparing the ratio between injured and uninjured sides multiplied by 100 (Revised from Kendall et al, 2006)[261].

2.8 Double immunofluorescence/Assessment of pro- / anti- inflammatory microglia

Activated pro- and anti-inflammatory microglial cells were stained for CD86 and CD206 following the same immunohistochemical protocol as described above, using a polyclonal rat anti-CD86 (1:1600 dilution, Dako, UK) and goat anti-CD206 (1:400 dilution, Dako, UK) primary antibodies, and a biotinylated donkey anti-rat (1:200 dilution, Vector Laboratories, UK) and donkey anti-goat-488 (1:200 dilution, Vector Laboratories, UK) secondary antibodies, respectively. After 3 washes in 0.01MPB the slides were incubated with tertiary antibodies: AvidinTexas Red (1:1000, Vector Laboratories, UK) and Alexa-Fluor488 conjugated rabbit anti-donkey (1:200, Vector Laboratories, UK), respectively. Finally, the sections were coverslipped with Vectashield mounting medium with DAPI (Vector Labs, UK) and the edges were sealed with nail polish. Table 4 summarised the antibodies used for double immunofluorescence.

5 slides per brain were assessed blindly. Pro-inflammatory, anti-inflammatory and pro- & anti-inflammatory microglial activation profiles (CD86 and CD2O6 immunoreactivity) were quantified in three different fields of the regions of interest. A Leica DM5500 B microscope with LASX Software was used to visualise the sections at 40x magnification. For each field of every region, four images were captured illustrating pro-inflammatory activation, anti-inflammatory activation, nuclear DAPI and the co-

localization of active pro- and anti-inflammatory microglia on nuclear DAPI and then were processed with ImageJ.

Table 4. **List of the antibodies and their respective dilutions used to stain for pro- / anti-inflammatory microglia.**

Staining	Primary antibody	Dilution and Manufacturer	Secondary antibody	Dilution and Manufacturer	Tertiary antibody	Dilution and Manufacturer
Pro-inflammatory microglia	Polyclonal Rat Anti-CD86	1:1600 Dako, UK	Biotinylated donkey anti-rat	1:200, Vector Laboratories Inc., UK	Avidin Texas Red	1:1000, Vector Laboratories Inc., UK
Anti-inflammatory microglia	Polyclonal goat anti-CD206	1:400 Dako, UK	Biotinylated donkey anti-got	1:200, Vector Laboratories Inc., UK	Rabbit anti-donkey-488	1:200, Vector Laboratories Inc., UK

2.9 Quantitative analysis of pro-, anti- inflammatory microglia activation

To quantitatively measure the activated phenotypes, CellProfiler 4, BMC Bioinformatics, was used with a MATLAB designated code for counting the activated pro-, anti- inflammatory microglia and the co-localising activated cells. The results obtained from CellProfiler were double checked using the ImageJ multi-point tool which enables manual counts of the activated cells.

Z-stacks spanning the whole thickness of the slice were taken within 3 fields of each brain region of interest. After imaging, the Z-stacks were compressed into one image using the LASX software. Cell number of CD86+ and CD206+ was manually counted using a clicker after importing the images to ImageJ. When co-localisation between different structures was investigated the resulting images from the z-stacks taken were

analysed using CellProfiler 4 software. A pipeline was used to automate the analysis by applying the same processing steps to all analysed images and finally obtain two numerical values associated with the amount of colocalisation between the antibodies and DAPI. The obtained values correspond to the Mander's coefficients indicating the degree of overlap between two channels.

2.10 Western blot analysis

For extraction of protein from brain tissue, the animals were sacrificed at 1h post-HI by intraperitoneal (i.p.) injection of pentobarbitone at a dose of 5ml/kg. The cortex and hippocampus were excised from extracted treated and control brains and snap frozen. The brain regions were homogenised in radio-immunoprecipitation assay (RIPA)+ cell lysis buffer (Sigma, UK) containing 10% protease inhibitor complex (Sigma, UK) using a handheld tissue homogeniser. The time point of 1h post-treatment was chosen as this coincides with the time of maximum expression of phosphorylated STAT3 Y705[181]. Total protein was extracted from the homogenised hippocampal tissue as follows: the homogenised tissue was incubated with the RIPA+ buffer on a rotating platform at 4°C for 2h, pipetting gently with regular intervals. Thereafter, the tissue homogenates were centrifuged at 16,000 g at 4°C for 20 min and the supernatant containing the extracted protein was collected. The protein extracts were measured by Bradfor protein assay, and then re-constituted in 2 × Laemmli sample buffer (BioRad, UK) containing 5% β-mercaptoethanol (Sigma, UK) and boiled for 5 min at 100°C. Proteins were separated by SDS-PAGE (approximately 10 µg of protein was loaded per lane), using 4–20% Mini-Protean TGX protein gels (BioRad, UK). Western blotting transfer was performed for 1h at 15V using the Trans-Blot Semi-Dry cell (BioRad, UK). Even transfer of

proteins to the nitrocellulose membranes (0.45 μm, BioRad, UK) was assessed using Ponceau S staining (Sigma, UK). The membranes were blocked for 1h at room temperature (RT) in 5% BSA (Sigma, UK) in Tris-buffered saline (TBS) with 0.01% Tween20 (TBS-T), followed by overnight incubation at 4°C with the following primary antibodies: anti-prohibitin (Abcam, UK; 1:1000 in TBS-T) for the assessment of changes in this mitochondrial house-keeping protein, Phospho-Stat3 (Ser727) (Cell Signaling, UK, 1:1000 in TBS-T), or Phospho-Stat3 (Tyr705) (Abcam, UK; 1:5000 in TBS-T). Thereafter, membranes were washed three times for 10 min in TBS-T, incubated for 1h at RT with an horseradish peroxidase (HRP)-labeled anti-rabbit IgG secondary antibody (BioRad, UK), followed by five TBS-T washes and one final TBS wash, and thereafter they were visualised using ECL (Amersham, UK) and the UVP BioDoc-ITTM System. HRP-conjugated anti-β-actin antibody (Abcam, UK; 1:5000 in TBS-T) was used for internal loading control and densitometry analysis was carried out using ImageJ.

2.11 Primary neuronal and N2A cell culture

Toxicity assay of WP1066 was performed on primary neuronal and N2A cells. For primary neurons cervical dislocation was performed on P0 C57Bl/6 mice and then head was transferred in clean 60 petri dish with PBS sitting on ice (1 petri dish /litter). The cortices were then placed in new clean petri dish with PBS sitting on ice. On the plate excess PBS was removed, the cortices were then cut in small pieces using scalpel and with plastic pipette 15ml tube with PBS + 25% Trypsin were transferred on the plate, for 20 min incubation in water bath. Excess PBS/trypsin was removed followed by neutralisation of trypsin with 2ml of DMEM (Thermo Fisher, UK) with 10%

FBS (Thermo Fisher, UK). DMEM/FBS was then added up to 10ml and the brain samples were centrifuged at 1000rpm for 3 min and finally 100ul added on a 96-well plate.

The number of cells per plate was 800,000 cells/well. For maintenance of the culture fresh neurobasal medium was added (1/2 original volume on cells), and then 2-3 times a week, the half of the medium was replaced by fresh neurobasal medium (Thermo Fisher, UK). Due to the sensitivity of primary neuron cultures, the cells died and therefore toxicity assay was performed on to neuro 2A (N2A) cells, a mouse neural crest-derived cell line, as they are more robust.

A total of 30,000 N2A cells (ATCC, UK) were seeded in 96-well plates using growth media, made in DMEM+GlutaMAX medium (Thermo Fisher, UK), 10% fetal calf serum (FCS, Thermo Fisher, UK), 1% penicillin-streptomycin (P/S, Merck,UK), 0.5mM Cyclic AMP (Cell Signalling, UK), 20μM Retinoic acid (Merck, UK). The next day the media was changed for differentiation media, made in DMEM+GlutaMAX, 2% FCS, 1% P/S, 1X NEAA, 0.5mM Cyclic AMP, 20μM retinoic acid and them the cells were maintained in this media for 5 days cultured in a humidified incubator at 37^{o}C, 5% CO_2, until further used for toxicity assay.

2.12 Cell viability assay

96-wells plates were used containing 100μl/well of cell culture medium. On the day of the assay, the medium was replaced with decreasing concentrations of WP1066 into the cell culture medium. In the starting solution, WP1066 was dissolved in 100% DMSO at a concentration of 320mg/ml. Considering the highest dose used in the *in*

vivo studies of 160µg/g BW, the maximum concentration present in the blood of a neonatal mouse (considering for a 4g mouse and a blood volume of 342µl) of 1.87 mg/ml was used as the highest concentration for the cell viability assay, and 10 consequent serial 1:2 dilutions were applied on the cells (100µl) in triplicates. Three wells per plate were left for living cells (positive control), while other 3 wells per plate were left without medium (dead cells) as the negative control and 3 wells were treated with 100% DMSO as control. Figure 11 illustrates the design of the cell viability plate.

N2A cells with WP1066 doses and cells with or without medium were incubated at 37ºC for 4.5h in a humidified incubator. Then, MTT assay was performed, where 10µl of 3-(4,5-dimethylthiazol-2-yl)-2,5-diphenyltetrazolium bromide (MTT, Sigma-Aldrich, UK) were added to each well. The plate was covered with aluminium foil and incubated for 3h at 37ºC, 5% CO_2. When ready, the media was removed and 100µl of DMSO (Sigma Aldrich, UK) were added to each well. The plate was then placed at room temperature on an orbital shaker for 15 min, still covered. The absorbance of each well was measured using a FluoStar Omega LVIS plate reader (BMG Labtech, Buckinghamshire, UK) spectrophotometer at a wavelength of 590µm. The triplicates were averaged and the background from the media was subtracted. The cell viability was calculated using the following formula:

%cell viability= (mean of absorbance for cells treated with WP1066/ mean of absorbance for cells not treated)*100

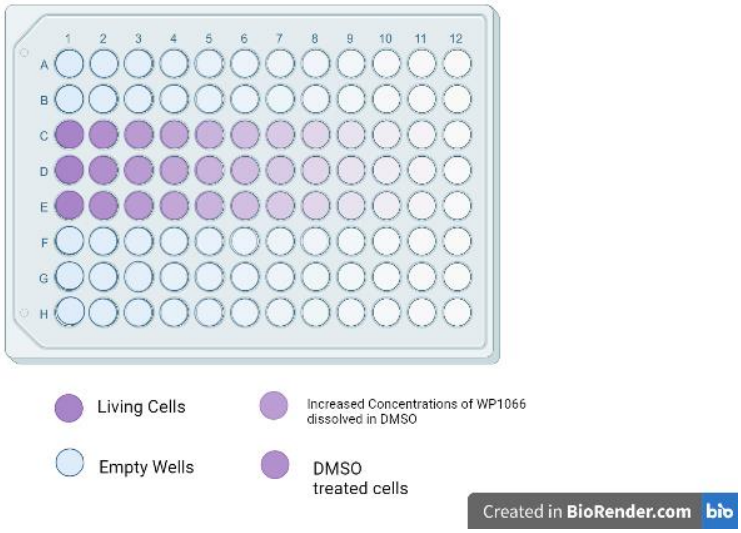

Figure 11. **Graphical representation of the plate design for the cell viability assay.**

2.13 Reverse Transcription and qRT-PCR

The brain samples were extracted as described above and hippocampus, cortex were used for qRT-PCR. Total RNA was isolated using an RNeasy Lipid Tissue Mini Kit (Qiagen, UK) in accordance with the manufacturer's instructions. RNA concentration was measured using a NanoDrop 1000 spectrophotometer (NanoDrop, Wilmington, USA). Reverse transcription was performed in duplicate using a QuantiTect Reverse Transcription Kit (Qiagen). qRT-PCR was performed on a QuantoStudio Real-time PCR system (Thermo Fisher, UK), using a QuantiFast SYBR Green PCR kit (Qiagen, UK) with the following cycling protocol: 10 s denaturation at 95◦C followed by 30s annealing/extension at 60◦C for 40 cycles. IL-6 and CD206 primers were purchased from Qiagen Table 5, while complement primers were purchased from Integrated DNA Technologies, UK (Table 6) and amplification specificity was confirmed by melting curve analysis, the assessment of the dissociation characteristics of double-stranded

DNA during heating. Relative quantitation was performed in accordance with the standard curve method and expression values were normalised to the reference gene glyceraldehyde 3-phosphate dehydrogenase (GAPDH).

Table 5. **Primers used for qRT-PCR**

Gene	Official Symbol	Entrez gene ID	Primer	Product number
Gapdh	Gapdh	14,433	Mm_Gapdh_3_SG	QT01658692
CD206	Mrc1 17	17,533	Mm_Mrc1_1_SG	QT00103012
IL-6	Il-6	16,193	Mm_Il6_1_SG	QT00098875

Table 6. **Primers used for qRT-PCR**

Gene	5′ Forward	3′ Reverse
C1QA	CCATCAGCAAAGGGCTGGAG	TACTAGGGTCATGGTCAGCA
C1QB	GACTTCCGCTTTCTGAGGAC	TGTGTCTTCATCAGCTCAGC
C1QC	GACGTCTCTGTGATTAGGCC	AGGGCCAGAAGAAACAGCAG
C1R	GAGGAGAATGGGACATCAT	GACACAGATGTTGGCATCGG
C1S	GTTTGGTCCTTACTGTGGTA	CCAAGGGTTCTTTTGCCCC

2.14 Enzyme-linked immunoassay (ELISA)

The animals were sacrificed at 1h post-HI by i.p. injection of pentobarbitone and the cortex was extracted from treated and untreated control brains and snap frozen before homogenization in RIPA+ buffer (Sigma, UK) containing 10% protease inhibitor complex (Sigma, UK). Total protein was extracted from the homogenised hippocampal tissue as follows: the homogenised tissue was incubated with the RIPA+ buffer on a rotating platform at 4°C for 2h, pipetting gently with regular intervals. Thereafter, the

tissue homogenates were centrifuged at 16,000 g at 4°C for 20 min and the supernatant containing the extracted protein was collected. The levels of IL-1β, IL-6, IL-12/IL-23 p40 were detected using ELISA kits (IL-6: KE10007, IL-1β KE10003, IL-12/IL-23 p40: KE10068 Proteintech Group, Inc., Europe). In brief, 100 mg tissue homogenate was mixed with 1 mL lysis solution containing 40 μL RIPA buffer+5 μL protease inhibitor+5 μL phosphatase inhibitor+5 μL phenylmethylsulfonyl fluoride (Thermo Fisher, UK). The mixture was then centrifuged at 15 000 rpm at 4°C for 10 min. Then, 800 μL supernatant was collected, and the protein concentration was determined using a bicinchoninic acid (BCA) method kit (Thermo Fisher, UK). A total of 20 μg protein was used for ELISA. Each blank well was loaded with 100 μL sample diluent, while the residual wells were loaded with either 100 μL standard or sample for test. The ELISA plate was covered with tectorial membrane for 120 min of warm incubation at 37°C. Then, each well was loaded with 100 μL working solution of primary antibodies, prepared 15 min prior to use. The plate was then sealed with membrane again for 1h of incubation at 37°C. Then, the liquid in wells was discarded, and each well was filled with 100 μL HRP-conjugated working solution, prepared 15 min prior to use for 40 min of warm incubation. Following colour development by addition of 2,4-diaminobutyric acid, the optical density (OD) value of each well at 450 nm was determined using a microplate reader.

2.15 Statistics

The statistical analysis was performed using GraphPad Prism v6.0. Each data set was checked for normality with D'Agostino-Pearson normality test and Shapiro-Wilk and Kolmogorov-Smirnov tests. Further, Kruskal-Wallis test with Dunn's post-hoc analysis

was carried out when data was not normally distributed to assess evidence for sub regional differences. In the case of normally distributed data, two-way ANOVA with Bonferonni's post-hoc correction was performed. The results were considered significant where a p-value <0.05 was obtained. The results are presented as mean ± standard error of mean (SEM) of each data set.

Having in mind the variability of the model and previous experiments with similar design[181] we need an average number of 16 animals/group for the histological assessment and an average of 5 animals/group for the western blot, qPCR and the ELISA assessments. The power calculations are based on αMβ2 immunoreactivity and detection of statistical difference between a group with a mean of 2.3, standard deviation 1.29, and a group with a mean of 1, power>0.8, p<0.05 (http://powerandsamplesize.com/Calculators/)[259].

The power calculations were performed based on the following equation:

nA=κnB and $nB=\left(1+\frac{1}{k}\right)\left(\sigma\frac{z1-\frac{\alpha}{2}+z1-\beta}{\mu A-\mu B}\right)^2$

$$1-\beta=\Phi\left(z-z1-\frac{\alpha}{2}\right)+\Phi\left(-z-z1-\frac{\alpha}{2}\right), z=\frac{\mu A-\mu B}{\sigma\sqrt{\frac{1}{nA}+\frac{1}{nB}}}$$

where,

κ=nA/nB is the matching ratio

σ is standard deviation

Φ is the standard Normal distribution function

Φ−1 is the standard Normal quantile function

α is Type I error

β is Type II error, meaning 1−β is power

R Code

R code to implement these functions:

```
1

2 muA=5

3 muB=10

4 kappa=1

5 sd=10

6 alpha=0.05

7 beta=0.20

8 (nB=(1+1/kappa)*(sd*(qnorm(1-alpha/2)+qnorm(1-beta))/(muA-muB))^2)

9 ceiling(nB) # 63

10 z=(muA-muB)/(sd*sqrt((1+1/kappa)/nB))

(Power=pnorm(z-qnorm(1-alpha/2))+pnorm(-z-qnorm(1-alpha/2)))
```

2.16 Behavioural Assessments

Negative geotaxis

The negative geotaxis is a motor test used to assess motor coordination and labyrinth reflex[262]. Following HI insult and WP1066 treatment at P9, P11 mice were placed facing downwards on a 45^{o} inclined platform. The time to turn face up was recorded. The test was repeated for 3 trials of 1 min intervals, and the times were averaged for the analysis. If the animals did not turn facing upwards, a maximum time of 30 seconds was allowed (Figure 12).

Slipping test

The slipping test is a motor balance and coordination test, modified from the balance beam test[263]. For this assessment, a 50cm long metal grid was placed between the housing cage and a clean new cage, elevated of about 20cm above a table surface. For assessment, the mouse (P28) was allowed to freely move on the grid from the clean to the housing cage, and a video was recorded from under the grid. The number of times each mouse slipped from the grid while walking from the new cage to the housing cage was counted by playing the videos in slow motion (Figure 12).

Novel Object Recognition test

The Novel Object Recognition (NOR) test measures cognition and preference for novelty, relying on the innate mouse nature to explore unknown objects (Figure 12). NOR test is particularly useful for detection of hippocampus-dependent tasks[264]. The housing cage containing P35 mice treated on P9 with 80µg/g BW WP1066 was moved

to the experimental room at least 30 min before the beginning of the test, to allow habituation to the new environment. The NOR test consisted of: • habituation: 5 min spent in a 40x30cm arena the day before the test; • familiarisation: the animal was allowed to explore 2 identical objects positioned at equal distance from the walls of the arena for 5 min; • 10 min rest in the housing cage; • test phase: one of the objects was replaced with another one of different shape and colour (Figure 12). At P36 the animals underwent the test phase only, to assess long-term recognition memory. The time the mouse spent exploring the 2 objects was recorded on both days. The discrimination index was calculated via the formula below:

$$(time\ with\ novel\ object - time\ with\ familiar\ object) / (time\ with\ familiar\ object + time\ with\ novel\ object)$$

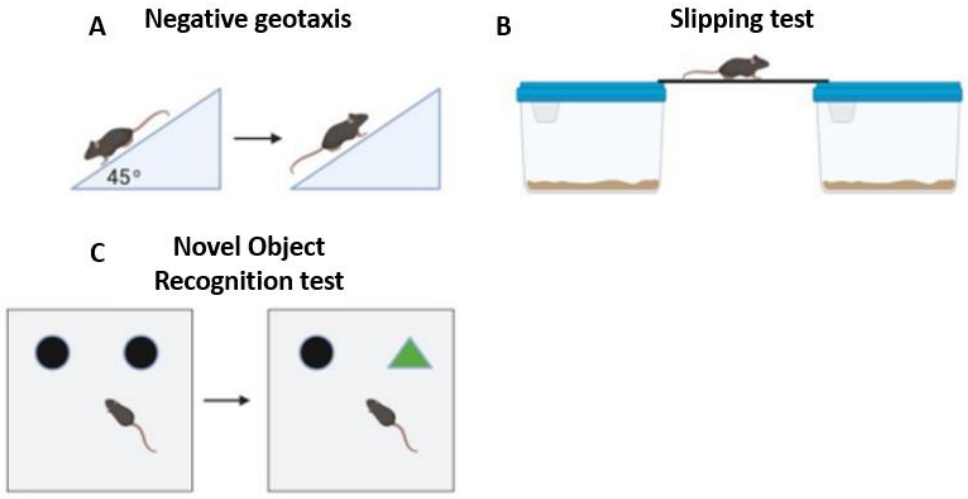

Figure 12. **Illustration of the different behavioural tests used for the long-term experiments.** A. Negative geotaxis is a motor test used to assess motor coordination and labyrinth reflex. B. The slipping test is a motor balance and coordination test, modified from the balance beam test. C. The Novel Object Recognition (NOR) test measures cognition and preference for novelty, relying on the innate mouse nature to explore unknown objects. Figure created on Biorender and based on publications[262–264].

Chapter 3: Effects of WP1066 application in a DMSO solution, in a P9 HI mouse model

3.1 AIMS

In this study, WP1066 is hypothesised to have neuroprotective effects in neonatal HI brain damage due to its ability to inhibit STAT3 phosphorylation, which is strongly upregulated after HI.

To test this hypothesis, we analysed the effects of WP1066 application on the extent of brain damage post-HI insult through assessment of glial response, tissue loss and cell death, as well as changes in levels of selected proteins and genes involved in HIE.

3.2 Methods

The ethical approvals were obtained, and neonatal HI model, brain extraction and immunohistochemical (IHC) analysis and statistics were performed as explained in Chapter 2.

3.2.1 Experimental groups

Immediately after the hypoxic insult, the animals were randomly divided into seven experimental groups as shown in Figure 13: three groups (n=16) treated with an intraperitoneal injection of WP1066 (40µg/g, 80µg/g, 160µg/g body weight (BW) in 100% DMSO, respectively), one with only an intraperitoneal injection of DMSO (n=16), one group subjected to HI without treatment (HI control) (n=16), as well as sham (n=6) and naïve control groups (n=6). HI and DMSO groups serve as control and the animals underwent HI insult, whereas naïve and sham animals did not undergo HI insult. Sham control group animals underwent anaesthesia and

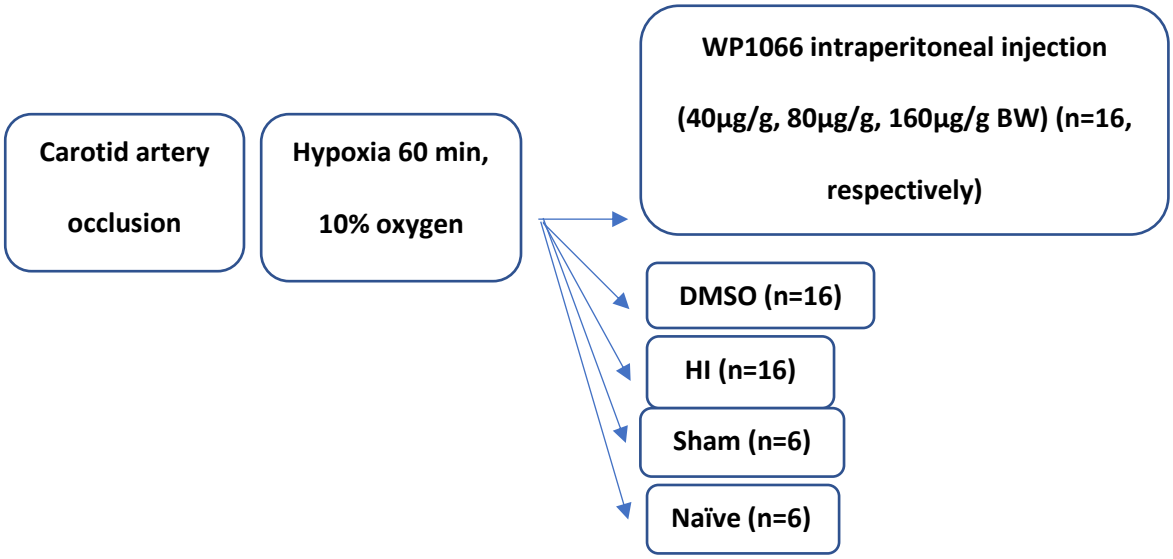

Figure 13. **Schematic representation of the experimental groups treated with WP1066/DMSO or DMSO alone after HI insult, as well as controls (untreated HI, sham and naïve littermates)**

3.3 Results

3.3.1 Cell viability assay

A cell viability assay was performed to explore WP1066 treatment toxicity. For this purpose, concentrations of WP1066 in the range between 1.89 mg/ml to 0.003mg/ml, starting from a solution of 320mg/ml WP1066 in DMSO were used. As expected, the results displayed in Figure 14 show that WP1066 at very low concentrations does not affect cell viability. Interestingly, WP1066 toxicity increases at 0.46mg/ml and then decreases again. This result may suggest that WP1066 acts as a hermetic compound, displaying toxicity at low doses rather than high doses.

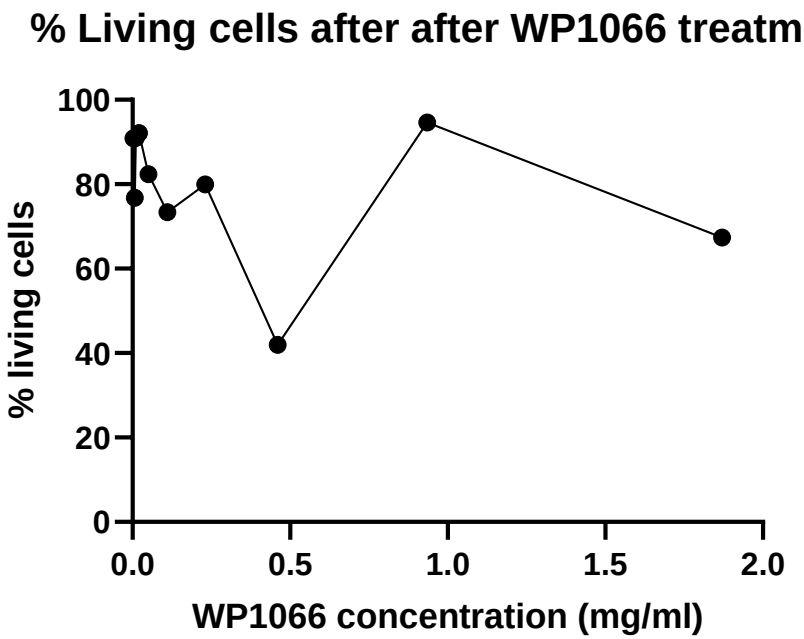

Figure 14. **Dose-response curve to different concentrations of WP1066 in N2A cells expressed as the percentage of living cells.**

3.3.2 WP1066 provides dose-dependent neuroprotection in neonatal HI

Following the previously successful neuroprotective results obtained from the split dose of 80µg/g WP1066 treatment pre- and post-HI[58], it was necessary to determine the optimal single dose required to provide a neuroprotective effect when applied post injury only. The animals were injected intraperitoneally with a dose of 40, 80 or 160µg/g of WP1066 immediately after HI insult. The damage was compared to control littermates treated with DMSO 0.5 µl/g BW after the induction of HI injury, HI, sham and naïve animals. The results are shown in Figure 15.

Assessment of TUNEL + cell death following i.p. application of 80µg/g WP1066, compared to untreated HI and DMSO treated groups, revealed an overall ipsilateral reduction in cell death (Figure 15A, Kruskal-Wallis test with Dunn's post-hoc, $p<0.05$) with sub-regional differences in cortex, striatum, external capsule, pyriform cortex, hippocampus, and thalamus ($p<0.05$ Kruskal-Wallis test with Dunn's post-hoc) (Figure 15A).

Immediate post-HI intraperitoneal application of 80µg/g WP1066 significantly reduced ipsilateral microglial activation in comparison to DMSO treated and untreated HI controls overall ($p=0.0001$, Kruskal-Wallis test with Dunn's post-hoc) and with sub-regional differences in cortex, hippocampus, striatum, pyriform cortex and thalamus ($p<0.05$ Kruskal-Wallis test with Dunn's post-hoc) (Figure 15B- inserts representing untreated HI (J), DMSO treated (K), WP1066 treated (L) groups). Immediate post-HI application of 80µg/g WP1066 also resulted in significant reduction of reactive astrogliosis compared to untreated HI and DMSO treated controls. Overall ipsilateral reduction of GFAP immunoreactivity was observed ($p=0.0001$, Kruskal-Wallis test with Dunn's post-hoc) with sub-regional differences in pyriform cortex, hippocampus, and

external capsule ($p<0.05$ Kruskal-Wallis test with Dunn's post-hoc) (Figure 15C-inserts representing untreated HI (O), DMSO treated (P), WP1066 treated (Q) groups).

Similarly, the animals treated with 80µg/g of WP1066 showed a significant reduction of ipsilateral tissue loss overall (Figure 15D-inserts representing untreated HI (T), DMSO treated (U), WP1066 treated (V), sham (W) and naïve (X) groups) (Kruskal-Wallis test, with Dunn's post-hoc, $p=0.0001$), as well as significant sub-regional decrease in striatum, external capsule, pyriform cortex, hippocampus, and thalamus compared to untreated HI or DMSO treated controls ($p<0.05$ with Kruskal-Wallis test, Dunn's post-hoc). Significant increase of cell death, microglial and astroglial activation and tissue loss was observed between HI, DMSO and WP1066 groups when compared sham and naïve controls (Kruskal-Wallis test with Dunn's post-hoc, $p<0.05$) (Figure 15A, B, C, D).

Immediate post-insult intraperitoneal application of 40 or 160µg/g, of WP1066 did not show neuroprotective effect in any marker of the IHC analysis (Supplementary Figure 1A, F, K, P). Surprisingly, on the contrary, intraperitoneal WP1066 application with a dose of 40µg/g significantly increased the damage after induction of HI. Specifically, TUNEL+ cell death was increased after 40µg/g WP1066 application compared to DMSO treated controls in striatum, external capsule, and hippocampus (Kruskal-Wallis test with Dunn's post-hoc, $p<0.01$), and in cortex, hippocampus and striatum compared to untreated HI control animals (Kruskal-Wallis test with Dunn's post-hoc, $p<0.05$) (Supplementary Figure 1A). Immediate intraperitoneal application of 40µg/g WP1066 also increased tissue loss compared to DMSO treated controls in cortex ($p<0.01$, Kruskal-Wallis test with Dunn's post-hoc) and in hippocampus compared to untreated HI control animals ($p<0.001$). Finally, immediate intraperitoneal application of 160µg/g WP1066 also upregulated tissue loss compared to control HI littermates in

hippocampus and thalamus (Kruskal-Wallis test with Dunn's post-hoc, $p<0.05$) (Supplementary Figure 1P).

These results together with the data from the application of 80μg/g BW, show that WP1066 acts as a neuroprotective therapeutic agent in neonatal HI in a dose specific manner, with 80μg/g BW being neuroprotective, whereas 40μg/g and 160μg/g are not.

All together, these results support greatly the possible application of WP1066 in neonatal HI at the specific dose of 80μg/g BW.

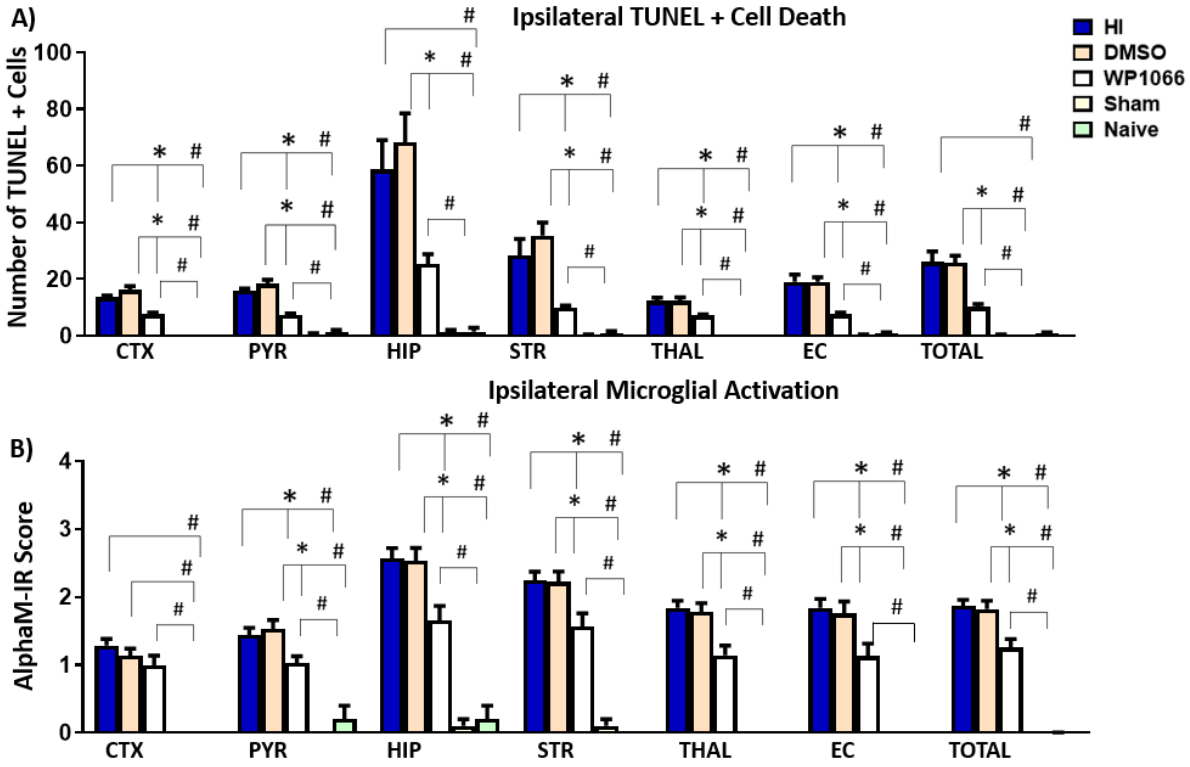

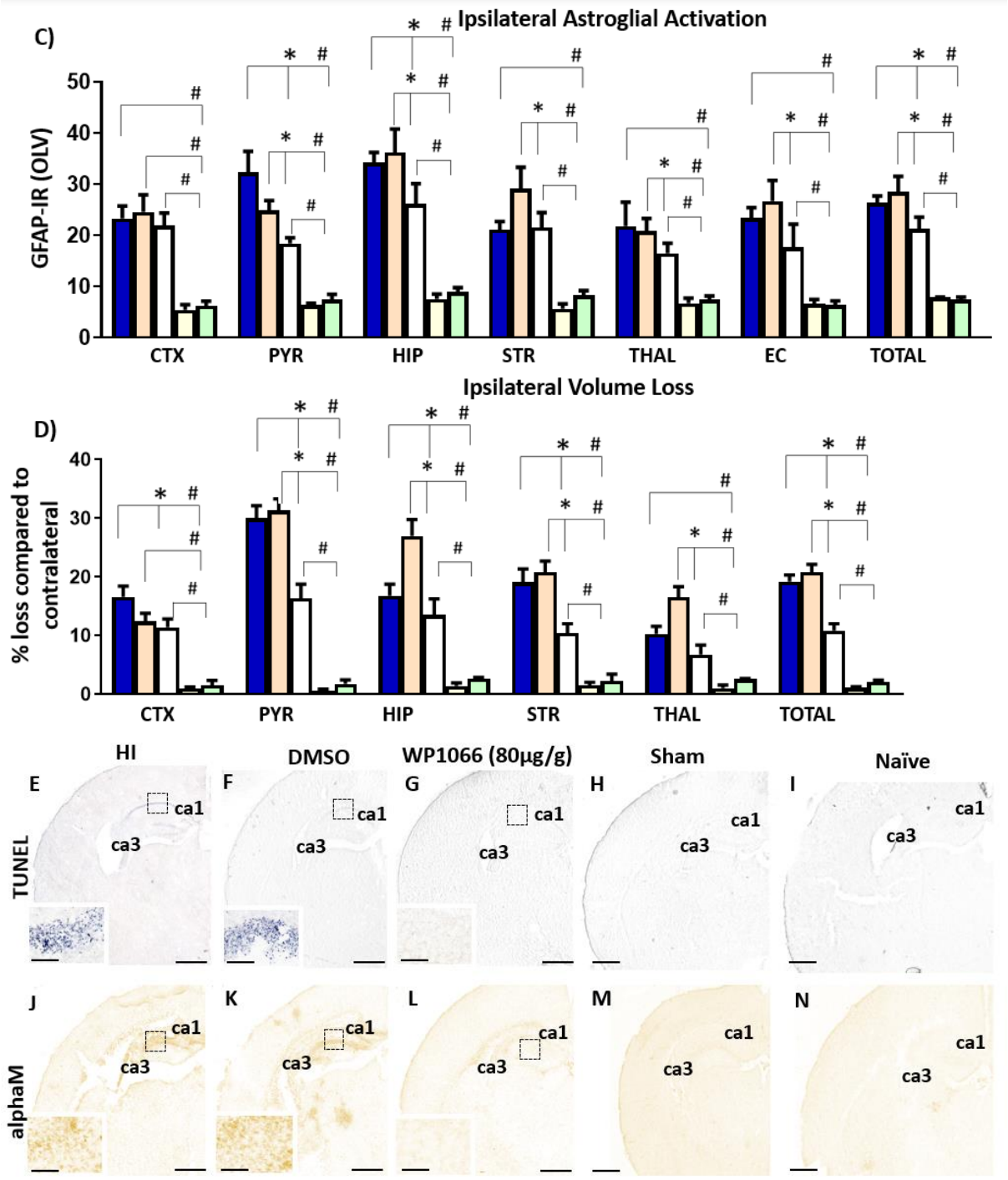
C)
Ipsilateral Astroglial Activation
GFAP-IR (OLV)
50
40
30
20
10
0
CTX
PYR
HIP
STR
THAL
EC
TOTAL
D)
Ipsilateral Volume Loss
% loss compared to contralateral
40
30
20
10
0
CTX
PYR
HIP
STR
THAL
TOTAL
HI
DMSO
WP1066 (80µg/g)
Sham
Naïve
E
F
G
H
I
TUNEL
ca1
ca3
J
K
L
M
N
alphaM

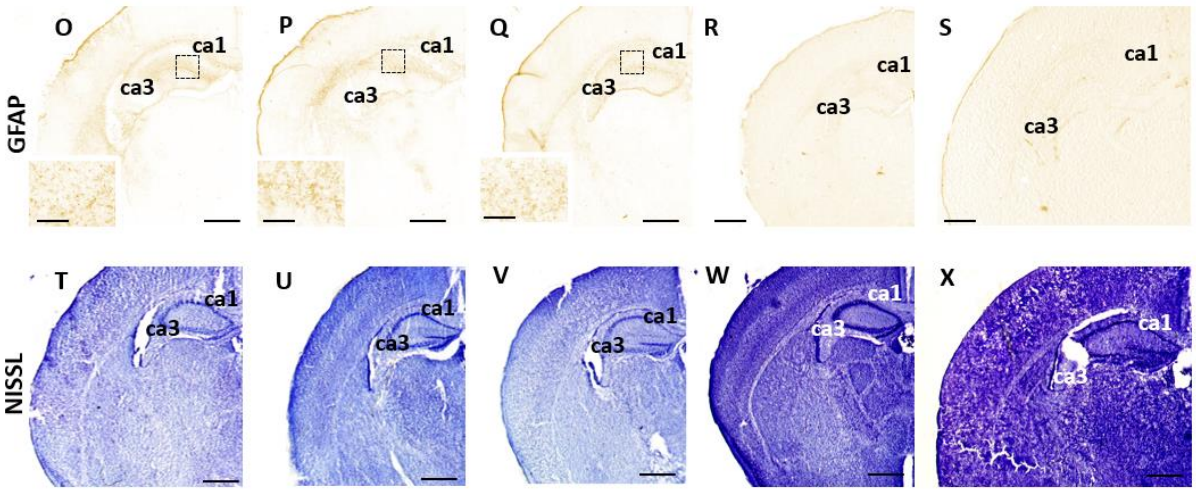

Figure 15. **Neuroprotective effect of immediate post-HI intraperitoneal application of 80µg/g BW WP1066 application.** A. Quantitative ipsilateral analysis of TUNEL+ cell death in animals treated with WP1066 80µg/ g (white) (n=16), DMSO (orange) (n=16) or untreated HI (blue) (n=16), naïve (green) (n=6), sham (pink) (n=6) control littermates. Intraperitoneal application of WP1066 80µg/g BW reduced cell death in cortex (p=0.0004), pyriform cortex (p=0.0005), striatum (p=0.005), external capsule (p=0.0006), hippocampus (p=0.0006), thalamus (p=0.0002) and overall (p=0.0007) compared to untreated HI and DMSO treated groups. An increase in cell death was observed in cortex, pyriform cortex, striatum, external capsule, hippocampus, thalamus, and overall in WP1066 80µg/g treated group compared to naïve and sham control groups (p=0.0001, Kruskal-Wallis test with Dunn's post-hoc). B. Quantitative analysis of alphaM immunoreactivity representing microglial activation in animals treated with 80µg/g BW WP1066 (G) compared to untreated HI, DMSO treated control groups. Intraperitoneal application of WP1066 80µg/g BW reduced microglial activation in thalamus (p=0.002), hippocampus (p<0.0006), striatum (p=0.0009), external capsule (p=0.03) and overall (p=0.0002) compared to DMSO and HI control groups. An increase in microglial activation was observed in cortex, pyriform cortex, striatum, external capsule, hippocampus, thalamus, and overall of WP1066 80µg/g treated group compared to naïve and sham groups (p=0.0001). C. Ipsilateral changes in astroglial activation assessed through GFAP immunoreactivity after treatment with 80µg/g BW WP1066 compared to DMSO, HI, sham, and

naïve littermates. Intraperitoneal application of WP1066 80µg/g BW reduced astroglial activation in pyriform cortex (p=0.002), hippocampus (p=0.04) and overall (p=0.04) compared DMSO treated and untreated HI control groups. An increase in astroglial activation was observed in cortex, pyriform cortex, striatum, external capsule, hippocampus, thalamus, and overall of WP1066 80µg/g treated group compared to naïve and sham groups (p=0.0001). D. Quantitative analysis showing the percentage of tissue loss assessed through Cresyl Violet staining consequent to HI insult on the ipsilateral side of the brain in the regions of interest immediate post-HI intraperitoneal application of 80µg/g WP1066 compared to untreated HI and DMSO treated control groups. WP1066 80µg/g application significantly reduced tissue loss in pyriform cortex (p=0.01) and striatum (p=0.0004) and overall (p=0.001, Kruskal-Wallis test with Dunn's post-hoc) compared to DMSO and HI control groups, with a visible trend towards reduction in the rest of the regions. An increase in tissue loss was observed in cortex, pyriform cortex, striatum, external capsule, hippocampus, thalamus, and overall in WP1066 80µg/g treated group compared to naïve and sham groups. E-I. Histochemical overview of the treatment groups stained for TUNEL+ cell death, HI (E), DMSO (F), 80µg/g BW WP1066 (G), sham (H), naïve (I) and low magnification ipsilateral overview in HI (E) and DMSO (F) groups. J-N. Histochemical overview of the treatment groups, of alphaM staining, HI (J), DMSO (K), 80µg/g BW WP1066 (L), sham (M), naïve (N) and low magnification ipsilateral overview in HI (J), DMSO (K) and WP1066 (L) groups. O-S. Histochemical overview of the treatment groups, HI (O), DMSO (P), 80µg/g BW WP1066 (Q), sham (R), naïve (S) and low magnification ipsilateral overview in HI (O), DMSO (P) and WP1066 (Q) groups. T-X. NISSL-stained forebrain of the treatment groups HI (T), DMSO (U), WP1066 (V), sham (W), naïve (X). Scale bars represent 400µm, inserts=62µm. (*$p<0.05$, #$p<0.05$ significant difference compared to sham-naïve control groups). CTX – cortex, PYR – pyriform cortex, HIP – hippocampus, STR – striatum, THAL -thalamus, EC – external capsule, Total - Average of all regions.

3.3.3 Immediate intraperitoneal application of 80µg/g WP1066 post-HI decreases myelin loss and oxidative stress

Intraperitoneal application of 80µg/g WP1066 resulted in higher levels of myelination compared to untreated HI and DMSO treated control littermates. MBP levels were also significantly lower in untreated HI controls and DMSO treated littermates compared to sham and naïve animals in external capsule and hippocampus (Figure 16A, $p<0.05$, Kruskal-Wallis test with Dunn's post-hoc). Higher levels in MBP expression were observed in the external capsule and striatum ($p<0.05$ Kruskal-Wallis test with Dunn's post-hoc) (Figure 16A). Oxidative stress, as assessed by iNOS, in animals treated with WP1066 80µg/g was significantly decreased compared to DMSO treated and untreated HI control littermates in the hippocampus ($p<0.05$ Kruskal-Wallis test with Dunn's post-hoc) of the ipsilateral side (Figure 16G). Significant increase of iNOS+ cells was observed in WP1066 treated animals compared to sham and naïve controls (Kruskal-Wallis test with Dunn's post-hoc, $p<0.05$) (Figure 16G).

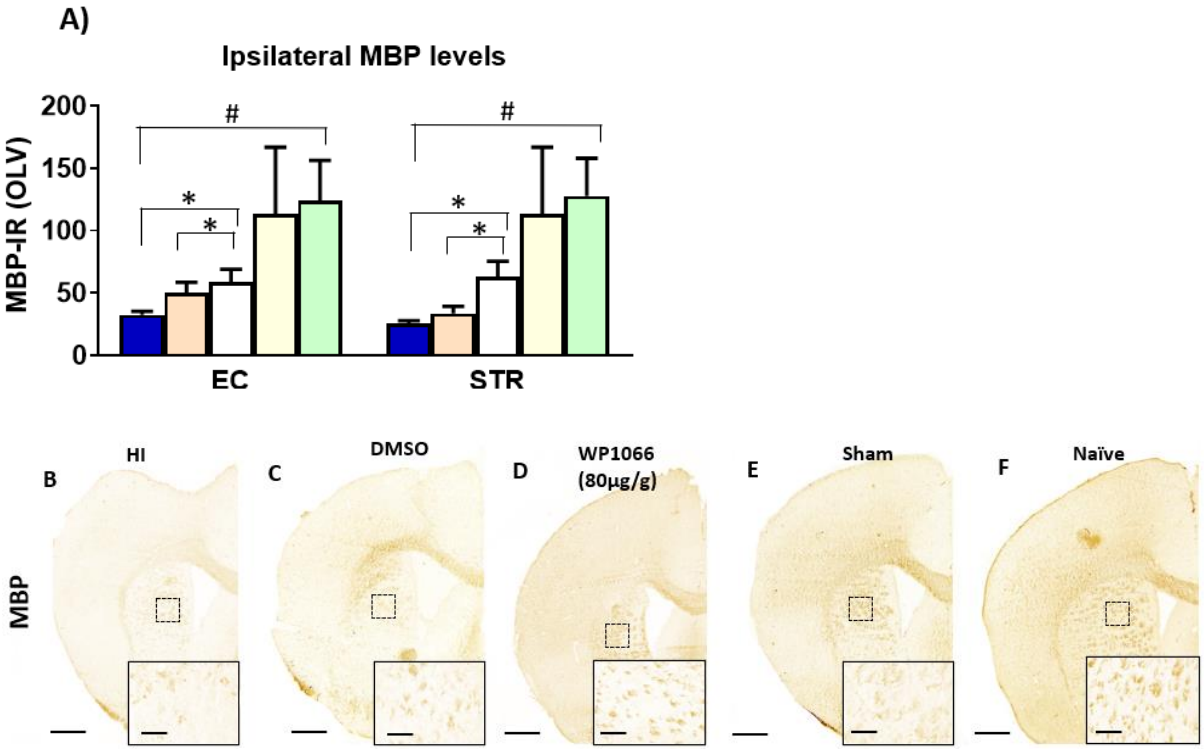

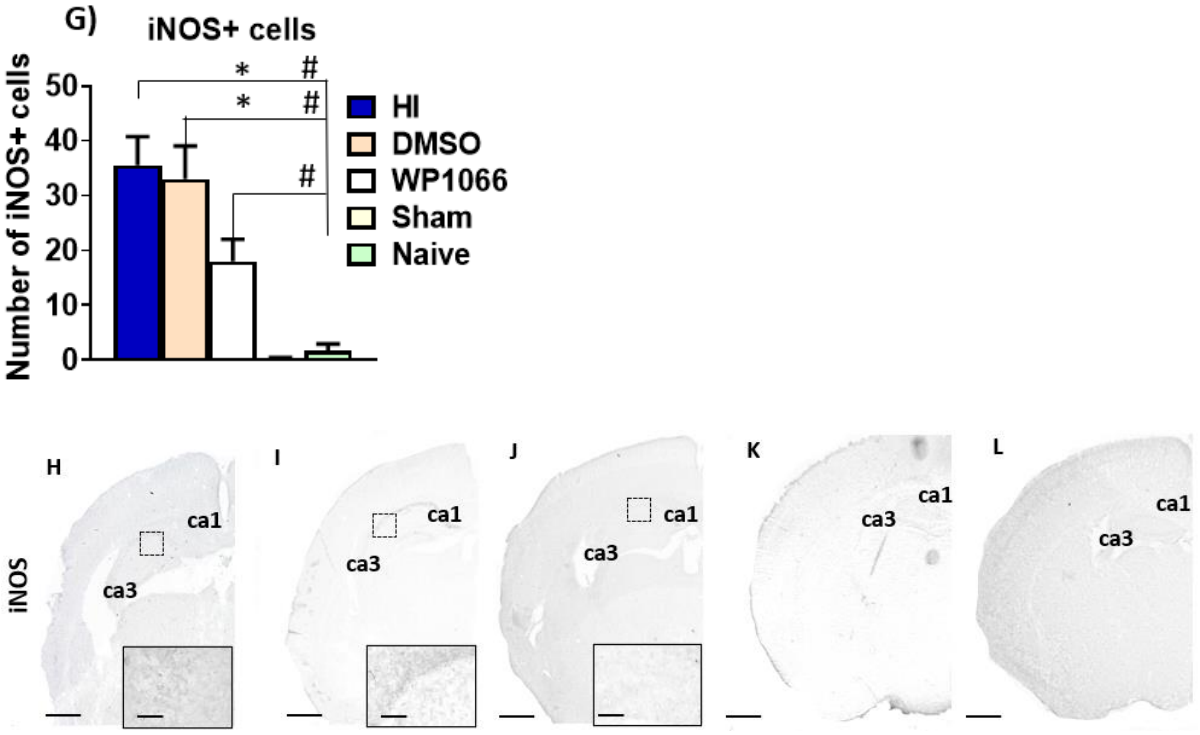

Figure 16. **Immediate intraperitoneal application of 80µg/g BW WP1066 increased myelination and decreased oxidative stress**. A. Quantitative ipsilateral analysis of MBP myelination levels in animals treated with WP1066 80µg/ g treated (white), DMSO treated (orange) or untreated HI (blue), naïve (green), sham (pink) control animals. An increase in cell death was observed in striatum (p=0.001) and external capsule (p=0.004) of WP1066 80µg/g treated group compared to untreated HI and DMSO treated groups. Lower levels of myelination were observed in striatum and external capsule of untreated HI and DMSO treated controls compared to naïve and sham groups (p=0.0001). B-F. Histochemical overview of the treatment groups, HI (B), DMSO (C), 80µg/g BW WP1066 (D), sham (E), naïve (F) and low magnification ipsilateral overview in HI (B) and DMSO (C) groups. G-L. Quantitative analysis of iNOS immunoreactivity in animals treated with 80µg/g BW WP1066 (G) and ipsilateral overview of the experimental groups (H-L). Graph G shows the reduction in iNOS+ cells hippocampus after 80µg/g WP1066 treatment compared to DMSO and HI groups (p=0.02) (Kruskal-Wallis test, with Dunn's post-hoc). An increase in iNOS+ cells was observed in hippocampus of WP1066 80µg/g treated group compared to naïve and sham groups

(p=0.0001). H-L. Histochemical overview of the treatment groups, HI (H), DMSO (I), 80µg/g BW WP1066 (J), sham (K), naïve (L) and low magnification ipsilateral overview in HI (H), DMSO (I) and WP1066 (J) groups. Abbreviations: EC, external capsule; HIP, hippocampus; STR, striatum. Scale bars: (B, C, D, E, F, H, I, J, K, L) = 1,000 µm; inserts = 62 µm. *p<0.05, #p<0.05, significant difference between sham and naïve control groups.

3.3.4 Immediate intraperitoneal application of 80µg/g WP1066 post-HI decreases pro- and anti-inflammatory microglial activation with an increase towards anti-inflammatory microglia

The pro-inflammatory phenotype activation pattern was significantly decreased in the 80µg/g WP1066 treated group compared to untreated HI and DMSO treated controls in cortex, hippocampus, external capsule, striatum thalamus and overall and in pyriform cortex, hippocampus, external capsule, striatum and thalamus, respectively (p<0.05, Kruskal-Wallis test with Dunn's post-hoc) (Figure 17B). The anti-inflammatory activation pattern was also significantly reduced in WP1066 treated animals compared with untreated HI and DMSO treated group in cortex, thalamus and in cortex, thalamus and external capsule, respectively (p<0.05, Kruskal-Wallis test with Dunn's post-hoc) (Figure 17C). Pro- & anti-inflammatory microglia co-localisation also showed significant reduction in cortex, hippocampus, thalamus, striatum, external capsule and the overall (p<0.05, Kruskal-Wallis test with Dunn's post-hoc) in the WP1066 treated group compared with the untreated HI controls, as well asin cortex, hippocampus, thalamus, striatum, pyriform cortex, external capsule and the overall, compared with DMSO treated control littermates (Figure 17D). Although WP1066 application reduced the levels of pro- and anti-inflammatory microglia, the levels remained significantly

higher when compared to naïve and sham controls (Kruskal-Wallis test with Dunn's post-hoc, $p<0.05$) (Figure 17).

To better understand the inter-relation between pro-inflammatory (CD86) and anti-inflammatory (CD206) microglia between the experimental groups after immediate intraperitoneal post-HI 80µg/g BW WP1066 application we assessed six different ratios between the two phenotypes in each of the six regions (Figure 17 E, F).

The ipsilateral anti-inflammatory / pro-inflammatory ratio was significantly increased in the pyriform cortex, hippocampus, striatum and external capsule ($p<0.01$, Kruskal-Wallis test with Dunn's post-hoc, Figure 17F) in the WP1066 experimental group, when compared with HI controls and in hippocampus and striatum when compared with DMSO treated animals ($p<0.01$, Kruskal-Wallis test with Dunn's post-hoc, Figure 17F), representing the higher population of anti-inflammatory microglia, >60% compared to pro-inflammatory microglia. Additionally, the pro-/anti- inflammatory microglia ratio was significantly decreased in cortex, pyriform cortex, hippocampus, striatum, thalamus, external capsule and overall between WP1066 treated animals and HI controls ($p<0.05$, Kruskal-Wallis test with Dunn's post-hoc, Figure 17E), as well as in cortex, pyriform cortex, hippocampus, striatum, external capsule and overall between WP1066 treated and DMSO treated animals (Figure 17E). In Supplementary Figure 2 a 3D representation of pro- and anti-inflammatory microglia cells is listed.

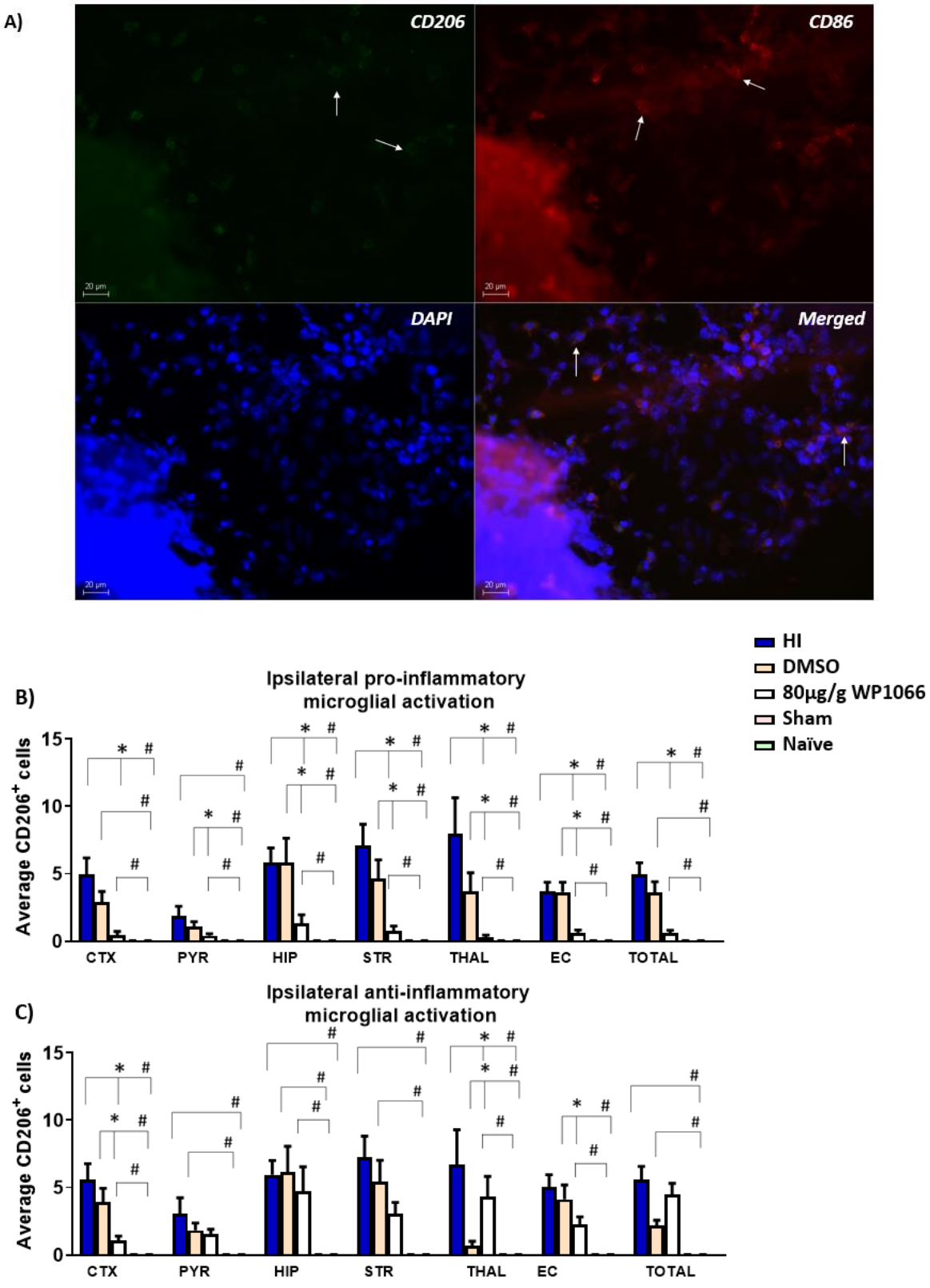
A)
CD206
CD86
DAPI
Merged
20 µm
B)
Ipsilateral pro-inflammatory microglial activation
Average CD206+ cells
0
5
10
15
CTX
PYR
HIP
STR
THAL
EC
TOTAL
HI
DMSO
80µg/g WP1066
Sham
Naïve
C)
Ipsilateral anti-inflammatory microglial activation
Average CD206+ cells
0
5
10
15
CTX
PYR
HIP
STR
THAL
EC
TOTAL

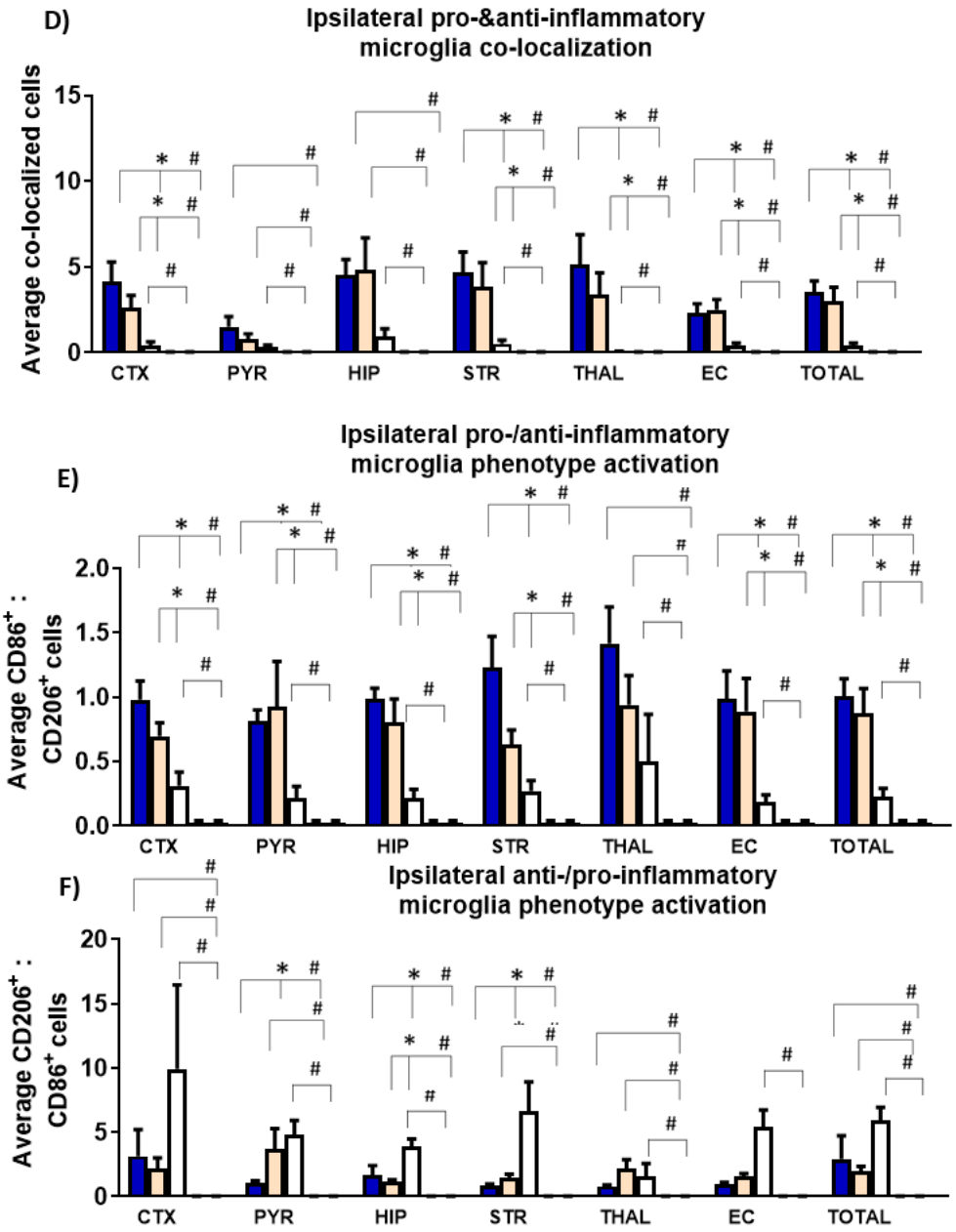

Figure 17. Immediate intraperitoneal application of 80µg/g BW WP1066 post-HI significantly reduces pro-, anti- inflammatory microglial phenotypes after HI insult. The graphs illustrate the averages of cell counts in six brain regions, for the HI, DMSO, WP1066 treatment, sham and naïve animals. A. Visual representation of pro-inflammator, anti-inflammatory and of pro- & anti- inflammatory microglia co-localization in the ipsilateral hemisphere. B. Activation profiles of CD86+, with significant decrease in cortex (p=0.0006), hippocampus (p=0.0006), striatum (p=0.0003), external capsule (p=0.0007), thalamus (p=0.004) and overall (p=0.0002) when comparing WP1066 treated animals and HI controls,

and in pyriform cortex (p=0.03), hippocampus (p=0.01), striatum (p=0.004), external capsule (p=0.0001) and thalamus (p=0.01) and overall (p=0.0002) when comparing WP1066 treated to DMSO treated animals (Kruskal-Wallis test with Dunn's post-hoc). An increase in pro-inflammatory microglial activation was observed in all the regions of interest in WP1066 80µg/g treated group compared to naïve and sham groups (p=0.0001). C. Activation profiles CD206+ microglial cells in the ipsilateral hemisphere. Anti-inflammatory cells were reduced in cortex (p=0.0006) and thalamus (p=0.01) in WP1066 group when compared to HI controls and in cortex (p=0.003), thalamus (p=0.01) and external capsule (p=0.006) when compared to DMSO treated animals Kruskal-Wallis test with Dunn's post-hoc). An increase in anti-inflammatory microglial activation was observed in all the regions of interest in WP1066 80µg/g treated group compared to naïve and sham groups (p=0.0001). D. Pro- & anti- inflammatory microglia co-localized cells were significantly reduced in cortex (p=0.001), pyriform cortex (p=0.03), hippocampus (p=0.0006), external capsule (p=0.001), striatum (p=0.001), thalamus (p=0.004) and overall (p=0.0007), Kruskal-Wallis test with Dunn's post-hoc) after WP1066 treatment compared to untreated HI control group and in cortex (p=0.02), striatum (p=0.009), thalamus (p=0.007), external capsule (p=0.0005) and overall 0.001) compared to DMSO group. An increase in pro- & anti- inflammatory microglial activation was observed in all the regions of interest in WP1066 80µg/g treated group compared to naïve and sham groups (p=0.0001). E. Significant reduction of pro- : anti- inflammatory microglia ratio in cortex (p=0.0006), pyriform cortex (p=0.0003), hippocampus (p=0.0001), striatum (p=0.0008), thalamus (p=0.03), external capsule (p=0.001) and overall (p=0.0001) in WP1066 treated group when compared to untreated HI and in cortex (p=0.0007), pyriform cortex (p=0.02), hippocampus (p=0.002), striatum (p=0.01), external capsule (p=0.009) and overall (p=0.001) when compared to DMSO treated group (Kruskal-Wallis test with Dunn's post-hoc) F. The graph illustrates significant decrease of CD206+: CD86+ ratio in pyriform cortex (p=0.003), hippocampus (p=0.02), striatum (p=0.004) and external capsule (p=0.0002) (Kruskal-Wallis test with Dunn's post-hoc) in WP1066 treated group when compared to untreated HI control littermates. A. Note the co-localization of CD86+ and CD206+ cells (white arrows) . Results

are presented as mean ± SEM. CTX – cortex, PYR – pyriform cortex, HIP – hippocampus, STR – striatum, THAL -thalamus, EC – external capsule, Total - Average of all regions. (*p<0.05).

3.3.5 WP1066 application immediately post-HI decreases phosphorylated STAT3 Tyr705 in ipsilateral hippocampus

Western Blot analysis for phosphorylated STAT3 Y705 (pSTAT3 Y705) in ipsilateral and contralateral hippocampus from animals with no treatment (HI), DMSO, or 80µg/g WP1066 treatment and following 1h recovery demonstrated some (albeit not statistically significant) ipsilateral increase in pSTAT3 Y705 in the DMSO treated group compared to the untreated HI controls (Figure 18A). WP1066 application significantly decreased levels of pSTAT3 Y705 on the ipsilateral side, compared with DMSO treated controls, but did not show significant reduction compared to the untreated HI group. WP1066 application did not result in significant changes in the contralateral side of any of the tested markers (Figure 18A). Western blotting analysis for phosphorylated STAT3 S727 (pSTAT3 S727) under the same conditions did not show significant changes between the experimental groups on either contralateral of ipsilateral side (Figure 18B). Western blotting analysis for PHB at 1h of untreated HI, DMSO-, or 80µg/g WP1066-treated animals showed a trend of ipsilateral increase of PHB protein levels in the WP1066, compared with the DMSO treated and untreated HI control animals, but did not reach statistical significance (Figure 18C). No significant differences were observed between the DMSO treated animals and the HI littermate controls. No differences between the three groups were registered on the contralateral side (Figure 18C). The values shown represent relative densitometry of protein bands

compared to β-actin, which was used as the internal loading control. We also observed no change in β-actin protein levels, across all experimental groups.

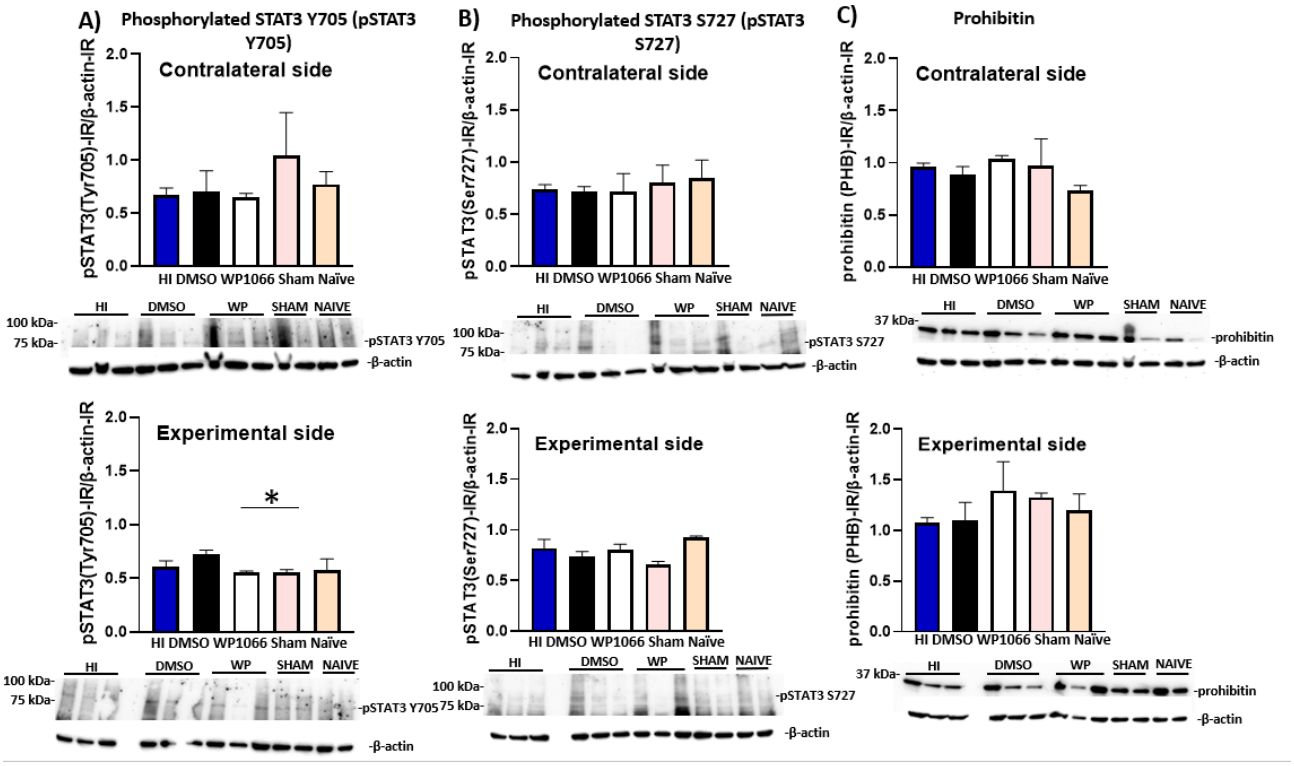

Figure 18. **Intraperitoneal application of 80µg/g BW WP1066 in P9 mice immediately post-HI decreases phosphorylated STAT3 Y705 in ipsilateral hippocampus.** (A) Western Blots for pSTAT3 Y705 in ipsilateral and contralateral hippocampus from untreated HI, DMSO- or 80µg/g WP1066- treated animals or sham and naïve control littermates and 1h recovery. β-actin protein levels served as control. WP1066 application decreases STAT3 Y705 protein levels ipsilaterally by 30% when compared to DMSO treated animals. (B) Western Blots for pSTAT3 S727 in ipsilateral and contralateral hippocampus from untreated HI, DMSO- or 80µg/g WP1066-treated animals after 1h recovery, as well as naïve and sham littermate controls. β-actin protein levels served as control. No significant change is observed both ipsi- and contralaterally when compared to HI, DMSO, sham and naïve groups. No significant change was observed on β-actin protein levels. (C) Western Blots for PHB in ipsilateral and contralateral hippocampus from untreated HI, DMSO- or 80µg/g WP1066- treated animals

after 1h recovery, and sham and naïve littermate controls. β-actin protein levels served as control. Note the trend of increase of PHB protein levels in the WP1066 treated animals compared to HI and DMSO groups. *p<0.05.

3.3.6 Immediate post-HI WP1066 application does not affect total STAT3 and STAT1 levels in cortex after 1h

Western Blot analysis for total STAT3 in ipsilateral cortex from untreated HI (n=6), DMSO- (n=6), or 80µg/g WP1066-treated (n=6) animals after 1h recovery demonstrated no significant difference in protein levels between the groups (Figure 19A). Western blotting analysis for phosphorylated STAT1 under the same conditions did not show significant changes between the experimental groups on the ipsilateral side of cortex (Figure 19B). The values represent relative densitometry compared to β-actin, which was used as the internal loading control.

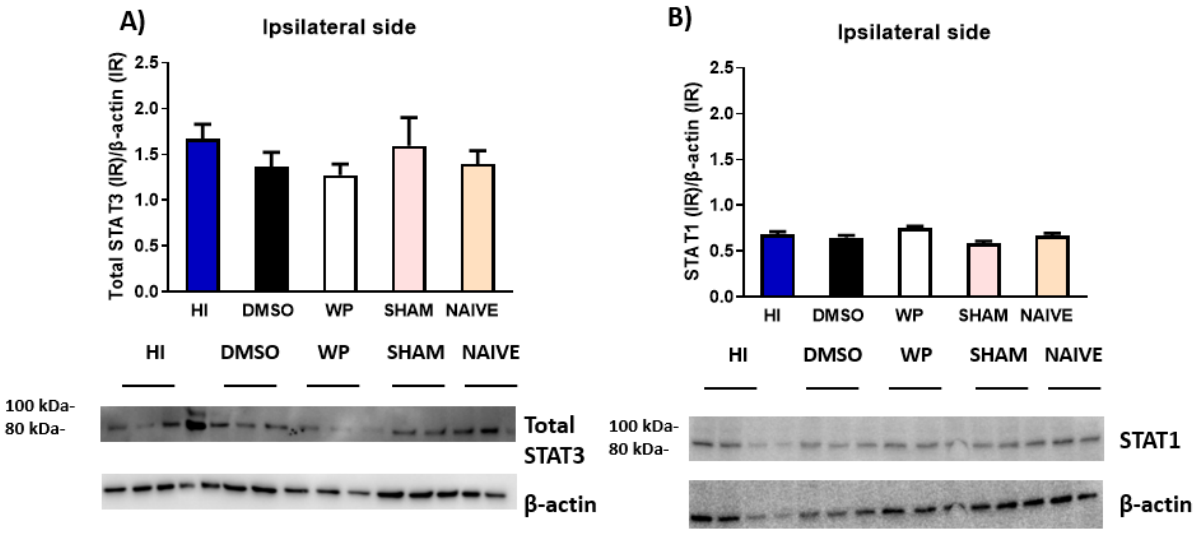

Figure 19. **Immediate post-HI application of 80µg/g BW WP1066 in P9 mice does not affect total STAT3 and STAT1 levels in cortex at 1h.** (A) Western blots for total STAT3 in ipsilateral cortex from untreated HI (n=6), DMSO- (n=6) or 80µg/g WP1066-treated (n=6)

animals after 1h recovery, or sham (n=5) and naïve littermate controls (n=5). β-actin protein levels served as loading control. WP1066 application does not affect total STAT3 protein levels. (B) Western Blots for STAT1 in ipsilateral cortex from untreated HI, DMSO- or 80µg/g WP1066-treated animals after 1h recovery, and sham and naïve littermate controls. β-actin protein levels served as loading control. No significant change is observed ipsilaterally in the WP1066-treated animals when compared to untreated HI, DMSO, sham and naïve groups. (p>0.05, Kruskal-Wallis test with Dunn's post-hoc).

3.3.7 Immediate post-HI intraperitoneal application WP1066 immediately does not affect pro-inflammatory cytokine levels in cortex at 1h

We tested the effect of 80µg/g WP1066 application immediately after HI insult, on multiple pro-inflammatory cytokine levels in cortex, using ELISA. The results showed that WP1066 application did not change the levels of IL-6, IL-1b and IL-12/IL-23 compared to untreated HI (n=5), DMSO treated (n=5), sham (n=4) or naïve (n=4) control groups (Figure 20) (p>0.05, Kruskal-Wallis test with Dunn's post-hoc).

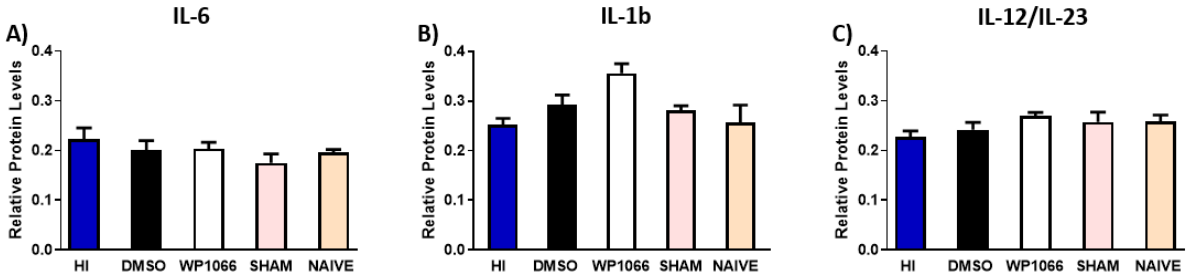

Figure 20. **Immediate post-HI intraperitoneal application of 80µg/g BW WP1066 in P9 mice does not change the protein levels of IL-6, IL-1b, IL-12/IL-23 in cortex.** A-C. Relative protein levels of IL-6 (A), IL-1b (B), IL-12/IL-23 (C) through ELISAs. No significant changes were observed among the experimental groups (p>0.05, Kruskal-Wallis test with Dunn's post-hoc). (HI n=5, DMSO n=5, WP1066 n=5, sham n=4, naïve n=4).

3.3.8 Immediate post-HI application of WP1066 increases anti-inflammatory CD206 gene levels and has no effect on IL-6 pro-inflammatory gene levels in hippocampus at 1h post-treatment

Pro- and anti-inflammatory gene levels are alternating after HI insult[265], therefore we investigated the effect of intraperitoneal 80µg/g WP1066 application immediately after HI insult, on IL-6 and CD206 gene levels in hippocampus through qPCR analysis. The results showed that WP1066 application (n=4) did not change the levels of the pro-inflammatory IL-6 gene (Figure 21A), but significantly increased the levels of the anti-inflammatory CD206 gene compared to DMSO treated (n=4) control group (Figure 21B) (p>0.05, Kruskal-Wallis test with Dunn's post-hoc).

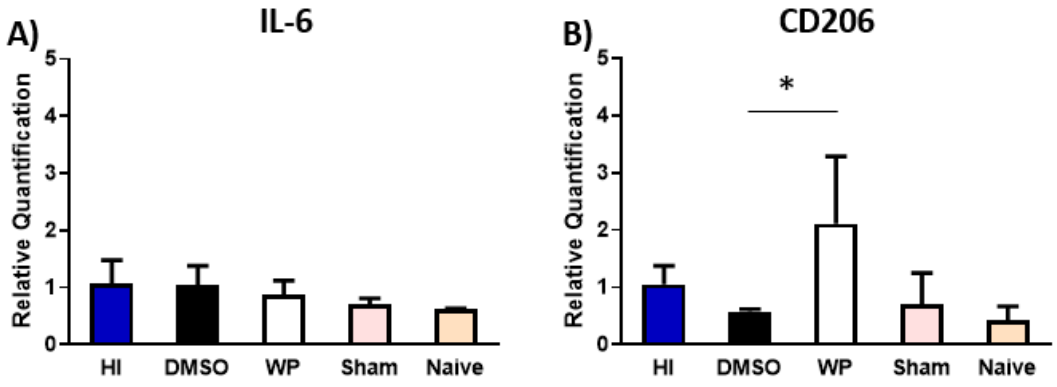

Figure 21**. Effect of immediate post-HI intraperitoneal application of 80µg/g BW WP1066 in P9 mice on IL-6 and CD206 gene levels in hippocampus.** A. No significant changes of pro-inflammatory IL-6 gene levels in hippocampus were observed among the experimental groups (p>0.05, Kruskal-Wallis test with Dunn's post-hoc). B. CD206 anti-inflammatory gene levels in hippocampus were significantly increased after immediate post-HI 80µg/g BW WP1066 intraperitoneal application compared to DMSO treated control littermates (p<0.05, Kruskal-Wallis test with Dunn's post-hoc). (HI n=4, DMSO n=4, WP1066 n=4, sham n=3, naïve n=3).*p<0.05.

3.3.9 Effects of immediate post-HI intraperitoneal WP1066 application on complement component C1qa in cortex

The classical complement (C) activation pathway contributes to HI brain injury[154] and therefore we aimed to investigate whether WP1066 treatment provides a neuroprotective role by affecting this pathway. Our results indicated that immediate intraperitoneal post-HI application of 80µg/g BW WP1066 (n=5) decreased C1qa gene levels compared to DMSO treated (n=5) control littermates ($p<0.05$, Kruskal-Wallis test with Dunn's post-hoc, Figure 22A) but had no significant effect on C1qb and C1qc gene levels ($p>0.05$, Kruskal-Wallis test with Dunn's post-hoc, Figure 22B, C).

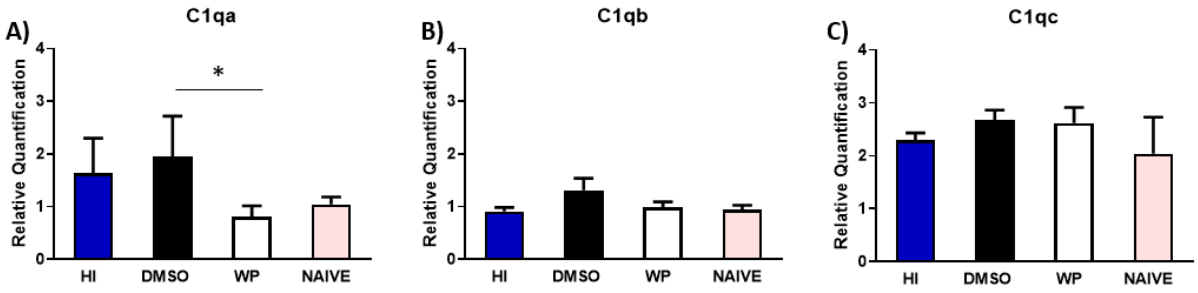

Figure 22. **Effect of immediate intraperitoneal post-HI application of 80µg/g BW of WP1066 in P9 mice on complement component C1q gene levels in cortex.** A. Relative quantification of C1qa levels indicated a statistically significant decrease in WP1066 group compared to DMSO controls, $p=0.04$, Kruskal-Wallis test with Dunn's post-hoc. B-C. No significant changes were observed in relative quantification levels of C1qb and C1qc levels among the experimental groups, $p>0.05$, Kruskal-Wallis test with Dunn's post-hoc. (HI n=5, DMSO n=5, WP1066 n=5, sham n=4, naïve n=4).*$p<0.05$.

3.3.10 Long-term assessments of 80µg/g BW WP1066 application immediately after HI insult

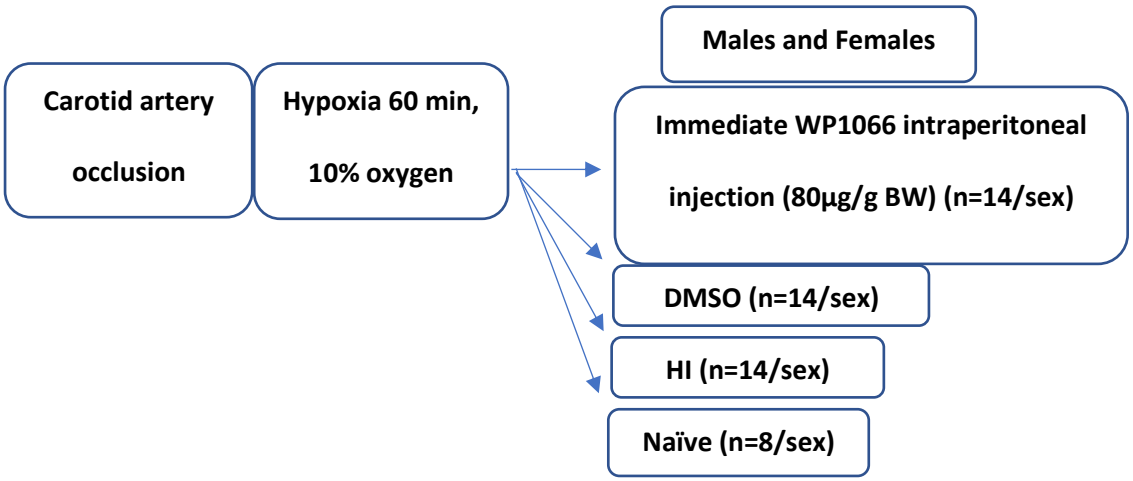

Figure 23. **Schematic representation of the experimental groups treated with either WP1066 or DMSO after HI brain damage, as well as their controls (untreated HI, naïve).**

3.3.11 Immunohistochemical analysis

In order to understand the long-term effects of application of WP1066 immediately post-HI, the brains of P36 mice untreated or treated with WP1066 80µg/g or DMSO were assessed for changes in infraction volume and myelination. At P36 Cresyl Violet staining was used to obtain the percentage of volume loss in the ipsilateral hemisphere compared to the contralateral one (Figure 24A-C). P36 WP1066 treated males showed a significant reduction of tissue loss compared to both untreated HI and DMSO treated male littermates in all brain regions ($p<0.05$, Kruskal-Wallis test with Dunn's post-hoc correction, Figure 24B). P36 WP1066 treated females showed similar pattern of reduction except for in the striatum ($p<0.05$, Kruskal-Wallis test with Dunn's post-hoc correction, Figure 24A). In line with the above data, when evaluating overall tissue loss (without separation between males and females), WP1066 application resulted in overall significantly reduced Cresyl Violet staining compared to both untreated HI and DMSO treated littermates ($p<0.05$, Kruskal-Wallis test with Dunn's post-hoc correction, Figure 24C).

When evaluating myelination, male animals treated with WP1066 treatment showed significantly higher MBP levels in the external capsule compared to untreated HI controls ($p<0.05$, Kruskal-Wallis test with Dunn's post-hoc), while no significant differences were recorded in MBP levels of the striatum (Figure 24E). Application of WP1066 resulted in higher MBP levels in both striatum and external capsule of females when compared DMSO treated control group ($p<0.05$, Kruskal-Wallis test with Dunn's post-hoc), and in overall brain, when compared to both untreated HI and DMSO treated control littermates ($p<0.05$, Kruskal-Wallis test with Dunn's post-hoc, Figure 24D, F).

Significant lower levels of myelination and increased levels of tissue loss were observed between experimental males and females untreated HI and DMSO treated groups compared to naïve control group (Kruskal-Wallis test, $p<0.05$) (Figure 24).

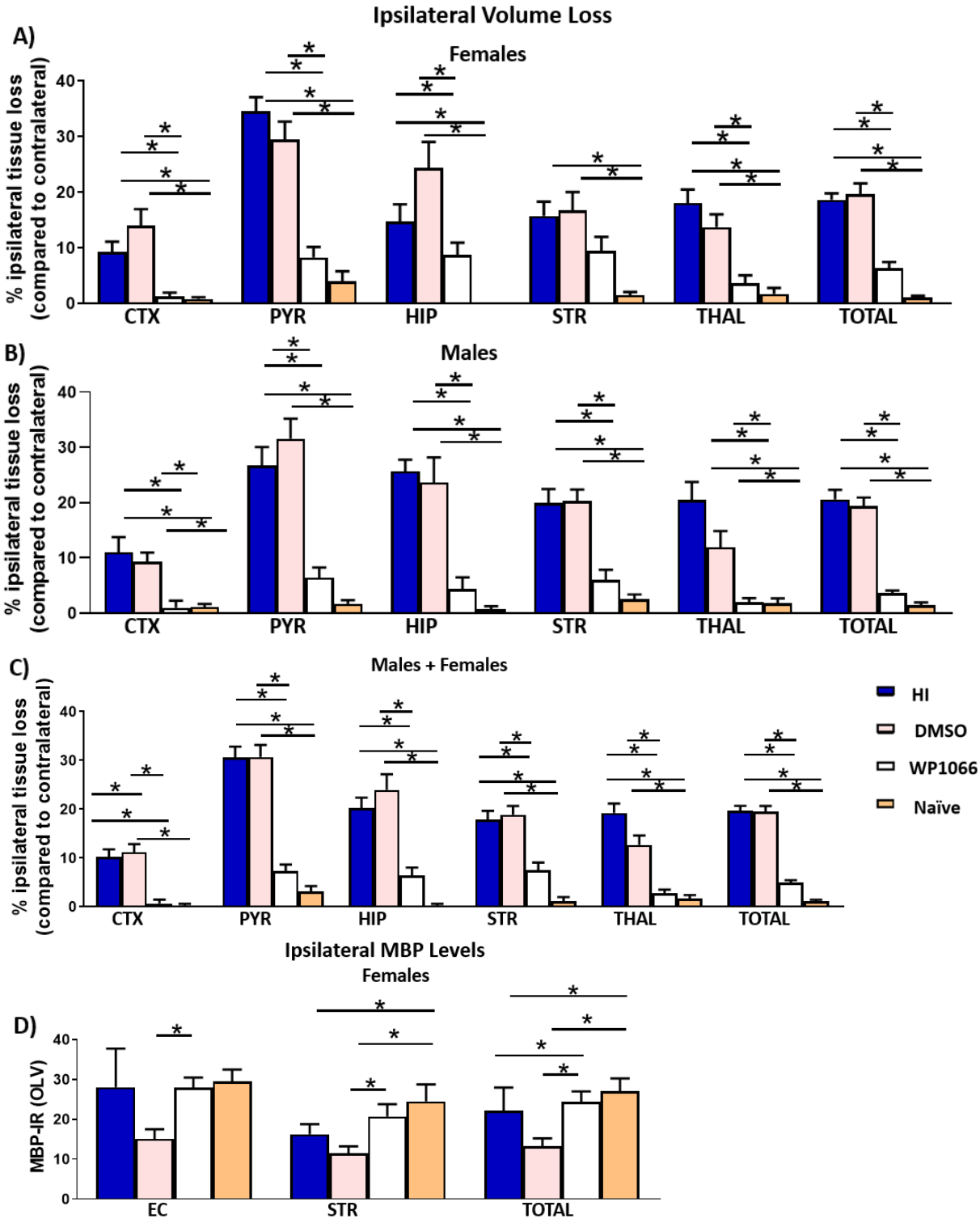

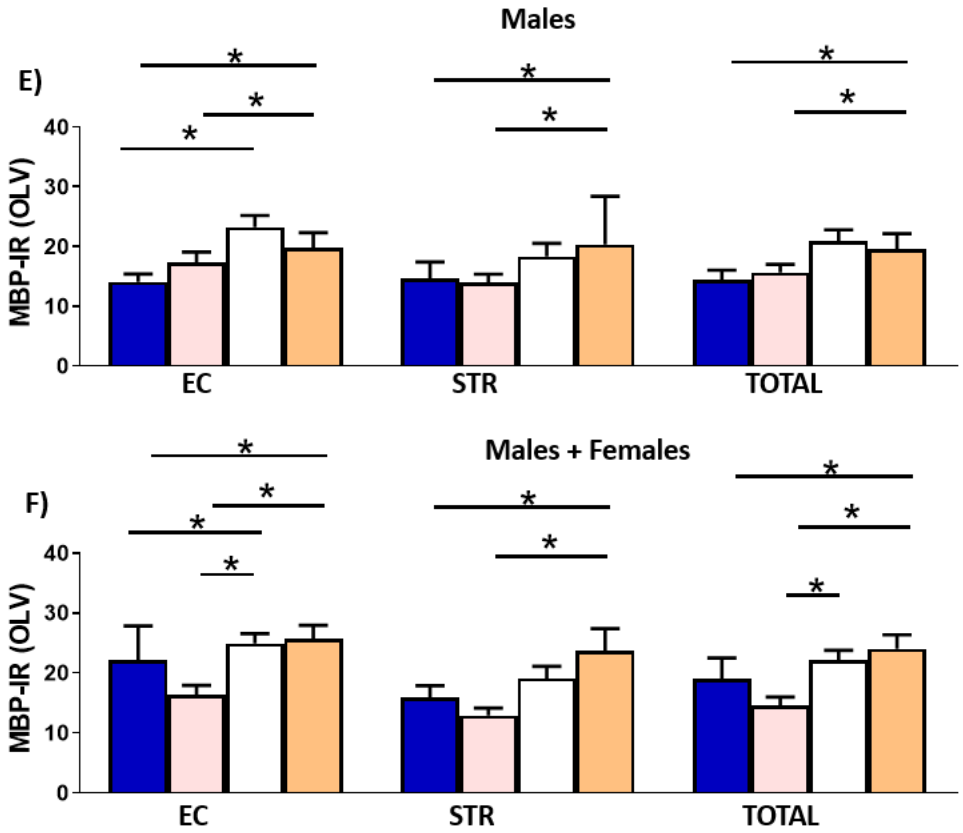

Figure 24. **Long-term effect immediate intraperitoneal post-HI application of 80µ/g BW WP1066 on tissue loss and myelination.** A-C. Percentage of tissue loss in the ipsilateral hemisphere of females (A), males (B) and overall (males+females) (C) at P36. WP1066 application significantly reduced tissue loss compared to female untreated HI (p=0.0001) and DMSO treated (p=0.0001) control animals in all brain regions (Kruskal-Wallis test with Dunn's post-hoc). Overall (C) significant difference was observed between WP1066 treated and untreated HI (p=0.002, Kruskal-Wallis test with Dunn's post-hoc correction) and between WP1066 and DMSO treatment (p=0.001, Kruskal-Wallis test with Dunn's post-hoc correction) in all brain regions assessed. D-F. Quantification of MBP immunoreactivity in the external capsule, striatum and overall in OLV. (D) Immediate intraperitoneal post-HI WP1066 application resulted in significantly higher MBP levels in striatum of the female group and significantly in the external capsule, compared to DMSO treated control female littermates (p=0.03, Kruskal-Wallis test with Dunn's post-hoc) and overall (p=0.001) compared to untreated HI and DMSO treated control. Significantly lower levels of myelination in striatum

were observed in untreated HI (p=0.02) and DMSO treated (p=0.001) groups compared to naïve control female littermates. In males (E) WP1066 application resulted in significantly higher levels of myelination in the external capsule (p=0.01) compared to male untreated HI control animals (Kruskal-Wallis test with Dunn's post-hoc). WP1066 application in combined males and females (F), resulted in significantly higher levels of myelination in external capsule compared to HI and DMSO control littermates (p=0.01, Kruskal-Wallis test with Dunn's post-hoc) and overall compared to DMSO treated controls (p=0.02, Kruskal-Wallis test with Dunn's post-hoc). Significantly decreased levels of myelination were observed in external capsule, striatum and overall of untreated HI and DMSO treated groups compared to naïve animals (p=0.001, Kruskal-Wallis test with Dunn's post-hoc).*p<0.05.

3.3.12 Behavioural assessments

The slipping test allowed the assessment of motor balance and coordination of P28 male and female mice. In this test, immediate intraperitoneal post-HI application of 80µg/g BW of WP1066 in DMSO significantly decreased the number of missed steps compared to untreated HI and DMSO treated control animals (p-value<0.05, Kruskal-Wallis test with Dunn's post-hoc, Figure 25A, B, C). Importantly, untreated HI and DMSO treated male and female control animals showed increased number of missed steps compared to naïve male and female littermates (p<0.05) but not when compared to WP1066 treated animals (p-value>0.05, Kruskal-Wallis test with Dunn's post-hoc, Figure 25B).

The NOR test was performed at P35 to assess the short-term memory, 10 min after the exposure to the novel object, of male and female mice and repeated at P36 to evaluate long-term memory, 24h after the exposure to the novel object. The short-term version of the test revealed that immediate intraperitoneal post-HI application of 80µg/g BW WP1066 on male mice, induced significantly improved memory compared

to DMSO treated and untreated HI controls (p-value<0.05, two-way ANOVA with Bonferroni correction, Figure 25D). Additionally, significant decrease in time spent with the novel object was recorded in untreated HI and DMSO treated controls when compared to naïve animals (p-value<0.05, two-way ANOVA with Bonferroni correction, Figure 25D). However, WP1066 treated females showed no significant difference compared to untreated HI controls (p-value>0.05, two-way ANOVA with Bonferroni correction, Figure 25E). Importantly, female DMSO treated animals spent significantly less time with the novel object compared to naïve littermates (p-value<0.05, two-way ANOVA with Bonferroni correction, Figure 25E). Figure 25F shows that when combined, males and female littermates treated with WP1066 showed a preference for the novel object when compared to untreated HI and DMSO controls (p-value<0.05, two-way ANOVA with Bonferroni correction). Finally, combined male and female DMSO treated animals spent less time with the novel object compared to naïve littermate controls (p-value<0.05, two-way ANOVA with Bonferroni correction, Figure 25F).

In P36, males (Figure 25G) and the overall group (Figure 25I), immediate post-HI WP1066 application induced significantly increased levels in discrimination index (p<0.05, two-way ANOVA with Bonferroni correction) compared to untreated HI and DMSO treated groups. The same pattern was recorded for untreated HI and DMSO treated males and combined animals compared to naïve littermates (p <0.05, two-way ANOVA with Bonferroni correction, Figure 25G, I). In females (Figure 25H), WP1066 application did not induce any significant change in discrimination index, although a trend towards an increase was observed compared to untreated HI and DMSO treated controls (p>0.05, two-way ANOVA with Bonferroni correction).

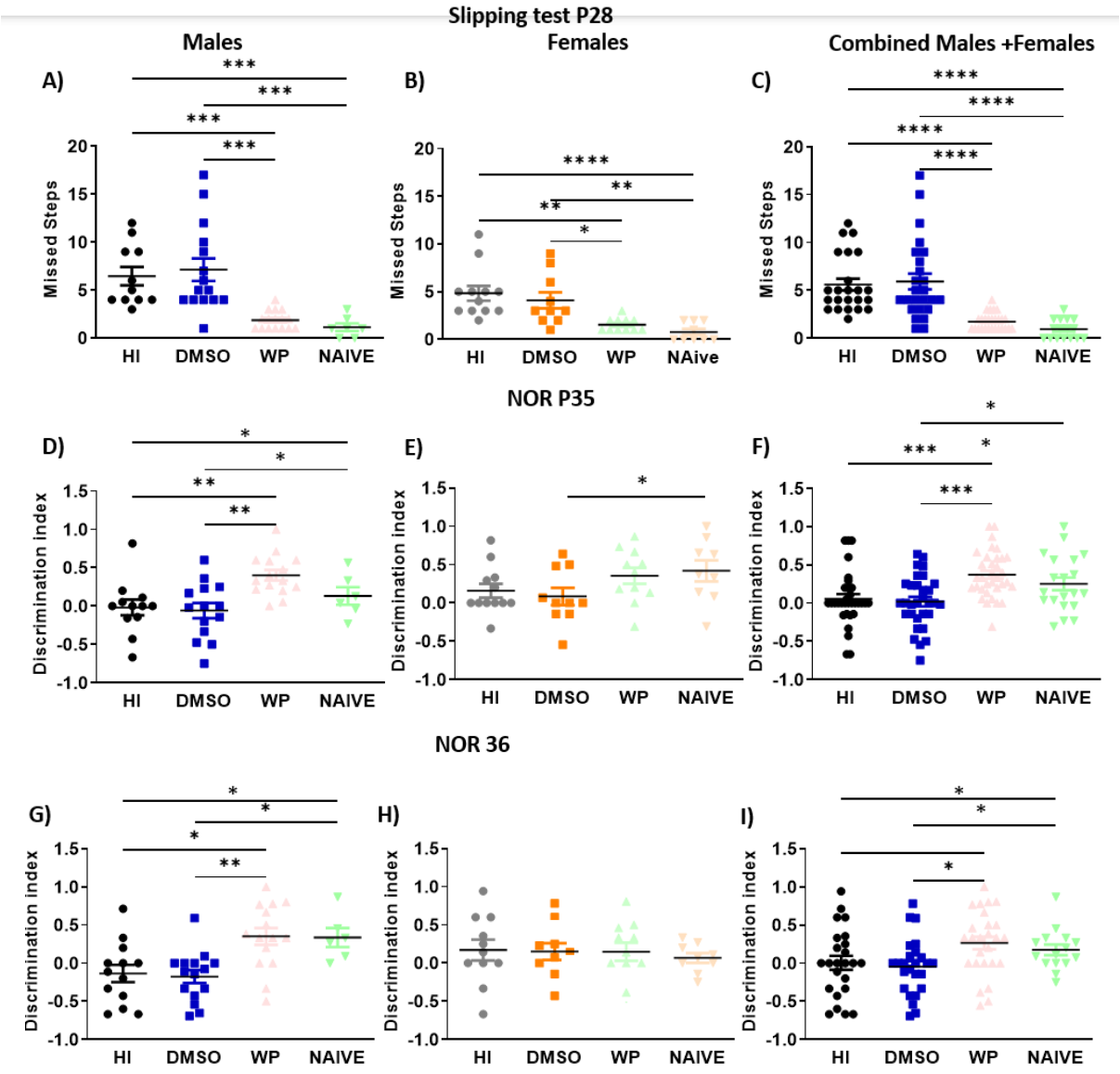

Figure 25. **Long-term effects (P28, P35, P36) of immediate intraperitoneal post-HI application of 80µg/g WP1066**. A-C. Application of 80µg/g WP1066 treatment immediately after HI reduced the number of missteps observed at 28 days in slipping test compared to untreated HI and DMSO treated control littermates in (A) males (B) females and (C) combined (males+females) assessed using Kruskal-Wallis test with Dunn's post-hoc correction (p=0.001). A significant increase in the missteps was also observed in untreated HI and DMSO treated controls compared to naïve littermate animals (p=0.001, Kruskal-Wallis test with Dunn's post-hoc). D-F. Immediate intraperitoneal post-HI application of 80µg/g WP1066 improved short-term memory measured with the NOR test at P35 in males (D) and combined

(males+females) (F) compared to DMSO treated or untreated HI animals assessed by two-way ANOVA with Bonferroni's correction. WP1066 treatment improved the short-term memory in females only, compared to DMSO treated control littermates (p=0.01, two-way ANOVA with Bonferroni's correction). G-I. Immediate intraperitoneal post-HI application of 80µg/g WP1066 improved long-term memory measured with the NOR test at P36 in males (G) and combined (males+females) (I) compared to DMSO treated or untreated HI animals assessed by two-way ANOVA with Bonferroni's correction. No significant changes were observed in females (p>0.05, by two-way ANOVA with Bonferroni's correction). All data presented as median and interquartile range.*p<0.05, **p<0.01, ***p<0.001, ****p<0.0001.

3.3.13 Delayed post-HI application of 80µg/g BW WP1066 at 1 or 2h after HI insult reduces brain damage in neonatal HI

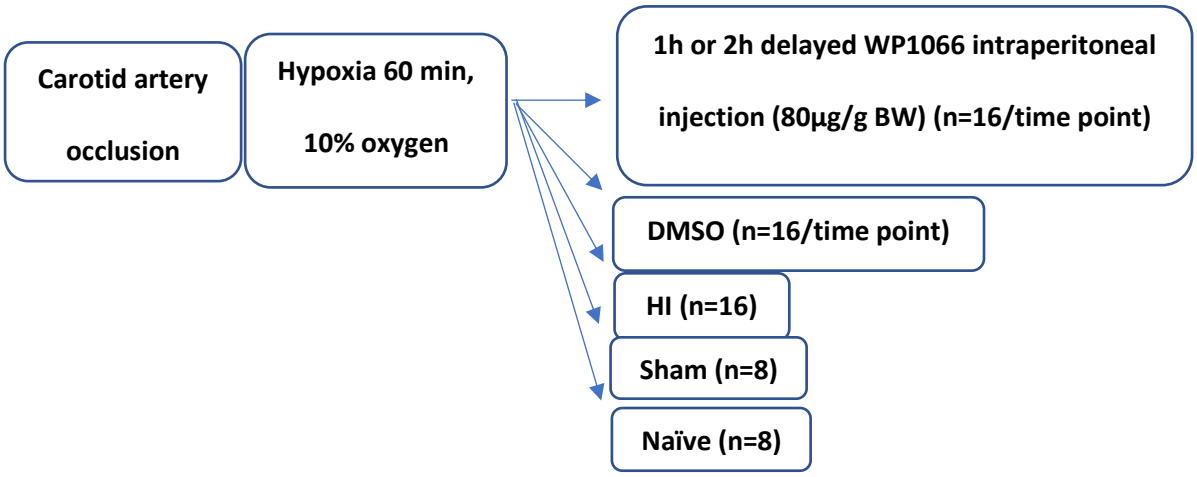

Figure 26. **Schematic representation of the experimental groups treated with either WP1066 or DMSO 1 or 2h after HI brain damage, as well as their controls (untreated HI, naïve and sham).**

3.3.14 Immunohistochemical analysis

In a clinical setting, when neonatal HI occurs, immediate treatment is not always feasible or possible. Therefore, we assessed whether the neuroprotective effects of 80µg/g WP1066 application would be maintained in the case of a delayed administration, 1h or 2h after HI insult. IHC analysis demonstrated that 48h after 1h delayed application of 80µg/g WP1066, cell death was significantly decreased compared to untreated HI and DMSO treated controls in the cortex, striatum and external capsule and in the pyriform cortex and overall in all brain regions assessed ($p<0.05$, Kruskal-Wallis test with Dunn's test, Figure 27A). Similar neuroprotective effect was observed in all the brain regions assessed compared to untreated HI and DMSO treated control groups at 2h delayed WP1066 application ($p<0.05$, Kruskal-Wallis test with Dunn's test, Figure 27E). In terms of microglial activation, assessed through alphaM immunoreactivity, 1h delayed WP1066 application significantly reduced microglial activation compared to both untreated HI and DMSO treated littermates in cortex, pyriform cortex, hippocampus, striatum, external capsule and overall ($p<0.05$, Kruskal-Wallis test with Dunn's test, Figure 27B). Furthermore, 2h delayed WP1066 application reduced microglial activation, specifically in the striatum, thalamus and external capsule compared to DMSO treated controls and in hippocampus, striatum, thalamus, external capsule and in all brain regions assessed compared to untreated HI littermates ($p<0.05$ Kruskal-Wallis test with Dunn's post-hoc, Figure 27F). WP1066 application reduced astroglial activation if applied after a delay of 1h or 2h post-HI, compared to untreated HI controls (Figure 27C, G). Specifically, GFAP immunoreactivity was decreased in in pyriform cortex, hippocampus, external capsule, striatum and overall following 1h delayed WP1066

application when compared to DMSO treated control group, and in all brain regions assessed when compared to untreated HI littermates (Figure 27C). A significant decrease in astroglial activation was observed in pyriform cortex, thalamus, striatum, external capsule and overall in animals treated with WP1066 at 2h compared to untreated HI and DMSO treated controls ($p<0.05$, Kruskal-Wallis test with Dunn's post-hoc, Figure 27G)

Delayed WP1066 application (at 1 or 2h post-HI) reduced the levels of volume loss assessed through Cresyl Violet staining (Figure 27D, H). Specifically, 1h delayed WP1066 application reduced tissue loss in cortex, pyriform cortex, striatum, hippocampus, external capsule and in all brain regions assessed when compared to untreated HI and DMSO treated control groups ($p<0.05$, Kruskal-Wallis test with Dunn's post-hoc, Figure 27D), while 2h delayed WP1066 application decreased volume loss in hippocampus and overall compared to untreated HI controls and in striatum, thalamus and external capsule compared to DMSO treated control littermates ($p<0.05$, Kruskal-Wallis test with Dunn's post-hoc, Figure 27H).

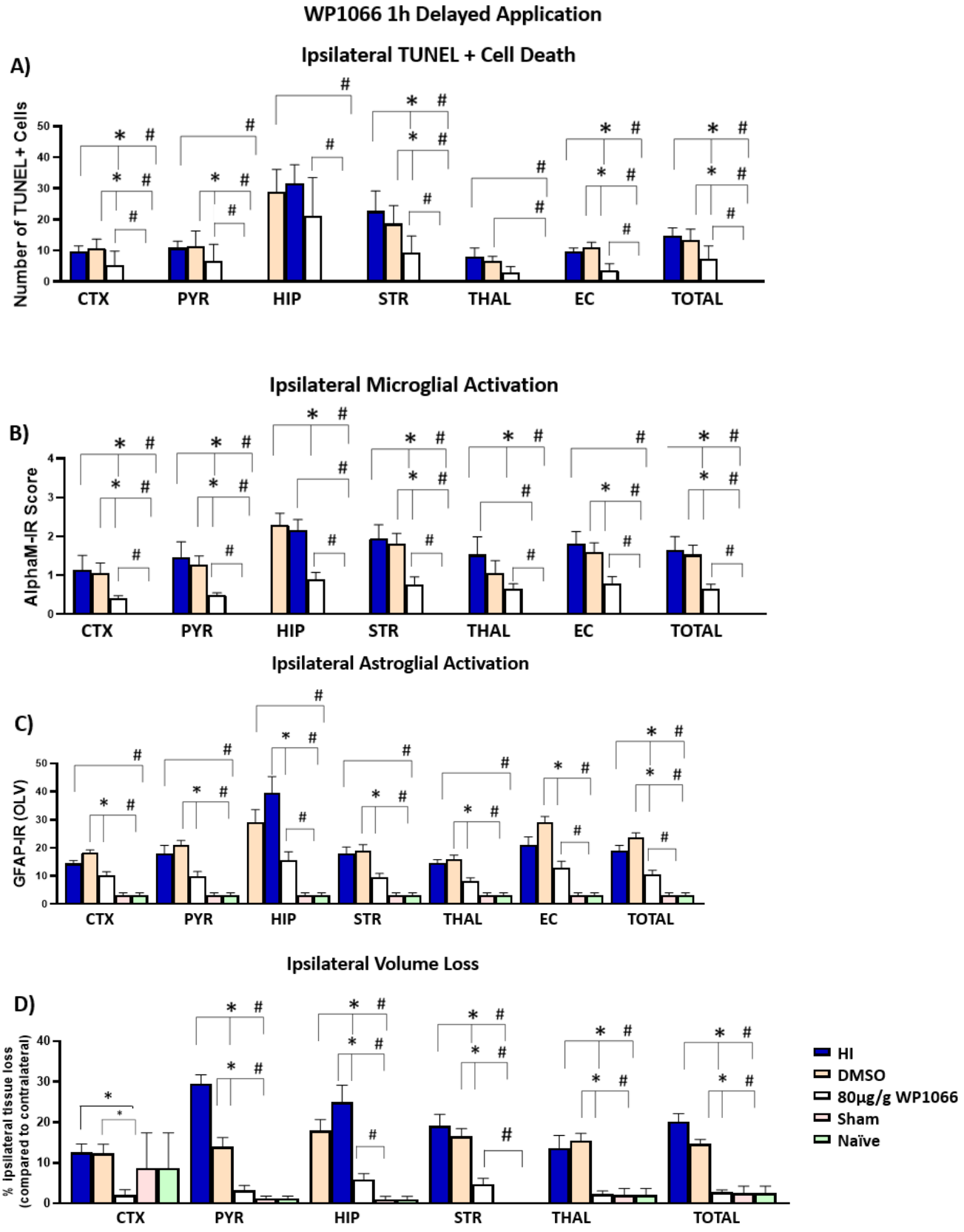
WP1066 1h Delayed Application
A)
Ipsilateral TUNEL + Cell Death
Number of TUNEL+ Cells
CTX
PYR
HIP
STR
THAL
EC
TOTAL
B)
Ipsilateral Microglial Activation
AlphaM-IR Score
C)
Ipsilateral Astroglial Activation
GFAP-IR (OLV)
D)
Ipsilateral Volume Loss
% Ipsilateral tissue loss (compared to contralateral)
HI
DMSO
80µg/g WP1066
Sham
Naïve

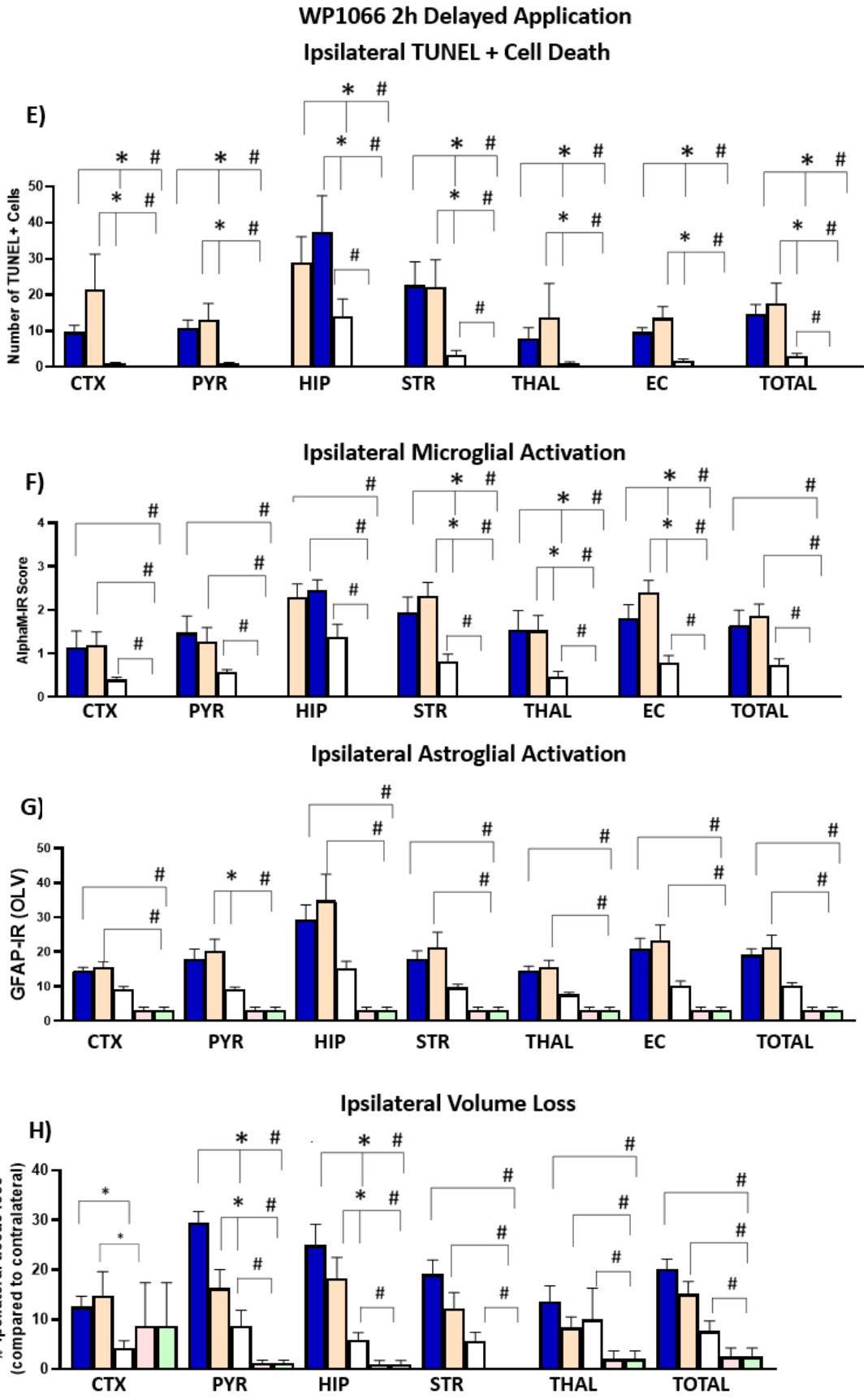
WP1066 2h Delayed Application
Ipsilateral TUNEL + Cell Death
E)
Number of TUNEL+ Cells
CTX
PYR
HIP
STR
THAL
EC
TOTAL
Ipsilateral Microglial Activation
F)
AlphaM-IR Score
Ipsilateral Astroglial Activation
G)
GFAP-IR (OLV)
Ipsilateral Volume Loss
H)
% Ipsilateral tissue loss
(compared to contralateral)

Figure 27. **Effects of a delayed 1 or 2h post-HI intraperitoneal WP1066 application.** A. 1h delayed intraperitoneal application of 80µg/g WP1066 significantly reduced TUNEL+ cell death in cortex (p=0.036), pyriform cortex (p=0.001), striatum (p=0.003), external capsule (p=0.02), and overall in the forebrain (p=0.002) compared to untreated HI controls, and in cortex (p=0.001), striatum (p=0.03) and external capsule (p=0.001) compared to DMSO treated controls (Kruskal-Wallis test with Dunn's post-hoc correction), WP1066 80µg/ g (white) (n=16), DMSO (orange) (n=16) or HI (blue) (n=16), sham (pink) (n=8), naïve (green) (n=8), B. Delayed application of WP1066 at 1h after HI reduces microglial activation assessed through alphaM immunoreactivity in cortex (p=0.028), pyriform cortex (p=0.01), hippocampus (p=0.0001), striatum (p=0.03), external capsule (p=0.001) and in all brain regions assessed (p=0.001) compared to untreated HI control littermates and the in the cortex (p=0.02), pyriform cortex (p=0.001), striatum (p=0.02), external capsule (p=0.032) and overall (p=0.001) compared to DMSO treated littermates (Kruskal-Wallis test with Dunn's post-hoc). C. Delayed application of 80µg/g WP1066 at 1h after HI insult reduced reactive astrogliosis visualised through GFAP OLV overall in the brain regions assessed (p=0.01) compared to untreated HI controls and in pyriform cortex (p=0.001), hippocampus (p=0.02), striatum (p=0.001), external capsule (p=0.001) and overall (p=0.002) compared to DMSO treated littermates (Kruskal-Wallis test with Dunn's post-hoc). D. Quantitative analysis of percentage of tissue loss assessed via Nissl staining showed that delayed WP1066 application at 1h post-HI significantly reduced tissue loss in cortex (p=0.001), pyriform cortex (p=0.002), striatum (p=0.0034), hippocampus (p=0.002), thalamus (p=0.001) and overall (p=0.001) compared to untreated HI and DMSO treated control groups ($p<0.05$, Kruskal-Wallis test with Dunn's post-hoc). E. Delayed WP1066 application at 2h after HI insult significantly reduced the number of TUNEL+ dying cells compared to untreated HI and DMSO treated controls in cortex (p=0.0064 and p=0.003, respectively), pyriform cortex (p=0.04 and p=0.013 respectively), hippocampus (p=0.003 and p=0.002 respectively), striatum (p=0.0001), thalamus (p=0.0001), external capsule (p=0.02, p=0.001) and in all the brain regions assessed (p=0.001 and p=0.012 respectively) (Kruskal-Wallis test with Dunn's post-hoc) F. Delayed WP1066 application at 2h

after HI insult significantly reduced microglial activation compared to untreated HI controls in striatum (p=0.002), thalamus (p=0.01), external capsule (p=0.006) and overall (p=0.004). AlphaM score was also significantly reduced by delayed WP1066 application at 2h post-HI compared to DMSO treated littermates in striatum (p=0.002), thalamus (p=0.001) and external capsule (p=0.002) (Kruskal-Wallis test, with Dunn's post-hoc). G. Delayed WP1066 application at 2h post-HI reduced astroglial activation compared to untreated HI in striatum (p=0.006), thalamus (p=0.002), external capsule (p=0.001) and overall (p=0.002), and in pyriform cortex compared to DMSO treated controls (p=0.02) ($p<0.02$, Kruskal-Wallis test with Dunn's post-hoc). H. Delayed application of WP1066 at 2h HI insult significantly reduced tissue loss in all the brain regions compared to untreated HI controls (p=0.001), and in cortex (p=0.03), pyriform cortex (p=0.01) and hippocampus (p=0.002) compared to DMSO treated littermates (Kruskal-Wallis test with Dunn's post-hoc). An increase in all the markers assessed was observed in cortex, pyriform cortex, striatum, external capsule, hippocampus, thalamus, and overall of WP1066 80µg/g treated group compared to naïve and sham controls (p=0.0001) (*$p<0.05$, # significant difference compared sham and naïve control groups, $p<0.05$). CTX – cortex, PYR – pyriform cortex, HIP – hippocampus, STR – striatum, THAL -thalamus, EC – external capsule, Total - Average of all brain regions assessed).

3.3.15 Behavioural assessments

The negative geotaxis test allowed the assessment of reflexes and coordination of P11 mice. Delayed intraperitoneal administration of 80µg/g WP1066 in DMSO at 1h or 2h after the HI insult significantly improved behavioural outcomes at 48h compared to untreated HI and DMSO control littermates. The Kruskal–Wallis test showed significant differences in the mean-time in seconds between treatment groups ($p<0.05$). Dunn's multiple comparisons test showed significant decrease of the time

necessary for change of orientation in the group treated with delayed WP1066 application (1 or 2h post-HI) compared to the untreated HI and DMSO treated groups ($p<0.05$, Figure 28).

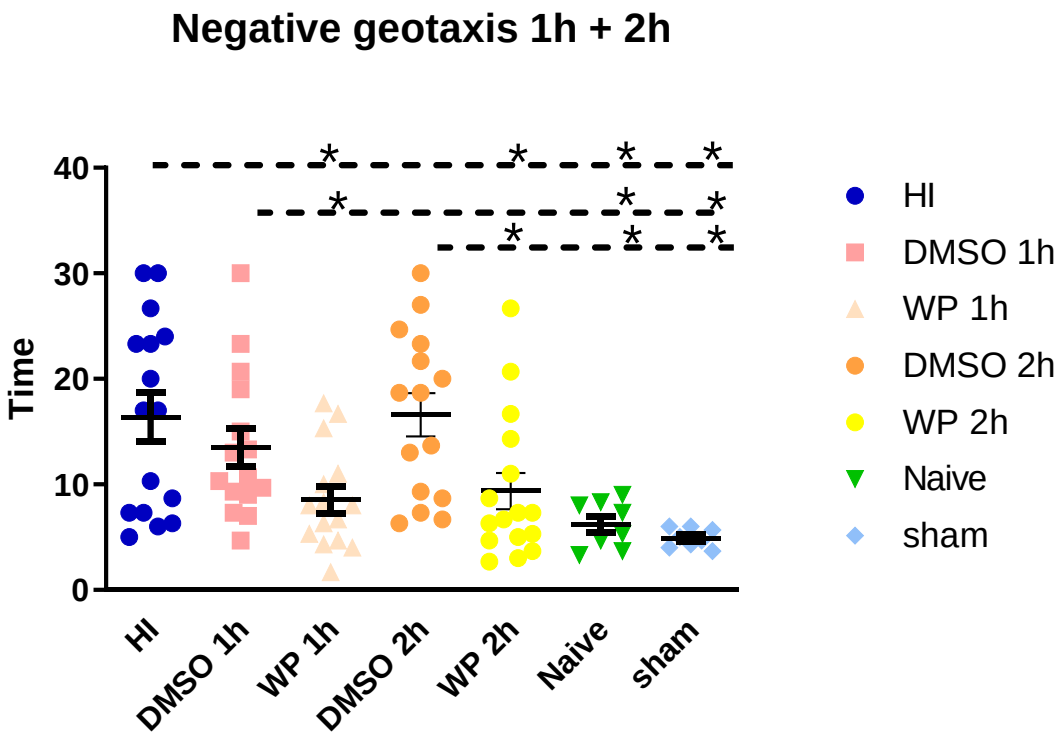

Figure 28. **Negative geotaxis test shows neuroprotective role of delayed intraperitoneal application of 80µg/g WP1066 at 1 or 2h after HI insult.** A-B. Delayed 80µg/g WP1066 application at 1h and 2h after HI insult reduced the reflex time in geotaxis reflex at P11 assessed using Kruskal-Wallis test with Dunn's post-hoc. All data presented as median and interquartile range. HI (n=16), DMSO (n=16), WP1066 (n=16), naïve (n=8), sham (n=8), *p<0.05.

Chapter 4: Discussion on WP1066 treatment

STAT3 is strongly upregulated after HI insult and targeted pharmacological inhibition of its expression with WP1066, a JAK-2 inhibitor could provide neuroprotective effect. Therefore, this study focuses on identifying the effect of WP1066 in neonatal HI damage. WP1066 was dissolved in DMSO, a common solvent used in preclinical studies, and the neuroprotective effects of three different doses of WP1066 were assessed in the P9 HI animal model, applying 40µg/g, 80µg/g and 160µg/g BW, respectively. The optimal dose after immediate application post-HI insult was investigated.

The current study supports previous work carried out by our group which determined the effect of combined 20 min pre-insult and immediate post-insult blockade of JAK2 with systemically applied WP1066 in a split dose of 80µg/g[181]. Specifically, pharmacological interference with WP1066 provided a protective effect similar to that observed in the neuron- and astroglia-specific STAT3 knock-out mice, but to a more moderate degree, where treatment with the inhibitor, significantly reduced pSTAT3 Y705 phosphorylation in cortex and hippocampus at 1h post-HI, as well as astro- and microglial activation at 48h post-HI[181]. However, this neuroprotective effect was weak and did not lead to a statistically significant reduction in brain tissue loss. Subsequently, the current research project investigates the effects of WP1066 treatment immediately after HI insult. The results demonstrated that immediate intraperitoneal post-HI application of 80µg/g BW WP1066 provides neuroprotection through reduction of brain tissue loss, cell death, microglial and astroglial activation in the most affected brain regions after HI insult in a P9 mouse model (Figure 15). However, the lower and higher doses of 40µg/g and 160µg/g BW respectively, did not

provide any neuroprotective effect but interestingly increased the damage as indicated by elevated cell death and tissue loss markers (Supplementary Figure 1).

Furthermore, this current study confirms that DMSO does not contribute to the neurological outcomes as no significant change was observed in tissue loss, cell death, microglial and astroglial activation between the untreated HI and DMSO treated groups ($p>0.05$, Figure 15). There seems to be a trend towards an increase in some of the experiments in the DMSO treated group compared to the HI group, however these differences do not reach significant values. Nevertheless, in the same set up we observe significant decrease in the WP1066 treated groups compared to the DMSO and/or HI groups, suggesting a protective effect of WP1066, therefore DMSO group was compared versus WP1066 treated group.

The current results are in line with other studies where WP1066 exhibited neuroprotective effects[172,266,267]. In particular, WP1066 demonstrated inhibitory effects on JAK2-mediated signalling and decreased infract volume and pSTAT3 levels in a rat model of focal cerebral ischaemia[268]. Moreover, WP1066 improved the degree of recovery of vestibular motor function and increased the levels of GABA-A receptor in a mouse model of traumatic brain injury[267]. In a status epilepticus rat model Grabenstatter and colleagues (2015) showed that WP1066 effectively reduced STAT3 phosphorylation in the dentate gyrus of hippocampus, as well as STAT3-targeted genes such as c-myc, ICER, cyclin D1, Bcl-xl and mcl-1[266]. In the same study, WP1066 reduced the severity of chronic epilepsy as shown in aEEG diagram but did not reduce cell death in hippocampus.

Increased levels of microglial IL-6 following neonatal HI-injury correlate with increase in pSTAT3 + astrocytes[31]. Interestingly, WP1066 strongly inhibits microglial IL-6

production[269], which in the current study could contribute to the reduction in reactive astrogliosis after 80µg/g BW WP1066 treatment.

Our results also indicate the dose-dependent efficacy of WP1066. Application of WP1066 at 80µg/g BW exerts neuroprotective effect. Interestingly, immediate application of a lower dose of WP1066 at 40µg/g post-HI increased tissue loss and cell death and a similar observation was made for a high dose of 160µg/g, which also upregulated tissue loss (Supplementary Figure 1), which may be attributed to hermetic properties of WP1066. This indicates a specific dose window for WP1066 application in the context of neuroprotection and will need consideration in different model species and for clinical translation.

Previous study from our lab demonstrated that pre- and post-HI split dose of 80µg/g BW WP1066 application reduced the protein levels of phosphorylated STAT3 Y705 in both cortex and hippocampus[181]. In line with this data, in the current study, a significant reduction was observed in the protein levels of phosphorylated STAT3 Y705 in the ipsilateral hippocampus of 80µg/g BW WP1066 treated animals post-HI (Figure 18A), compared with DMSO treated littermates, but not when compared with untreated HI controls. Detrimental effects of DMSO treatment have previously been reported[270] and our results suggest that DMSO treatment may increase levels of STAT3 Y705, possible reflective of harmful effects of DMSO, which is counteracted by the application of WP1066 (Figure 18A). Effects of WP1066 on protein levels of STAT3 S727, total STAT3 and STAT1 in cortex were not statistically significant at 1h post-HI and this was expected as WP1066 inhibits only the Tyr705 phosphorylation site of STAT3[181] (Figure 18B, Figure 19). Therefore, we could conclude that WP1066 does not interfere with the Ser727 STAT3 phosphorylation site, total STAT3 and STAT1 levels.

Moreover, at 1h post-HI some changes were observed for PHB levels, a multifaceted protein with key roles in mitochondrial housekeeping, cell survival and apoptosis[271,272]. PHB acts as a scaffold protein in mitochondria, regulates mitochondrial dynamics and plays important roles in stress responses[271]. In the current study, some increase (albeit not statistically significant) in PHB protein levels was observed in the ipsilateral hippocampus of the WP1066 treated compared with DMSO treated controls (Figure 18C) and may be indicative of some protective effects on mitochondria in response to WP1066 treatment. This is similar to findings in a previous study assessing neuroprotective effects of curcumin in the neonatal HIE model, where a trend in increased PHB protein expression was observed in the ipsilateral side[255]. Furthermore, increased neural expression of PHB has been found to be related to neuroprotection in a focal cerebral ischaemia mouse model[256] and to reduce free radical production by mitochondria, protecting brain cells from injury[256]. It must be noted that in the current study the hippocampus was only assessed at 1h post-HI and further time points should be investigated for PHB protein modulation by WP1066 to fully understand effects on PHB in neuroprotection in this model. In the current study, we did not observe any significant differences between the β-actin levels along all the experimental groups and markers. However, normalisation to the total protein could be considered for future research as HI might have an effect on β-actin levels.

In the current study, we tested the effects of immediate intraperitoneal 80µg/g BW WP1066 application on cytokine levels and genes involved in HI. Interestingly, we did not observe any changes on cytokine levels of IL-6, IL-1b, IL-12/IL-23, nor at IL-6 gene levels (Figure 20), all which are downstream molecular targets of the STAT3 pathway. Therefore, based on the current findings, we can conclude that WP1066 is a specific inhibitor of the STAT3 Tyr705 phosphorylation site and has no significant effect on the

feedback loop of the pathway where we would expect to have an effect on the cytokines involved. On the other hand, immediate application of WP1066 increased the levels of the CD206 anti-inflammatory gene (Figure 21B). This correlates with the immunofluorescence results presented in this study showing that WP1066 treatment increased the levels of CD206+ cells (Figure 17). Thus, we can assume that immediate WP1066 application after HI insult may exhibit its protective effects via increasing the anti-inflammatory levels of CD206 resulting in induced repair.

Several studies have shown the contribution of the classical complement pathway to HI brain injury[160,273]. In line with those studies, we observed a significant reduction in C1qa gene levels in hippocampus of WP1066 treated animals compared to DMSO treated controls (Figure 22A), while no changes were seen for C1qb and C1qc levels. Our results are in line with the study of Vadim and colleagues (2005) where deletion of C1qa gene in C57Bl/6 mice that underwent HI at P7 led to significantly decreased activation of circulating neutrophils associated with diminished local accumulation and attenuation of brain injury[274]. Remarkably, this is the first study to provide evidence of WP1066's role on the complement system and potential neuroprotective effects via this pathway.

Interestingly, WP1066 treatment resulted in neuroprotection even if applied with a delay of 1 or 2h post-HI by reducing glial activation, tissue loss and cell death (Figure 27). This result is particularly relevant for clinical application as the immediate administration of treatment after neonatal HI is challenging and not always possible, including the western and the developing world. Negative geotaxis test, which is a measurement for motor coordination and labyrinth reflex, also showed a significant decrease in the reflex time of animals treated with WP1066 1 or 2h post-HI insult.

WP1066 application provided long-term neuroprotection (36 days post-HI), as shown in P36 male and female mice, with a significant reduction of brain tissue loss compared to untreated HI and DMSO treated controls (Figure 24A-C). Similarly, untreated HI and DMSO treated controls significantly decrease MBP levels in P36 females in the striatum and external capsule in comparison to WP1066 (80 µg/g BW) application and in males' external capsule (Figure 24D-F). Behavioural tests exploring motor skills, and memory were performed at P28, P35 and P36 using the slipping test and NOR tests. Both assessments showed improvement of motor and memory skills following WP1066 (80 µg/g BW) application immediately after HI (Figure 25), thus expressing beneficial effects on cognitive damages generated by the HI insult. Many studies have indeed reported that HI injured rodents show impairments in auditory and memory/learning processing[275–277]. Considering this, NOR tests were performed in the current study to examine short-term (at P35) and long-term memory (at P36) (Figure 25D-I). Interestingly, male animals treated with WP1066 (80 µg/g BW) immediate post-HI showed improved short- and long-term memory compared to untreated HI littermates, while no changes were observed in females short- and long-term memory. In clinical settings, HI brain injury appears to have more severe consequences for males rather than females[278], due to the interplay between hormonal modulation and genetically determined apoptotic mechanisms protecting females to a degree against HI[279]. Therefore, it is not surprising that a memory improvement was observed in male mice, as these will show a higher level of injury. NOR behavioural tasks explore the functionality of a working memory in the mouse but from a slightly different perspective[280,281]. The recognition of novelty in the NOR test is dependent on the hippocampal connections with the perirhinal cortex[281,282]. It is, therefore, possible to

speculate that the ability of WP1066 in improvement of long-term memory is due to the improvement of hippocampal memory.

Overall, the data from the current study suggests a critical role for STAT3, including possibly also a contribution to neonatal HI-brain damage via Tyr705 phosphorylation.

Chapter 5: Effects of curcumin application in DMSO solution, in a P9 HI mouse model

5.1 AIMS

We have previously shown that curcumin provides neuroprotection when administered in a P7 HI mouse model, corresponding to slightly pre-term human brain development[255]. Therefore, in this current study we hypothesise that curcumin therapy will be neuroprotective in a P9 neonatal HI mouse model, corresponding to term human brain development, based on the well documented anti-oxidant, and anti-inflammatory properties of this natural compound.

To test this hypothesis, we investigated the neuroprotective effects of i.p. administered curcumin dissolved in DMSO, on glial response, tissue loss, and cell death in HI brain damage via immunohistochemical analysis and developed a controlled drug delivery system for curcumin by encapsulation in Poly(3-Hydroxybutyrate) microspheres, for intranasal application in HI.

5.2 Methods

All ethical approvals were obtained, and the neonatal HI model, brain extraction, and IHC analysis and statistics were performed as explained in Chapter 2.

5.2.1 Pharmacological Treatment

After the induction of HI insult, the pups were immediately treated with an intraperitoneal injection of curcumin dissolved in 0.5ul 100% DMSO at a dosage of 200µg/g BW. Additionally, for controlled curcumin delivery with Poly(3-Hydroxybutyrate) microspheres, animals received intranasal delivery of 66µg/g BW encapsulated curcumin.

5.3 Results

5.3.1 Immediate post-HI intraperitoneal application of 200µg/g BW curcumin in DMSO is neuroprotective

Intraperitoneal injection of 200µg/g curcumin dissolved in DMSO, applied immediately after the HI insult, reduced all brain damage markers assessed, thus signifying neuroprotection (Figure 29). Curcumin treatment reduced cell death overall in all brain regions assessed (Kruskal-Wallis test, with Dunn's post-hoc $p<0.05$), and in cortex, pyriform cortex, striatum, thalamus, and external capsule, compared to DMSO treated and untreated HI control animals ($p<0.05$) (Figure 29A).

In addition, the immediate i.p. curcumin post-HI application triggered a significant reduction in both ipsilateral astroglial and microglial activation, as assessed through GFAP and alphaM immunoreactivity, respectively. Microglial activation was significantly reduced after immediate post-HI intraperitoneal curcumin application in hippocampus, compared to DMSO treated animals ($p=0.001$); and in hippocampus and external capsule ($p=0.01$), compared to untreated HI controls (Figure 29B). Similarly, astroglial activation was also downregulated after immediate post-HI curcumin application in cortex ($p=0.001$) and in hippocampus ($p<0.01$), compared to untreated HI control animals; and in hippocampus, striatum and overall forebrain ($p<0.05$), when compared to DMSO treated littermates (Figure 29C). Furthermore, GFAP immunoreactivity was significantly decreased in contralateral hippocampus of the curcumin treated animals compared to DMSO treated controls ($p=0.004$, Kruskal-Wallis test with Dunn's post-hoc) (Figure 29E).

Similarly, compared to untreated HI and DMSO treated control littermates, curcumin treated animals showed a reduction in overall brain infraction volume (Kruskal-Wallis test with Dunn's post-hoc, $p<0.01$), as well as in infarction volume of all the specific brain regions of interest (Figure 29D).

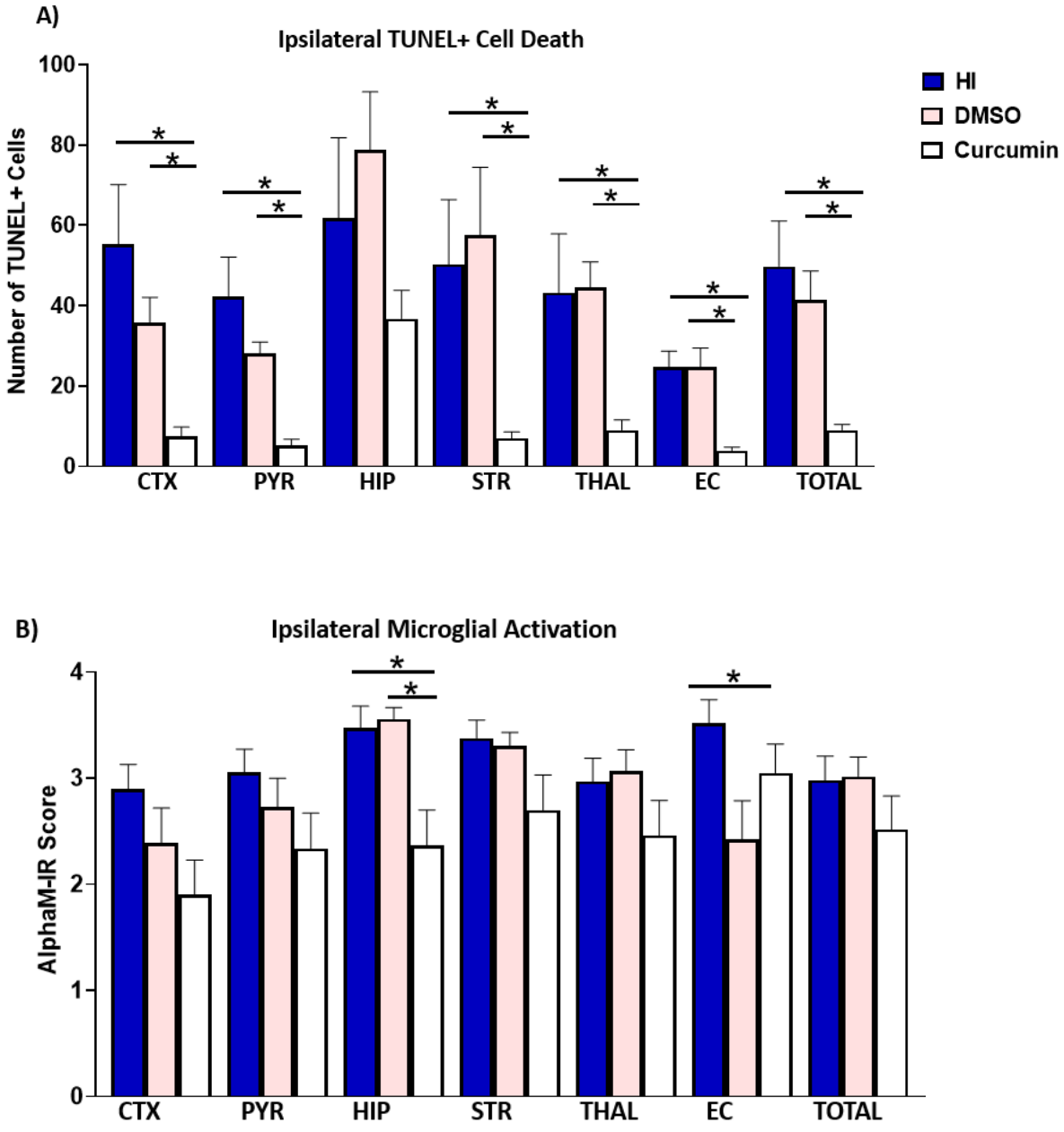

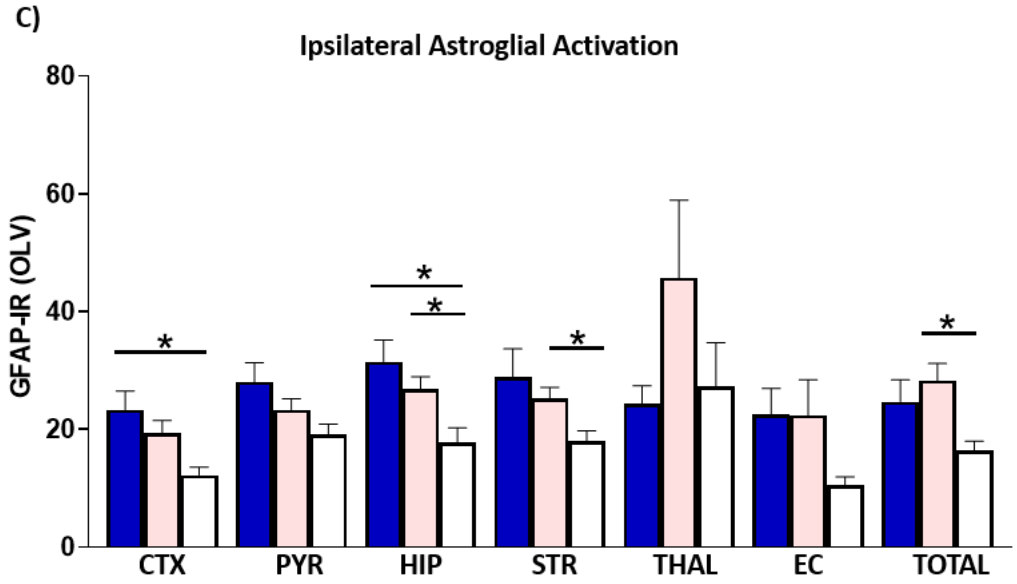
C)
Ipsilateral Astroglial Activation
GFAP-IR (OLV)
80
60
40
20
0
CTX
PYR
HIP
STR
THAL
EC
TOTAL

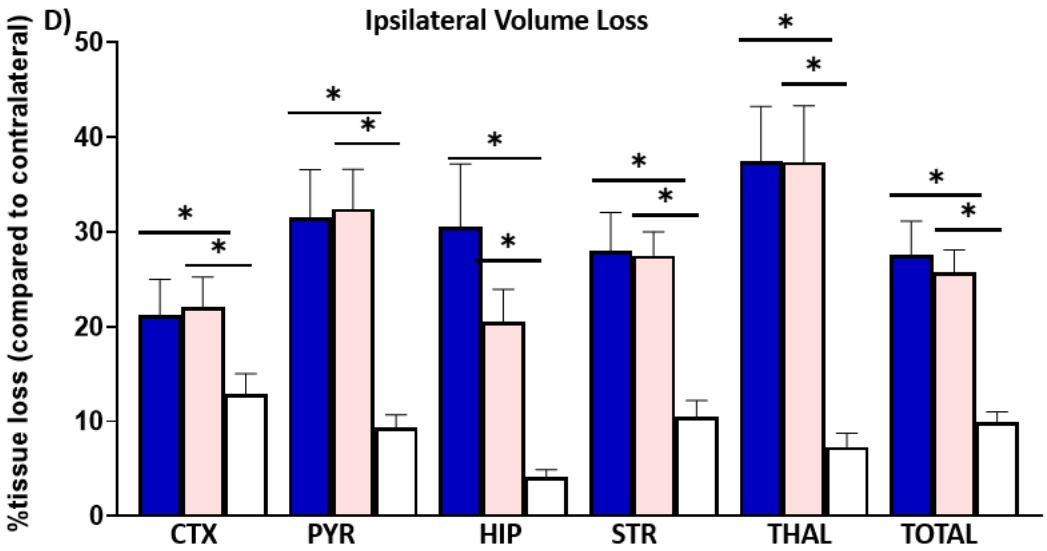
D)
Ipsilateral Volume Loss
%tissue loss (compared to contralateral)
50
40
30
20
10
0
CTX
PYR
HIP
STR
THAL
TOTAL

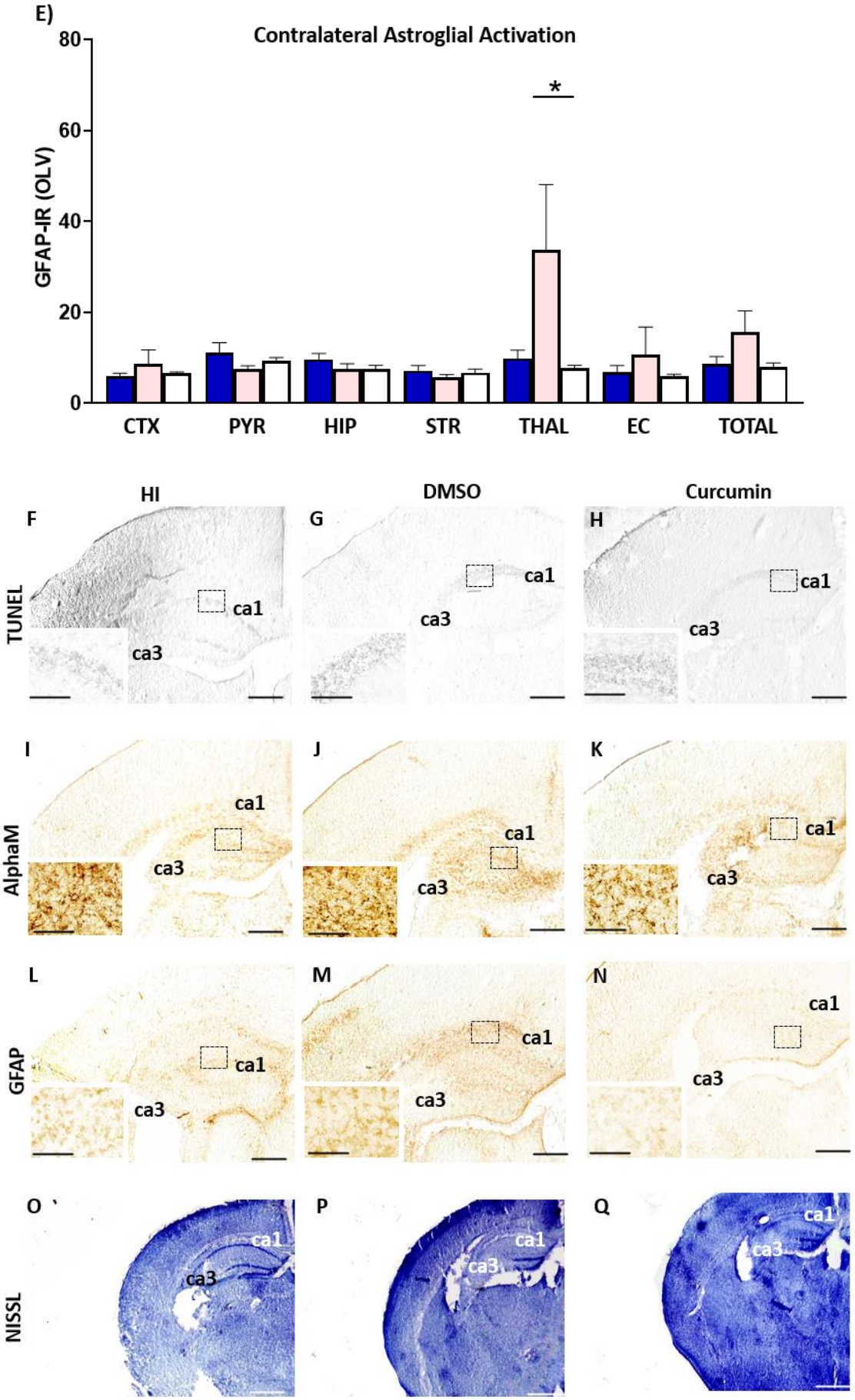
E)
Contralateral Astroglial Activation
GFAP-IR (OLV)
80
60
40
20
0
*
CTX
PYR
HIP
STR
THAL
EC
TOTAL
HI
DMSO
Curcumin
F
G
H
TUNEL
ca1
ca3
I
J
K
AlphaM
L
M
N
GFAP
O
P
Q
NISSL

Figure 29. **Neuroprotective effects of immediate intraperitoneal post-HI 200µg/g BW curcumin application at 48h.** A. Quantitative analysis of TUNEL+ cells in the ipsilateral hemisphere after HI damage (n=15), compared with curcumin (n=15) or DMSO (n=15) control treatment. The reduction of TUNEL+ cells was significant (Kruskal-Wallis test with Dunn's post-hoc) in cortex (p=0.0008), pyriform cortex (p=0.0001), striatum (p=0.002), thalamus (p=0.007), external capsule (p=0.0005), and overall brain (p=0.0003) in the animals treated with curcumin (white) compared to DMSO (pink) treated controls and untreated HI (blue) control animals**.** B. Semi-quantitative score of microglial activation (alphaM immunoreactivity) after HI brain damage and immediate intraperitoneal curcumin or DMSO treatment, reduced microglial activation in curcumin treated animals compared to DMSO controls, in hippocampus (p=0.001), and compared to HI control animals, showing a significant reduction in hippocampus (p=0.01), and external capsule (p=0.01). C. Astroglial activation measured through GFAP OLVs in the ipsilateral hemisphere after treatment with curcumin or DMSO only, in HI animals. A significant reduction of GFAP immunoreactivity was observed in cortex (p=0.001) and hippocampus (p=0.002) after curcumin treatment compared to untreated HI control animals, and compared to hippocampus (p=0.005), striatum (p=0.005) and overall brain (p=0.0006), when compared to the DMSO treated control littermates. D. Percentage tissue volume loss due to HI insult on the ipsilateral side following immediate post-HI treatment with 200µg/g BW of curcumin, DMSO or untreated HI is shown. Significant reduction following curcumin treatment was observed in pyriform cortex (p=0.0001), hippocampus (p=0.0001), striatum (p=0.0005), thalamus (p=0.001) as well as in overall forebrain (p=0.001, Kruskal-Wallis test with Dunn's post-hoc) compared to both DMSO treated and untreated HI group. E. Significant reduction of contralateral astroglial activation following curcumin treatment was observed in hippocampus (p=0.004, Kruskal-Wallis test with Dunn's post-hoc) compared to the DMSO treated group. F-H. Ipsilateral overview of TUNEL stained brain sections of untreated HI controls, (F) animals treated with curcumin (H) or DMSO treated littermates (G). The inserts in F, G (untreated HI and DMSO treated brains respectively) show at high magnification the pyknotic nuclei typical of dying cells, which are not observable in H (curcumin

treated group). I-K. Low magnification images of brain sections, showing the reduction in alphaM (microglial marker) immunoreactivity in the curcumin treated (K) compared to the DMSO treated (J) and untreated HI groups (I). The inserts in I and J show the typical morphology of activated microglial cells with a phagocytic phenotype, while insert K illustrates the phenotype of normal ramified microglia. L-N. Ipsilateral images representing the reduction in GFAP immunoreactivity in brains of curcumin treated animals (N) compared to DMSO treated (M) and untreated HI control littermates (L). The inserts at high magnification in K and L highlight the presence of activated astroglial cells, which are not detectable in the insert (N). O-Q. Overview of ipsilateral hemispheres stained with Cresyl Violet for Nissl bodies, showing less tissue loss in brains of curcumin treated animals (Q) compared to brains of DMSO treated (P) and untreated HI littermate controls (O). Scale bars represent 400µm in all low magnification figures and 62µm in the magnified inserts. CTX – cortex, PYR – pyriform cortex, HIP – hippocampus, STR – striatum, THAL -thalamus, EC – external capsule, Total - Average of all brain regions.

Furthermore, our results confirm that curcumin also provides neuroprotection by significantly reducing iNOS oxidative stress, in P9 mice, as seen in Figure 30. Application of 200µg/g BW of curcumin immediately post-HI, reduced the number of iNOS+ cells (p value =0.0023, Kruskal-Wallis test with Dunn's post-hoc), when directly compared to brains of the untreated HI control group. Additionally, there was a significant downregulation in the number of iNOS+ cells (p=0.0024, Kruskal-Wallis test with Dunn's post-hoc), when comparing brains from curcumin treated to those of the DMSO treated controls (Figure 30B). No significant differences were found between the DMSO treated control group and the HI non treatment group (p>0.05, Kruskal-Wallis test with Dunn's post-hoc), as shown in Figure 30.

We further assessed effects of curcumin treatment on levels of myelination, and our data did not show statistically significant difference in the curcumin treated group compared to the DMSO treated control group, or the untreated HI group, in either external capsule or striatum (p>0.05, Kruskal-Wallis test with Dunn's post-hoc, Figure 30A).

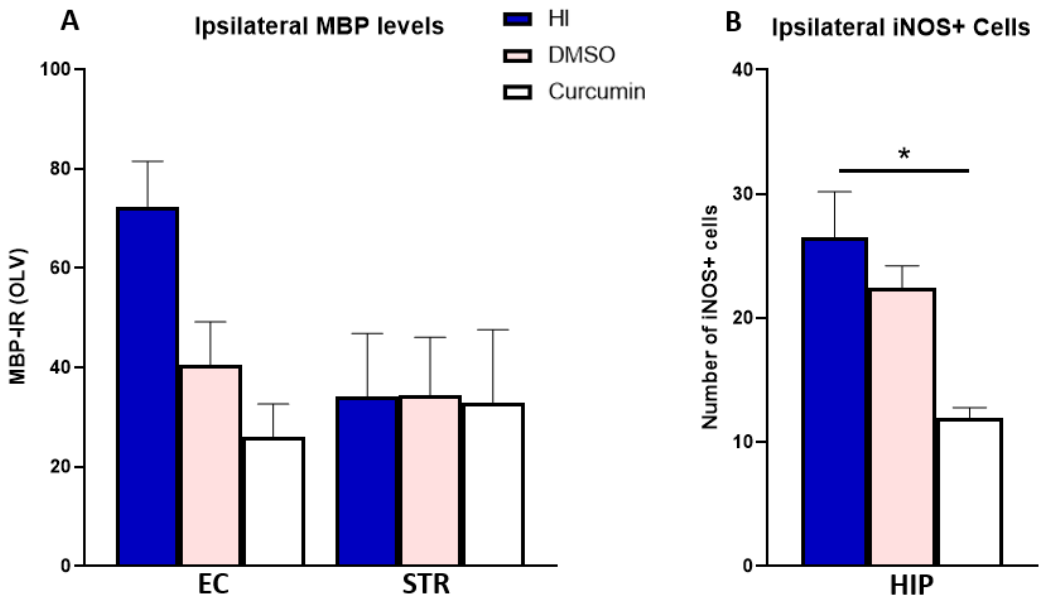

Figure 30. **Effects of immediate intraperitoneal post-HI application of 200µg/g BW curcumin on myelination and iNOS+ cells.** A. Myelination measured through MBP OLVs in the ipsilateral hemisphere after treatment with curcumin or DMSO in HI animals. No significant changes were observed after curcumin treatment (p>0.05, Kruskal-Wallis test with Dunn's post-hoc). B. Quantitative analysis of iNOS+ cells after immediate post-HI curcumin application compared to untreated HI control animals, showing a significant reduction in hippocampus (p=0.001, Kruskal-Wallis test with Dunn's post-hoc). Abbreviations: EC: external capsule, STR: striatum, HIP: hippocampus

Chapter 6: Effects of curcumin P(3HB) encapsulated microspheres application in a P9 HI mouse model

6.1 Synthesis of Poly(3-Hydroxybutyrate) Microspheres P(3HB) microspheres with encapsulated Curcumin

Poly(3-hydroxybutyrate)-Hyaluronic Acid biopolymers with encapsulated curcumin were created and provided by Prof Ipsita Roy's Research Group. Firstly, (3HB) solution of 0.65 % w/v was prepared in chloroform (CHCl3) and Polyvinyl Alcohol (PVA) solution. Curcumin was added in the polymer solution, dissolved and added to PVA. The particles were then collected by centrifuging the emulsion, washed by suspension in 10% of ethanol. The particles were then ultimately suspended in distilled water (40 ml) and again centrifuged 500 ul of 50mg/ml trehalose dehydrogenase were then added. Finally, the particles were frozen at -20 ^{o}C and then transferred to a freeze dryer for 1-2 days.

6.2 Surface morphology and particle size analysis

The surface morphology and size distribution of the microspheres was assessed and imaged using SEM (FEI XL30 FEG Scanning Electron Microscope (FEI, Eindhoven, Netherlands)), at Eastman Dental Institute, UCL, UK. Image J software was used to quantify particle distribution using images captured using SEM. The images were appropriated to suitable thresholds and the analysis was calibrated using pixel to scale bar. As demonstrated in Figure 31B, the biopolymer microsphere encapsulated curcumin for a delayed release upon degradation of the biopolymer and featured an outer layer of curcumin for a more immediate release upon administration. Figure 32

shows an SEM image of curcumin loaded biopolymers, and a theoretical mock-up of the two-step drug release.

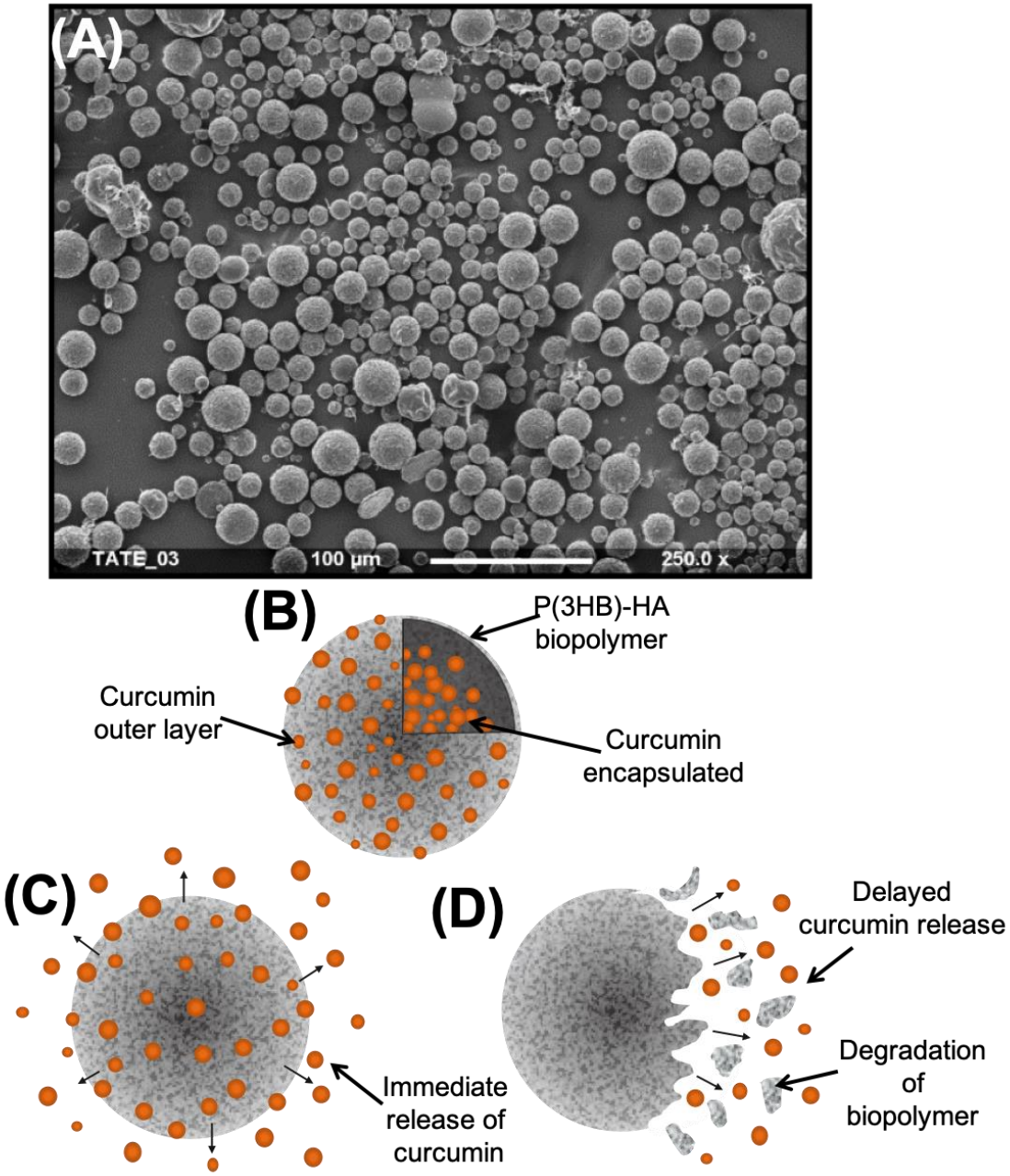

Figure 31. **Schematic representation of P(H3B)-HA biopolymers**. A. A scanning electron microscope image of Poly(3-hydroxybutyrate) biopolymer encapsulated curcumin, created by Prof Ipsita Roy's Research Group. Polyhydroxyaklanoates (PHA) are a type of biodegradable polymer, synthesised by bacteria during fermentation under conditions with excess carbon and nutrient limitations[283]. Hyaluronic acid (HA) was conjugated with P(3HB) microspheres as

it can support the structure of the biopolymer and aid in water solubility and bioavailability as a drug delivery vehicle[284]. B. A theoretical graphical image of a single P(3HB)-HA biopolymer microspheres used in this study. Drug delivery strategy is shown in the image. The microsphere features an outer layer of curcumin on the surface (shown in orange) for immediate release and encapsulated curcumin inside for a delayed release. C. Theoretical image showing the outer layer of the P(3HB)-HA biopolymer releasing curcumin immediately. D. Theoretical image showing the delayed release of curcumin due to the degradation of the biopolymer.

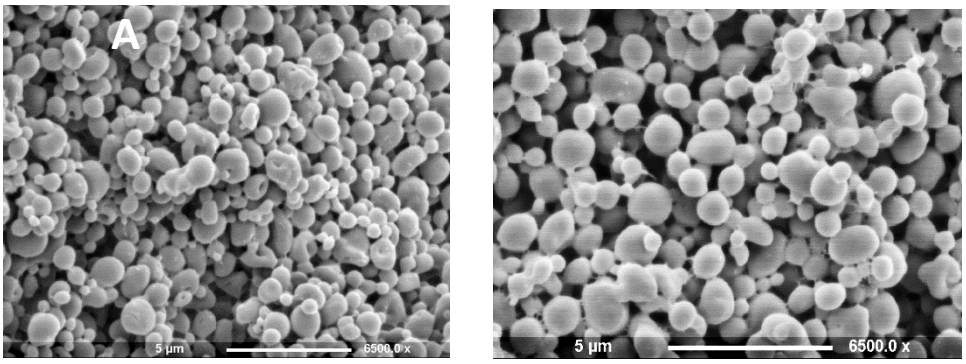

Figure 32. **Surface morphology and size distribution. A.** SEM image of P(3HB) microspheres, average particle size= 0.551 ± 0.108µm. **B.** SEM image of P(3HB) microspheres with encapsulated curcumin, average particle size= 0.551 ± 0.108µm

6.3 Encapsulation efficiency

Encapsulation efficiency was calculated using the supernatant that was obtained from centrifuging the microspheres and assessed with a Fourier-transform infrared spectroscopy (FTIR) spectrometer (Figures 33B-D)

Drug release kinetics:

Drug-encapsulated microspheres (10 mg) were immersed in 2ml of PBS. One ml samples were drawn periodically and 1ml fresh PBS was added to the samples.

Curcumin was quantified using measuring absorbance at 420nm (Figure 33A).

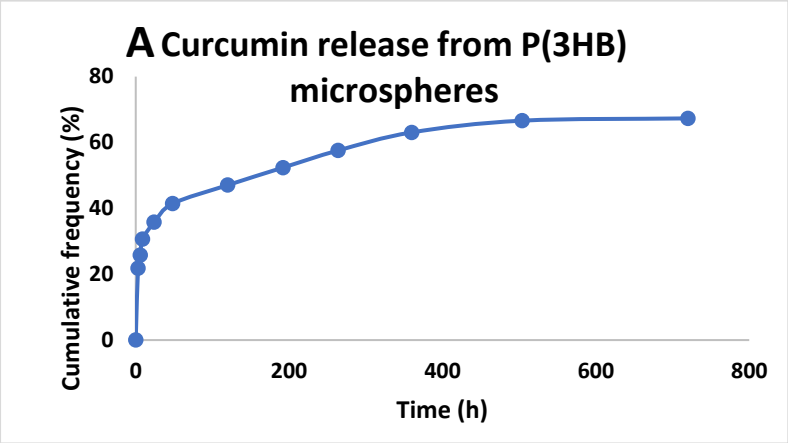

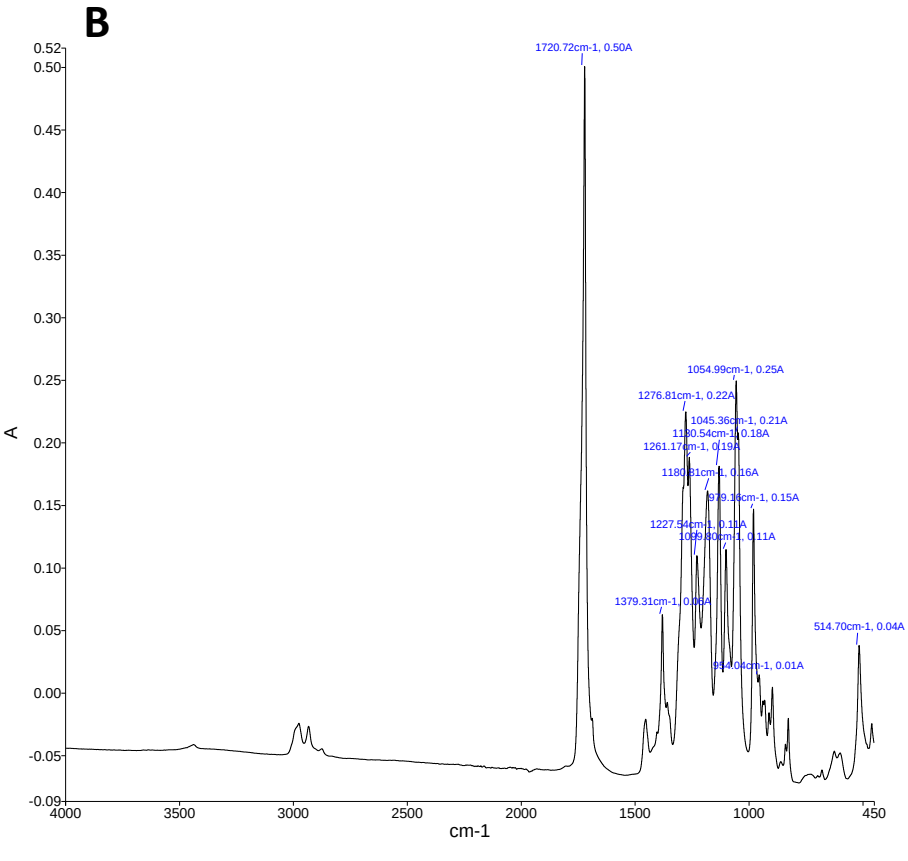

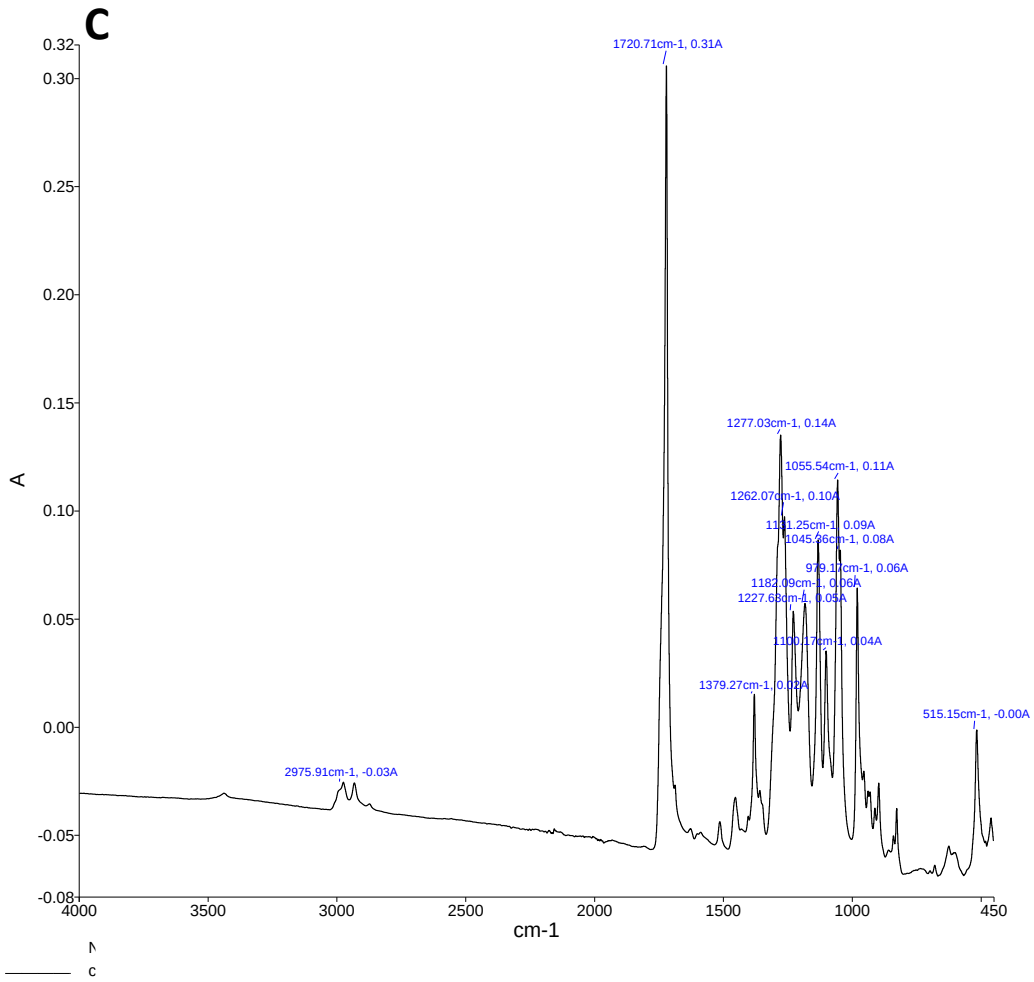
C
1720.71cm-1, 0.31A
1277.03cm-1, 0.14A
1055.54cm-1, 0.11A
1262.07cm-1, 0.10A
1045.26cm-1, 0.08A
1182.09cm-1, 0.06A
1227.63cm-1, 0.05A
1379.27cm-1, 0.03A
515.15cm-1, -0.00A
2975.91cm-1, -0.03A
A
cm-1
0.32
0.30
0.25
0.20
0.15
0.10
0.05
0.00
-0.05
-0.08
4000
3500
3000
2500
2000
1500
1000
450
c

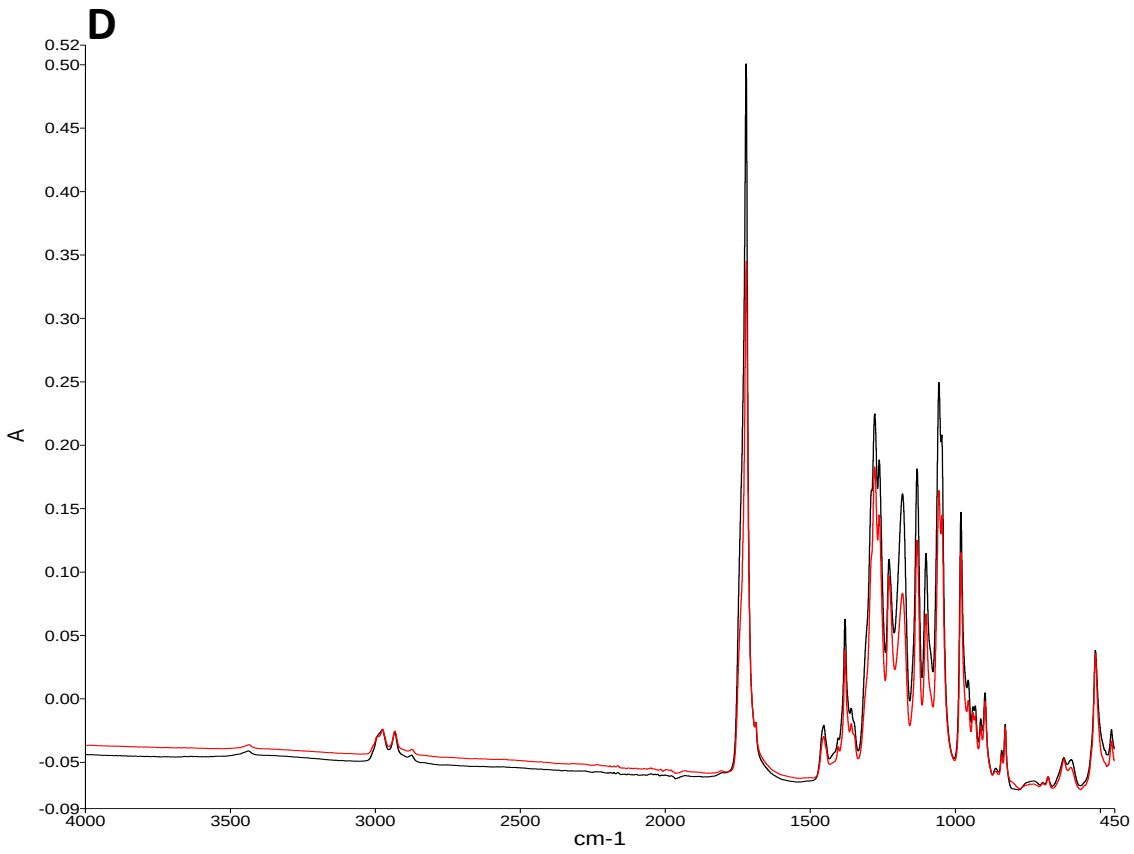

Figure 33. **Release kinetics and chemical characterisation: FTIR.** A. Curcumin release from P(3HB) microspheres, encapsulation efficiency= 63.82 ± 3.21%. Curcumin was quantified using measuring absorbance at 420nm. B. FTIR spectra of empty P(3HB) microspheres. C. FTIR spectra of empty P(3HB) microspheres with curcumin. D. Overlap of FTIR spectra of empty P(3HB) microspheres and microspheres with curcumin.

6.4 Pharmacological treatment

Based on previously published data from our lab where 200µg/g BW curcumin provided neuroprotection after i.p. administration in a P7 HI mouse model[255] and unpublished data after intranasal administration of curcumin in DMSO and curcumin in nanoparticles formulation, we investigated the effect of intranasal route, since this

route of administration consists in the administration of the product of interest in the nasal cavity. Intranasal route of administration, allows the compounds to bypass the BBB by entering perivascular channels in the intranasal epithelium or by extracellular and intracellular pathways via the olfactory and trigeminal nerve[285]. Therefore, two intranasal doses of 33µg/g encapsulated curcumin in 6µl of vehicle (empty microspheres) were administrated, to reach a total dose of 66µg/g curcumin. The curcumin treatment group received one intranasal dose of encapsulated curcumin immediately post-HI, and an additional dose 30 minutes later. The Biopolymer group received two doses of the biopolymer vehicle only. The HI group did not receive any pharmacological treatment.

6.5 Results

6.5.1 Intranasal delivery of curcumin via P(3HB) microspheres immediately post-HI reduces cell death, tissue loss and microglial activation

Compared to biopolymers-treated animals and untreated HI controls, intranasal delivery of 66µg/g BW P(3HB) encapsulated curcumin straight after the HI-insult significantly reduced brain damage markers (tissue loss, TUNEL+ cell death and microglial activation) at 48h post-HI. Immediate intranasal post-HI application of P(3HB) encapsulated curcumin downregulated TUNEL+ cell death (Figure 34A). Figure 34A shows that encapsulated curcumin treatment straight HI significantly reduced the number of TUNEL+ cells compared to empty P(3HB) microspheres treated littermates and untreated HI control group (Kruskal-Wallis test with Dunn's post-hoc, $p=0.001$) with individual significant decrease of 70–90% in cortex, pyriform cortex, hippocampus, striatum, external capsule, thalamus and overall ($p<0.05$ in Kruskal-Wallis test with Dunn's post-hoc). The TUNEL+ cells displayed the typical pyknotic nuclear morphology (Figure 34-insert, ipsilateral hippocampus empty P(3HB) microspheres (G) and HI (F)).

Immediate intranasal post-HI P(3HB) encapsulated curcumin application had a similar effect on microglia activation score (Figure 34B) based on alphaM integrin immunoreactivity (Figures 34B, I-K). Regional assessment shown in Figure 34B revealed a reduction in activation score in the P(3HB) encapsulated curcumin treated group (Kruskal-Wallis test with Dunn's post-hoc, $p=0.0001$), with significant decrease of 50–80% in all six individual ipsilateral brain regions compared to empty P(3HB) microspheres treated group and in hippocampus and external capsule compared to untreated HI group ($p<0.05$, Kruskal-Wallis test with Dunn's post-hoc).

Application of P(3HB) encapsulated curcumin immediately post-HI had no significant effect on astroglial activation compared to empty P(3HB) microspheres treated and untreated HI controls as shown in Figure 34C ($p>0.05$, Kruskal-Wallis test with Dunn's post-hoc). As shown in Figure 34D, post-HI intranasal application of curcumin loaded P(3HB) microspheres markedly decreased ipsilateral forebrain tissue loss. Regional assessment presented in Figure 34D revealed strong decrease across the different forebrain regions (Kruskal-Wallis test with Dunn's post-hoc, $p=0.001$). Immediate intranasal post-HI application of P(3HB) encapsulated curcumin significantly reduced tissue loss in relation to empty P(3HB) microsphere treated only control littermates and untreated HI controls by 50–70% in cortex, pyriform cortex, hippocampus, striatum, external capsule, thalamus, and overall in the brain regions assessed ($p<0.05$ in Kruskal-Wallis test with Dunn's post-hoc).

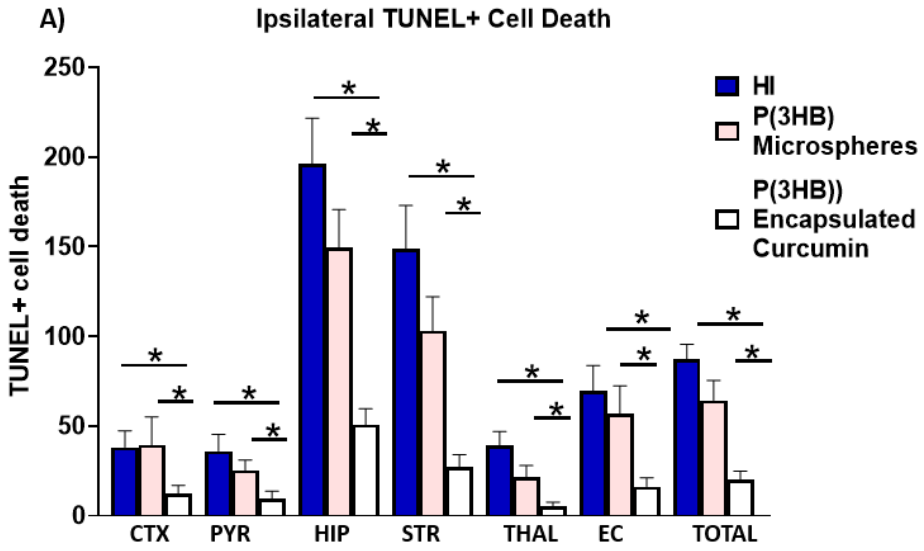

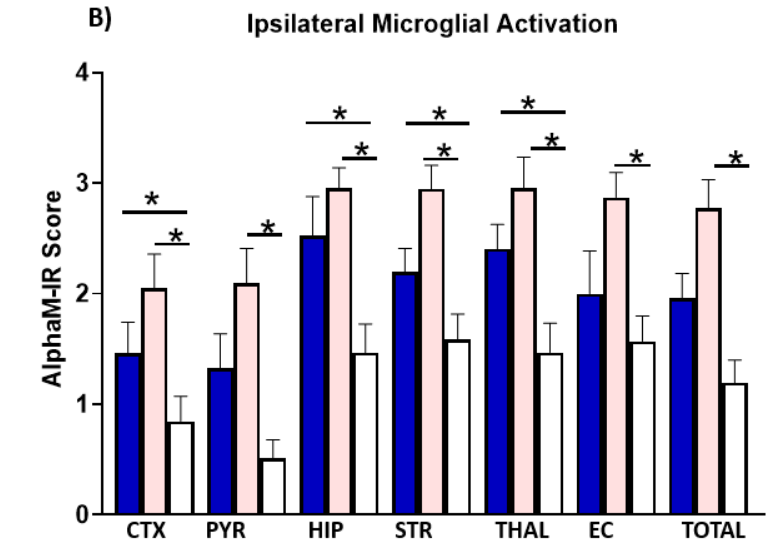
B)
Ipsilateral Microglial Activation
AlphaM-IR Score
0
1
2
3
4
CTX
PYR
HIP
STR
THAL
EC
TOTAL

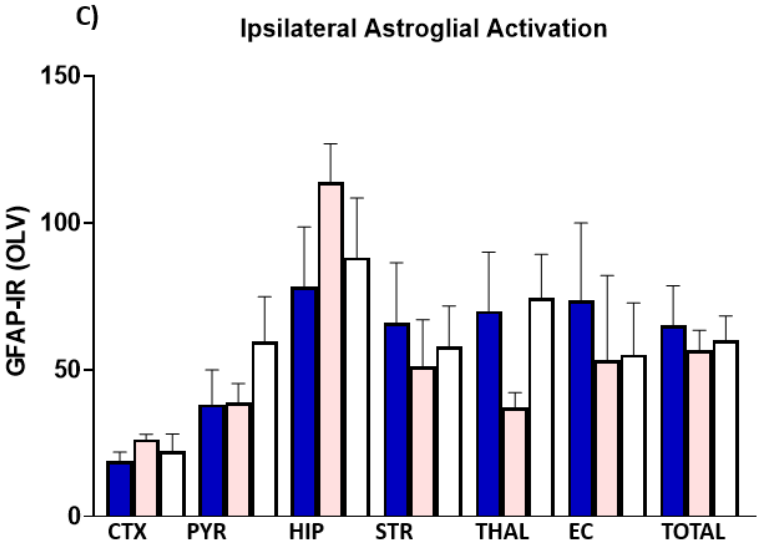
C)
Ipsilateral Astroglial Activation
GFAP-IR (OLV)
0
50
100
150
CTX
PYR
HIP
STR
THAL
EC
TOTAL

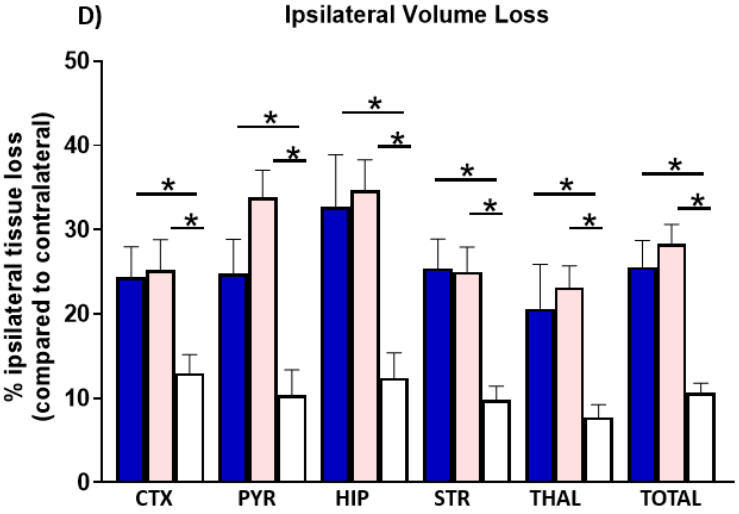
D)
Ipsilateral Volume Loss
% ipsilateral tissue loss
(compared to contralateral)
0
10
20
30
40
50
CTX
PYR
HIP
STR
THAL
TOTAL

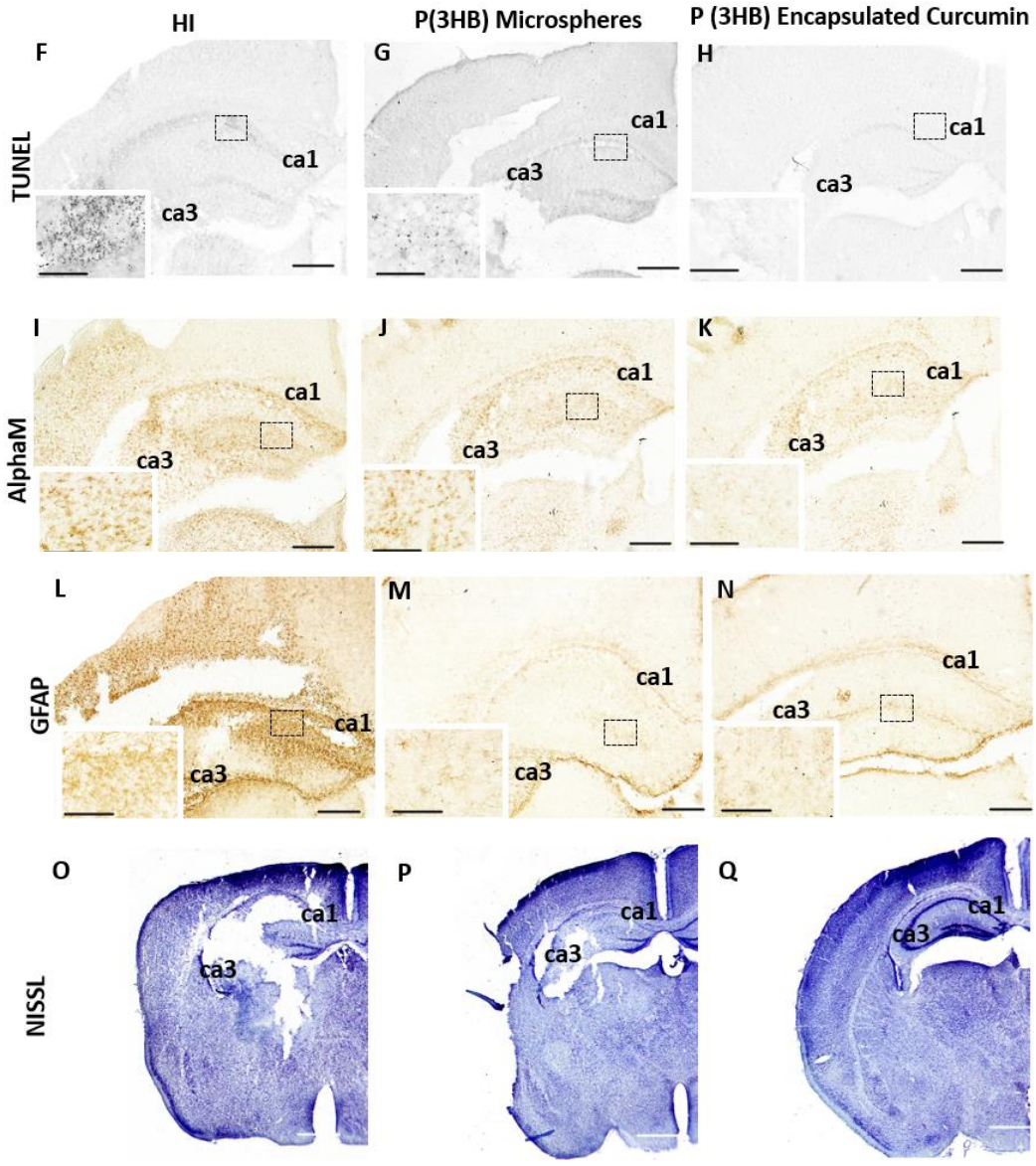

Figure 34. **Neuroprotective effects of immediate intranasal post-HI application of 66µg/g BW curcumin encapsulated P(3HB) microspheres at 48h.** A. Curcumin encapsulated P(3HB) microspheres treatment reduced TUNEL+ cell death across all 6 examined forebrain regions, with significant, individual decrease (Kruskal-Wallis test with Dunn's post-hoc) in cortex (p = 0.01), pyriform cortex (p = 0.004), hippocampus (p = 0.003), striatum (p=0.0001), external capsule (p=0.0001), thalamus (p=0.0001) and overall forebrain (p=0.005) compared to untreated HI group and in cortex (p=0.04), pyriform cortex (p=0.01), hippocampus (p=0.003), striatum (p=0.0001), external capsule (p=0.006), thalamus (p=0.006) and overall forebrain (p=0.0002) when compared to empty P(3HB) microspheres treated controls. B.

Quantitative analysis of AlphaM immunoreactivity representing microglial activation in animals treated with 66µg/g BW curcumin encapsulated P(3HB). Graph B shows the reduction in microglial activation in cortex (p=0.01), pyriform cortex (p=0.001), hippocampus (p=0.01), striatum (p=0.02), external capsule (p=0.004) and overall (p=0.003) after 66µg/g curcumin encapsulated P(3HB) microspheres treatment compared to untreated HI group and in cortex (p=0.0004), pyriform cortex (p=0.003), hippocampus (p=0.0001), striatum (p=0.004), external capsule (p=0.007), thalamus and overall (p=0.007) compared to empty P(3HB) microspheres group. C. Ipsilateral changes in astroglial activation assessed through GFAP immunoreactivity at 48h after application of 66µg/g BW curcumin encapsulated P(3HB) microspheres compared to empty P(3HB) microspheres and untreated HI control littermates. Graph C shows no significant change in astroglial activation after 66µg/g curcumin encapsulated P(3HB) microspheres treatment compared to empty P(3HB) microspheres and untreated HI groups. D. Quantitative ipsilateral analysis of tissue loss in animals treated with 66µg/ g of curcumin encapsulated P(3HB) microspheres (white), empty P(3HB) microspheres (pink) or untreated HI (blue) control animals. A reduction in tissue loss was observed in cortex (p=0.004), pyriform cortex (p=0.004), striatum (p=0.0006), hippocampus (p=0.001), thalamus (p=0.003) and overall (p=0.0001) of curcumin-P(3HB) microspheres treated group compared to untreated HI and in cortex (p=0.002), pyriform cortex (p=0.004), striatum (p=0.0004), hippocampus (p=0.0003), thalamus (p=0.004) and overall forebrain (p=0.0006) compared to empty P(3HB) microspheres groups. F-H. TUNEL+ staining of dying brain cells with fragmented DNA at 48h following HI-insult-histochemical overview of the ipsilateral forebrain in untreated HI (F), empty P(3HB) microspheres (G) and curcumin encapsulated P(3HB) microspheres (H) treated animals. Note the typical pyknotic nuclear morphology of the TUNEL+ cells observed in the untreated HI (F) and empty P(3HB) microspheres group (G) (- insert, hippocampus) and the lack of such cells in the curcumin encapsulated P(3HB) microspheres group (H). I-K. Histochemical overview of the treatment groups with alphaM staining, untreated HI (I), empty P(3HB) microspheres (J), 66µg/g BW curcumin encapsulated P(3HB) microspheres (K), and low magnification ipsilateral overview in untreated HI (I), empty P(3HB) microspheres (J) and

curcumin encapsulated P(3HB) microspheres (K) groups. L-N. GFAP, histochemical overview of the treatment groups, untreated HI (L), empty P(3HB) microspheres (M), 66µg/g curcumin encapsulated P(3HB) microspheres curcumin groups (N). O-Q. Histochemical NISSL-stained overview of the treatment groups, untreated HI (O), empty P(3HB) microspheres (P), 66µg/g BW curcumin encapsulated P(3HB) microspheres (Q). Scale bars 400µm, inserts=62µm. (*$p<0.05$).

Chapter 7: Discussion on curcumin application

Curcumin's anti-inflammatory, anti-oxidant and anti-apoptotic properties make it an appealing target for drug discovery in many neurodegenerative disorders[249,250,252,255]. Hence, this research focuses on identifying the effect of curcumin in neonatal HI damage. Considering the low bioavailability, lipophilic properties and reported quick clearance from the body[286], we dissolved curcumin in the first instance in DMSO, a common solvent used in preclinical studies, and investigated the neuroprotective effect of 200µg/g BW curcumin in P9 HI animals in order to compare with previous studies in a P7 HI mouse model[255]. The P9 mouse model corresponds to human term infant therefore this current study is more translational to the clinic compared to the P7 mouse model study[255].

The current study supports previous work carried out by our group which determined the neuroprotective effects of immediate 200µg/g BW intraperitoneal curcumin treatment in the P7 mouse with severe HI brain damage[255]. Our results confirmed our hypothesis that an immediate dose of 200µg/g BW curcumin i.p. reduces tissue loss, cell death, microglial and astroglial activation in the most affected brain regions after HI insult in the P9 HI mouse model (Figure 29, Figure 30). Overall, curcumin administered i.p. at a dose of 200µg/g immediately after HI provided neuroprotection.

Moreover, our study is accordance with our previous findings and corroborates with our hypothesis that DMSO does not contribute to the neurological outcome as no significant change in tissue loss, cell death, microglial and astroglial activation was observed between the untreated HI and DMSO treated groups ($p>0.05$, Figure 29).

Our results are in line with other studies demonstrating the neuroprotective effect of curcumin. Specifically, in a study conducted by Cui and colleagues (2017), curcumin was administrated to P7 rats at a dose of 150mg/kg per day for three days, 24h after HI-injury, and resulted in prevention of myelin loss[287]. Expression of nuclear factor erythroid-2-related factor 2 (Nrf2), which has been linked to increased neuroprotection[287], was measured and found to be increased in the curcumin treated mice. Curcumin treatment also significantly attenuated the increased expression of iNOS and caspase-3 activity when compared to untreated HI control group. Attenuation of these pro-inflammatory and pro-apoptotic markers suggests that curcumin treatment acts to supress these pathways in order to confer neuroprotection. Our results in the Rice-Vannucci mouse model show a reduction of TUNEL+ cell death and tissue loss, which was not explored in the rat study[287].

Furthermore, curcumin treatment reduced microglial activation and the infarction volume of the injured brain area, compared to untreated control animals in a mouse model of stroke[288]. The same study showed that curcumin treatment reduced microglial gene expression of pro-inflammatory and oxidative stress markers, such as TNF-α, IL-12 and iNOS. Additionally, pro-inflammatory cytokines expression was reduced after curcumin treatment in *in vitro* incubation of LPS-INFγ activated microglia[288].

In our P9 mouse model, as well as in the P7 HI mice[255], immediate curcumin post-HI treatment reduced astroglial activation both ipsi- and contralaterally when compared to DMSO treated control group (Figure 29 I, Q). Although the contralateral hemisphere is considered as control, it undergoes hypoxia and is subjected to delayed atrophy[125]. Bilateral acidosis and upregulation of pSTAT3, have been reported in previous studies suggesting changes in both hemispheres after HI insult[181]. Additionally, STAT3 is

critical in astroglial maturation[181] and curcumin is reported to inhibit STAT3 phosphorylation[110], therefore an effect causing reduction of astrogliosis was to be expected. Curcumin reduced glial scar formation in a rat model of spinal cord injury[289]. In this model, astroglial cells have a major contribution to the formation of glial scar, impeding tissue regeneration[289]. Specifically, curcumin seems to inhibit NF-kB signalling pathway, which reduces GFAP expression in astrocytes[289]. Hence, it is likely that after HI brain damage curcumin reduces astroglial activation by acting on NF-kB and STAT3 pathways, which both play an important role in stimulating apoptosis and inflammation therefore explaining the reduction in tissue loss and cell death. The inhibition of NF-kB pathway also prevents the upregulation and production of iNOS. Curcumin's application in the P7 and P9 mouse model of HI resulted in significantly reduced levels of tissue loss along with reduced number of iNOS positive cells[255]. These results may suggest that the decline in oxidative stress due to curcumin treatment is crucial in lessening neuronal tissue injury. Studies carried out in term fetal guinea pigs following HI brain damage found significant levels of iNOS expressed by both glial and neuronal cells in all brain regions where significant tissue loss was observed. Furthermore, inhibition of iNOS with the selective inhibitor N-iminoethyl-L-lysine (L-NIL), demonstrated that the majority of HI induced increase of the free radical NO was reflected by an excess iNOS activity and thus reduced or eliminated the injury[290]. Our data is in line with these findings, suggesting that the observed reduction in tissue loss, cell death and glial response, could depend on curcumin's ability to resolve inflammation through downregulation of pro-inflammatory cytokines and reducing oxidative stress through suppression of iNOS transcription.

The significant reduction in iNOS+ cells in our study can be explained as well by curcumin's ability to scavenge and clear ROS and free radicals due to its o-methoxy

phenolic group[291]. Curcumin is able to attenuate oxidative stress by inducing the polarisation of murine RAW264.7 macrophages from a pro-inflammatory phenotype to an anti-inflammatory phenotype[292]. Therefore, the effect of curcumin on inflammation and oxidative stress could be through the reduction of pro-inflammatory cytokines such as IL-1β and iNOS levels, and due to the upregulation of ani-inflammatory factors[292,293]. Furthermore, Mukherjee and colleagues (2019) demonstrated that curcumin upregulates antioxidant compounds, such as SOD, which could also explain the reduction of iNOS+ cells after curcumin treatment. With the increased production of ROS and free radicals following a severe HI insult, there is a decrease in endogenous antioxidant proteins such as glutathione and SOD, existing in low levels and exacerbates neuronal cell death and tissue loss[294]. A study conducted in neonatal rat cerebral ischaemic reperfusion model found that polyethylene glycolylated polylactide-co-glycolide nano-capsulated curcumin restored SOD activity to normal levels[294]. Additionally, curcumin protected cultured HT22 neuronal cells against oxygen-glucose deprivation and reoxygenation by upregulating type-2 superoxide dismutase (SOD2) protein, decreasing intracellular ROS and the accumulation of mitochondrial superoxides, thus improving mitochondrial function and cell integrity[224].

In an adult male rat model of HI, treatment with oral curcumin dissolved in DMSO application demonstrates an ability to target NOS[296]. Interestingly, this study also found that curcumin treatment resulted in reduced expression of Aquaporin-4, (AQP-4), a water channel protein expressed at the BBB, upregulation of which may contribute to increased oedema in HI injury. However, whether this applies in cases of neonatal HI injury remains to be investigated.

Finally, our results also showed no significant difference in MBP levels in P9 mice treated with curcumin compared to DMSO treated or untreated HI control littermates

(Figure 30A). This result differed compared to our previous study in P7 mice, where i.p. curcumin treatment immediately after HI insult resulted in higher levels of MBP in the external capsule and striatum, compared to DMSO treated and untreated HI controls. A study by a different group on neonatal (P9-P10) HI mice found that the expression of MBP protein and its transcripts significantly reduced in the external capsule, striatum, corpus callosum and white matter tracts (in which microglia are most abundant) at 24h following the HI insult. However, our results did not show this effect on the P9 HI mouse model[297]. Our data from the P9 HI mouse model is also not in line with other studies which have investigated the effects of curcumin on myelination, where researchers concluded that higher levels of MBP were associated with neuroprotection of white matter following neonatal HI injury[287,298]. Therefore, we cannot conclude that curcumin affects demyelination in P9 mice. Our results may have been affected by the low number of animals, hence future studies with an increased sample group size will be needed to verify the findings from the current study.

Due to curcumin's low bioavailability, further routes of administration for treatment in neonatal HI injury have been tested. Curcumin loaded poly (lactic-co-glycolic acid)-poly (ethylene glycol) (PLGA-PEG) nanoparticles at a dose of 50mg/kg were intraperitoneal injected into P7 rat pups 30 minutes after HI insult[299]. Quantification of the nanoparticles in the parenchyma of the HI brain showed successful uptake. Furthermore, histological investigation of injury in coronal slices suggested that the curcumin loaded nanoparticles showed a significant neuroprotective effect, especially compared to curcumin dissolved in DMSO alone. Therefore, this study suggests that successful delivery of curcumin into the neonatal rat brain was able to attenuate HI tissue volume loss.

The results from the current study, using curcumin encapsulated P(3HB) microspheres, indicate that the P(3HB)-HA biopolymer was able to successfully provide neuroprotection, as can be observed in Figure 33. Curcumin has been the focus of several drug delivery studies aiming to increase its bioavailability[300,301]. A study by Joseph and colleagues[302] used curcumin loaded polylactic-co-glycolic acid-polyethylene glycol nanoparticles in a similar model of unilateral HI brain injury in neonatal rats. The results, although indicating an overall neuroprotective effect, did not lead to a significant difference observed between the vehicle control and the curcumin nanoparticle treatment. This was suggested to be due to the possible neuroprotective effects of the polymer itself. It is therefore important to find a more appropriate polymer structure for the delivery of curcumin. Furthermore, previous results from our lab (unpublished data Hristova lab) are in line with the results in this study, indicating that intranasal administration of encapsulated curcumin in TPGS nanoparticles is neuroprotective by reducing cell death, tissue loss and glial activation.

The use of the Polyhydroxyaklanoates P(3HB) conjugated with HA for increased solubility has been shown to be a good candidate for controlled drug delivery. Low molecular weights of P(3HB) are present in humans and animals, leading to a high level of biocompatibility[284]. Furthermore, P(3HB) elicit lower immune responses compared to other commercial medical polymers[284]. The two-step curcumin release strategy of the biopolymer used in this study (Figure 31) would be advantageous for the treatment of HI injury due to its ability to elicit both an immediate and delayed neuroprotective effect from the latent phase and onwards, if given between 30 minutes to 6h after the initial injury.

Overall, this study provided evidence that curcumin is neuroprotective in a term (P9) mouse model of HI brain injury through the reduction of cell death, tissue loss and

microglial activation. Moreover, this study represents a novel success in the use of P(3HB)-HA biopolymers for the controlled drug delivery of curcumin in HI treatment, via intranasal delivery. These results suggest that the use of curcumin as an intranasal treatment for neonatal HI is a valid neuroprotective strategy, removing any need for invasive procedures. Future experiments should focus on investigating the long-term effects of curcumin loaded biopolymer's administration.

Chapter 8: Effects of microglial TGFβR-1 specific deletion on microglial population in a P7 HI mouse model

8.1 AIMS

Microglial-specific TGFβR-1 deletion is neuroprotective following severe HI insult (unpublished data Hristova lab), we hypothesised that a potential mechanism behind this neuroprotective effect is due to the reduction of pro- and increase of anti-inflammatory microglial activation after HI insult. Furthermore, we set out to assess whether there is a shift in the ratio between the pro- and anti- inflammatory microglia in the brain regions most affected by the insult, with more activation of the anti-inflammatory phenotype thus inducing repair.

To test this hypothesis, we investigated the effects of microglia-specific TGFβR-1 deletion in a P7 mouse model on microglial activation via immunohistochemical analysis.

8.2 Methods

All ethical approvals were obtained, brain extraction and statistics were performed as explained in Chapter 2. The surgical procedures to induce HI were performed as described previously. However, HI insult was performed in the P7 mouse late pre-term model and the pups were exposed to humidified 8% oxygen/ 92% nitrogen (3L/min) at 36^{o}C for 60 minutes.

8.2.1 TGFβR-1 deletion

The mouse brains used in this study were previously obtained in our laboratory and display microglia targeted TGFβR-1 deletion. A global deletion of the receptor is lethal in embryonic stage[303], thus a LoxP-mediated knockout of TGFβR-1 was used that targets only macrophages/ microglia (MAC1::CRE). Genetically engineered mice by homologous recombination carrying the LoxP site at each flanking intronic sequences of the TGFβR-1 exon 9-11 (TGFβR-1$^{Fl/Fl}$) were obtained from Professor Stefan Karlsson, Lund University, Division of Molecular Medicine and Gene Therapy, Sweden. These mice were crossed with the Mac1/Cd11b-Cre^{+} mice, obtained from Hellenic Pasteur Institute, Athens, Greece, resulting in Mac1-Cre^{+}-TGFβR-1$^{Fl/-}$. The progeny was crossed for two generations with the TGFβR-1$^{Fl/Fl}$ mice to obtain the experimental (TGFβR-1$^{\Delta}$) and control (TGFβR-1$^{Fl/Fl}$) groups. All animals were genotyped for TGFβR-1 flox and Cre.

8.2.2 Statistical analysis

The statistics were performed as explained in Chapter 2.

8.3 Results

8.3.1 Pro-, anti- inflammatory microglia phenotype activation and pro- & anti-microglia co-localization

The pro-inflammatory phenotype activation pattern was significantly decreased in TGFβR-1$^{\Delta}$ (experimental) compared to TGFβR-1$^{Fl/F}$ (control) animal group in hippocampus, external capsule and overall forebrain ($p<0.05$, Kruskal-Wallis test) (Figure 35B). The anti-inflammatory activation pattern was also significantly downregulated in TGFβR-1$^{\Delta}$ mice, compared to the TGFβR-1$^{Fl/F}$ group after induction of HI, in cortex, hippocampus, external capsule, pyriform cortex, striatum and overall in all brain regions assessed ($p<0.05$, Kruskal-Wallis test with Dunn's post-hoc) (Figure 35D). Pro- and anti-inflammatory microglia co-localisation, indicative of pro- and anti- inflammatory microglia double-labelling also showed significant reduction in hippocampus and external capsule ($p<0.05$, Kruskal-Wallis test with Dunn's post-hoc) in TGFβR-1$^{\Delta}$ group (Figure 35D).

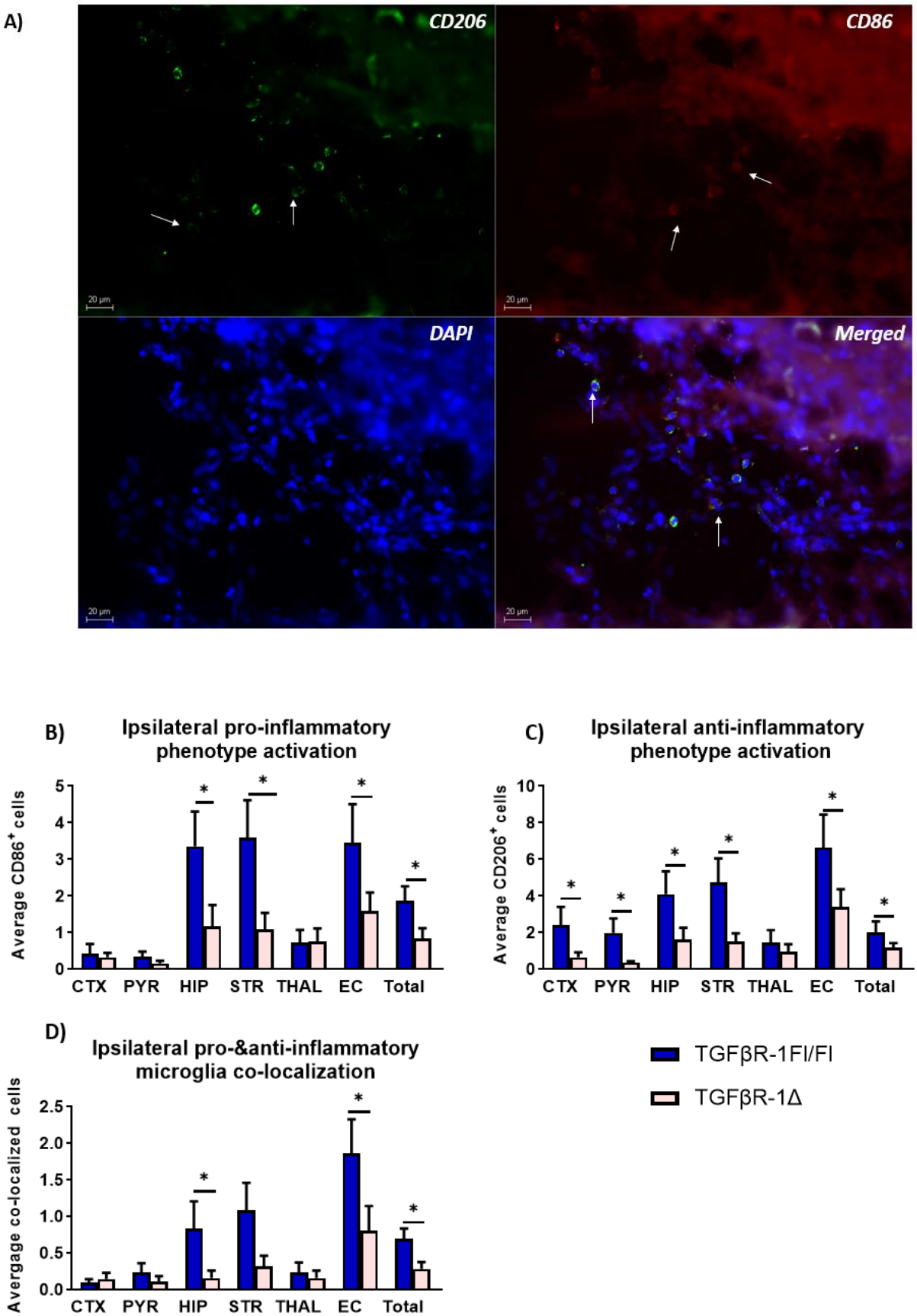
A)
CD206
CD86
DAPI
Merged
20 µm
B)
Ipsilateral pro-inflammatory phenotype activation
Average CD86+ cells
CTX PYR HIP STR THAL EC Total
C)
Ipsilateral anti-inflammatory phenotype activation
Average CD206+ cells
CTX PYR HIP STR THAL EC Total
D)
Ipsilateral pro-&anti-inflammatory microglia co-localization
Avergage co-localized cells
CTX PYR HIP STR THAL EC Total
TGFβR-1Fl/Fl
TGFβR-1Δ

Figure 35. **Microglia-specific TGFβR-1 deletion significantly reduces pro and anti-inflammatory microglial phenotypes after HI insult.** The graphs illustrate the averages of cell counts in six brain regions, for the TGFβR-$1^{Fl/Fl}$ (control) (n=10) and the TGFβR-1^{Δ} (experimental) (n=19) group. A. Visual representation of CD86+, CD206+ and co-localised CD86+, CD206+ microglial cells. B. Activation profiles of pro-inflammatory (or CD86+), with significant decrease in hippocampus (p=0.03), striatum (p=0.007), external capsule (p=0.04) and overall forebrain (p=0.01) in TGFβR-1^{Δ} compared to TGFβR-$1^{Fl/Fl}$ (Kruskal-Wallis test with Dunn's post-hoc). C. Activation profiles anti-inflammatory or CD206+ microglial cells in the ipsilateral hemisphere. Anti-inflammatory microglia cells were reduced in cortex (p=0.01), pyriform cortex (p=0.03), hippocampus (p=0.03), striatum (p=0.003), external capsule (p=0.04) and overall (p=0.04, Kruskal-Wallis test with Dunn's post-hoc) in TGFβR-1^{Δ} when compared to TGFβR-$1^{Fl/Fl}$. D. Pro- & anti- inflammtory microglia co-localised cells were significantly reduced in hippocampus (p=0.01), external capsule (p=0.04) and overall (p=0.009, Kruskal-Wallis test with Dunn's post-hoc) after TGFβR-1 deletion compared to TGFβR-$1^{Fl/Fl}$ animals. A. Immunofluorescence for rat monoclonal anti- CD86, in red and goat monoclonal anti- CD206), in green, superimposed on nuclear DAPI fluorescence, in blue in the ipsilateral hippocampus of TGFβR-1^{Δ}. Results are presented as mean ± standard error of mean (SEM). CTX – cortex, PYR – pyriform cortex, HIP – hippocampus, STR – striatum, THAL -thalamus, EC- external capsule, Total - Average of all brain regions. *p<0.05.

8.3.2 Ratios between pro-, anti-, pro- & anti- and pro- + anti- inflammatory microglial populations

To better understand the inter-relation between pro- and anti- inflammatory activation in TGFβR-1$^{\Delta}$ (n=19) and TGFβR-1$^{Fl/F}$ (n=10) animal groups after HI insult we assessed six different ratios between the two phenotypes in each of the six regions (Figure 36).

We assessed pro- inflammatory microglia as a percentage from: the total number of activated microglia (pro- inflammatory: total); and as a percentage from the anti-inflammatory population, excluding (pro- inflammatory: anti- inflammatory) and then including (pro- inflammatory: all anti- inflammatory) the co-localised cells. Similarly, we assessed anti- inflammatory: total, and the percentage of pro-inflammaroy: co-localised with anti- inflammatory and vice versa.

When comparing the ratios pro-inflammatory microglia/total and anti-inflammatory microglia/total (Figure 36E, F), anti-inflammatory microglia cells represented the biggest population of the total number of activated microglia >70%, in both TGFβR-1$^{\Delta}$ and TGFβR-1$^{Fl/Fl}$ groups. For both phenotypes, the highest percent of active cells was reported in TGFβR-1$^{Fl/Fl}$ hippocampus, 60% (Figure 36E, F) and statistically significant increase was observed in hippocampus and thalamus anti-inflammatory microglia /total of TGFβR-1$^{\Delta}$ group (Figure 36F), ($p<0.05$, Kruskal-Wallis test, with Dunn's post-hoc) compared to TGFβR-1$^{Fl/Fl}$ but no significant difference was observed in pro-inflammatory microglia/total ratio. Ipsilateral anti- / pro- inflammatory ratio comparison between the two experimental groups was significantly increased in hippocampus and overall, 66% and 80% respectively of TGFβR-1$^{\Delta}$ animals ($p<0.01$, Kruskal-Wallis test with Dunn's post-hoc, Figure 36A) compared to TGFβR-1$^{Fl/Fl}$ and siginificantly decreased in cortex ($p<0.01$, Kruskal-Wallis test with Dunn's post-hoc, Figure 36A). In

contrast, pro- / anti- inflammatory microglia ratio was significantly decreased in hippocampus and striatum of TGFβR-1$^{\Delta}$ compared to TGFβR-1$^{Fl/Fl}$ ($p<0.05$, Kruskal-Wallis test with Dunn's post-hoc, Figure 36B). Figure 36C, D illustrates the ipsilateral ratio of pro-inflammatory microglia: co-localised cells and anti-inflammatory microglia: co-localised cells, respectively. The pro-inflammatory microglia: co-localised cells ratio was significantly reduced in hippocampus ($p=0.001$, Kruskal-Wallis test with Dunn's post-hoc) and the anti-inflammatory microglia: co-localised cells ratio in striatum of TGFβR-1$^{\Delta}$ animals compared to TGFβR-1$^{Fl/Fl}$ ($p=0.04$, Kruskal-Wallis test with Dunn's post-hoc).

Finally, Figure 36H represents the ratio of anti-inflammatory microglia: pro-inflammatory microglia cells in the TGF-R1$^{\Delta}$ group of animals. The ratio overall was decreased in all of the regions of interest, with significant reduction in hippocampus, striatum and external capsule, 45%, 33%, 65% respectively, ($p<0.05$, Kruskal-Wallis test with Dunn's post-hoc), indicating an overall bigger population of anti-inflammatory microglia cells in the group of microglia-specific TGFβR-1 deletion following neonatal HI injury.

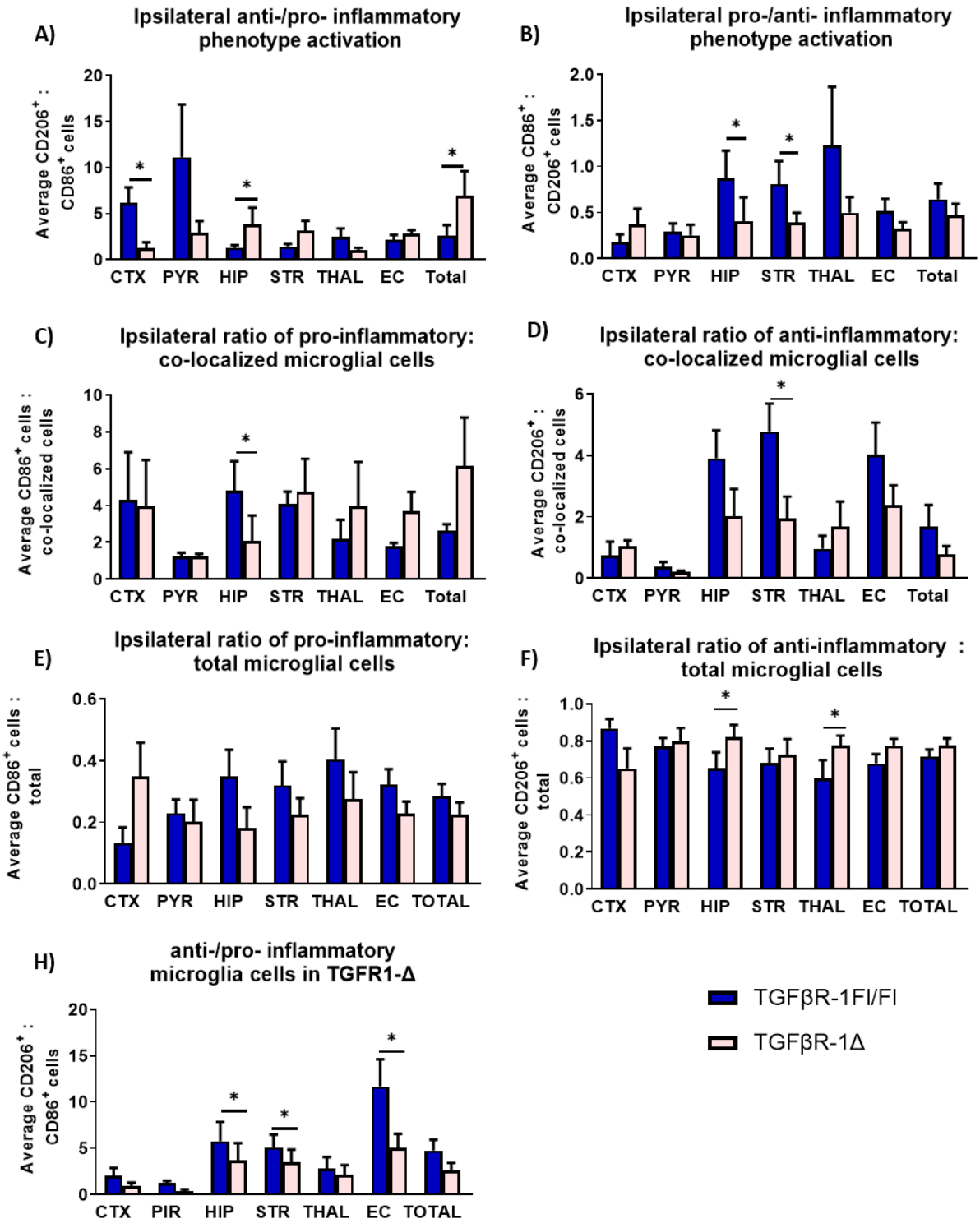
A)
Ipsilateral anti-/pro- inflammatory phenotype activation
Average CD206+ : CD86+ cells
CTX PYR HIP STR THAL EC Total
B)
Ipsilateral pro-/anti- inflammatory phenotype activation
Average CD86+ : CD206+ cells
CTX PYR HIP STR THAL EC Total
C)
Ipsilateral ratio of pro-inflammatory: co-localized microglial cells
Average CD86+ cells : co-localized cells
CTX PYR HIP STR THAL EC Total
D)
Ipsilateral ratio of anti-inflammatory: co-localized microglial cells
Average CD206+ : co-localized cells
CTX PYR HIP STR THAL EC Total
E)
Ipsilateral ratio of pro-inflammatory: total microglial cells
Average CD86+ cells : total
CTX PYR HIP STR THAL EC TOTAL
F)
Ipsilateral ratio of anti-inflammatory : total microglial cells
Average CD206+ cells : total
CTX PYR HIP STR THAL EC TOTAL
H)
anti-/pro- inflammatory microglia cells in TGFR1-Δ
Average CD206+ : CD86+ cells
CTX PIR HIP STR THAL EC TOTAL
TGFβR-1Fl/Fl
TGFβR-1Δ

Figure 36. **Microglia-specific TGFβR-1 deletion results in anti-inflammatory microglial phenotype polarization after HI insult** A. Significant reduction of anti- : pro- inflammatory ratio in cortex and significant increase in hippocampus (p=0.04) and overall (p=0.01, Kruskal-Wallis test with Dunn's post-hoc) in TGFβR-1$^{\Delta}$ group (n=19) when compared to TGFβR-1$^{Fl/Fl}$ (n=10). B. The graph illustrates significant decrease of pro- : anti-inflammatory microglia ratio in hippocampus (p=0.04) and striatum (p=0.01, Kruskal-Wallis test with Dunn's post-hoc in TGFβR-1$^{\Delta}$ group when compared to TGFβR-1$^{Fl/Fl}$. C. Ipsilateral ratio of pro-inflammatory : co-localised microglia cells significantly reduced in hippocampus (p=0.001, Kruskal-Wallis test with Dunn's post-hoc) in TGFβR-1$^{\Delta}$ group compared to TGFβR-1$^{Fl/Fl}$ group. D. Anti-inflammatory: co-localised cells ratio is significantly reduced in striatum (p=0.04, Kruskal-Wallis test with Dunn's post-hoc) in TGFβR-1$^{\Delta}$ group when compared to TGFβR-1$^{Fl/Fl}$. E. No significant difference is observed in pro-inflammatory: total cells ratio between the two experimental groups. F. Significant increase of anti-inflammatory: total cells in hippocampus (p=0.01 and thalamus (p=0.01, Kruskal-Wallis test with Dunn's post-hoc) in TGFβR-1$^{\Delta}$ group when compared to TGFβR-1$^{Fl/Fl}$. H. The graph represents the significantly lower number of pro-inflammatory microglia cells compared to anti-inflammatory microglia cells in TGFβR-1$^{\Delta}$ animal group in hippocampus (p=0.04), striatum (p=0.04) and external capsule (p=0.02, Kruskal-Wallis test with Dunn's post-hoc) compared to TGFβR-1$^{Fl/Fl}$ animals.

Chapter 9: Discussion on TGFβR-1 deletion

TGFβ1 and its receptor, TGFβR-1, are up-regulated after HI insult[304] (unpublished data Hristova lab). Our group previously identified that microglia-specific deletion of TGFβR-1 in severe HI reduces tissue loss, microglial and astroglial activation, overall resulting in neuroprotection (unpublished data Hristova lab). Microglial cells are the first line of defence against injury, constantly surveying their environment. Microglia become highly active after tissue damage[305], and their activation is a hallmark event involved in almost all neuropathologies and experimental lesions, including HI brain damage[306]. Therefore, we sought to further assess the microglial polarisation into the pro- and anti-inflammatory phenotypes in the same knockout TGFβ mouse strain and HI model and whether the neuroprotective effect may be partly attributed to a shift between these microglial phenotypes. As activated microglia can be both pro- and anti-inflammatory, overall reduction of all microglial activation might not necessarily point towards positive outcome. However, even if the overall microglial activation was not changed, protective effects might still be there due to decrease of the pro-inflammatory phenotype and an increase of the anti- inflammatory phenotype.

Based on the findings of the current study, our results indicate overall significantly low levels of both pro- and anti- inflammatory cells after microglia-specific TGFβR-1 deletion (Figure 35), which was to be expected based on the previous preliminary data showing overall reduction of microglial activation in the mutants. Furthermore, the polarization into the anti- inflammatory phenotype was overall higher than into pro-inflammatory in the experimental (TGFβR-1$^{\Delta}$e) group (Figure 36). This was also observed when assessing the percentage of pro- and anti- inflammatory microglia cells from the total number of microglial cells, with >82% expressing the anti- inflammatory

and <30% expressing the pro- inflammatory phenotype in the experimental animal group (Figure 35). Assessing co-localization of pro- anti- inflammatory allowed us to better examine the activation profiles and the shift pattern, since pro- and anti-inflammatory can be expressed simultaneously in the same cell. We observed that >86% of the total anti-inflammatory microglia cells in the ipsilateral hemisphere of both experimental and control groups were pure anti-inflammatory phenotype microglia, as indicated by CD206 microglial marker counts. Over 75% of all microglia cells appeared to be anti- inflammatory phenotype when compared to the number of total cells (Figure 36F), out of which <10% co-localised with pro- inflammatory phenotype (Figure 36C). This trend confirmed our hypothesis that the neuroprotective effects provided by microglia-specific deletion of TGFβR-1 (unpublished data Hristova lab) can be due to a shift between the pro- and anti- inflammatory phenotypes towards the anti-inflammatory one. The number of anti- inflammatory microglial cells was significantly higher in the TGFβR-1Δ group, compared to pro- inflammatory positive cells, indicating that TGFβR-1 deletion induces an increase of anti-inflammatory microglial phenotype, which subsequently can contribute to the observed reduced damage.

Previous results from our lab demonstrated that microglia targeted deletion of TGFβR-1 resulted in reduced alphaM immunoreactivity and neuronal cell loss, based on the injury score, with significant differences in the pyriform cortex and striatum (unpublished data). Therefore, the decrease in alphaM immunoreactivity, combined with the reduced damage, might be consistent with overall reduced microglial activation and predominance of anti- inflammatory microglial phenotype observed in our results.

A study from Ryu and colleagues (2012) is in line with our observations in this study, since they showed that increased expression of TGFβ, as a result of HI insult, could

prolong the activated state of microglia, hence, TGFβR-1 deletion would suppress it[307]. Additionally, other *in vitro* and *in vivo* studies suggested that TGFβ is crucial for the development of CNS specific microglia and that its presence is essential for the survival of mature microglia, and postnatal development[308]. The same group reported that TGFβ1 deletion led to reduction in microglia numbers observed from P20 in an HI mouse model[308]. Zöller and colleagues (2018), presented TGFβ1 as a crucial endogenous factor required in earlier postnatal stages for an adequate microglial maturation and thus normal microglial function in the adult CNS[309]. That study also suggested that the silencing of TGFβ in mature microglia increases TAK1 phosphorylation (TGFβ-activated kinase 1, a CNS regulator of cell death and production of pro- and anti- inflammatory cytokines), thus disturbing microglial quiescence[310].

TGFβR-1 deletion might present both pro- or anti-inflammatory effects. Bain and colleagues (2010) emphasised the dependence of the oligodendrocyte precursor differentiation on the balance between pro- and anti-inflammatory cytokines and demonstrated that global inhibition of TGFβR-1 in severe HI suppresses abnormal astrogliogenesis from pro-oligodendroglia precursors. Our results from a previous study (unpublished) showed that astroglial activation was significantly reduced after TGFβR-1 deletion, which is in line with Bain and colleagues' study. As TGFβR-1 deletion decreased alphaM immunoreactivity (unpublished data Hristova lab), and there was a trend towards anti-inflammatory polarization, it would be interesting to further assess the response of other important cells, such as oligodendrocytes, and the changes in cytokines balance in response to these events.

Chapter 10: Infection-sensitised HI model

10.1 Materials and Methods

All animal experiments and care protocols were approved by the Home Office and carried out according to the UK Animals (Scientific procedures) Act 1986, following the ARRIVE guidelines. IHC and statistical analysis were performed as described in Chapter 2.

10.1.1 Mouse model of ascending vaginal infection

Virgin female C57Bl/6 Tyrc-2J mice (Charles River, Kent, UK) were time mated (evidence of vaginal plug designated was embryonic day (E) 0.5). On E16.5, mice were anaesthetised by the inhalation of isoflurane (5% for induction, 1.5% for maintenance in oxygen) and *E. coli* K12 MG1655-lux[311] was delivered intravaginally as previously described[89]. Briefly, 20µL of midlogarithmic-phase *E. coli* (1 x 10^9 CFU resuspended in phosphate-buffered saline (PBS)) or PBS (vehicle control) was administered into the vagina using a 200-µL pipette tip, then 20µL of 20% Pluronic® F-127 gel (Sigma) was delivered to prevent leakage. Animals were individually caged and monitored by CCTV for the delivery of pups. Time to delivery was recorded as the number of hours from the time of intravaginal delivery of *E. coli* or PBS to the delivery of the first pup.

10.1.2 Neonatal HI brain damage model

A modified version of the Rice-Vannucci model was used to induce neonatal HI brain damage in C57Bl/6 mice at P7, corresponding to term human brain maturation[70] as described in Chapter 2, although the animals were placed in a 36°C humidified hypoxic chamber and exposed to a mixture of 8% oxygen and 92% nitrogen for 30 min.

10.2 Results

To evaluate the effects of intrauterine maternal *E.coli* K12 infection in a HI mouse model, IHC was conducted to assess alphaM, GFAP, TUNEL, NISSL, iNOS, MBP and NG2 markers in different brain regions. The effect was assessed at 48h following HI, in PBS, untreated HI, and *E.coli* K12 experimental groups and the results are presented in Figures 37-39.

The animals injected with *E.coli* showed a significant increase of ipsilateral TUNEL+ cell death overall (Figure 37A) (Kruskal-Wallis test, with Dunn's post-hoc, $p=0.0001$), as well as significant sub-regional upregulation in striatum, external capsule, thalamus and overall brain regions compared to untreated HI controls ($p<0.05$ with Kruskal-Wallis test, Dunn's post-hoc) and in cortex, striatum and external capsule when compared to PBS treated control group ($p<0.05$ with Kruskal-Wallis test, Dunn's post-hoc) (Figure 37A).

Microglial activation, assessed with alphaM marker, in the *E.coli* K12 group was significantly increased compared to untreated HI and PBS treated control animals in external capsule and in cortex, pyriform cortex, striatum, thalamus and overall forebrain respectively ($p<0.05$ Kruskal-Wallis test with Dunn's post-hoc) (Figure 37B). Significant increase was observed also in the reactive astrogliosis, assessed with

GFAP OLV, in the *E.coli* K12 group compared to PBS treated controls. Increase in GFAP expression was observed overall in the ipsilateral hemisphere (p=0.0001, Kruskal-Wallis test with Dunn's post-hoc) with sub-regional differences observed in striatum and hippocampus (p<0.05 Kruskal-Wallis test with Dunn's post-hoc) (Figure 37C).

Similarly, ipsilateral assessment of tissue loss following *E.coli* injection compared to HI group revealed an overall increase (Kruskal-Wallis test with Dunn's post-hoc, p<0.05) with sub-regional differences in striatum, external, hippocampus, and overall (p<0.05 Kruskal-Wallis test with Dunn's post-hoc) (Figure 37D).

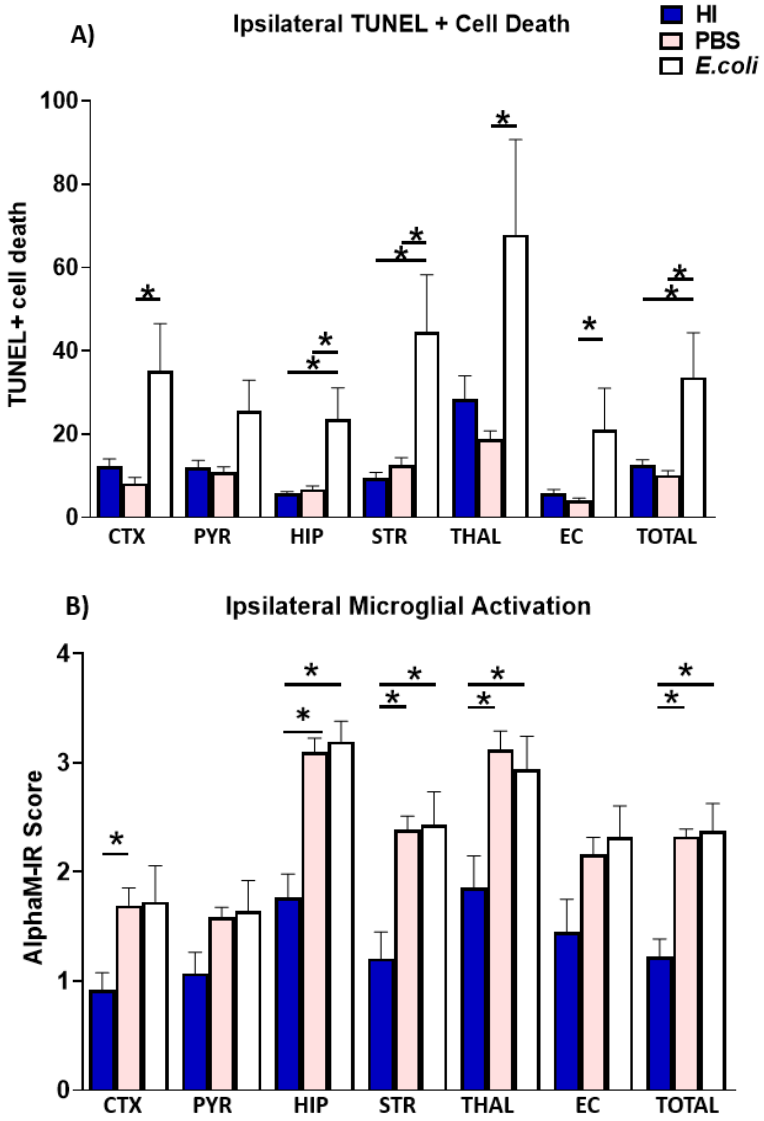

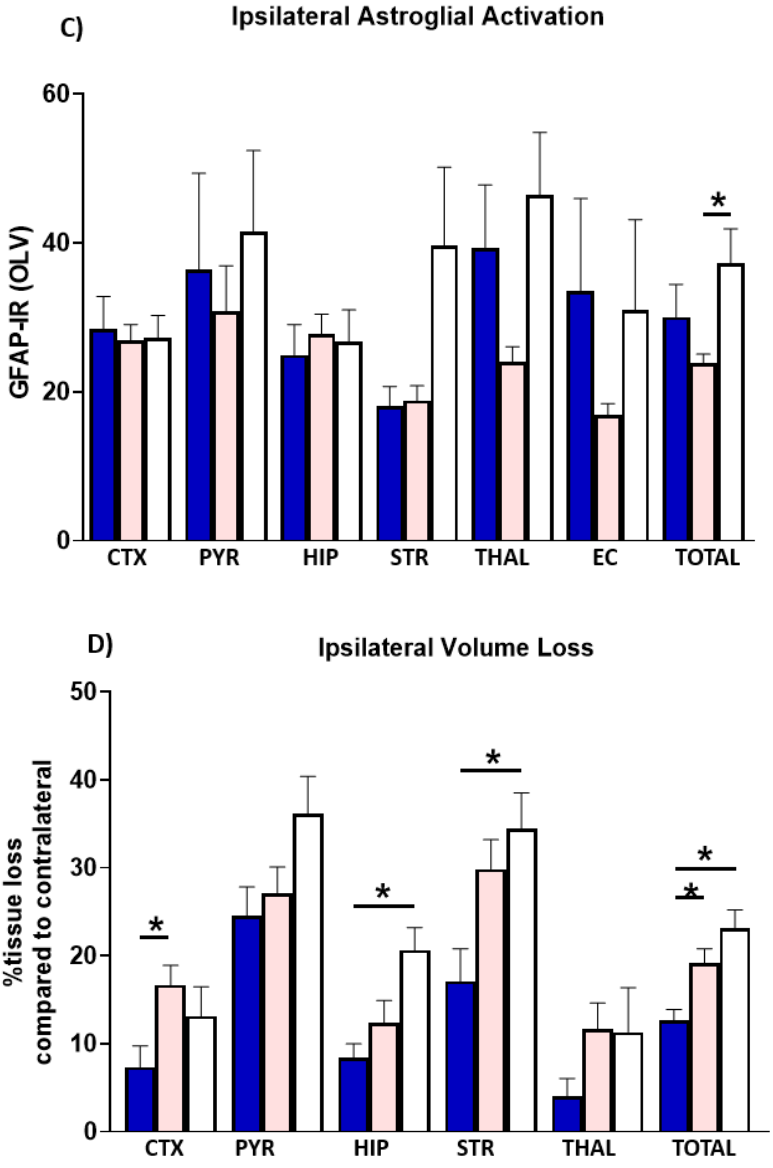
C)
Ipsilateral Astroglial Activation
GFAP-IR (OLV)
60
40
20
0
*
CTX
PYR
HIP
STR
THAL
EC
TOTAL
D)
Ipsilateral Volume Loss
%tissue loss compared to contralateral
50
40
30
20
10
0
*
*
*
*
*
CTX
PYR
HIP
STR
THAL
TOTAL

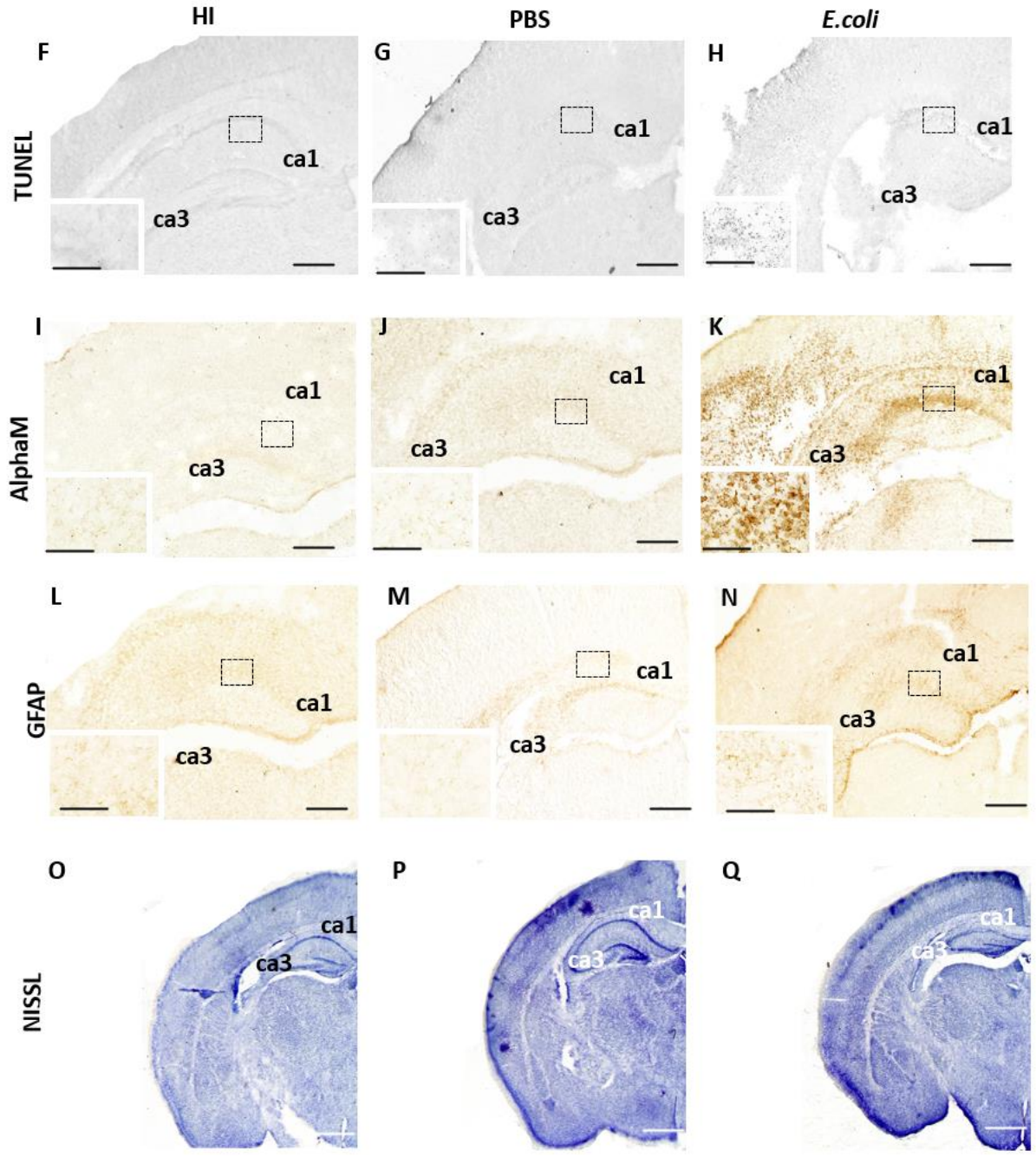

Figure 37. **Ipsilateral TUNEL+ cell death, glial activation and tissue loss in infection-sensitised HI, PBS-treated HI and untreated HI animals** A. Quantitative ipsilateral analysis of TUNEL+ cell death in *E.coli* K12 treated animals (white), PBS (pink) or HI (blue) control animals. An increase in cell death was observed in cortex (p=0.0004), pyriform cortex

(p=0.0005), striatum (p=0.005), external capsule (p=0.0006), hippocampus (p=0.0006), thalamus (p=0.0002) and overall forebrain (p=0.0007) of the *E.coli* treated group compared to untreated HI and PBS treated groups. (p=0.0001). B. Quantitative analysis of alphaM immunoreactivity representing microglial activation. Graph B shows the increase in microglial activation in thalamus (p=0.002), hippocampus (p<0.0006), striatum (p=0.0009), external capsule (p=0.03) and overall forebrain (p=0.0002) in *E.coli* treated animals compared to PBS treated and untreated HI groups. C. Ipsilateral increase in astroglial activation assessed through GFAP immunoreactivity after *E.coli* intrauterine infection compared to PBS and Hi control groups. Significant increase in astroglial activation was observed in pyriform cortex (p=0.002), hippocampus (p=0.04) and overall forebrain (p=0.04) in *E.coli* K12 treated group compared to PBS treated and untreated HI groups. D. Quantitative analysis showing the increased percentage of tissue loss assessed through Cresyl Violet staining consequent to HI insult on the ipsilateral side of the brain in the regions of interest after *E.coli* intrauterine infection compared to HI and PBS groups. In D, significant increase after *E.coli* K12 infection was observed in pyriform cortex (p=0.01) and striatum (p=0.0004) and overall forebrain (p=0.001, Kruskal-Wallis test with Dunn's post-hoc) compared to PBS treated and untreated HI control groups. F-H. Histochemical overview of the TUNEL+ cells in the treatment groups, untreated HI (F), PBS treated (G), *E.coli* treated (H). I-K Ipsilateral overview of microglial activation in the experimental groups, untreated HI (I), PBS- (J) and *E.coli* treated (K) and inserts of HI (I), PBS (J) and *E.coli* groups (K). L-N. Histochemical overview of GFAP immunoreactivity in the treatment groups, untreated HI (L), PBS treated (M), *E.coli* treated (N) groups. O-Q. Ipsilateral overview of NISSL stained forebrain in HI (O), PBS (P) and *E.coli* (Q) groups. Scale bars 400µm, inserts=62µm. (*p<0.05). CTX – cortex, PYR – pyriform cortex, HIP – hippocampus, STR – striatum, THAL -thalamus, EC – external capsule, Total - Average of all brain regions assessed.

Compared to PBS treated and HI untreated animals, *E.coli* K12 intrauterine infection had no significant effect on MBP levels and number of the number of NG2 + cells (p>0.05, t-test) Figure 38A, Figure 39B.

E.coli intrauterine infection increase the levels of oxidative stress assessed through iNOS immunoreactivity, compared to untreated HI controls, with individual significant increase of 80% in hippocampus (Figure 38B, p-value<0.05, t-test).

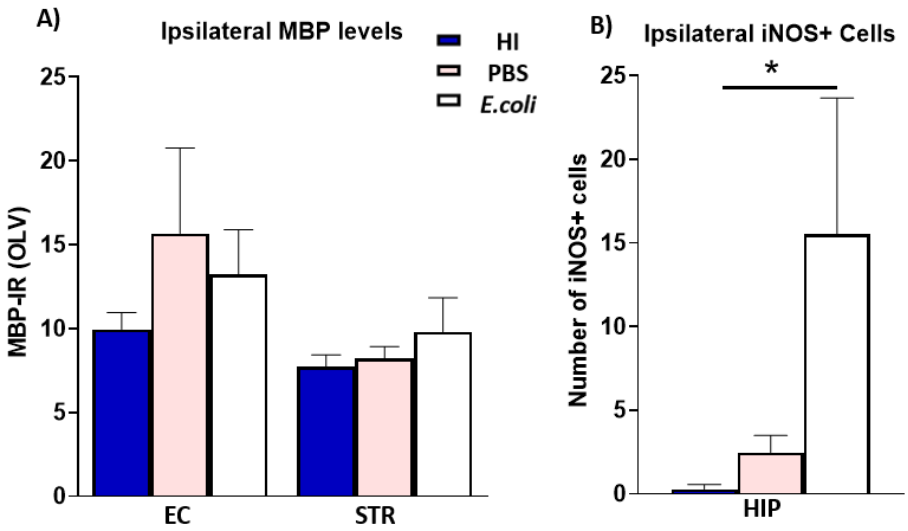

Figure 38. **Ipsilateral MBP and iNOS immunoreactivity in infection-sensitised HI, PBS-treated HI and untreated HI animals**. A. Quantitative ipsilateral analysis of MBP immunoreactivity as a marker of myelination levels in animals with *E.coli* K12 infection (blue), PBS treated (grey) or untreated HI (black) control animals. No significant difference was observed in MBP levels between the groups (p>0.05, Kruskal-Wallis test with Dunn's post-hoc). B. Quantitative analysis of iNOS immunoreactivity as a marker of oxidative stress. Graph B shows the increase in iNOS+ cells in hippocampus after *E.coli* intrauterine infection compared to untreated HI control group (p=0.02, Kruskal-Wallis test with Dunn's post-hoc) and no significant change compared to PBS treated group (p>0.05, Kruskal-Wallis test with Dunn's post-hoc).

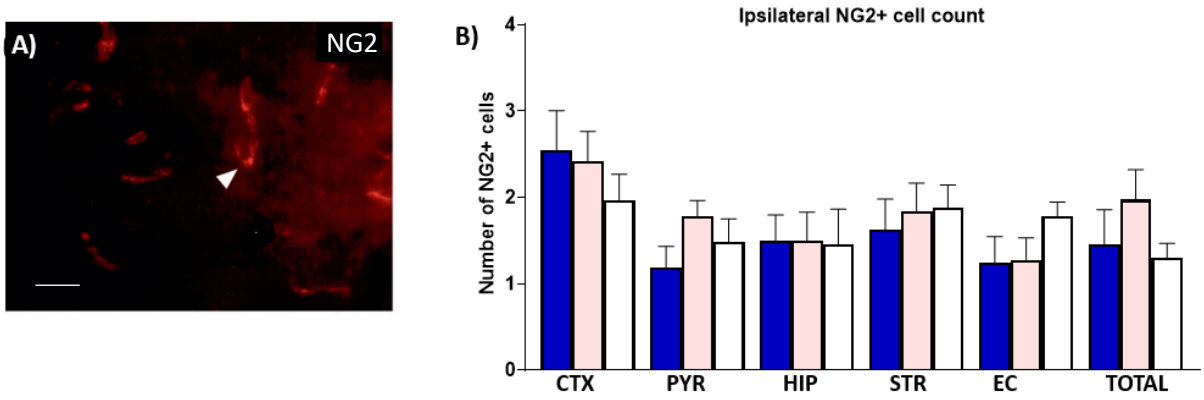

Figure 39**. Ipsilateral NG2 immunoreactivity in infection-sensitised HI, PBS-treated HI and untreated HI animals** (A) The mean and SEM of NG2 manual counts following immunohistochemistry staining for NG2 expression in cortex (CTX), external capsule (EC), hippocampus (HIP), pyriform cortex (PYR), striatum (STR), and thalamus (THA) in neonatal mice 48h following PBS or *E.coli* intra-uterine exposure with HI at P7, and untreated HI alone treatment groups. The combined average expression in all sub regions is also presented (total) (Kruskal-Wallis test with Dunn's post-hoc (p=0.3325). (B) Ipsilateral cortex of NG2 expression at 40x magnification in untreated HI, PBS treated and *E.coli* P7 mouse pups. (B) Immunofluorescence for NG2 and DAPI. Arrows= NG2+ cell. Scale bars= 20μm

Chapter 11: Discussion on Infection-sensitised HI

This study investigated the sensitising effects of maternal intrauterine infection on the neonatal mouse brain, combined with a unilateral HI insult. The aim of this study was to improve current pre-clinical infection-sensitised HI models to resemble more closely the clinical state in term asphyxiated infants, where gram-negative infections dominate. To elucidate the effects of intrauterine infections, a non-pathogenic *E. coli* K12 strain was intravaginally administered on embryonic day 16 to challenge the fetal immune system which could possibly have a sensitisation effect when an additional inflammatory trigger, such as HI insult, is introduced neonatally. Overall, this study found statistically significant increase of glial activation, tissue loss, cell death and oxidative stress of intrauterine *E. coli* infection further sensitising the neonatal brain to HI insult. However, no significant difference was observed for myelination. This investigation builds on previous research which highlights the exacerbation in HI brain damage after LPS sensitisation in animal models leading to increased rates of mortality and detrimental long-term outcomes such as cerebral palsy[312].

Previous studies have demonstrated an increase in microglial activation and proliferation in response to an infection[313]. Consistent with these reports, our study found a significant increase in microglial activation in multiple brain regions, in animals pre-exposed to *E.coli* compared to untreated HI and PBS treated control groups (Figure 37E). This is associated with the 'two-hit hypothesis' in which pre-exposure to LPS interact with TLR4-MyD-88 dependent pathway in the neonatal brain, exacerbating the HI insult[102,115,314]. Subsequently, this markedly increases the NF-kB signalling pathway upregulating the infection/inflammation response. A comparable study carried out by Suff and colleagues demonstrated pathogenic *E. coli* K1 strains

to render O-antigen in the LPS outer cell wall, thus increasing TLR4 interaction, due to O-antigen recognition, to evade the host compared to K12 stain, which lack O-antigens[315].

Reactive astrogliosis can further exacerbate the extent of brain injury by upregulating the production of pro-inflammatory (IL-1β, IL-6, and TNF-α) cytokines increasing NO toxicity, tissue loss, and initiating cellular death pathways. In addition, reactive astrogliosis produces chemokines (CXCL10) which enable migration of immune cells to the site of injury[129]. Our results on GFAP immunoreactivity results indicated an equivalent significantly increased ipsilateral astroglial activation in cortex and hippocampus, in the *E.coli* group compared to untreated HI and PBS treated controls (Figure 37I). This is in accordance with previous findings, which reported increased regions of astroglia activation in P7 rat pups after LPS-stimuli[315].

Furthermore, a recent study by Lively and colleagues compared changes in gene expression of pro- and anti-inflammatory cytokines after activation of microglia by either LPS or INFa/TNF-α[313]. The results showed that in both scenarios, activated microglia upregulate pro-inflammatory cytokines expression, leading to a proinflammatory state. Interestingly, while the administration of anti-inflammatory cytokines IL-4 and IL-10 resolved the established pro-inflammatory state, the application of such anti-inflammatory molecules did not completely reverse LPS induced inflammation[313]. This outcome suggests that LPS generates a more severe pro-inflammatory response compared to other stimuli, offering a possible explanation for our results in the *E.coli*-sensitised HI model.

Several studies in P7 rat and newborn piglet models evaluating the activation of proteolytic cleaved caspase-3 enzyme (CC3) following HI have revealed a caspase-

dependent pathway resulting in apoptotic cell death in the neonatal brain[96,215]. Alternatively, studies have indicated low CC3 cell counts to correlate with increased TUNEL+ cell death[96]. This is attributed to caspase-independent cell death pathway which initiates cell death via necrosis, necroptosis, and non-caspase mediated apoptosis. Caspase is protein, which will be expressed only during a particular phase of the apoptotic cell death process, while DNA fragmentation, which is detected with TUNEL, lasts longer and is detected for a longer period of time. This confirms that neuronal cell death commence in an 'apoptosis-necrosis continuum' which occurs in a hybrid form within the spectrum following HI insult as opposed to apoptosis or necrosis alone[1].

Our study also demonstrated a significant increase in iNOS expression in ipsilateral hippocampus following *E.coli* sensitisation and HI in comparison to untreated HI alone control groups (Figure 38B). These results support our hypothesis that infection sensitises the neonatal brain to HI damage resulting in increased oxidative stress. An increase in iNOS expression in the hippocampus can be explained by the two-hit hypothesis. LPS acts as a TLR agonist triggering MyD88 adaptor protein or Toll/IL-1R domain-containing adaptor recruitment producing IFN-β signal transduction and NF-kB cell activation[314,316]. Srivastava and colleagues (2018) have shown that microglial activation results in polarisation into pro- and anti- inflammatory microglial phenotypes responsible for macrophage-like tendencies, capable of phagocytosis, proinflammatory and anti-inflammatory cytokine release and iNOS production[317]. Pro-inflammatory polarisation is associated with upregulation of iNOS production[318]. It is well established that high concentrations of NO synthesised via oxidation of L-arginine by iNOS, inhibits mitochondrial respiration due to competition with O2 in cytochrome c oxidase. NO subsequently reacts with superoxide free radicals to create toxic

peroxynitrate, nitrogen peroxide, nitrogen dioxide and hydroxyl radicals, ultimately leading to increased damage to cellular components and cell death. Earlier investigations have highlighted peak iNOS production at 48h after HI[319]. In our study we observed iNOS positive cells at 48h post-HI, which may align with the excessive increase in pro-inflammatory cytokines due to microglial activation during the secondary energy failure. NO is a product of all three NOS isoforms, thus iNOS may not be a major contributor under HI insult, as shown by Rao and colleagues (2011) in a near-term rabbit HI model[320]. However, when combined with LPS sensitisation as modelled in our study, a significant increase in iNOS is likely to result in an exacerbation of damage to the neonatal brain.

No significant difference in MBP expression in the external capsule and striatum was identified in the *E.coli* sensitised group in comparison to PBS treated or untreated HI control groups (Figure 38A). Myelination is a process primarily driven by oligodendrocytes, but other glial cells such as microglia and astrocytes also contribute to myelin development. Astrocytes share a common lineage with oligodendrocytes. Under normal oxygen conditions, astrocytes express fibroblast growth factor 2 (FGF2) and PDGF which control the production of oligodendrocytes. In HI P7 rat models, astrocytes upregulate TNF-α and IL-1β, resulting in increased levels of oligodendrocyte apoptosis via interactions of astrocytes with TNF-receptor 1 present on oligodendrocytes[321]. Wan and colleagues (2022) have suggested that astrocyte activation during HI insult in mice allows astrocytic apoptosis, as degraded MBP is colocalised with lysosomal associated membrane protein 1 (LAMP1) in GFAP+ astrocytes. However, previous investigations using 1h hypoxia in LPS sensitised P7 C57Bl/6 mice have found a 15% mortality rate, with 70% of deaths occurring during the hypoxia phase. Hence, our study used a reduced hypoxia period of 30 minutes[322].

Additionally, Martinello and colleagues (2019) used a piglet model to display increased reactive astrogliosis following LPS sensitisation in naive animals. Reactive astrogliosis was lower following LPS sensitisation and HI, but still higher than HI alone controls[96], therefore less OPCs differentiate into oligodendrocytes, resulting in reduced myelination. Thus, the results in our study were unexpected and do not support the hypothesis that intra-uterine infection sensitises the neonates to HI conditions, diminishing myelination in a P7 mouse model.

Different levels of myelin transcripts and proteins at developmental stages differ between mouse strains[323]. Within C57Bl/6 mice, some investigations have identified initiation of MBP expression at P14, whereas others have identified MBP at P7[324]. Because the MBP levels were approximately equal in each treatment group, we concluded that *E.coli* K12 did not cause a significant delay in oligodendrocyte differentiation. Therefore, as a precursor of MBP, NG2 expression was assessed. Affeldt and colleagues (2017) have proposed that alterations in oligodendrocyte transcription factor expression is regional, with a significant delay in myelination in the external capsule following HI[325].

Immunofluorescent analysis of NG2 immunoreactivity found no significant difference in expression levels between the treatment groups (Figure 39). In an *in utero* P7 LPS sensitised non-HI mouse model, Borhani-Hagighi and colleagues (2019) presented that significant demyelination occurs, reducing the levels of MBP expressed by mature oligodendrocytes, as well as Olig2 expressed by both mature oligodendrocytes and OPCs[326]. Maternal inflammation due to in utero infection reduces the level of oligodendrocyte precursors[326]. The additional upregulation of microglia and macrophages in response to LPS exacerbates myelin phagocytosis and oligodendrocyte cell death[326].

In a rat model, NG2 is initially expressed by OPCs at P4. Following HI, the impact on the OPC population has been assessed via NG2 expression in the cortex at 24h, 48h and 72h post-HI, and a significant increase in NG2 positive cells was observed compared to the contralateral hemisphere[327]. Additionally, GFAP, expressed by activated astrocytes, was not co-localised with NG2 expression. OPC proliferation following HI may be indicative of rapid maturation, in an attempt to replenish the oligodendrocyte population[327]. In line with this data, Ahrendsen and colleagues (2016) reported that OPC numbers remaining elevated for a number of days post-HI with seemingly healthy myelin processes 24h post-HI in P20-25 mice. The same resistance was not noted in adult mice (8-12 weeks of age) as a result of altered K+ homeostasis triggering proliferation of NG2 expressing cells[328].

Overall, the current study established that in utero exposure to *E.coli* K12, followed by normal vaginal delivery and HI insult of the pups at P7 sensitised the neonatal brain. This is characterised by an increase in glial activation, cell death, tissue loss and iNOS expression in comparison to PBS-treated and untreated HI alone controls, which exacerbates the damage caused by the HI insult. Thus, *E. coli* K12 intravaginal infection directly induces a sensitisation in HI damage.

Chapter 12: Discussion, Limitations and Future Experiments

12.1 Overview

The lack of effective treatments for neonatal HI and infection sensitised HI was the leading point that drove the present research. Finding better and new treatments, explicitly targeting pathways of interest is of great significance in the field. This thesis aimed to further the understanding of STAT3's pathway involvement in HI brain damage. The following are the key findings from the study:

- WP1066, a JAK2/STAT3 inhibitor, provided short- and long- term neuroprotective effects after immediate or 1h, 2h delayed application, by reducing tissue loss, cell death, oxidative stress, glial activation, increasing myelination and improving behavioural outcomes.
- Curcumin, a natural compound with anti-inflammatory properties, exhibited short-term neuroprotective effects in DMSO solution, and encapsulated in P(3HB) microspheres, by reducing tissue loss, cell death, microglial and astroglial activation.
- Microglial-specific TGFβR1 deletion, reduced pro-inflammatory microglia and increased anti-inflammatory phenotype microglia, inducing repair after HI insult, indicating the potential mechanism of action on inflammation.
- Maternal intrauterine delivery of *E.coli* K12 strain, sensitised the pups brain by increasing tissue loss, cell death and glial activation, leading to the establishment of a new infection-sensitised HI model. Further studies are needed to investigate the involvement of STAT3 pathway in this infection-sensitised HI mouse model.

12.2 WP1066 application

WP1066

In this current study, WP1066 application, a low-molecular-weight kinase inhibitors targeting JAK2/STAT3 pathway, demonstrated neuroprotective effects in a P9 HI mouse model. Specifically, as shown in Chapter 3 immediate application of 80µg/g BW of WP1066, reduced cell death, tissue loss, glial activation, oxidative stress, increased myelination and anti-inflammatory microglia therefore inducing neuroprotection when assessed 48h after the initial HI insult. WP1066's application was dose-dependent as 40µg/g and 160µg/g BW doses did not provide protective effects. Additionally, WP1066 exhibited short-term neuroprotective effects by reducing cell death, tissue loss and glia activation, when administered with 1 or 2h delay after HI insult. These results are significantly important for translational research, as in a clinical setting diagnosis of affected infants can be delayed and therefore their treatment. Infants diagnosed with HI could develop long-term deficits, such as cerebral palsy and epilepsy, thus we investigated the long-term effects of immediate WP1066 application. The results showed a significant reduction of tissue loss, higher levels of myelination, and improvement of motor coordination and memory impairment. When exploring in detail the mechanism of action by which WP1066 can exploit its neuroprotective effects, we observed modulation of pSTAT3 Y705 levels in comparison to untreated HI and DMSO treated groups. We also observed a significant reduction in C1qa gene levels in hippocampus of WP1066 treated animals compared to DMSO treated controls, while no changes were seen for C1qb and C1qc levels.

Remarkably, this is the first study to provide evidence of WP1066's role on the complement system and potential neuroprotective effects via this pathway.

The current study supports previous work carried out by our group which determined the effect of combined 20 min pre-insult and immediate post-insult blockade of JAK2 with systemically applied WP1066 in a split dose of 80µg/g[181]. There are other studies in line with our results, indicating the neuroprotective role of WP1066[172,266,267]. In particular, WP1066 demonstrated inhibitory effects on JAK2-mediated signalling and decreased infract volume and pSTAT3 levels in a rat model of focal cerebral ischaemia[268]. In the current study, we observed a significant reduction in the levels of pSTAT3 compared to the DMSO control group, which is in line with our previous study from our lab[181]. However, we did not observe any significant difference on pSTAT3 levels between HI and naïve groups which could be contributed to the number of animals used for this study or to the chosen time-point (1h after HI insult). Therefore, further studies are needed to explore the effects of WP1066 levels on pSTAT3 at different time points and with larger number of animals.

Additionally, immediate application of WP1066 increased the levels of the CD206 anti-inflammatory gene, which correlates with the immunofluorescence results presented in this study showing that WP1066 treatment increased the levels of CD206+ cells Thus, we can assume that one potential neuroprotective mechanism of WP1066 application after HI insult may be via increasing the anti-inflammatory levels of CD206 resulting in induced repair. Remarkably, this is the first study to provide evidence of WP1066's role on the complement system and potential neuroprotective effects via this pathway, since we observed decreased levels of C1qa levels after WP1066 application. This result is line with the study of Vadim and colleagues (2005) where deletion of C1qa gene in C57Bl/6 mice that underwent HI at P7 led to significantly

decreased activation of circulating neutrophils associated with diminished local accumulation and attenuation of brain injury[274].

Overall, the data from the current study suggests a critical role for STAT3, including possibly also a contribution to neonatal HI-brain damage via Tyr705 phosphorylation.

12.3 Curcumin application

Curcumin is a compound widely studied for its anti-inflammatory, anti-oxidant and anti-apoptotic properties make it an appealing target for drug discovery in many neurodegenerative disorders[249,250,252,255]. The presence of a clear overlap between the mechanism of action of curcumin and the pathways involved in the pathology of neonatal HI positively supports the investigation of curcumin application in neonatal HI brain damage. Chapter 5 focused on exploring the therapeutic potential of a solution of curcumin in DMSO. The main findings reported that when applied immediately after HI insult an immediate dose of 200µg/g BW curcumin i.p. reduces tissue loss, cell death, microglial and astroglial activation, oxidative stress and increases myelination. These results are in line with previous study by our group in a P7 mouse with severe HI brain damage, where curcumin application dissolved in DMSO reduced glial activation, tissue loss and cell death[255]. Additionally, the results replicate and expand the results from previous studies performed in rats, in which curcumin provided neuroprotection[287]. In the current study, on the P9 mouse model, as well as in the P7 HI mice[255], immediate curcumin post-HI treatment reduced astroglial activation both ipsi- and contralaterally when compared to DMSO treated control group, and effect which can be attributed to bilateral acidosis and upregulation of pSTAT3, resulting in changes in both hemispheres after HI insult[181]. Additionally, curcumin is reported to

inhibit STAT3 phosphorylation[110], and seems to inhibit NF-kB signalling pathway, which reduces GFAP expression in astrocytes[289]. Hence, it is likely that after HI brain damage curcumin reduces astroglial activation by acting on NF-kB and STAT3 pathways, which both play an important role in stimulating apoptosis and inflammation therefore explaining the reduction in tissue loss and cell death. Curcumin's application in the P7 and P9 mouse model of HI also resulted in significantly reduced levels of tissue loss along with reduced number of iNOS positive cells[255]. These results may suggest that the decline in oxidative stress due to curcumin treatment is crucial in lessening neuronal tissue injury. These results are in line with a study, in an adult male rat model of HI, treatment with oral curcumin dissolved in DMSO application demonstrates an ability to target NOS[296].

A significant limitation of these studies is curcumin's low solubility, therefore the choice of DMSO as a solvent. To overcome this limitation, the research presented in Chapter 6 focused on exploring alternatives to increase curcumin solubility while removing DMSO from the formulation. This resulted in the manufacturing of P(3HB) microspheres of diameter around 0.551µm. These microspheres were stable at RT for and were tested in a P9 mouse model of neonatal HI, administered intranasally thus increasing efficacy and direct delivery to the brain. The two-step curcumin release strategy of the microspheres used in this study (Figure 31) could potentially be effective as a treatment for HI injury due to its ability to elicit both an immediate and delayed neuroprotective effect from the latent phase and onwards, if given between 30 minutes to 6h after the initial injury. Treatment with encapsulated curcumin P(3HB) microspheres showed promising neuroprotective results through reduction of tissue loss, cell death and microglial activation. However, these results did not match the

extend of neuroprotection observed with the DMSO formulation as astroglial activation was not significantly reduced, probably because of the low curcumin concentration. A possible way to increase the therapeutic effect of encapsulated curcumin could be the delivery of the microspheres in specific injured areas of the brain. Our results are in line with previous studies from our lab (unpublished data Hristova lab), where encapsulated curcumin in TPGS nanoparticles provided neuroprotective effects by reducing cell death, tissue loss and glial activation.

Overall, this study exhibited curcumin's neuroprotective role in a term (P9) mouse model of HI brain injury through the reduction of cell death, tissue loss and glial activation, in two different formulations; dissolved in DMSO and encapsulated in P(3HB) microspheres. Therefore, the use of curcumin as treatment for neonatal HI may be a valid neuroprotective strategy, while removing any need for invasive procedures when administered intranasally.

12.4 Microglial-specific TGFβR1 deletion

TGFβ1, a pleiotropic cytokine, and its receptor, TGFβR-1, are up-regulated after HI insult[304] (unpublished data Hristova lab). Microglia-specific TGFβR-1 deletion, exhibited neuroprotective effects by promoting prevalence of anti-inflammatory microglia, which induces repair after HI insult. TGFβ has been reported to act synergistically on STAT3 pathway[179] and therefore its effect on inflammation can provide a new insight into STAT3 pathway's involvement in HI brain damage.

Our group previously identified that microglia-specific deletion of TGFβR-1 in severe HI reduces tissue loss, microglial and astroglial activation, overall resulting in

neuroprotection (unpublished data Hristova lab). Based on the findings of the current study, our results indicate overall significantly low levels of both pro- and anti-inflammatory cells after microglia-specific TGFβR-1 deletion, which was to be expected based on the previous preliminary data showing overall reduction of microglial activation in the mutants. A study from Ryu and colleagues (2012) is in line with our observations in this study, since they showed that increased expression of TGFβ, as a result of HI insult, could prolong the activated state of microglia, hence, TGFβR-1 deletion would suppress it[307]. In conclusion, TGFβ and STAT3 pathways act synergistically on HI insult and the potential mechanism of neuroprotection may be by the increase of anti-inflammatory microglia, which induces repair.

12.5 Infection-sensitised HI model

This study investigated the sensitising effects of maternal intrauterine infection on the neonatal mouse brain, combined with a unilateral HI insult. Overall, the results showed statistically significant increase of glial activation, tissue loss, cell death and oxidative stress of intrauterine *E. coli* infection further sensitising the neonatal brain to HI insult. This investigation builds on previous research which highlights the exacerbation in HI brain damage after LPS sensitisation in animal models leading to increased rates of mortality and detrimental long-term outcomes such as cerebral palsy[312]. Our results are line with previous studies, which demonstrated an increase in microglial activation and proliferation in response to an infection[313]. This effect is associated with the 'two-hit hypothesis' in which pre-exposure to LPS interact with TLR4-MyD-88 dependent pathway in the neonatal brain, exacerbating the HI insult[102,115,314]. Subsequently, this markedly increases the NF-kB signalling pathway upregulating the

infection/inflammation response. This current study, also reported a significant increase in iNOS expression in ipsilateral hippocampus following *E.coli* sensitisation, which is line with previous studies[317] and can be explained by the two-hit hypothesis. LPS acts as a TLR agonist triggering MyD88 adaptor protein or Toll/IL-1R domain-containing adaptor recruitment producing IFN-β signal transduction and NF-kB cell activation[316].

Overall, the current study established that in utero exposure to *E.coli* K12, followed by normal vaginal delivery and HI insult of the pups at P7 sensitised the neonatal brain, by increasing glial activation, cell death, tissue loss and iNOS expression. Thus, *E. coli* K12 intravaginal infection directly induces a sensitisation in HI damage**.**

12.6 Conclusion

Neonatal HI and infection-sensitised HI brain injury are among the primary cause of neonatal morbidity and mortality worldwide. There is a paucity of treatments available for these pathologies, with TH being the clinical standard treatment for neonatal HI and efficacious in only half of the cases especially in the developing world. New therapeutic strategies are targeting specific pathways activated during HI, interfering with inflammation, oxidative stress and cell death. The lack of effective treatments for neonatal HI and the role of STAT3 on cell death pathways of the disease was the leading point that drove the present research. Finding new and promising treatments, targeting specific pathways, as STAT3, is of great significance in the field. The current study, provided significant results indicating the neuroprotective role of WP1066 and curcumin by acting on inflammation, oxidative stress and cell death.

In conclusion, the work presented in this thesis builds a solid base for further research on developing WP1066 and curcumin as treatments for neonatal HI brain damage and exploring further the role of STAT3 as a therapeutic target for the disease.

12.7 Limitations

There were two main limitations in the studies presented here; first, *in vivo* experiments on curcumin and TGFβR-1 deletion would have benefited from a deeper understanding of the molecular pathways involved. This limitation was not approached mainly due to lack of time: the high variability of the model would require a large sample size, and once the histological data was obtained, the same experiments should have been repeated to collect samples for molecular analysis. The collection of brain tissue and blood for each experiment to dedicate to molecular studies was not possible in the time allowed for this PhD. Specifically, on Chapter 3 we observed that after extracting the brain samples for western blot analysis at 1h after HI insult, the levels of pSTAT3 on the HI group are similar to naïve control animals, which highlights the significance of exploring different time points of brain samples extraction. This could also be a result of number of animals used for this experiment, therefore larger number of animals is needed to further explore the effects of HI insult on pSTAT3 levels. Second, during this PhD the Home Office Animal License expired and therefore no animal work was feasible for one year. This fact impacted my research as more *in vivo* experiments could have been conducted especially for the WP1066 Chapter 3. In conclusion, I recommend that these limitations should be considered by future researchers.

12.8 Future Research

Future research should focus on design and optimisation of a new WP1066 nanoparticle formulation, since DMSO's toxicity can be an obstacle for translational research and a less invasive and efficient way of delivery such as intranasal route of administration. It will be also important to determine the *in vivo* effects of this formulation and application in neonatal HI and in the presence of an infection-sensitisation. Furthermore, this study established a new infection-sensitised HI model based on *E.coli* maternal intravaginal injection, therefore it would be beneficial to test whether treatment of the pups with WP1066 and curcumin provides neuroprotection. Finally, studies on the ability of WP1066 and curcumin to cross the placenta and their toxicity in this context could shed light on their potential as pregnancy supplements to prevent brain damage from neonatal HI or to minimise its detrimental effects.

Bibliography

1. Rocha-Ferreira E, Hristova M. Plasticity in the Neonatal Brain following Hypoxic-Ischaemic Injury. *Neural Plasticity*. 2016;2016:1-16. doi:10.1155/2016/4901014

2. Osredkar D, Sabir H, Falck M, et al. Hypothermia Does Not Reverse Cellular Responses Caused by Lipopolysaccharide in Neonatal Hypoxic-Ischaemic Brain Injury. *Developmental Neuroscience*. 2015;37(4-5):390-397. doi:10.1159/000430860

3. Osredkar D, Thoresen M, Maes E, Flatebø T, Elstad M, Sabir H. Hypothermia is not neuroprotective after infection-sensitized neonatal hypoxic-ischemic brain injury. *Resuscitation*. 2014;85(4):567-572. doi:10.1016/j.resuscitation.2013.12.006

4. Wintermark P, Boyd T, Gregas MC, Labrecque M, Hansen A. Placental pathology in asphyxiated newborns meeting the criteria for therapeutic hypothermia. *American Journal of Obstetrics and Gynecology*. 2010;203(6):579.e1-579.e9. doi:10.1016/j.ajog.2010.08.024

5. Rocha-Ferreira E, Phillips E, Francesch-Domenech E, et al. The role of different strain backgrounds in bacterial endotoxin-mediated sensitization to neonatal hypoxic–ischemic brain damage. *Neuroscience*. 2015;311:292-307. doi:10.1016/j.neuroscience.2015.10.035

6. Rocha-Ferreira E, Hristova M. Plasticity in the neonatal brain following hypoxic-ischaemic injury. *Neural Plasticity*. 2016;2016:4901014. doi:10.1155/2016/4901014

7. Perrone S, Stazzoni G, Tataranno ML, Buonocore G. New pharmacologic and therapeutic approaches for hypoxic-ischemic encephalopathy in the newborn. In: *Journal of Maternal-Fetal and Neonatal Medicine*. Vol 25. J Matern Fetal Neonatal Med; 2012:83-88. doi:10.3109/14767058.2012.663168

8. Lundgren C, Brudin L, Wanby AS, Blomberg M. Ante- and intrapartum risk factors for neonatal hypoxic ischemic encephalopathy. *Journal of Maternal-Fetal and Neonatal Medicine*. 2018;31(12):1595-1601. doi:10.1080/14767058.2017.1321628

9. Ferriero DM. Neonatal Brain Injury. *New England Journal of Medicine*. 2004;351(19):1985-1995. doi:10.1056/nejmra041996

10. Sanders RD, Manning HJ, Robertson NJ, et al. Preconditioning and postinsult therapies for perinatal hypoxic-ischemic injury at term. *Anesthesiology*. 2010;113(1):233-249. doi:10.1097/ALN.0b013e3181dc1b84

11. Baburamani AA, Ek CJ, Walker DW, Castillo-Melendez M. Vulnerability of the developing brain to hypoxic-ischemic damage: contribution of the cerebral

vasculature to injury and repair? *Front Physiol*. 2012;3:424. doi:10.3389/fphys.2012.00424

12. Jensen A, Berger R. Fetal circulatory responses to oxygen lack. *Journal of developmental physiology*. 1991;16(4):181-207.

13. Vannucci RC. Experimental biology of cerebral hypoxia-ischemia: Relation to perinatal brain damage. *Pediatric Research*. 1990;27(4):317-326. doi:10.1203/00006450-199004000-00001

14. Jensen A, Garnier Y, Berger R. Dynamics of fetal circulatory responses to hypoxia and asphyxia. In: *European Journal of Obstetrics and Gynecology and Reproductive Biology*. Vol 84. Elsevier Ireland Ltd; 1999:155-172. doi:10.1016/S0301-2115(98)00325-X

15. Babcock MA, Kostova FV, Ferriero DM, et al. Injury to the Preterm Brain and Cerebral Palsy: Clinical Aspects, Molecular Mechanisms, Unanswered Questions, and Future Research Directions. *J Child Neurol*. 2009;24(9):1064-1084. doi:10.1177/0883073809338957

16. Amess PN, Penrice J, Cady EB, et al. Mild hypothermia after severe transient hypoxia-lschemia reduces the delayed rise in cerebral lactate in the newborn piglet. *Pediatric Research*. Published online 1997. doi:10.1203/00006450-199706000-00002

17. Hope PL, Cady EB, Tofts PS, et al. CEREBRAL ENERGY METABOLISM STUDIED WITH PHOSPHORUS NMR SPECTROSCOPY IN NORMAL AND BIRTH-ASPHYXIATED INFANTS. *The Lancet*. 1984;324(8399):366-370. doi:10.1016/S0140-6736(84)90539-7

18. Jantzie LL, Talos DM, Jackson MC, et al. Developmental Expression of N-Methyl-D-Aspartate (NMDA) Receptor Subunits in Human White and Gray Matter: Potential Mechanism of Increased Vulnerability in the Immature Brain. Published online 2013. doi:10.1093/cercor/bht246

19. Paoletti P, Bellone C, Zhou Q. NMDA receptor subunit diversity: impact on receptor properties, synaptic plasticity and disease. *Nat Rev Neurosci*. 2013;14(6):383-400. doi:10.1038/nrn3504

20. Rossi B, Maton G, Collin T. Calcium-permeable presynaptic AMPA receptors in cerebellar molecular layer interneurones. *J Physiol*. 2008;586(21):5129-5145. doi:10.1113/jphysiol.2008.159921

21. Kehrer JP. The Haber-Weiss reaction and mechanisms of toxicity. *Toxicology*. 2000;149(1):43-50. doi:10.1016/S0300-483X(00)00231-6

22. Mello Filho AC, Meneghini R. In vivo formation of single-strand breaks in DNA by hydrogen peroxide is mediated by the Haber-Weiss reaction. *BBA - Gene Structure and Expression*. 1984;781(1-2):56-63. doi:10.1016/0167-4781(84)90123-4

23. Traystman RJ, Kirsch JR, Koehler RC. Oxygen radical mechanisms of brain injury following ischemia and reperfusion. *J Appl Physiol (1985)*. 1991;71(4):1185-1195. doi:10.1152/jappl.1991.71.4.1185

24. Davies KJ, Goldberg AL. Oxygen radicals stimulate intracellular proteolysis and lipid peroxidation by independent mechanisms in erythrocytes. *Journal of Biological Chemistry*. 1987;262(17):8220-8226. doi:10.1016/S0021-9258(18)47552-7

25. Vasiljevic B, Maglajlic-Djukic S, Gojnic M, Stankovic S. The role of oxidative stress in perinatal hypoxic-ischemic brain injury. *Srpski arhiv za celokupno lekarstvo*. 2012;140(1-2):35.

26. Gunn AJ, Parer JT, Mallard EC, Williams CE, Gluckman PD. Cerebral histologie and electrocorticographic changes after asphyxia in fetal sheep. *Pediatric Research*. 1992;31(5):486-491. doi:10.1203/00006450-199205000-00016

27. Drury PP, Bennet L, Gunn AJ. Mechanisms of hypothermic neuroprotection. *Seminars in Fetal and Neonatal Medicine*. 2010;15(5):287-292. doi:10.1016/j.siny.2010.05.005

28. Iwata O, Iwata S, Thornton JS, et al. “Therapeutic time window” duration decreases with increasing severity of cerebral hypoxia-ischaemia under normothermia and delayed hypothermia in newborn piglets. *Brain Research*. 2007;1154(1):173-180. doi:10.1016/j.brainres.2007.03.083

29. Quiniou C, Kooli E, Joyal JS, et al. Interleukin-1 and Ischemic Brain Injury in the Newborn: Development of a Small Molecule Inhibitor of IL-1 Receptor. *Seminars in Perinatology*. 2008;32(5):325-333. doi:10.1053/j.semperi.2008.07.001

30. Ådén U, Favrais G, Plaisant F, et al. Systemic inflammation sensitizes the neonatal brain to excitotoxicity through a pro-/anti-inflammatory imbalance: Key role of TNFα pathway and protection by etanercept. *Brain, Behavior, and Immunity*. 2010;24(5):747-758. doi:10.1016/j.bbi.2009.10.010

31. Shrivastava K, Llovera G, Recasens M, et al. Temporal expression of cytokines and signal transducer and activator of transcription factor 3 activation after neonatal hypoxia/ischemia in mice. In: *Developmental Neuroscience*. Vol 35. ; 2013:212-225. doi:10.1159/000348432

32. Janowska J, Sypecka J. Therapeutic Strategies for Leukodystrophic Disorders Resulting from Perinatal Asphyxia: Focus on Myelinating Oligodendrocytes. *Molecular Neurobiology*. 2018;55(5):4388-4402. doi:10.1007/s12035-017-0647-7

33. Segovia KN, McClure M, Moravec M, et al. Arrested oligodendrocyte lineage maturation in chronic perinatal white matter injury. *Annals of Neurology*. 2008;63(4):520-530. doi:10.1002/ana.21359

34. Penrice J, Lorek A, Cady EB, et al. Proton magnetic resonance spectroscopy of the brain during acute hypoxia-ischemia and delayed cerebral energy failure in

the newborn piglet. *Pediatric Research*. 1997;41(6):795-802. doi:10.1203/00006450-199706000-00001

35. Peng TI, Greenamyre JT. Privileged access to mitochondria of calcium influx through N-methyl-D- aspartate receptors. *Molecular Pharmacology*. 1998;53(6):974-980.

36. Puka-Sundvall M, Wallin C, Gilland E, et al. Impairment of mitochondrial respiration after cerebral hypoxia-ischemia in immature rats: Relationship to activation of caspase-3 and neuronal injury. *Developmental Brain Research*. 2000;125(1-2):43-50. doi:10.1016/S0165-3806(00)00111-5

37. Johnston M V, Nakajima W, Hagberg H. Mechanisms of hypoxic neurodegeneration in the developing brain. *The Neuroscientist : a review journal bringing neurobiology, neurology and psychiatry*. 2002;8(3):212-220. doi:10.1177/1073858402008003007

38. Northington FJ, Zelaya ME, O'Riordan DP, et al. Failure to complete apoptosis following neonatal hypoxia-ischemia manifests as "continuum" phenotype of cell death and occurs with multiple manifestations of mitochondrial dysfunction in rodent forebrain. *Neuroscience*. 2007;149(4):822-833. doi:10.1016/j.neuroscience.2007.06.060

39. Moynagh PN. The interleukin-1 signalling pathway in astrocytes: a key contributor to inflammation in the brain. *Journal of Anatomy*. 2005;207(3):265-269. doi:10.1111/j.1469-7580.2005.00445.x

40. O'Hare FM, Watson RWG, O'Neill A, et al. Serial cytokine alterations and abnormal neuroimaging in newborn infants with encephalopathy. *Acta Paediatrica*. 2017;106(4):561-567. doi:10.1111/apa.13745

41. Bilbo SD, Schwarz JM. Early-Life Programming of Later-Life Brain and Behavior: A Critical Role for the Immune System. *Front Behav Neurosci*. 2009;3:14. doi:10.3389/neuro.08.014.2009

42. Ca M, Hj S, S C, T P, Jm S. Spinal cord injury-induced expression of the immune-regulatory chemokine interleukin-16 caused by activated microglia/macrophages and CD8+ cells. *Journal of neurosurgery Spine*. 2006;4(3). doi:10.3171/spi.2006.4.3.233

43. Iyer SS, Cheng G. Role of Interleukin 10 Transcriptional Regulation in Inflammation and Autoimmune Disease. *Crit Rev Immunol*. 2012;32(1):23-63.

44. Descloux C, Ginet V, Clarke PGH, Puyal J, Truttmann AC. Neuronal death after perinatal cerebral hypoxia-ischemia: Focus on autophagy-mediated cell death. *Int J Dev Neurosci*. 2015;45:75-85. doi:10.1016/j.ijdevneu.2015.06.008

45. Lu Y, Tucker D, Dong Y, Zhao N, Zhuo X, Zhang Q. Role of Mitochondria in Neonatal Hypoxic-Ischemic Brain Injury. Journal of neuroscience and rehabilitation 2015; 2: 1–14 -

46. Johnston M V, Trescher WH, Ishida A, Nakajima W. Neurobiology of hypoxic-ischemic injury. *Pediatric Research*. Published online 2001.

47. Skoff RP, Bessert D, Barks JDE, Silverstein FS. Plasticity of neurons and glia following neonatal hypoxic-ischemic brain injury in rats. *Neurochemical Research*. 2007;32(2):331-342. doi:10.1007/s11064-006-9188-6

48. Tetorou, K., Sisa, C., Iqbal, A., Dhillon, K., & Hristova, M. (2021). Current Therapies for Neonatal Hypoxic–Ischaemic and Infection-Sensitised Hypoxic–Ischaemic Brain Damage. Frontiers in Synaptic Neuroscience, 13. https://doi.org/10.3389/fnsyn.2021.709301

49. Lang JT, McCullough LD. Pathways to ischemic neuronal cell death: are sex differences relevant? *Journal of Translational Medicine*. 2008;6(1):33. doi:10.1186/1479-5876-6-33

50. Cotten CM, Shankaran S. Hypothermia for hypoxic-ischemic encephalopathy. *Expert Rev Obstet Gynecol*. 2010;5(2):227-239. doi:10.1586/eog.10.7

51. Cregan SP, Dawson VL, Slack RS. Role of AIF in caspase-dependent and caspase-independent cell death. *Oncogene*. 2004;23(16):2785-2785. doi:10.1038/sj.onc.1207517

52. Thornton C, Leaw B, Mallard C, Nair S, Jinnai M, Hagberg H. Cell Death in the Developing Brain after Hypoxia-Ischemia. *Frontiers in Cellular Neuroscience*. 2017;11(August):1-19. doi:10.3389/fncel.2017.00248

53. Wajant H. The Fas signaling pathway: more than a paradigm. *Science*. 2002;296(5573):1635-1636. doi:10.1126/science.1071553

54. Hagberg H, Mallard C, Rousset CI, Thornton C. Mitochondria: hub of injury responses in the developing brain. *Lancet Neurol*. 2014;13(2):217-232. doi:10.1016/S1474-4422(13)70261-8

55. Sutcliffe TC, Winter AN, Punessen NC, Linseman DA. Procyanidin B2 Protects Neurons from Oxidative, Nitrosative, and Excitotoxic Stress. *Antioxidants (Basel)*. 2017;6(4):77. doi:10.3390/antiox6040077

56. Wang X, Han W, Du X, et al. Neuroprotective effect of Bax-inhibiting peptide on neonatal brain injury. *Stroke*. 2010;41(9):2050-2055. doi:10.1161/STROKEAHA.110.589051

57. Jänicke RU, Sprengart ML, Wati MR, Porter AG. Caspase-3 is required for DNA fragmentation and morphological changes associated with apoptosis. *J Biol Chem*. 1998;273(16):9357-9360. doi:10.1074/jbc.273.16.9357

58. Galluzzi L, Blomgren K, Kroemer G. Mitochondrial membrane permeabilization in neuronal injury. *Nat Rev Neurosci*. 2009;10(7):481-494. doi:10.1038/nrn2665

59. Fatokun AA, Dawson VL, Dawson TM. Parthanatos: mitochondrial-linked mechanisms and therapeutic opportunities. *Br J Pharmacol*. 2014;171(8):2000-2016. doi:10.1111/bph.12416

60. Northington FJ, Ferriero DM, Graham EM, Traystman RJ, Martin LJ. Early Neurodegeneration after Hypoxia-Ischemia in Neonatal Rat Is Necrosis while Delayed Neuronal Death Is Apoptosis. *Neurobiology of Disease*. 2001;8(2):207-219. doi:10.1006/nbdi.2000.0371

61. Lyu H, Sun DM, Ng CP, et al. A new Hypoxic Ischemic Encephalopathy model in neonatal rats. *Heliyon*. 2021;7(12):e08646. doi:10.1016/j.heliyon.2021.e08646

62. Leist M, Single B, Castoldi AF, Kühnle S, Nicotera P. Intracellular Adenosine Triphosphate (ATP) Concentration: A Switch in the Decision Between Apoptosis and Necrosis. *J Exp Med*. 1997;185(8):1481-1486.

63. Millar LJ, Shi L, Hoerder-Suabedissen A, Molnár Z. Neonatal hypoxia ischaemia: Mechanisms, models, and therapeutic challenges. *Frontiers in Cellular Neuroscience*. Published online 2017. doi:10.3389/fncel.2017.00078

64. He C, Klionsky DJ. Regulation mechanisms and signaling pathways of autophagy. *Annu Rev Genet*. 2009;43:67-93. doi:10.1146/annurev-genet-102808-114910

65. Shintani T, Klionsky DJ. Autophagy in health and disease: a double-edged sword. *Science*. 2004;306(5698):990-995. doi:10.1126/science.1099993

66. Boland B, Nixon RA. Neuronal macroautophagy: from development to degeneration. *Mol Aspects Med*. 2006;27(5-6):503-519. doi:10.1016/j.mam.2006.08.009

67. Matyja E, Taraszewska A, Nagańska E, Rafałowska J. Autophagic degeneration of motor neurons in a model of slow glutamate excitotoxicity in vitro. *Ultrastruct Pathol*. 2005;29(5):331-339. doi:10.1080/01913120500214333

68. Shacka JJ, Lu J, Xie ZL, Uchiyama Y, Roth KA, Zhang J. Kainic acid induces early and transient autophagic stress in mouse hippocampus. *Neurosci Lett*. 2007;414(1):57-60. doi:10.1016/j.neulet.2006.12.025

69. Wang Y, Han R, Liang ZQ, et al. An autophagic mechanism is involved in apoptotic death of rat striatal neurons induced by the non-N-methyl-D-aspartate receptor agonist kainic acid. *Autophagy*. 2008;4(2):214-226. doi:10.4161/auto.5369

70. Rice JE, Vannucci RC, Brierley JB. The influence of immaturity on hypoxic-ischemic brain damage in the rat. *Annals of Neurology*. 1981;9(2):131-141. doi:10.1002/ana.410090206

71. Koike M, Shibata M, Tadakoshi M, et al. Inhibition of Autophagy Prevents Hippocampal Pyramidal Neuron Death after Hypoxic-Ischemic Injury. *Am J Pathol*. 2008;172(2):454-469. doi:10.2353/ajpath.2008.070876

72. Laptook AR. Birth Asphyxia and Hypoxic-Ischemic Brain Injury in the Preterm Infant. *Clinics in Perinatology*. 2016;43(3):529-545. doi:10.1016/j.clp.2016.04.010

73. Ohshima M, Coq JO, Otani K, et al. Mild intrauterine hypoperfusion reproduces neurodevelopmental disorders observed in prematurity. *Scientific Reports*. 2016;6. doi:10.1038/srep39377

74. McQuillen PS, Sheldon RA, Shatz CJ, Ferriero DM. Selective vulnerability of subplate neurons after early neonatal hypoxia-ischemia. *Journal of Neuroscience*. 2003;23(8):3308-3315. doi:10.1523/jneurosci.23-08-03308.2003

75. Kendall GS, Hirstova M, Horn S, et al. TNF gene cluster deletion abolishes lipopolysaccharide-mediated sensitization of the neonatal brain to hypoxic ischemic insult. *Laboratory Investigation*. 2011;91(3):328-341. doi:10.1038/labinvest.2010.192

76. Volpe JJ. Perinatal brain injury: From pathogenesis to neuroprotection. *Mental Retardation and Developmental Disabilities Research Reviews*. 2001;7(1):56-64. doi:10.1002/1098-2779(200102)7:1<56::AID-MRDD1008>3.0.CO;2-A

77. Back SA, Riddle A, McClure MM. Maturation-dependent vulnerability of perinatal white matter in premature birth. In: *Stroke*. Vol 38. ; 2007:724-730. doi:10.1161/01.STR.0000254729.27386.05

78. Volpe JJ, Kinney HC, Jensen FE, Rosenberg PA. The developing oligodendrocyte: Key cellular target in brain injury in the premature infant. *International Journal of Developmental Neuroscience*. 2011;29(4):423-440. doi:10.1016/j.ijdevneu.2011.02.012

79. Fern R, Möller T. Rapid ischemic cell death in immature oligodendrocytes: A fatal glutamate release feedback loop. *Journal of Neuroscience*. 2000;20(1):34-42. doi:10.1523/jneurosci.20-01-00034.2000

80. Baud O, Greene AE, Li J, Wang H, Volpe JJ, Rosenberg PA. Glutathione Peroxidase-Catalase Cooperativity Is Required for Resistance to Hydrogen Peroxidase by Mature Rat Oligodendrocytes. *Journal of Neuroscience*. 2004;24(7):1531-1540. doi:10.1523/JNEUROSCI.3989-03.2004

81. Jantzie LL, Talos DM, Jackson MC, et al. Developmental Expression of N-Methyl-D-Aspartate (NMDA) Receptor Subunits in Human White and Gray Matter: Potential Mechanism of Increased Vulnerability in the Immature Brain. Published online 2013. doi:10.1093/cercor/bht246

82. Martin LJ, Brambrink A, Koehler RC, Traystman RJ. Primary sensory and forebrain motor systems in the newborn brain are preferentially damaged by hypoxia-ischemia. *Journal of Comparative Neurology*. Published online 1997. doi:10.1002/(SICI)1096-9861(19970113)377:2<262::AID-CNE8>3.0.CO;2-1

83. Johnston M V., Trescher WH, Ishida A, Nakajima W, Zipursky A. Neurobiology of hypoxic-ischemic injury in the developing brain. *Pediatric Research*. 2001;49(6):735-741. doi:10.1203/00006450-200106000-00003

84. Menkes JH, Curran J. Clinical and MR correlates in children with extrapyramidal cerebral palsy. *AJNR American journal of neuroradiology*. 1994;15(3):451-457.

85. Wood T, Moralejo D, Corry K, et al. A Ferret Model of Inflammation-sensitized Late Preterm Hypoxic-ischemic Brain Injury. *Journal of visualized experiments : JoVE*. 2019;(153):1-9. doi:10.3791/60131

86. McLean C, Ferriero D. Mechanisms of hypoxic-ischemic injury in the term infant. *Seminars in Perinatology*. 2004;28(6):425-432. doi:10.1053/j.semperi.2004.10.005

87. Jisa KA, Clarey DD, Peeples ES. Magnetic Resonance Imaging Findings of Term and Preterm Hypoxic-Ischemic Encephalopathy: A Review of Relevant Animal Models and Correlation to Human Imaging. *The Open Neuroimaging Journal*. Published online 2018. doi:10.2174/1874440001812010055

88. Eklind S, Mallard C, Leverin AL, et al. Bacterial endotoxin sensitizes the immature brain to hypoxic-ischaemic injury. *European Journal of Neuroscience*. 2001;13(6):1101-1106. doi:10.1046/j.0953-816X.2001.01474.x

89. Suff N, Karda R, Diaz JA, et al. Ascending Vaginal Infection Using Bioluminescent Bacteria Evokes Intrauterine Inflammation, Preterm Birth, and Neonatal Brain Injury in Pregnant Mice. *Am J Pathol*. 2018;188(10):2164-2176. doi:10.1016/j.ajpath.2018.06.016

90. O'Callaghan ME, MacLennan AH, Gibson CS, et al. Epidemiologic associations with cerebral palsy. *Obstetrics and Gynecology*. Published online 2011. doi:10.1097/AOG.0b013e31822ad2dc

91. Suff N, Karda R, Perocheau D, et al. *ImmuNologicAl AsPects of GeNe TheRAPy i A Light-Producing Model of Infection-Related Preterm Birth*.; 2016. doi:10.1038/mt.2016.78

92. Agrawal V, Hirsch E. Intra-uterine infection and preterm labor. Seminars in Fetal and Neonatal Medicine. 2012 Feb 1;17(1):12–9.

93. Blencowe H, Cousens S, Oestergaard MZ, et al. National, regional, and worldwide estimates of preterm birth rates in the year 2010 with time trends since 1990 for selected countries: a systematic analysis and implications. *Lancet*. 2012;379(9832):2162-2172. doi:10.1016/S0140-6736(12)60820-4

94. Dammann O, Leviton A. Does prepregnancy bacterial vaginosis increase a mother's risk of having a preterm infant with cerebral palsy? *Developmental Medicine & Child Neurology*. 2008;39(12):836-840. doi:10.1111/j.1469-8749.1997.tb07554.x

95. Lipopolysaccharide Sensitizes Neonatal Hypoxic-Ischemic Brain Injury in a MyD88-Dependent Manner | The Journal of Immunology. Accessed October 2, 2022. https://www.jimmunol.org/content/183/11/7471

96. Martinello KA, Meehan C, Avdic-Belltheus A, et al. Acute LPS sensitization and continuous infusion exacerbates hypoxic brain injury in a piglet model of neonatal encephalopathy. *Scientific Reports*. 2019;9(1):10184. doi:10.1038/s41598-019-46488-y

97. Lehnardt S, Massillon L, Follett P, et al. Activation of innate immunity in the CNS triggers neurodegeneration through a Toll-like receptor 4-dependent pathway. *Proceedings of the National Academy of Sciences of the United States of America*. 2003;100(14):8514-8519. doi:10.1073/pnas.1432609100

98. Yang D, Sun YY, Lin X, et al. Intranasal delivery of cell-penetrating anti-NF-κB peptides (Tat-NBD) alleviates infection-sensitized hypoxic–ischemic brain injury. *Experimental Neurology*. 2013;247:447-455. doi:10.1016/j.expneurol.2013.01.015

99. Cunha C, Gomes C, Vaz AR, Brites D. Exploring New Inflammatory Biomarkers and Pathways during LPS-Induced M1 Polarization. *Mediators of Inflammation*. 2016;2016:1-17. doi:10.1155/2016/6986175

100. Serdar M, Kempe K, Rizazad M, et al. Early Pro-inflammatory Microglia Activation After Inflammation-Sensitized Hypoxic-Ischemic Brain Injury in Neonatal Rats. *Frontiers in Cellular Neuroscience*. 2019;13:237. doi:10.3389/fncel.2019.00237

101. Kapitanović Vidak H, Catela Ivković T, Jokić M, Spaventi R, Kapitanović S. The association between proinflammatory cytokine polymorphisms and cerebral palsy in very preterm infants. *Cytokine*. 2012;58(1):57-64. doi:10.1016/j.cyto.2011.12.018

102. Mallard Anders Elmgren C, Gan L, Eriksson K, et al. MyD88-Dependent Manner Hypoxic-Ischemic Brain Injury in a Lipopolysaccharide Sensitizes Neonatal. *J Immunol References*. 2009;183:7471-7477. doi:10.4049/jimmunol.0900762

103. Kendall GS, Hirstova M, Horn S, et al. TNF gene cluster deletion abolishes lipopolysaccharide-mediated sensitization of the neonatal brain to hypoxic ischemic insult. *Laboratory Investigation*. 2011;91(3):328-341. doi:10.1038/labinvest.2010.192

104. Stolp HB, Ek CJ, Johansson PA, et al. Effect of minocycline on inflammation-induced damage to the blood-brain barrier and white matter during development. *European Journal of Neuroscience*. 2007;26(12):3465-3474. doi:10.1111/j.1460-9568.2007.05973.x

105. Hagberg H, Mallard C, Ferriero DM, et al. The role of inflammation in perinatal brain injury. doi:10.1038/nrneurol.2015.13

106. Tribe RM, Moriarty P, Dalrymple A, Hassoni AA, Poston L. Interleukin-1β induces calcium transients and enhances basal and store operated calcium entry in human myometrial smooth muscle. Biology of Reproduction. 2003 May;68(5):1842–9.

107. Counsell SJ, Maalouf EF, Fletcher AM, et al. MR imaging assessment of myelination in the very preterm brain. *AJNR Am J Neuroradiol*. 2002;23(5):872-881.

108. Foster-Barber A, Dickens B, neuroscience DFD, 2001 undefined. Human perinatal asphyxia: correlation of neonatal cytokines with MRI and outcome. *karger.com*.

109. Sävman K, Blennow M, Gustafson K, … ETP, 1998 undefined. Cytokine response in cerebrospinal fluid after birth asphyxia. *nature.com*.

110. Fjalstad JW, Stensvold HJ, Bergseng H, et al. Early-Onset Sepsis and Antibiotic Exposure in Term Infants. *The Pediatric Infectious Disease Journal*. 2015;35(1):1. doi:10.1097/INF.0000000000000906

111. Falck M, Osredkar D, Maes E, et al. Hypothermic Neuronal Rescue from Infection-Sensitised Hypoxic-Ischaemic Brain Injury Is Pathogen Dependent. *Developmental Neuroscience*. 2017;39(1-4):238-247. doi:10.1159/000455838

112. Mottahedin A, Svedin P, Nair S, et al. Systemic activation of Toll-like receptor 2 suppresses mitochondrial respiration and exacerbates hypoxic-ischemic injury in the developing brain. *Journal of Cerebral Blood Flow and Metabolism*. 2017;37(4):1192-1198. doi:10.1177/0271678X17691292

113. Yang D, Sun YY, Nemkul N, et al. Plasminogen activator inhibitor-1 mitigates brain injury in a rat model of infection-sensitized neonatal hypoxia-ischemia. *Cerebral Cortex*. Published online 2013. doi:10.1093/cercor/bhs115

114. Lehnardt S, Lachance C, Patrizi S, et al. The toll-like receptor TLR4 is necessary for lipopolysaccharide-induced oligodendrocyte injury in the CNS. *The Journal of neuroscience : the official journal of the Society for Neuroscience*. 2002;22(7):2478-2486. doi:20026268

115. Dean JM, Wang X, Kaindl AM, et al. Microglial MyD88 signaling regulates acute neuronal toxicity of LPS-stimulated microglia in vitro. *Brain, Behavior, and Immunity*. 2010;24(5):776-783. doi:10.1016/j.bbi.2009.10.018

116. Yamamuro K, Kimoto S, Rosen KM, Kishimoto T, Makinodan M. Potential primary roles of glial cells in the mechanisms of psychiatric disorders. *Front Cell Neurosci*. 2015;9:154. doi:10.3389/fncel.2015.00154

117. Kalla R, Liu Z, Xu S, et al. Microglia and the early phase of immune surveillance in the axotomized facial motor nucleus: Impaired microglial activation and lymphocyte recruitment but no effect on neuronal survival or axonal regeneration in macrophage-colony stimulating factor-defici. *Journal of Comparative Neurology*. 2001;436(2):182-201. doi:10.1002/cne.1060

118. Li Q, Barres BA. Microglia and macrophages in brain homeostasis and disease. *Nat Rev Immunol*. 2018;18(4):225-242. doi:10.1038/nri.2017.125

119. Ginhoux F, Greter M, Leboeuf M, et al. Fate mapping analysis reveals that adult microglia derive from primitive macrophages. *Science*. 2010;330(6005):841-845. doi:10.1126/science.1194637

120. Lund H, Pieber M, Parsa R, et al. Competitive repopulation of an empty microglial niche yields functionally distinct subsets of microglia-like cells. *Nat Commun*. 2018;9(1):4845. doi:10.1038/s41467-018-07295-7

121. Graeber MB, López-Redondo F, Ikoma E, et al. The microglia/macrophage response in the neonatal rat facial nucleus following axotomy. *Brain Research*. 1998;813(2):241-253. doi:10.1016/S0006-8993(98)00859-2

122. Colonna M, Butovsky O. Microglia Function in the Central Nervous System During Health and Neurodegeneration. *Annu Rev Immunol*. 2017;35:441-468. doi:10.1146/annurev-immunol-051116-052358

123. Shi Y, Wu W, Chai Q, et al. LTβR controls thymic portal endothelial cells for haematopoietic progenitor cell homing and T-cell regeneration. *Nat Commun*. 2016;7(1):12369. doi:10.1038/ncomms12369

124. Yao HW, Kuan CY. Early neutrophil infiltration is critical for inflammation-sensitized hypoxic-ischemic brain injury in newborns. *J Cereb Blood Flow Metab*. 2020;40(11):2188-2200. doi:10.1177/0271678X19891839

125. Omlin FX, Webster HD, Palkovits CG, Cohen SR. Immunocytochemical localization of basic protein in major dense line regions of central and peripheral myelin. *J Cell Biol*. 1982;95(1):242-248. doi:10.1083/jcb.95.1.242

126. Rasband MN. Glial Contributions to Neural Function and Disease. *Mol Cell Proteomics*. 2016;15(2):355-361. doi:10.1074/mcp.R115.053744

127. Michaluk P, Heller JP, Rusakov DA. Rapid recycling of glutamate transporters on the astroglial surface. Elife. 2021;10(1):e64714.

128. Jha MK, Kim JH, Song GJ, et al. Functional dissection of astrocyte-secreted proteins: Implications in brain health and diseases. *Prog Neurobiol*. 2018;162:37-69. doi:10.1016/j.pneurobio.2017.12.003

129. Cekanaviciute E, Buckwalter MS. Astrocytes: Integrative Regulators of Neuroinflammation in Stroke and Other Neurological Diseases. *Neurotherapeutics*. 2016;13(4):685-701. doi:10.1007/s13311-016-0477-8

130. Bell KF, Al-Mubarak B, Fowler JH, et al. Mild oxidative stress activates Nrf2 in astrocytes, which contributes to neuroprotective ischemic preconditioning. *Proc Natl Acad Sci U S A*. 2011;108(1):E1-2; author reply E3-4. doi:10.1073/iti0111108

131. Jiao M, Li X, Chen L, et al. Neuroprotective effect of astrocyte-derived IL-33 in neonatal hypoxic-ischemic brain injury. *J Neuroinflammation*. 2020;17:251. doi:10.1186/s12974-020-01932-z

132. Hardy R, Reynolds R. Proliferation and differentiation potential of rat forebrain oligodendroglial progenitors both in vitro and in vivo. *Development*. 1991;111(4):1061-1080. doi:10.1242/dev.111.4.1061

133. Snaidero N, Möbius W, Czopka T, Hekking LHP, Mathisen C, Verkleij D, et al. Myelin membrane wrapping of CNS axons by PI(3,4,5)P3-dependent polarized growth at the inner tongue. Cell

134. Naruse M, Ishino Y, Kumar A, et al. The Dorsoventral Boundary of the Germinal Zone is a Specialized Niche for the Generation of Cortical Oligodendrocytes

during a Restricted Temporal Window. *Cereb Cortex*. 2016;26(6):2800-2810. doi:10.1093/cercor/bhv141

135. Huang W, Bhaduri A, Velmeshev D, et al. Origins and Proliferative States of Human Oligodendrocyte Precursor Cells. *Cell*. 2020;182(3):594-608.e11. doi:10.1016/j.cell.2020.06.027

136. Kucharova K, Stallcup WB. The NG2 proteoglycan promotes oligodendrocyte progenitor proliferation and developmental myelination. *Neuroscience*. 2010;166(1):185-194. doi:10.1016/j.neuroscience.2009.12.014

137. Seo JH, Miyamoto N, Hayakawa K, et al. Oligodendrocyte precursors induce early blood-brain barrier opening after white matter injury. *J Clin Invest*. 2013;123(2):782-786. doi:10.1172/JCI65863

138. Akay LA, Effenberger AH, Tsai LH. Cell of all trades: oligodendrocyte precursor cells in synaptic, vascular, and immune function. *Genes Dev*. 2021;35(3-4):180-198. doi:10.1101/gad.344218.120

139. Matrix metalloproteinase 7 promoted Schwann cell migration and myelination after rat sciatic nerve injury | Molecular Brain | Full Text. Accessed October 2, 2022. https://molecularbrain.biomedcentral.com/articles/10.1186/s13041-019-0516-6

140. Kaplan S, Geuna S, Ronchi G, Ulkay MB, von Bartheld CS. Calibration of the stereological estimation of the number of myelinated axons in the rat sciatic nerve: A multicenter study. *J Neurosci Methods*. 2010;187(1):90-99. doi:10.1016/j.jneumeth.2010.01.001

141. Fünfschilling U, Supplie LM, Mahad D, et al. Glycolytic oligodendrocytes maintain myelin and long-term axonal integrity. *Nature*. 2012;485(7399):517-521. doi:10.1038/nature11007

142. Impact of neonatal hypoxia-ischaemia on oligodendrocyte survival, maturation and myelinating potential. Accessed October 2, 2022. https://www.ncbi.nlm.nih.gov/pmc/articles/PMC5742723/

143. Norton WT, Poduslo SE. Myelination in rat brain: method of myelin isolation. *J Neurochem*. 1973;21(4):749-757. doi:10.1111/j.1471-4159.1973.tb07519.x

144. Zaidi AU, Bessert DA, Ong JE, et al. New oligodendrocytes are generated after neonatal hypoxic-ischemic brain injury in rodents. *Glia*. 2004;46(4):380-390. doi:10.1002/glia.20013

145. Bohnert S, Wirth C, Schmitz W, et al. Myelin basic protein and neurofilament H in postmortem cerebrospinal fluid as surrogate markers of fatal traumatic brain injury. *Int J Legal Med*. 2021;135(4):1525-1535. doi:10.1007/s00414-021-02606-y

146. Zhao H, Gao XY, Liu ZH, et al. Effects of the transcription factor Olig1 on the differentiation and remyelination of oligodendrocyte precursor cells after focal

cerebral ischemia in rats. *Molecular Medicine Reports*. 2019;20(5):4603-4611. doi:10.3892/mmr.2019.10713

147. Liu B, Staron M, Hong F, et al. Essential roles of grp94 in gut homeostasis via chaperoning canonical Wnt pathway. *Proceedings of the National Academy of Sciences of the United States of America*. 2013;110(17):6877. doi:10.1073/PNAS.1302933110

148. Astrocytic p75NTR expression provoked by ischemic stroke exacerbates the blood–brain barrier disruption - Qin - 2022 - Glia - Wiley Online Library. Accessed October 2, 2022. https://onlinelibrary.wiley.com/doi/10.1002/glia.24146

149. Greenwood, N.N. and Earnshaw, A. (1998) Chemistry of the Elements. 2nd Edition, Butterworth-Heinemann, Oxford. - References - Scientific Research Publishing.

150. Zhao M, Zhu P, Fujino M, et al. Oxidative Stress in Hypoxic-Ischemic Encephalopathy: Molecular Mechanisms and Therapeutic Strategies. *Int J Mol Sci*. 2016;17(12):E2078. doi:10.3390/ijms17122078

151. Silachev DN, Plotnikov EY, Pevzner IB, Zorova LD, Balakireva A v., Gulyaev M v., et al. Neuroprotective Effects of Mitochondria-Targeted Plastoquinone in a Rat Model of Neonatal Hypoxic–Ischemic Brain Injury. Molecules : A Journal of Synthetic Chemistry and Natural Product Chemistry [Internet]. 2018 Aug 1 [cited 2022 Jul 25];23(8).

152. Grant PE, Roche-Labarbe N, Surova A, et al. Increased cerebral blood volume and oxygen consumption in neonatal brain injury. *J Cereb Blood Flow Metab*. 2009;29(10):1704-1713. doi:10.1038/jcbfm.2009.90

153. Barkhuizen M, Van de Berg WDJ, De Vente J, Blanco CE, Gavilanes AWD, Steinbusch HWM. Nitric Oxide Production in the Striatum and Cerebellum of a Rat Model of Preterm Global Perinatal Asphyxia. *Neurotox Res*. 2017;31(3):400-409. doi:10.1007/s12640-017-9700-6

154. Schäfer MK, Schwaeble WJ, Post C, et al. Complement C1q is dramatically up-regulated in brain microglia in response to transient global cerebral ischemia. *J Immunol*. 2000;164(10):5446-5452. doi:10.4049/jimmunol.164.10.5446

155. Arumugam TV, Magnus T, Woodruff TM, Proctor LM, Shiels IA, Taylor SM. Complement mediators in ischemia-reperfusion injury. *Clin Chim Acta*. 2006;374(1-2):33-45. doi:10.1016/j.cca.2006.06.010

156. Liu F, Mccullough LD. Inflammatory responses in hypoxic ischemic encephalopathy. *Acta Pharmacologica Sinica*. 2013;34(9):1121-1130. doi:10.1038/aps.2013.89

157. Kouser L, Madhukaran SP, Shastri A, et al. Emerging and Novel Functions of Complement Protein C1q. *Frontiers in Immunology*. 2015;6. Accessed January 24, 2023. https://www.frontiersin.org/articles/10.3389/fimmu.2015.00317

158. Rocha-Ferreira E, Hristova M. Antimicrobial Peptides and Complement in Neonatal Hypoxia-Ischemia Induced Brain Damage. *Front Immunol*. 2015;6:56. doi:10.3389/fimmu.2015.00056

159. Ten VS, Sosunov SA, Mazer SP, et al. C1q-deficiency is neuroprotective against hypoxic-ischemic brain injury in neonatal mice. *Stroke*. 2005;36(10):2244-2250. doi:10.1161/01.STR.0000182237.20807.d0

160. Ten VS, Yao J, Ratner V, et al. Complement Component C1q Mediates Mitochondria-Driven Oxidative Stress in Neonatal Hypoxic-Ischemic Brain Injury. *Journal of Neuroscience*. 2010;30(6):2077-2087. doi:10.1523/JNEUROSCI.5249-09.2010

161. Chu Y, Jin X, Parada I, et al. Enhanced synaptic connectivity and epilepsy in C1q knockout mice. *Proc Natl Acad Sci U S A*. 2010;107(17):7975-7980. doi:10.1073/pnas.0913449107

162. Perry VH, O'Connor V. C1q: the perfect complement for a synaptic feast? *Nat Rev Neurosci*. 2008;9(11):807-811. doi:10.1038/nrn2394

163. Complement: The Emerging Architect of the Developing Brain - PubMed. Accessed January 24, 2023. https://pubmed.ncbi.nlm.nih.gov/29606485/

164. Brennan FH, Gordon R, Lao HW, et al. The Complement Receptor C5aR Controls Acute Inflammation and Astrogliosis following Spinal Cord Injury. *J Neurosci*. 2015;35(16):6517-6531. doi:10.1523/JNEUROSCI.5218-14.2015

165. Levy DE, Lee C kuo. What does Stat3 do? *Journal of Clinical Investigation*. 2002;109(9):1143-1148. doi:10.1172/jci15650

166. Mitchell TJ, John S. Signal transducer and activator of transcription (STAT) signalling and T-cell lymphomas. *Immunology*. 2005;114(3):301-312. doi:10.1111/j.1365-2567.2005.02091.x

167. Fukushi S, Yamasaki K, Aiba S. Nuclear localization of activated STAT6 and STAT3 in epidermis of prurigo nodularis. *British Journal of Dermatology*. 2011;165(5):990-996. doi:10.1111/j.1365-2133.2011.10498.x

168. Elango C, Devaraj S. Immunomodulatory effect of Hawthorn extract in an experimental stroke model. *Journal of Neuroinflammation*. 2010;7(1):97. doi:10.1186/1742-2094-7-97

169. Sriram K, Benkovic SA, Hebert MA, Miller DB, O'Callaghan JP. Induction of gp130-related cytokines and activation of JAK2/STAT3 pathway in astrocytes precedes up-regulation of glial fibrillary acidic protein in the 1-methyl-4-phenyl-1,2,3,6-tetrahydropyridine model of neurodegeneration: Key signaling pathway for astrogliosis in vivo? *Journal of Biological Chemistry*. 2004;279(19):19936-19947. doi:10.1074/jbc.M309304200

170. D'Angelo B, Joakim Ek C, Sun Y, Zhu C, Sandberg M, Mallard C. GSK3β inhibition protects the immature brain from hypoxic-ischaemic insult via reduced

STAT3 signalling. *Neuropharmacology*. 2016;101:13-23. doi:10.1016/j.neuropharm.2015.09.017

171. Aggarwal BB, Kunnumakkara AB, Harikumar KB, et al. Signal transducer and activator of transcription-3, inflammation, and cancer: How intimate is the relationship? In: *Annals of the New York Academy of Sciences*. Vol 1171. Blackwell Publishing Inc.; 2009:59-76. doi:10.1111/j.1749-6632.2009.04911.x

172. Wen TC, Peng H, Hata R, Desaki J, Sakanaka M. Induction of phosphorylated-Stat3 following focal cerebral ischemia in mice. *Neuroscience Letters*. 2001;303(3):153-156. doi:10.1016/S0304-3940(01)01711-6

173. Yang XP, Irani K, Mattagajasingh S, et al. Signal transducer and activator of transcription 3α and specificity protein 1 interact to upregulate intercellular adhesion molecule-1 in ischemic-reperfused myocardium and vascular endothelium. *Arteriosclerosis, Thrombosis, and Vascular Biology*. 2005;25(7):1395-1400. doi:10.1161/01.ATV.0000168428.96177.24

174. Yang R, Rincon M. Mitochondrial Stat3, the need for design thinking. *International Journal of Biological Sciences*. 2016;12(5):532-544. doi:10.7150/ijbs.15153

175. Lahiri T, Brambilla L, Andrade J, Askenazi M, Ueberheide B, Levy DE. Mitochondrial STAT3 regulates antioxidant gene expression through complex I-derived NAD in triple negative breast cancer. *Mol Oncol*. 2021;15(5):1432-1449. doi:10.1002/1878-0261.12928

176. Planas AM, Soriano MA, Berruezo M, et al. Induction of Stat3, a signal transducer and transcription factor, in reactive microglia following transient focal cerebral ischaemia. *European Journal of Neuroscience*. 1996;8(12):2612-2618. doi:10.1111/j.1460-9568.1996.tb01556.x

177. Han HS, Choi JS, Park J, Suk K, Moon C, Park YK. Mild hypothermia attenuates intercellular adhesion molecule-1 induction via activation of extracellular signal-regulated kinase-1/2 in a focal cerebral ischemia model. *Stroke Research and Treatment*. 2011;2011:846716-846716. doi:10.4061/2011/846716

178. Yi JH, Park SW, Kapadia R, Vemuganti R. Role of transcription factors in mediating post-ischemic cerebral inflammation and brain damage. *Neurochemistry International*. 2007;50(7-8):1014-1027. doi:10.1016/j.neuint.2007.04.019

179. Bain JM, Ziegler A, Yang Z, Levison SW, Sen E. TGFß1 stimulates the over-production of white matter astrocytes from precursors of the “brain marrow” in a rodent model of neonatal encephalopathy. *PLoS ONE*. 2010;5(3). doi:10.1371/journal.pone.0009567

180. Nobuta H, Ghiani CA, Paez PM, et al. STAT3-Mediated astrogliosis protects myelin development in neonatal brain injury. *Annals of Neurology*. 2012;72(5):750-765. doi:10.1002/ana.23670

181. Hristova M, Rocha-Ferreira E, Fontana X, et al. Inhibition of Signal Transducer and Activator of Transcription 3 (STAT3) reduces neonatal hypoxic-ischaemic brain damage. *Journal of Neurochemistry*. 2016;136(5):981-994. doi:10.1111/jnc.13490

182. Meydan N, Grunberger T, Dadi H, et al. Inhibition of acute lymphoblastic leukaemia by a Jak-2 inhibitor. *Nature*. 1996;379(6566):645-648. doi:10.1038/379645a0

183. Hussain SF, Kong LY, Jordan J, et al. A novel small molecule inhibitor of signal transducers and activators of transcription 3 reverses immune tolerance in malignant glioma patients. *Cancer Research*. 2007;67(20):9630-9636. doi:10.1158/0008-5472.CAN-07-1243

184. Grabenstatter HL, Del Angel YC, Carlsen J, et al. The effect of STAT3 inhibition on status epilepticus and subsequent spontaneous seizures in the pilocarpine model of acquired epilepsy. *Neurobiology of Disease*. 2014;62:73-85. doi:10.1016/j.nbd.2013.09.003

185. Xue ZJ, Shen L, Wang ZY, Hui SY, Huang YG, Mah C. STAT3 inhibitor WP1066 as a novel therapeutic agent for bCCI neuropathic pain rats. *Brain Research*. 2014;1583(1):79-88. doi:10.1016/j.brainres.2014.07.015

186. Groot J de, Ott M, Wei J, et al. A first-in-human Phase I trial of the oral p-STAT3 inhibitor WP1066 in patients with recurrent malignant glioma. *CNS Oncology*. 2022;11(02):CNS87. doi:10.2217/cns-2022-0005

187. Lindholm D, Castren E, Kiefer R, Zafra F, Thoenen H. Transforming growth factor-β1 in the rat brain: Increase after injury and inhibition of astrocyte proliferation. *Journal of Cell Biology*. 1992;117(2):395-400. doi:10.1083/jcb.117.2.395

188. Vivien D, Bernaudin M, Buisson A, Divoux D, MacKenzie ET, Nouvelot A. Evidence of Type I and Type II Transforming Growth Factor-β Receptors in Central Nervous Tissues: Changes Induced by Focal Cerebral Ischemia. *Journal of Neurochemistry*. 2002;70(6):2296-2304. doi:10.1046/j.1471-4159.1998.70062296.x

189. Mantovani A, Sica A, Sozzani S, Allavena P, Vecchi A, Locati M. The chemokine system in diverse forms of macrophage activation and polarization. *Trends in Immunology*. 2004;25(12):677-686. doi:10.1016/j.it.2004.09.015

190. Li JJ, Lu J, Kaur C, Sivakumar V, Wu CY, Ling EA. Effects of hypoxia on expression of transforming growth factor-β1 and its receptors I and II in the amoeboid microglial cells and murine BV-2 cells. *Neuroscience*. 2008;156(3):662-672. doi:10.1016/j.neuroscience.2008.07.061

191. Ruff CA, Staak N, Patodia S, et al. Neuronal c-Jun is required for successful axonal regeneration, but the effects of phosphorylation of its N-terminus are moderate. *Journal of Neurochemistry*. 2012;121(4):607-618. doi:10.1111/j.1471-4159.2012.07706.x

192. Brionne TC, Tesseur I, Masliah E, Wyss-Coray T. Loss of TGF-β1 leads to increased neuronal cell death and microgliosis in mouse brain. *Neuron*. 2003;40(6):1133-1145. doi:10.1016/S0896-6273(03)00766-9

193. Dünker N, Schuster N, Krieglstein K. TGF-beta modulates programmed cell death in the retina of the developing chick embryo. Development. 2001 Jun;128(11):1933-42. doi: 10.1242/dev.128.11.1933.

194. Massagué J. How cells read TGF-β signals. *Nature Reviews Molecular Cell Biology*. 2000;1(3):169-178. doi:10.1038/35043051

195. Xu P, Liu J, Derynck R. Post-translational regulation of TGF-β receptor and Smad signaling. *FEBS Letters*. 2012;586(14):1871-1884. doi:10.1016/j.febslet.2012.05.010

196. Lim CP, Cao X. Regulation of Stat3 Activation by MEK Kinase 1. *Journal of Biological Chemistry*. 2001;276(24):21004-21011. doi:10.1074/jbc.M007592200

197. Schust J, Sperl B, Hollis A, Mayer TU, Berg T. Stattic: A Small-Molecule Inhibitor of STAT3 Activation and Dimerization. *Chemistry and Biology*. 2006;13(11):1235-1242. doi:10.1016/j.chembiol.2006.09.018

198. Sikka S, Surana R, Dai X, et al. Targeting the STAT3 signaling pathway in cancer: Role of synthetic and natural inhibitors. *Biochimica et Biophysica Acta - Reviews on Cancer*. 2014;1845(2):136-154. doi:10.1016/j.bbcan.2013.12.005

199. Laptook AR, Shankaran S, Tyson JE, et al. Effect of therapeutic hypothermia initiated after 6 hours of age on death or disability among newborns with hypoxic-ischemic encephalopathy a randomized clinical trial. *JAMA - Journal of the American Medical Association*. 2017;318(16):1550-1560. doi:10.1001/jama.2017.14972

200. Kerenyi A, Kelen D, Faulkner SD, et al. Systemic effects of whole-body cooling to 35°C, 33.5°C, and 30°C in a piglet model of perinatal asphyxia: Implications for therapeutic hypothermia. *Pediatric Research*. 2012;71(5):573-582. doi:10.1038/pr.2012.8

201. Gluckman PD, Wyatt JS, Azzopardi D, et al. Selective head cooling with mild systemic hypothermia after neonatal encephalopathy: multicentre randomised trial. *The Lancet*. 2005;365(9460):663-670. doi:10.1016/S0140-6736(05)17946-X

202. Srinivasakumar P, Zempel J, Wallendorf M, Lawrence R, Inder T, Mathur A. Therapeutic Hypothermia in Neonatal Hypoxic Ischemic Encephalopathy: Electrographic Seizures and Magnetic Resonance Imaging Evidence of Injury. *The Journal of Pediatrics*. 2013;163(2):465-470. doi:10.1016/j.jpeds.2013.01.041

203. Jacobs SE, Hunt R, Tarnow-Mordi WO, Inder TE, Davis PG. Cooling for newborns with hypoxic ischaemic encephalopathy. In: Jacobs SE, ed. *Cochrane Database of Systematic Reviews*. John Wiley & Sons, Ltd; 2007:CD003311. doi:10.1002/14651858.CD003311.pub2

204. Ezzati M, Bainbridge A, Broad KD, et al. Immediate remote ischemic postconditioning after hypoxia ischemia in piglets protects cerebral white matter but not grey matter. *Journal of Cerebral Blood Flow and Metabolism*. 2016;36(8):1396-1411. doi:10.1177/0271678X15608862

205. Edwards AD, Brocklehurst P, Gunn AJ, et al. Neurological outcomes at 18 months of age after moderate hypothermia for perinatal hypoxic ischaemic encephalopathy: Synthesis and meta-analysis of trial data. *BMJ (Online)*. 2010;340(7743):409. doi:10.1136/bmj.c363

206. Schulzke SM, Rao S, Patole SK. A systematic review of cooling for neuroprotection in neonates with hypoxic ischemic encephalopathy – are we there yet? *BMC Pediatrics*. 2007;7(1):30. doi:10.1186/1471-2431-7-30

207. Pauliah SS, Shankaran S, Wade A, Cady EB, Thayyil S. Therapeutic Hypothermia for Neonatal Encephalopathy in Low- and Middle-Income Countries: A Systematic Review and Meta-Analysis. *PLoS ONE*. 2013;8(3). doi:10.1371/journal.pone.0058834

208. Sisa C, Turroni S, Amici R, Brigidi P, Candela M, Cerri M. Potential role of the gut microbiota in synthetic torpor and therapeutic hypothermia. *World Journal of Gastroenterology*. 2017;23(3):406. doi:10.3748/wjg.v23.i3.406

209. Kuffler DP. Neuroprotection by hypothermia plus alkalinization of dorsal root ganglia neurons through ischemia. In: *Annals of the New York Academy of Sciences*. Vol 1199. Blackwell Publishing Inc.; 2010:158-163. doi:10.1111/j.1749-6632.2009.05358.x

210. Ogawa Y, Tanaka E, Sato Y, Tsuji M. Brain damage caused by neonatal hypoxia-ischemia and the effects of hypothermia in severe combined immunodeficient (SCID) mice. *Experimental Neurology*. 2021;337. doi:10.1016/j.expneurol.2020.113577

211. Nakamura T, Yamada S, Yoshioka T. Brain hypothermic therapy dramatically decreases elevated blood concentrations of high mobility group box 1 in neonates with hypoxic-ischemic encephalopathy. *Disease markers*. 2013;35(5):327-330. doi:10.1155/2013/327604

212. Osredkar D, Thoresen M, Maes E, Flatebø T, Elstad M, Sabir H. Hypothermia is not neuroprotective after infection-sensitized neonatal hypoxic–ischemic brain injury. *Resuscitation*. 2014;85(4):567-572. doi:10.1016/j.resuscitation.2013.12.006

213. Osredkar D, Sabir H, Falck M, et al. Hypothermia Does Not Reverse Cellular Responses Caused by Lipopolysaccharide in Neonatal Hypoxic-Ischaemic Brain Injury. *Developmental neuroscience*. 2015;37(4-5):390-397. doi:10.1159/000430860

214. Wintermark P, Boyd T, Gregas MC, Labrecque M, Hansen A. Placental pathology in asphyxiated newborns meeting the criteria for therapeutic hypothermia.

American Journal of Obstetrics and Gynecology. 2010;203(6):579.e1-579.e9. doi:10.1016/j.ajog.2010.08.024

215. Martinello, KA 1, 2, Meehan C1, Avdic-Belltheus A1, Lingam I1, Mutshiya T1, Yang Q1, Price D1, Sokolska M1, Bainbridge A1, Hristova M1, Tann CJ1, Peebles D1, Hagberg H3, Wolfs TG4, Klein N1, Kramer BW4, Tachtsidis I1, Fleiss B3, Gressens P3, Golay X1 RN. Hypothermia is not therapeutic in a piglet model of lps sensitised neonatal encephalopathy. *Journal of Paediatrics and Child Health*. 2019;55(S1):33-33. doi:10.1111/jpc.14409_82

216. Chalak LF, Sánchez PJ, Adams-Huet B, Laptook AR, Heyne RJ, Rosenfeld CR. Biomarkers for Severity of Neonatal Hypoxic-Ischemic Encephalopathy and Outcomes in Newborns Receiving Hypothermia Therapy. *The Journal of Pediatrics*. 2014;164(3):468-474.e1. doi:10.1016/j.jpeds.2013.10.067

217. Nakamura T, Yamada S, Yoshioka T. Brain hypothermic therapy dramatically decreases elevated blood concentrations of high mobility group box 1 in neonates with hypoxic-ischemic encephalopathy. *Disease markers*. 2013;35(5):327-330. doi:10.1155/2013/327604

218. Jenkins DD, Lee T, Chiuzan C, et al. Altered Circulating Leukocytes and Their Chemokines in a Clinical Trial of Therapeutic Hypothermia for Neonatal Hypoxic Ischemic Encephalopathy*. *Pediatric Critical Care Medicine*. 2013;14(8):786-795. doi:10.1097/PCC.0b013e3182975cc9

219. Yoshimura A, Lien E, Ingalls RR, Tuomanen E, Dziarski R, Golenbock D. Cutting edge: recognition of Gram-positive bacterial cell wall components by the innate immune system occurs via Toll-like receptor 2. J Immunol. 1999 Jul 1;163(1):1-5.

220. Hakobyan M, Dijkman KP, Laroche S, et al. Outcome of Infants with Therapeutic Hypothermia after Perinatal Asphyxia and Early-Onset Sepsis. *Neonatology*. 2019;115(2):127-133. doi:10.1159/000493358

221. Wu YW, Mathur AM, Chang T, et al. High-dose erythropoietin and hypothermia for hypoxic-Ischemic encephalopathy: A phase II trial. *Pediatrics*. 2016;137(6). doi:10.1542/peds.2016-0191

222. Zhang L, Wang L, Ning FB, Wang T, Liang YC, Liu YL. *EPO for Treatment of Hypoxic Ischemic Brain Damage*.

223. Gunes T, Ozturk MA, Koklu E, Kose K, Gunes I. Effect of allopurinol supplementation on nitric oxide levels in asphyxiated newborns. *Pediatric neurology*. 2007;36(1):17-24. doi:10.1016/j.pediatrneurol.2006.08.005

224. Kaandorp JJ, Benders MJNL, Schuit E, et al. Maternal allopurinol administration during suspected fetal hypoxia: a novel neuroprotective intervention? A multicentre randomised placebo controlled trial. *Archives of disease in childhood Fetal and neonatal edition*. 2015;100(3):F216-23. doi:10.1136/archdischild-2014-306769

225. Rodríguez-Fanjul J, Fernández-Feijóo CD, Lopez-Abad M, et al. Neuroprotection with hypothermia and allopurinol in an animal model of hypoxic-ischemic injury: Is it a gender question? *PLoS ONE*. 2017;12(9). doi:10.1371/journal.pone.0184643

226. Dingley J, Tooley J, Liu X, et al. Xenon ventilation during therapeutic hypothermia in neonatal encephalopathy: A feasibility study. *Pediatrics*. 2014;133(5):809-818. doi:10.1542/peds.2013-0787

227. Azzopardi D, Robertson NJ, Bainbridge A, et al. Moderate hypothermia within 6 h of birth plus inhaled xenon versus moderate hypothermia alone after birth asphyxia (TOBY-Xe): A proof-of-concept, open-label, randomised controlled trial. *The Lancet Neurology*. 2016;15(2):145-153. doi:10.1016/S1474-4422(15)00347-6

228. Landucci E, Filippi L, Gerace E, Catarzi S, Guerrini R, Pellegrini-Giampietro DE. Neuroprotective effects of topiramate and memantine in combination with hypothermia in hypoxic-ischemic brain injury in vitro and in vivo. *Neuroscience Letters*. 2018;668:103-107. doi:10.1016/j.neulet.2018.01.023

229. Liu Y, Barks JD, Xu G, Silverstein FS. Topiramate extends the therapeutic window for hypothermia-mediated neuroprotection after stroke in neonatal rats. *Stroke*. 2004;35(6):1460-1465. doi:10.1161/01.STR.0000128029.50221.fa

230. Noh MR, Kim SK, Sun W, et al. Neuroprotective effect of topiramate on hypoxic ischemic brain injury in neonatal rats. *Experimental neurology*. 2006;201(2):470-478. doi:10.1016/j.expneurol.2006.04.038

231. Robertson NJ, Lingam I, Meehan C, et al. High-Dose Melatonin and Ethanol Excipient Combined with Therapeutic Hypothermia in a Newborn Piglet Asphyxia Model. *Scientific Reports*. 2020;10(1). doi:10.1038/s41598-020-60858-x

232. Robertson NJ, Martinello K, Lingam I, et al. Melatonin as an adjunct to therapeutic hypothermia in a piglet model of neonatal encephalopathy: A translational study. *Neurobiology of Disease*. 2019;121:240-251. doi:10.1016/j.nbd.2018.10.004

233. Robertson NJ, Faulkner S, Fleiss B, et al. Melatonin augments hypothermic neuroprotection in a perinatal asphyxia model. *Brain*. 2013;136(1):90-105. doi:10.1093/brain/aws285

234. van der Kooij MA, Groenendaal F, Kavelaars A, Heijnen CJ, van Bel F. Combination of deferoxamine and erythropoietin: Therapy for hypoxia–ischemia-induced brain injury in the neonatal rat? *Neuroscience Letters*. 2009;451(2):109-113. doi:10.1016/j.neulet.2008.12.013

235. Shishodia S, Sethi G, Aggarwal BB. Curcumin: Getting Back to the Roots. *Ann NY Acad Sci*. 2005;1056:206-217. doi:10.1196/annals.1352.010

236. Pescosolido N, Giannotti R, Plateroti AM, Pascarella A, Nebbioso M. Curcumin: Therapeutical potential in ophthalmology. *Planta Medica*. 2014;80(4):249-254. doi:10.1055/s-0033-1351074

237. Ahmad MZ, Alkahtani SA, Akhter S, et al. Progress in nanotechnology-based drug carrier in designing of curcumin nanomedicines for cancer therapy: current state-of-the-art. *Journal of Drug Targeting*. 2016;24(4):273-293. doi:10.3109/1061186X.2015.1055570

238. Naksuriya O, Okonogi S, Schiffelers RM, Hennink WE. Curcumin nanoformulations: A review of pharmaceutical properties and preclinical studies and clinical data related to cancer treatment. *Biomaterials*. 2014;35(10):3365-3383. doi:10.1016/j.biomaterials.2013.12.090

239. Sandur SK, Pandey MK, Sung B, et al. Curcumin, demethoxycurcumin, bisdemethoxycurcumin, tetrahydrocurcumin and turmerones differentially regulate anti-inflammatory and anti-proliferative responses through a ROS-independent mechanism. *Carcinogenesis*. 2007;28(8):1765-1773. doi:10.1093/carcin/bgm123

240. Kim JE, Kim AR, Chung HY, Han SY, Kim BS, Choi JS. In vitro peroxynitrite scavenging activity of diarylheptanoids fromCurcuma longa. *Phytotherapy Research*. 2003;17(5):481-484. doi:10.1002/ptr.1179

241. Liu Y, Hong XQ. [Effect of three different curcumin pigmens on the prdiferation of vascular smooth muscle cells by ox-LDL and the expression of LDL-R]. *Zhongguo Zhong yao za zhi = Zhongguo zhongyao zazhi = China journal of Chinese materia medica*. 2006;31(6):500-503.

242. Nishiyama T, Mae T, Kishida H, et al. Curcuminoids and Sesquiterpenoids in Turmeric (*Curcuma longa* L.) Suppress an Increase in Blood Glucose Level in Type 2 Diabetic KK-A ^{y} Mice. *Journal of Agricultural and Food Chemistry*. 2005;53(4):959-963. doi:10.1021/jf0483873

243. Spagnuolo C, Napolitano M, Tedesco I, Moccia S, Milito A, Russo GL. Neuroprotective Role of Natural Polyphenols. *Current topics in medicinal chemistry*. 2016;16(17):1943-1950.

244. Shehzad A, Qureshi M, Anwar MN, Lee YS. Multifunctional Curcumin Mediate Multitherapeutic Effects. *Journal of Food Science*. 2017;82(9):2006-2015. doi:10.1111/1750-3841.13793

245. Daugherty DJ, Marquez A, Calcutt NA, Schubert D. A novel curcumin derivative for the treatment of diabetic neuropathy. *Neuropharmacology*. 2018;129:26-35. doi:10.1016/j.neuropharm.2017.11.007

246. Priyadarsini K. The Chemistry of Curcumin: From Extraction to Therapeutic Agent. *Molecules*. 2014;19(12):20091-20112. doi:10.3390/molecules191220091

247. Tang M, Taghibiglou C, Liu J. The Mechanisms of Action of Curcumin in Alzheimer's Disease. *Journal of Alzheimer's Disease*. 2017;58(4):1003-1016. doi:10.3233/JAD-170188

248. Wang XS, Zhang ZR, Zhang MM, Sun MX, Wang WW, Xie CL. Neuroprotective properties of curcumin in toxin-base animal models of Parkinson's disease: A

systematic experiment literatures review. *BMC Complementary and Alternative Medicine*. 2017;17(1). doi:10.1186/s12906-017-1922-x

249. Hewlings S, Kalman D. Curcumin: A Review of Its Effects on Human Health. *Foods*. 2017;6(10):92. doi:10.3390/foods6100092

250. Alizadeh M, Kheirouri S. Curcumin reduces malondialdehyde and improves antioxidants in humans with diseased conditions: a comprehensive meta-analysis of randomized controlled trials. *BioMedicine*. 2019;9(4):23. doi:10.1051/bmdcn/2019090423

251. Maheshwari RK, Singh AK, Gaddipati J, Srimal RC. Multiple biological activities of curcumin: A short review. In: *Life Sciences*. Vol 78. Pergamon; 2006:2081-2087. doi:10.1016/j.lfs.2005.12.007

252. Alexandrow MG, Song LJ, Altiok S, Gray J, Haura EB, Kumar NB. Curcumin: A novel Stat3 pathway inhibitor for chemoprevention of lung cancer. *European Journal of Cancer Prevention*. 2012;21(5):407-412. doi:10.1097/CEJ.0b013e32834ef194

253. Trujillo J, Granados-Castro LF, Zazueta C, Andérica-Romero AC, Chirino YI, Pedraza-Chaverrí J. Mitochondria as a target in the therapeutic properties of curcumin. *Archiv der Pharmazie*. 2014;347(12):873-884. doi:10.1002/ardp.201400266

254. Anand P, Kunnumakkara AB, Newman RA, Aggarwal BB. Bioavailability of curcumin: Problems and promises. *Molecular Pharmaceutics*. 2007;4(6):807-818. doi:10.1021/mp700113r

255. Rocha-Ferreira E, Sisa C, Bright S, et al. Curcumin: Novel Treatment in Neonatal Hypoxic-Ischemic Brain Injury. *Frontiers in Physiology*. 2019;10. doi:10.3389/fphys.2019.01351

256. Kahl A, Anderson CJ, Qian L, et al. Neuronal expression of the mitochondrial protein prohibitin confers profound neuroprotection in a mouse model of focal cerebral ischemia. *J Cereb Blood Flow Metab*. 2018;38(6):1010-1020. doi:10.1177/0271678X17720371

257. REVIEW: Curcumin and Alzheimer's disease - PubMed. Accessed January 26, 2023. https://pubmed.ncbi.nlm.nih.gov/20406252/

258. Kendall GS, Hirstova M, Horn S, et al. TNF gene cluster deletion abolishes lipopolysaccharide-mediated sensitization of the neonatal brain to hypoxic ischemic insult. *Laboratory Investigation*. 2011;91(3):328-341. doi:10.1038/labinvest.2010.192

259. Kendall GS, Robertson NJ, Iwata O, Peebles D, Raivich G. N-Methyl-isobutyl-amiloride Ameliorates Brain Injury When Commenced Before Hypoxia Ischemia in Neonatal Mice. *Pediatric Research*. 2006;59(2):227-231. doi:10.1203/01.pdr.0000196805.68082.22

260. Möller JC, Klein MA, Haas S, Jones LL, Kreutzberg GW, Raivich G. Regulation of thrombospondin in the regenerating mouse facial motor nucleus. *GLIA*. 1996;17(2):121-132. doi:10.1002/(SICI)1098-1136(199606)17:2<121::AID-GLIA4>3.0.CO;2-5

261. Kendall GS, Robertson NJ, Iwata O, Peebles D, Raivich G. N-methyl-isobutyl-amiloride ameliorates brain injury when commenced before hypoxia ischemia in neonatal mice. *Pediatric Research*. 2006;59(2):227-231. doi:10.1203/01.pdr.0000196805.68082.22

262. Thiessen DD, Lindzey G. Negative geotaxis in mice: Effect of balancing practice on incline behaviour in C57BL/6J male mice. *Animal Behaviour*. 1967;15(1):113-116. doi:10.1016/S0003-3472(67)80020-4

263. Feather-Schussler DN, Ferguson TS. A Battery of Motor Tests in a Neonatal Mouse Model of Cerebral Palsy. *J Vis Exp*. 2016;(117):53569. doi:10.3791/53569

264. Antunes M, Biala G. The novel object recognition memory: neurobiology, test procedure, and its modifications. *Cogn Process*. 2012;13(2):93-110. doi:10.1007/s10339-011-0430-z

265. Hellström Erkenstam N, Smith PLP, Fleiss B, et al. Temporal Characterization of Microglia/Macrophage Phenotypes in a Mouse Model of Neonatal Hypoxic-Ischemic Brain Injury. *Frontiers in Cellular Neuroscience*. 2016;10.

266. Grabenstatter HL, Del Angel YC, Carlsen J, et al. The effect of STAT3 inhibition on status epilepticus and subsequent spontaneous seizures in the pilocarpine model of acquired epilepsy. *Neurobiology of Disease*. 2014;62:73-85. doi:10.1016/j.nbd.2013.09.003

267. Raible DJ, Frey LC, Del Angel YC, et al. JAK/STAT pathway regulation of GABAA receptor expression after differing severities of experimental TBI. *Exp Neurol*. 2015;271:445-456. doi:10.1016/j.expneurol.2015.07.001

268. Zhou Y, Wang S, Zhao J, Fang P. Asiaticoside attenuates neonatal hypoxic–ischemic brain damage through inhibiting TLR4/NF-κB/STAT3 pathway. *Annals of Translational Medicine*. 2020;8(10):641-641. doi:10.21037/atm-20-3323

269. Lambertsen KL, Biber K, Finsen B. Inflammatory cytokines in experimental and human stroke. *Journal of Cerebral Blood Flow and Metabolism*. 2012;32(9):1677-1698. doi:10.1038/jcbfm.2012.88

270. Galvao J, Davis B, Tilley M, Normando E, Duchen MR, Cordeiro MF. Unexpected low-dose toxicity of the universal solvent DMSO. *FASEB Journal*. 2014;28(3):1317-1330. doi:10.1096/fj.13-235440

271. Hernando-Rodríguez B, Artal-Sanz M. Mitochondrial Quality Control Mechanisms and the PHB (Prohibitin) Complex. *Cells*. 2018;7(12):238. doi:10.3390/cells7120238

272. Signorile A, Sgaramella G, Bellomo F, De Rasmo D. Prohibitins: A Critical Role in Mitochondrial Functions and Implication in Diseases. *Cells*. 2019;8(1):71. doi:10.3390/cells8010071

273. Sonntag J, Wagner MH, Strauss E, Obladen M. Complement and contact activation in term neonates after fetal acidosis. *Archives of Disease in Childhood: Fetal and Neonatal Edition*. 1998;78(2):F125-F128. doi:10.1136/fn.78.2.F125

274. Ten VS, Sosunov SA, Mazer SP, Stark RI, Caspersen C, Sughrue ME, Botto M, Connolly ES Jr, Pinsky DJ. C1q-deficiency is neuroprotective against hypoxic-ischemic brain injury in neonatal mice. Stroke. 2005 Oct;36(10):2244-50. doi: 10.1161/01.STR.0000182237.20807.d0. Epub 2005 Sep 22. -

275. Alexander M, Garbus H, Smith AL, Rosenkrantz TS, Fitch RH. Behavioral and histological outcomes following neonatal HI injury in a preterm (P3) and term (P7) rodent model. *Behav Brain Res*. 2014;259:85-96. doi:10.1016/j.bbr.2013.10.038

276. McClure MM, Threlkeld SW, Rosen GD, Holly Fitch R. Auditory processing deficits in unilaterally and bilaterally injured hypoxic-ischemic rats. *Neuroreport*. 2005;16(12):1309-1312. doi:10.1097/01.wnr.0000175613.16183.6c

277. McClure MM, Threlkeld SW, Rosen GD, Holly Fitch R. Rapid auditory processing and learning deficits in rats with P1 versus P7 neonatal hypoxic-ischemic injury. *Behav Brain Res*. 2006;172(1):114-121. doi:10.1016/j.bbr.2006.05.003

278. Mayoral SR, Omar G, Penn AA. Sex Differences in a Hypoxia Model of Preterm Brain Damage. *Pediatr Res*. 2009;66(3):248-253. doi:10.1203/PDR.0b013e3181b1bc34

279. Hill CA, Fitch RH. Sex differences in mechanisms and outcome of neonatal hypoxia-ischemia in rodent models: implications for sex-specific neuroprotection in clinical neonatal practice. *Neurol Res Int*. 2012;2012:867531. doi:10.1155/2012/867531

280. Vogel-Ciernia A, Wood MA. Examining object location and object recognition memory in mice. *Curr Protoc Neurosci*. 2014;69:8.31.1-17. doi:10.1002/0471142301.ns0831s69

281. Barker GR, Warburton EC. When is the hippocampus involved in recognition memory? J Neurosci. 2011 Jul 20;31(29):10721-31. doi: 10.1523/JNEUROSCI.6413-10.2011

282. Denninger JK, Smith BM, Kirby ED. Novel Object Recognition and Object Location Behavioral Testing in Mice on a Budget. J Vis Exp. 2018 Nov 20;(141):10.3791/58593. doi: 10.3791/58593

283. Philip S, Keshavarz T, Roy I. Polyhydroxyalkanoates: biodegradable polymers with a range of applications. *Journal ofChemical Technology and Biotechnology*. 2007;82(July 2006):329-333. doi:10.1002/jctb

284. Puthussery H. *Biosynthesis of Poly-3-Hydroxybutyrate and Its Application in Controlled Drug Delivery*. 2019.

285. Dhuria SV, Hanson LR, Frey WH. Intranasal delivery to the central nervous system: mechanisms and experimental considerations. *J Pharm Sci*. 2010;99(4):1654-1673. doi:10.1002/jps.21924

286. Davis BM, Pahlitzsch M, Guo L, et al. Topical Curcumin Nanocarriers are Neuroprotective in Eye Disease. *Scientific Reports*. 2018;8(1):11066. doi:10.1038/s41598-018-29393-8

287. Cui X, Song H, Su J. Curcumin attenuates hypoxic-ischemic brain injury in neonatal rats through induction of nuclear factor erythroid-2-related factor 2 and heme oxygenase-1. *Experimental and Therapeutic Medicine*. 2017;14(2):1512-1518. doi:10.3892/etm.2017.4683

288. Liu Z, Ran Y, Huang S, et al. Curcumin protects against ischemic stroke by titrating microglia/macrophage polarization. *Frontiers in Aging Neuroscience*. 2017;9(JUL). doi:10.3389/fnagi.2017.00233

289. Yuan J, Liu W, Zhu H, et al. Curcumin inhibits glial scar formation by suppressing astrocyte-induced inflammation and fibrosis in vitro and in vivo. *Brain Research*. 2017;1655:90-103. doi:10.1016/j.brainres.2016.11.002

290. Dong Y, Yu Z, Sun Y, et al. Chronic fetal hypoxia produces selective brain injury associated with altered nitric oxide synthases. In: *American Journal of Obstetrics and Gynecology*. Vol 204. Mosby Inc.; 2011:254.e16-254.e28. doi:10.1016/j.ajog.2010.11.032

291. Parada E, Buendia I, Navarro E, Avendaño C, Egea J, López MG. Microglial HO-1 induction by curcumin provides antioxidant, antineuroinflammatory, and glioprotective effects. *Mol Nutr Food Res*. 2015;59(9):1690-1700. doi:10.1002/mnfr.201500279

292. Chen F, Guo N, Cao G, Zhou J, Yuan Z. Molecular analysis of curcumin-induced polarization of murine RAW264.7 macrophages. *J Cardiovasc Pharmacol*. 2014;63(6):544-552. doi:10.1097/FJC.0000000000000079

293. Gao S, Zhou J, Liu N, et al. Curcumin induces M2 macrophage polarization by secretion IL-4 and/or IL-13. *J Mol Cell Cardiol*. 2015;85:131-139. doi:10.1016/j.yjmcc.2015.04.025

294. Mukherjee A, Sarkar S, Jana S, Swarnakar S, Das N. Neuro-protective role of nanocapsulated curcumin against cerebral ischemia-reperfusion induced oxidative injury. *Brain Res*. 2019;1704:164-173. doi:10.1016/j.brainres.2018.10.016

295. Wang Y, Zhang Y, Yang L, Yuan J, Jia J, Yang S. SOD2 Mediates Curcumin-Induced Protection against Oxygen-Glucose Deprivation/Reoxygenation Injury in HT22 Cells. *Evid Based Complement Alternat Med*. 2019;2019:2160642. doi:10.1155/2019/2160642

296. Yu L, Yi J, Ye G, et al. Effects of curcumin on levels of nitric oxide synthase and AQP-4 in a rat model of hypoxia-ischemic brain damage. *Brain Research*. 2012;1475:88-95. doi:10.1016/j.brainres.2012.07.055

297. Skoff RP, Bessert DA, Barks JD, Song D, Cerghet M, Silverstein FS. Hypoxic-ischemic injury results in acute disruption of myelin gene expression and death of oligodendroglial precursors in neonatal mice. *Int J Dev Neurosci*. 2001;19(2):197-208. doi:10.1016/s0736-5748(00)00075-7

298. Carlsson Y, Wang X, Schwendimann L, et al. Combined effect of hypothermia and caspase-2 gene deficiency on neonatal hypoxic-ischemic brain injury. *Pediatric Research*. 2012;71(5):566-572. doi:10.1038/pr.2012.15

299. Joseph A, Wood T, Chen CC, et al. Curcumin-loaded polymeric nanoparticles for neuroprotection in neonatal rats with hypoxic-ischemic encephalopathy. *Nano Research*. 2018;11(10):5670-5688. doi:10.1007/s12274-018-2104-y

300. Kamaraj S, Palanisamy UM, Kadhar Mohamed MSB, Gangasalam A, Maria GA, Kandasamy R. Curcumin drug delivery by vanillin-chitosan coated with calcium ferrite hybrid nanoparticles as carrier. *European Journal of Pharmaceutical Sciences*. Published online 2018. doi:10.1016/j.ejps.2018.01.023

301. Samrot AV, Burman U, Philip SA, Shobana N, Chandrasekaran K. Synthesis of curcumin loaded polymeric nanoparticles from crab shell derived chitosan for drug delivery. *Informatics in Medicine Unlocked*. 2018;10(December 2017):159-182. doi:10.1016/j.imu.2017.12.010

302. Joseph A, Wood T, Chen CC, et al. Curcumin-loaded polymeric nanoparticles for neuroprotection in neonatal rats with hypoxic-ischemic encephalopathy. *Nano Research*. 2018;11(10):5670-5688. doi:10.1007/s12274-018-2104-y

303. Larsson J, Goumans MJ, Sjöstrand LJ, et al. Abnormal angiogenesis but intact hematopoietic potential in TGF-β type I receptor-deficient mice. *EMBO Journal*. Published online 2001. doi:10.1093/emboj/20.7.1663

304. Li JJ, Lu J, Kaur C, Sivakumar V, Wu CY, Ling EA. Effects of hypoxia on expression of transforming growth factor-β1 and its receptors I and II in the amoeboid microglial cells and murine BV-2 cells. *Neuroscience*. 2008;156(3):662-672. doi:10.1016/j.neuroscience.2008.07.061

305. Raivich G, Bluethmann H, Kreutzberg GW. Signaling Molecules and Neuroglial Activation in the Injured Central Nervous System. *The Keio Journal of Medicine*. 1996;45(3):239-247. doi:10.2302/kjm.45.239

306. Hristova M, Cuthill D, Zbarsky V, et al. Activation and deactivation of periventricular white matter phagocytes during postnatal mouse development. *GLIA*. 2010;58(1):11-28. doi:10.1002/glia.20896

307. Ryu KY, Cho GS, Piao HZ, Kim WK. Role of TGF-β in Survival of Phagocytizing Microglia: Autocrine Suppression of TNF-α Production and Oxidative Stress. *Experimental Neurobiology*. 2012;21(4):151-157. doi:10.5607/en.2012.21.4.151

308. Butovsky O, Jedrychowski MP, Moore CS, et al. Identification of a unique TGF-β–dependent molecular and functional signature in microglia. *Nature Neuroscience*. 2014;17(1):131-143. doi:10.1038/nn.3599

309. Zöller T, Schneider A, Kleimeyer C, et al. Silencing of TGFβ signalling in microglia results in impaired homeostasis. *Nature Communications*. 2018;9(1):4011. doi:10.1038/s41467-018-06224-y

310. Mihaly SR, Ninomiya-Tsuji J, Morioka S. TAK1 control of cell death. *Cell Death & Differentiation*. 2014;21(11):1667-1676. doi:10.1038/cdd.2014.123

311. Cronin M, Akin AR, Collins SA, Meganck J, Kim JB, Baban CK, Joyce SA, van Dam GM, Zhang N, van Sinderen D, O'Sullivan GC, Kasahara N, Gahan CG, Francis KP, Tangney M. High resolution in vivo bioluminescent imaging for the study of bacterial tumour targeting. PLoS One. 2012;7(1):e30940. doi: 10.1371/journal.pone.0030940

312. Fragopoulou AF, Qian Y, Diaz Heijtz R, Forssberg H. Correction to: Can Neonatal Systemic Inflammation and Hypoxia Yield a Cerebral Palsy-Like Phenotype in Periadolescent Mice? *Mol Neurobiol*. 2019;56(10):6901. doi:10.1007/s12035-019-1610-6

313. Lively S, Schlichter LC. Microglia Responses to Pro-inflammatory Stimuli (LPS, IFNγ+TNFα) and Reprogramming by Resolving Cytokines (IL-4, IL-10). *Front Cell Neurosci*. 2018;12:215. doi:10.3389/fncel.2018.00215

314. Wang X, Stridh L, Li W, et al. Lipopolysaccharide Sensitizes Neonatal Hypoxic-Ischemic Brain Injury in a MyD88-Dependent Manner. *The Journal of Immunology*. 2009;183(11):7471-7477. doi:10.4049/jimmunol.0900762

315. Suff N, Karda R, Perocheau D, et al. 437. A Light-Producing Model of Infection-Related Preterm Birth. *Molecular Therapy*. 2016;24:S173. doi:10.1016/S1525-0016(16)33246-4

316. Brochu ME, Girard S, Lavoie K, Sébire G. Developmental regulation of the neuroinflammatory responses to LPS and/or hypoxia-ischemia between preterm and term neonates: An experimental study. *Journal of neuroinflammation*. 2011;8:55. doi:10.1186/1742-2094-8-55

317. Srivastava S, Katorcha E, Makarava N, Barrett JP, Loane DJ, Baskakov IV. Inflammatory response of microglia to prions is controlled by sialylation of PrPSc. *Scientific Reports*. 2018;8. doi:10.1038/s41598-018-29720-z

318. Chen AQ, Fang Z, Chen XL, et al. Microglia-derived TNF-α mediates endothelial necroptosis aggravating blood brain–barrier disruption after ischemic stroke. *Cell Death Dis*. 2019;10(7):487. doi:10.1038/s41419-019-1716-9

319. Iadecola C, Zhang F, Casey R, Clark HB, Ross ME. Inducible nitric oxide synthase gene expression in vascular cells after transient focal cerebral ischemia. *Stroke*. 1996;27(8):1373-1380. doi:10.1161/01.str.27.8.1373

320. Rao S, Lin Z, Drobyshevsky A, et al. Involvement of Neuronal Nitric Oxide Synthase in Ongoing Fetal Brain Injury following Near-Term Rabbit Hypoxia-Ischemia. *Dev Neurosci*. 2011;33(3-4):288-298. doi:10.1159/000327241

321. Deng Y, Xie D, Fang M, et al. Astrocyte-Derived Proinflammatory Cytokines Induce Hypomyelination in the Periventricular White Matter in the Hypoxic Neonatal Brain. *PLoS One*. 2014;9(1):e87420. doi:10.1371/journal.pone.0087420

322. Burnsed JC, Chavez-Valdez R, Hossain MS, et al. Hypoxia-Ischemia and Therapeutic Hypothermia in the Neonatal Mouse Brain – A Longitudinal Study. *PLoS One*. 2015;10(3):e0118889. doi:10.1371/journal.pone.0118889

323. Goudriaan A, Loos M, Spijker S, Smit AB, Verheijen MHG. Genetic Variation in CNS Myelination and Functional Brain Connectivity in Recombinant Inbred Mice. *Cells*. 2020;9(9):2119. doi:10.3390/cells9092119

324. Korrell KV, Disser J, Parley K, et al. Differential effect on myelination through abolition of activity-dependent synaptic vesicle release or reduction of overall electrical activity of selected cortical projections in the mouse. *J Anat*. 2019;235(3):452-467. doi:10.1111/joa.12974

325. Affeldt BM, Obenaus A, Chan J, Pardo AC. Region specific oligodendrocyte transcription factor expression in a model of neonatal hypoxic injury. *Int J Dev Neurosci*. 2017;61:1-11. doi:10.1016/j.ijdevneu.2017.05.001

326. Borhani-Haghighi M, Mohamadi Y, Kashani IR. In utero transplantation of neural stem cells ameliorates maternal inflammation-induced prenatal white matter injury. *J Cell Biochem*. 2019;120(8):12785-12795. doi:10.1002/jcb.28548

327. Sizonenko SV, Camm EJ, Dayer A, Kiss JZ. Glial responses to neonatal hypoxic-ischemic injury in the rat cerebral cortex. *Int J Dev Neurosci*. 2008;26(1):37-45. doi:10.1016/j.ijdevneu.2007.08.014

328. Ahrendsen JT, Grewal HS, Hickey SP, et al. Juvenile striatal white matter is resistant to ischemia-induced damage. *Glia*. 2016;64(11):1972-1986. doi:10.1002/glia.23036

Appendix

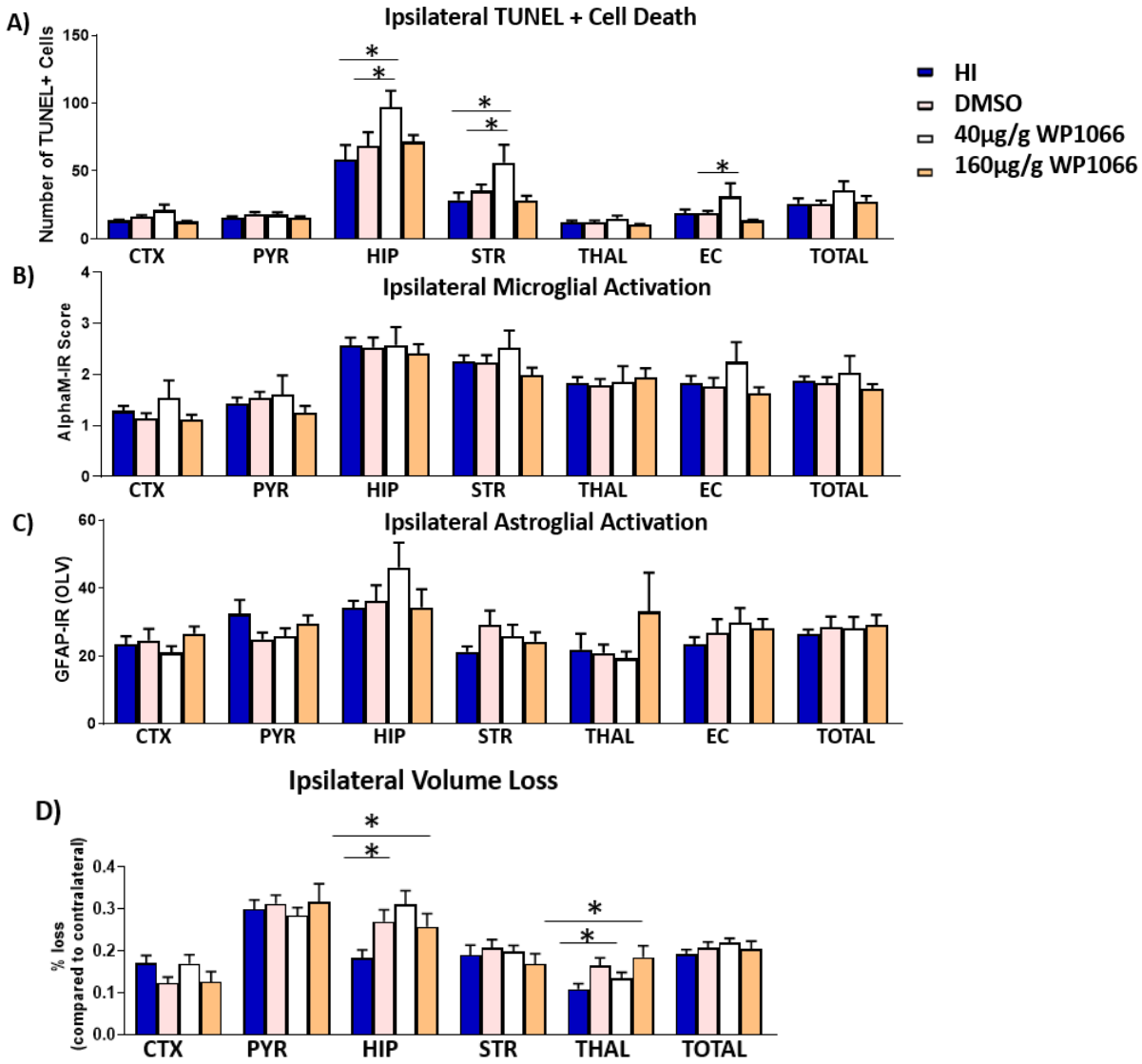
A)
Ipsilateral TUNEL + Cell Death
Number of TUNEL+ Cells
150
100
50
0
CTX
PYR
HIP
STR
THAL
EC
TOTAL
HI
DMSO
40µg/g WP1066
160µg/g WP1066
B)
Ipsilateral Microglial Activation
AlphaM-IR Score
4
3
2
1
0
C)
Ipsilateral Astroglial Activation
GFAP-IR (OLV)
60
40
20
0
D)
Ipsilateral Volume Loss
% loss
(compared to contralateral)
0.4
0.3
0.2
0.1
0.0

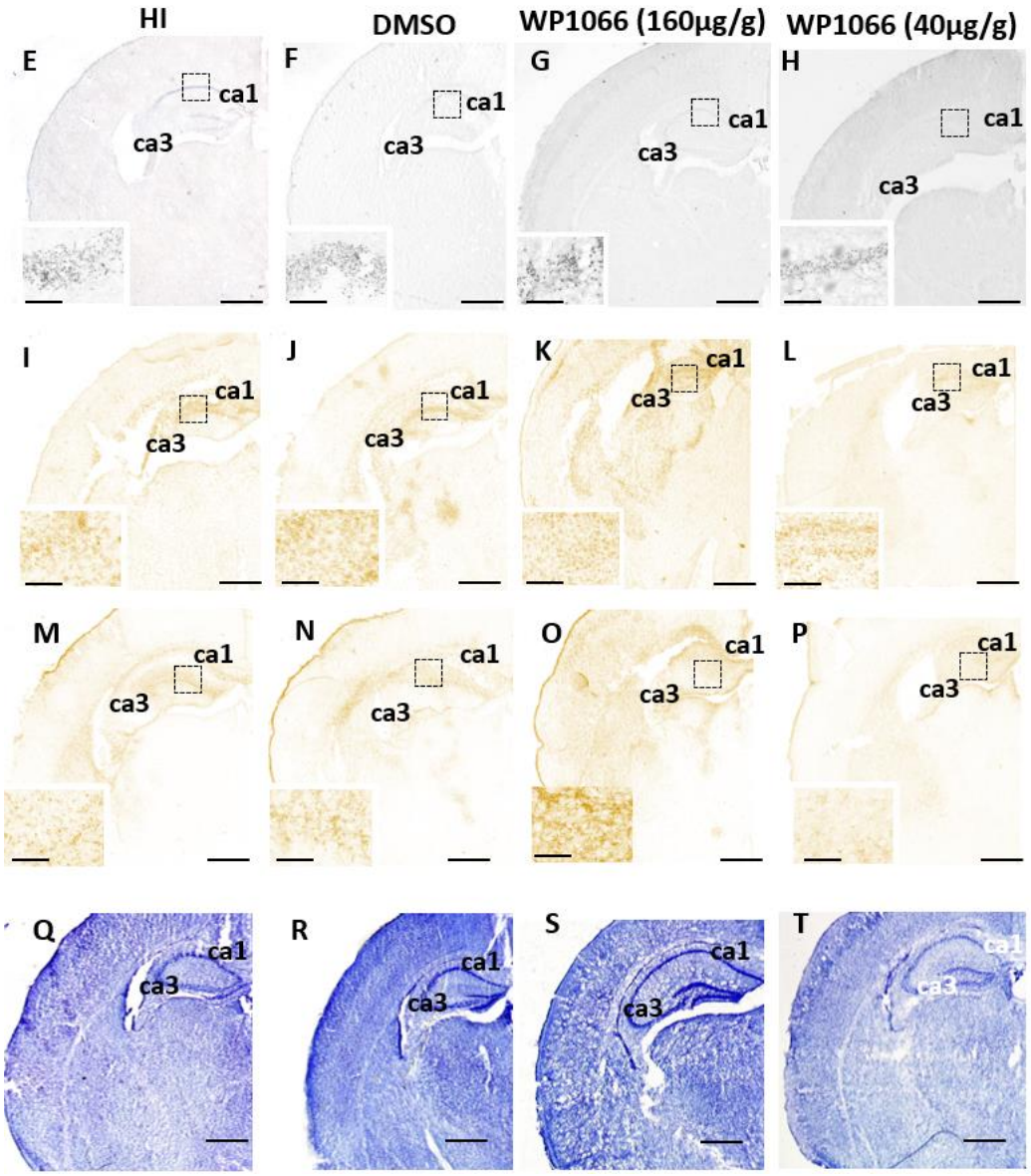

Supplementary Figure 1. **Effect of immediate intraperitoneal post-HI application of 40µg/g and 160µg/g BW WP1066 at 48h**. A. Quantitative ipsilateral analysis of cell death assessed with TUNEL+ cells count in animals treated with WP1066 40µg/g (white), 160µg/g (orange), DMSO (pink) or with no treatment, HI (blue). The graph highlights no significant changes in cell death after treatment with 160µg/g WP1066 in HI animals, but significant increase after treatment with 40µg/g WP1066 in cortex ($p=0.03$), hippocampus ($p=0.04$), striatum ($p=0.04$) when compared to HI controls ($p<0.05$) and in striatum ($p=0.02$), external capsule ($p=0.03$) and hippocampus ($p=0.01$) when compared to DMSO treatment (Kruskal-Wallis test, Dunn's post-hoc). B. No ipsilateral differences in microglial activation are observed after 40µg/g or 160µg/g BW WP1066 treatment. C. The graph shows no significant change in astroglial

activation after treatment with 40µg/g and 160µg/g BW WP1066 compared to DMSO treated and untreated HI animal groups. D. Quantitative analysis showing the percentage of ipsilateral tissue loss assessed through Cresyl Violet staining at 48h following HI insult in the regions of interest after treatment with 40µg/g, or 160µg/g BW of WP1066. In D, significant increase after 40µg/g BW WP1066 treatment was observed in cortex ($p=0.02$, Kruskal-Wallis test, Dunn's post-hoc) compared to DMSO and in hippocampus ($p=0.0007$) and thalamus ($p=0.02$) compared to HI littermates (Kruskal-Wallis test, Dunn's post-hoc). Significant increase of tissue loss is also observed after 160µg/g BW WP1066 in hippocampus ($p=0.02$) and thalamus ($p=0.0006$) compared to untreated HI control animals (Kruskal-Wallis test with Dunn's post-hoc). E-H. Ipsilateral histological overview of cell death in the experimental groups, untreated HI (E), DMSO treated (F), 160µg/g BW WP1066 treated (G), 40µg/g BW WP1066 treated (H)and high magnification of all the experimental groups in the inserts. I-L. Histochemical overview of microglial activation in the treatment groups, untreated HI (I), DMSO treated (J), 40µg/g BW WP1066 treated (K), 160µg/g BW WP1066 treated (L) and low magnification ipsilateral overview in HI (I), DMSO (J), 40µg/g BW WP1066 (K) and 160µg/g BW WP1066 (L) groups. M-P Histochemical overview of astroglial activation in the treatment groups, HI (M), DMSO (N), 40µg/g BW WP1066 (O), 160µg/g BW WP1066 (P) and low magnification ipsilateral overview in HI (M), DMSO (N), 40µg/g BW WP1066 (O) and 160µg/g BW WP1066 (P) groups. Q-T. Histochemical overview of tissue loss in the treatment groups, HI (Q), DMSO (R), 40µg/g BW WP1066 (S), 160µg/g BW WP1066 (T). Scale bars 1000µm. inserts=62µm. (*$p<0.05$).

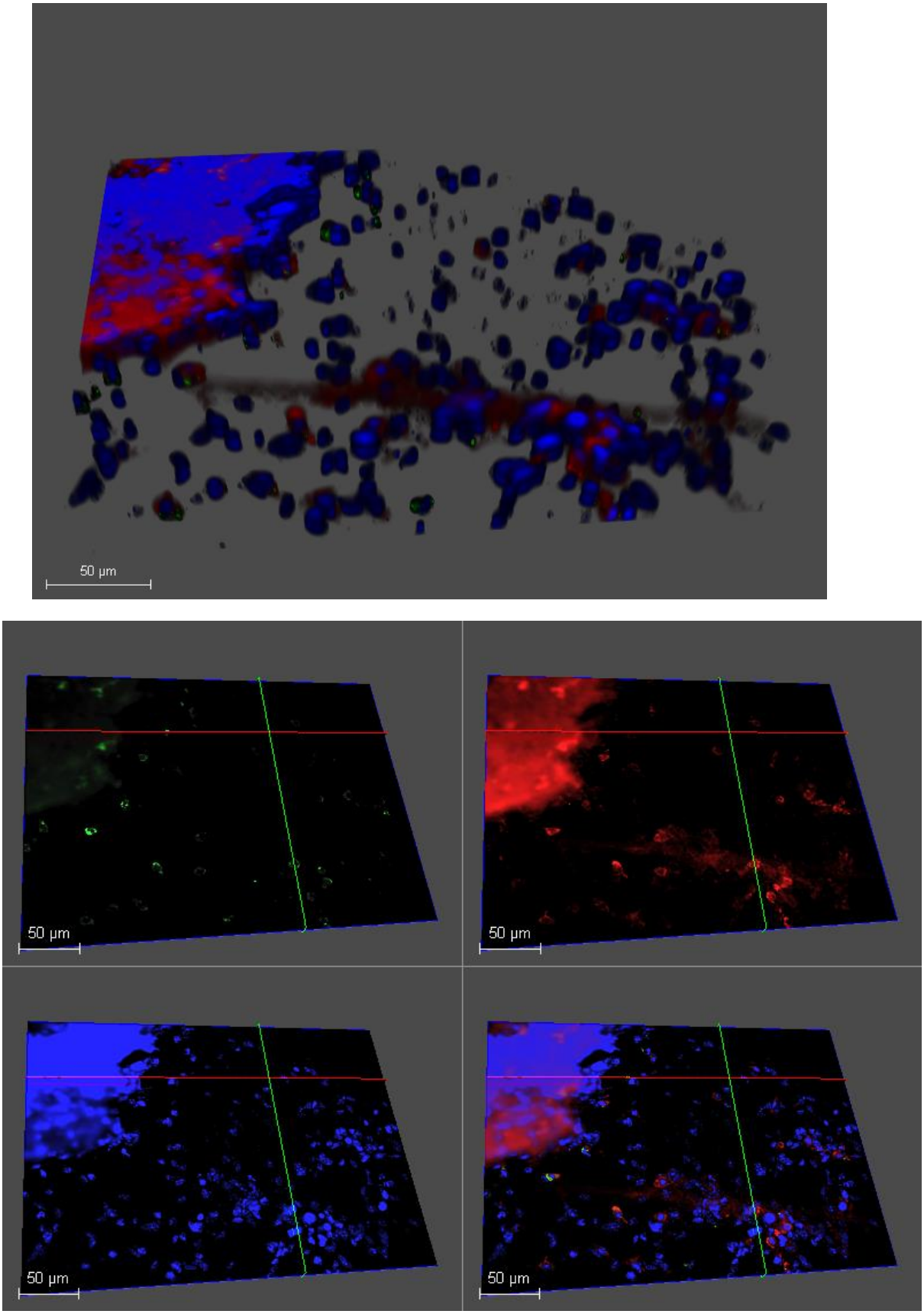

Supplementary Figure 2. **3D visual representation of CD86+ and CD206+ cells on WP1066 treated animals.**

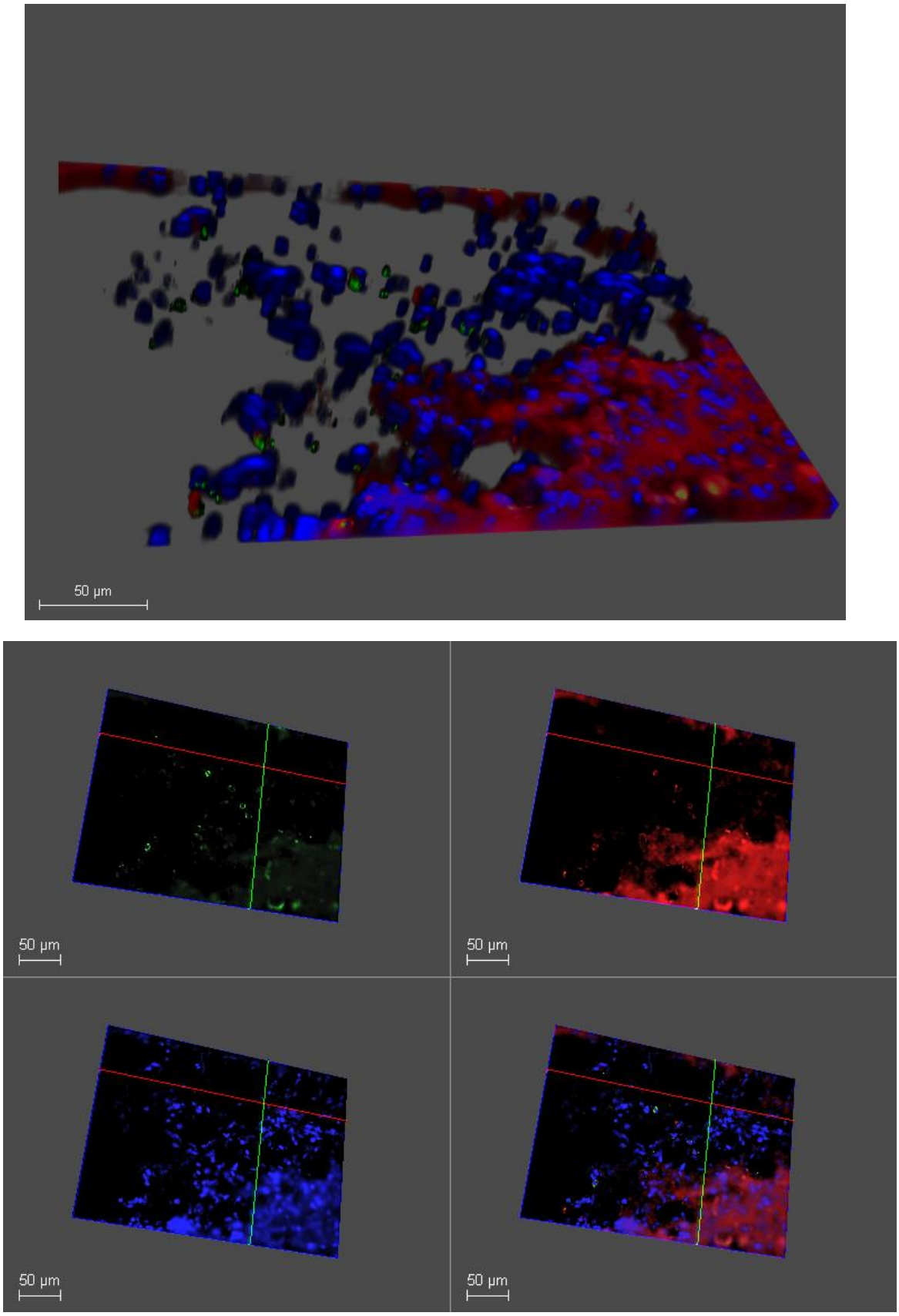

Supplementary Figure 3. **3D visual representation of CD86+ and CD206+ cells on TGFβR1 knockout mice.**